

THÈSE DE DOCTORAT

de l'Université de recherche Paris Sciences et Lettres
PSL Research University

Préparée à Institut Curie

Interplay between ABC membrane transporter BmrA and its
membrane environment

Ecole doctorale n°515

Complexité du vivant

Spécialité MICROBIOLOGIE

Soutenue par Su-Jin PAIK
le 11/10/2018

Dirigée par **Daniel LEVY**

COMPOSITION DU JURY :

Mme. CALLEBAUT Isabelle
Institut de Minéralogie et de Physique
des Minéraux, Présidente du jury

M. BOUTRY Marc
Université Catholique de Louvain,
Rapporteur

Mme. SALOME Laurence
Institut de Pharmacologie et de Biologie
Structurale, Rapportrice

M. PICOT Daniel
Institut de Biologie Physico-Chimique,
Membre du jury

M. RONDARD Philippe
Institut de Génomique Fonctionnelle,
Membre du jury

M. LEVY Daniel
Institut Curie, Directeur de thèse

Acknowledgement

First of all, I would like to express my sincere gratitude to my supervisor, Daniel Lévy, for his patience, guidance, enthusiasm, disposition, support, and the opportunity to work on this wonderful project during the last four years.

I would also like to thank our collaborators: Emmanuel Margeat, Ajay Mahalka, Aurélie Di Cicco, John Manzi, and Alicia Damm for their guidance, stimulating discussions, and advices. I feel privileged to be part of this project. Especially, Patricia Bassereau and Maxime Dahan for their disposition and willing to help. Sometimes I had the feeling of having three supervisors.

I am grateful to all the members of the jury, Isabelle Callebaut, Daniel Picot, and Philippe Rondard, especially to Laurence Salomé and Marc Boutry for taking time and putting effort in evaluating my work. It was an honor for me to have them.

The TAC committee members, Rémi Fronzes, Isabelle Callebaut, Joel Pothier who kept on the track of the project were great help. Your advice was very helpful to make progress in my research work. The guidance of Chiara Rapisarda, who inspired me to pursue a doctoral program after master's internship, was another great help.

I am deeply thankful to our group members with whom I spent a lot of time in a pleasant work environment. I gained weight while working on my thesis thanks to your generous and sweet presents nicely displayed on the desk.

To Cyntia Taveneau, I appreciate for providing models of BmrA. To Amanda Remorino, Mohamed El Beheiry, Aurélien Duboin, and Feng Tsai Ching, thank you for the image acquisition advice. To Matthias Garten, your tips to grow GUVs were amazing. To Clément Caporal, thank you for sharing your code to calculate liposome size. To Julien Pernier, Tea-Young Yoon, Tae-Sun Lee, and Chanwoo Lee, I very much appreciate for helping me to deal with the surface treatment.

To HiJee Kang, my lunch friend, and Rodrigo Caceres, who was constantly tapping my head, I express my gratitude. To Cyntia Taveneau, Estefania Barreto-Ojeda, Amélie Le Corre, Claire Jacquenod, Natalie Busch, Marina Sanchez, and Vincent Michet, thank you for your continuous support and friendship during my thesis works. I also thank the Asian Girls' Dinner Group, Feng Tsai Ching, Ayako Yamada, and Azumi Yoshimura. Our professional and personal discussions with beers were always insightful.

I would especially thank Alicia Damm (my acceptor) who has become a best friend and an amazing colleague. I would always count on her.

To all the people at UMR168, you made of our unit such a pleasant environment even when nothing worked in the lab.

Thanks to my family in Paris, Kumbong Paik, Namsuk Pyun, Jieun Ham, and Namjun Pyun, who gave me a great opportunity to study in Paris. I also thank my cousins, Julie Ju-Hee Paik and Michelle Sung-Jin Paik who have been always supportive.

Finally, I am thankful to my beloved family, Il-Woo Paik, Young-Hee Choi, Sung-Hee Wendy Paik, and Yonghwi Kim for their never-ending spiritual support throughout my life.

Table of Contents

Abbreviations	4
Introduction	5
I. ABC exporters	8
a. Cellular functions	8
b. Classification of ABC transporters	9
c. Topology of ABC transporters	10
1. Nucleotide binding domains of ABC transporters	10
2. Transmembrane domains of ABC transporters	11
d. Structures of ABC transporters	12
e. Substrate translocation mechanisms of type I exporter	14
II. ABCs exporter and membrane	17
a. Cell membranes	17
1. Lipids	17
2. Lipid composition in biological membrane	18
3. Membrane curvature and tension	19
4. Interaction between protein and membrane	21
b. Function of ABC transporters and membrane	22
c. Conformation of ABCs and their surrounding environment	25
d. Annular and structural lipids	25
e. Membrane curvature and thickness	26
f. Oligomerization of ABC transporters	27
III. Dynamics of ABC exporters	28
IV. Reconstitution of ABC transporters in membrane models	30
a. Membrane models	30
b. Reconstitution into SUVs	32
1. Reconstitution methods	32
2. Detergent removal	33
3. Characteristics of proteoliposomes for accurate quantitative measurements	35
4. Reconstitution by direct incorporation into pre-formed liposomes	36
c. Reconstitution into GUVs	37
V. BmrA, an homodimeric ABC from <i>B. subtilis</i>	39
a. Dynamics and structural studies of BmrA	41
b. Interplay between BmrA and membrane at high protein density	42
c. Aims of the thesis	44
Material and methods	45
I. Expression and purification of BmrA	46
a. Expression	46
1. Plasmid	46
2. Transformation	46
3. Culture medium	46
4. Expression	46
b. Membrane preparation	46
c. Purification of BmrA	47
II. Labeling of BmrA with fluorescent dyes	49
a. Labeling by thiol-maleimide reaction	49
b. Preparation of fluorescent dyes	49
c. Purification of labeled BmrA	50
III. Method and characterization of reconstitution of BmrA in proteoliposome	51
a. Preparation of lipids	52
b. Preparation of detergent	53
c. Reconstitution by detergent removal	53
1. Preparation of BioBeads	53
2. Reconstitution from micelles of lipid/detergent/protein	54

3.	Direct incorporation reconstitution	54
d.	Protein orientation	55
1.	Preparation of trypsin	55
2.	Preparation of PMSF	55
3.	Proteolysis	55
e.	Protein incorporation	55
f.	Size of liposomes by dynamic light scattering (DLS)	56
g.	Size and lamellarity of liposomes by cryo-electron microscopy	57
IV.	Reconstitution of BmrA into GUVs	57
a.	Fusion of small proteoliposomes to GUVs	57
b.	Incorporation of BmrA in GUVs by electroformation	58
V.	ATPase hydrolysis measurement	59
a.	Preparation of ATP	59
b.	Preparation of ADP	59
c.	Preparation of orthovanadate	59
d.	Preparation of AMP-PNP	59
e.	Preparation of ATP-γ-S	59
f.	Preparation of cocktail of enzymes:	60
g.	Preparation of 5X cocktail of enzymes:	60
h.	ATPase activity measurement	60
VI.	Ensemble FRET measurement by fluorescence spectroscopy	61
a.	Fluorescence spectroscopy	61
b.	Fluorescence spectroscopy analysis	61
VII.	Fluorescence Cross-Correlation Spectroscopy	62
a.	Measurement of fluorescent lifetime	63
1.	Ensemble FRET by FCCS	63
2.	Analysis of ensemble FRET	63
b.	Single-molecule FRET	63
1.	Single-Molecule FRET by FCCS	63
2.	Analysis Single-Molecule FRET	63
Results.....		65
I.	ATP hydrolysis of BmrA in micelles and reconstituted in membranes.	66
a.	Experimental conditions	67
1.	Inhibition rate of different inhibitors	67
2.	Effect of substrate on ATPase activity	67
b.	ATPase activity of BmrA in micelles of detergent and detergent/lipid	68
1.	ATPase activity depends on the type of detergent	68
2.	No lipid specificity on ATPase activity in micelles of detergent/lipid	69
c.	Functional analysis according to lipid composition in membrane	70
1.	Lipid specificity of ATPase activity in membrane	70
2.	ATPase activity depending on negatively charged lipids	71
3.	ATPase activity in PC vesicles	72
d.	Complete characterization of reconstituted proteoliposomes	73
1.	Protein orientation	74
2.	Protein incorporation	76
3.	Unilamellarity and sizes of liposomes	78
e.	Characteristics of EPC/EPA and <i>E. coli</i> proteoliposomes	78
f.	Conclusion	79
II.	Functional analysis according to membrane curvature	80
a.	Liposome size	80
1.	Comparison between DLS and cryo-EM images	80
2.	Measurement of sizes of liposomes from Cryo-EM images	81
3.	Liposome size modulation with same lipid composition	84
b.	ATPase activity of BmrA is decreased in highly positively curved membrane	85
1.	ATPase activity depending on membrane curvature	85
2.	Characterization of EPC/EPA proteoliposomes with two different sizes	86
III.	Sorting and spatio-temporal distribution of BmrA in curved membrane according to its catalytic states	88
a.	Experimental approaches	88
b.	Reconstitution methods and challenges	88
1.	Fusion of small proteoliposomes to GUVs	88

2.	Electroformation method	89
c.	Characterization of reconstitution of BmrA in small liposomes for reconstitution in GUVs	90
1.	Activity preservation after freezing in the presence of trehalose	91
2.	ATPase activity after buffer exchange to low salt.....	91
3.	ATPase activity in the presence of PEG lipids	92
4.	ATPase activity at 20 °C compared to 37 °C.....	92
d.	Reconstitution of BmrA into GUVs and tube pulling experiment	93
1.	Reconstitution of BmrA in GUVs	93
2.	Sorting of BmrA according to its catalytic state	94
3.	Clusters of apo-BmrA on the neck of nanotubes	95
4.	Orientation of apo-BmrA in GUVs and in nanotube.....	96
5.	Addition of ATP- γ -S at sorted apo-BmrA.....	97
6.	Redistribution of BmrA during catalytic cycle	98
IV.	Fluorescent labeling for analysis of the dynamics of BmrA.....	100
a.	Labeling of BmrA at native single Cys residue	100
b.	Labeling with a single fluorescent dye	101
1.	Depending on time and temperature	101
2.	Concentration of dyes	102
3.	Specificity of labeling.....	102
4.	Rate of labeling and activities.....	103
c.	Labeling with two fluorescent dyes for FRET	104
1.	Different location of labeling by single mutagenesis.....	104
2.	Optimization of ratio of two fluorescent dyes.....	105
3.	ATPase activity depending on labeling yield	107
d.	Conclusion.....	110
V.	Dynamics of BmrA by smFRET	112
Discussion		114
Mechanism of proteoliposomes formation.....		115
Membrane states, lipids composition and ATPase activity of BmrA.....		119
Membrane curvature and ATPase activity.....		121
Membrane curvature and protein distribution		121
Clustering of BmrA.....		124
Spatial distribution of ABCs in cell membranes.....		124
Annexe I : Dynamics of BmrA by smFRET		128
a.	Optimization of experimental conditions for FRET measurements of reconstituted BmrA.....	129
b.	Ensemble FRET measurement	130
1.	Fluorescence spectroscopy.....	130
2.	Fluorescence lifetime measurement by FCS	131
3.	InterFRET	133
c.	smFRET by FCCS.....	134
1.	Experimental approaches	134
2.	smFRET of BmrA solubilized in micelles of detergent	134
3.	smFRET of BmrA solubilized in micelles of lipid/detergent	135
4.	smFRET of BmrA solubilized in proteoliposome.....	135
d.	Conclusion.....	141
Résumé		142
a.	Introduction.....	143
b.	Résultats	144
1.	Hydrolyse d'ATP de BmrA dans les micelles et reconstitué dans les membranes.....	144
2.	Analyse fonctionnelle en fonction de la courbure membranaire.....	145
3.	Tri et distribution spatio-temporelle de BmrA dans la membrane courbée en fonction de ses états catalytiques.....	146
c.	Discussion.....	147
Figures and tables		151
Bibliography		156

Abbreviations

ABC	ATP-Binding Cassette transporter
CL	Cardiolipin
CMC	Critical micelle concentration
DDM	N-dodecyl- β -d-maltoside
DEER	Double electron electron resonance
DLS	Dynamic light scattering
DMPC	1,2-Dimyristoyl-sn-glycero-3-Phosphocholine
DOM	Dodecyl maltoside
DPPC	1,2-Dipalmitoyl-sn-glycero-3-Phosphocholine
<i>E. coli</i>	<i>Escherichia coli</i>
EM	Electron microscopy
EPC	Egg PC
EPR	Relative proximity ratio
FRET	Fluorescence resonance energy transfer
GUV	Giant unilamellar vesicle
HDX	Hydrogen/deuterium exchange
ICD	Intracellular domains
LLO	Lipid-linked oligosaccharyl
LPR	Lipid/protein ratio
LPS	Lipopolysaccharide
LRET	Luminescence resonance energy transfer
LUV	Large unilamellar vesicle
MATE	Multidrug and toxic compound extrusion
MD	Molecular dynamics
MDR	Multi-drug resistance
MFS	Major facilitator superfamily
MS	Mass spectroscopy
NBD	Nucleotide-binding domains
ND	Nanodisc
NMR	Nuclear magnetic resonance
OG	Octylglucoside
PC	Phosphatidylcholine
PDB	Protein data bank
PE	Phosphatidylethanolamine
PG	Phosphatidylglycerol
PgP	P-glycoprotein, ABCB1
PI	Phosphatidylinositol
PMSF	Phenylmethylsulfonyl fluoride
PS	Phosphatidylserine
RND	Resistance-nodulation-cell division
SMALP	Styrene maleic acid lipid particle
SMR	Small MDR
SUV	Small unilamellar vesicle
TMD	Transmembrane domain
Vi	Orthovanadate
v/v	Volume/volume
w/w	Weight/weight

Introduction

Cells are compartmentalized by membranes, which are composed of a lipid bilayer with transmembrane proteins and membrane bound proteins. The membrane acts as a barrier to protect the cell from the outside. Every molecule must pass through the membrane to enter or exit cells regardless of its size. This exchange of molecules e.g. nutrients, metabolites, ions is carried out in a selective and controlled manner by transporter or channels.

ATP-binding cassette (ABC) transporters are one of the largest transmembrane protein families present in all living organism. ABCs transport various types and size of substrates across the membrane including drugs, lipids, bile salts, hormones, micronutrients, nucleotides, sugars, vitamins, metals, peptides and many others (Beek, Guskov, & Slotboom, 2014; Locher, 2016). These proteins are ubiquitous, essential for cellular life because of their important cellular functions such as cell detoxification, lipid homeostasis, osmotic homeostasis, nutrient uptake, cell-volume regulation, immune system and others (P. M. Jones & George, 2004). The substrate transport is carried out by ATP hydrolysis dependent process. In *Escherichia coli* (*E. coli*), the genome of ABCs represents approximately 5% with 80 distinct systems (Rees, Johnson, & Lewinson, 2009). 48 and 20 ABCs have been identified in human and in *Bacillus subtilis*, respectively (Chen et al., 2016; Hassan et al., 2017).

ABCs allow unidirectional substrate transport as importers or exporters (Figure 1), which transport substrates inside or outside cells through the membrane, respectively. There are seven ABC superfamilies (Figure 2). ABC exporters are present in all living organisms whereas ABC importers are present exclusively in prokaryotes (Rees et al., 2009) and require accessory component called substrate binding protein for substrate translocation (Biemans-Oldehinkel, Doeven, & Poolman, 2006).

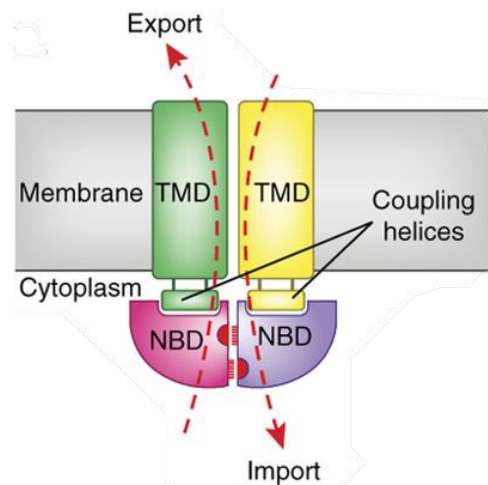


Figure 1 Domains of ABC transporters

ABCs share a common architecture, which consist of 2 TMDs and 2 NBDs. ATP-binding site in interface between two NBDs are represented in RED. The coupling helices allows conformational changes between NBDs and TMDs. (Locher, 2016)

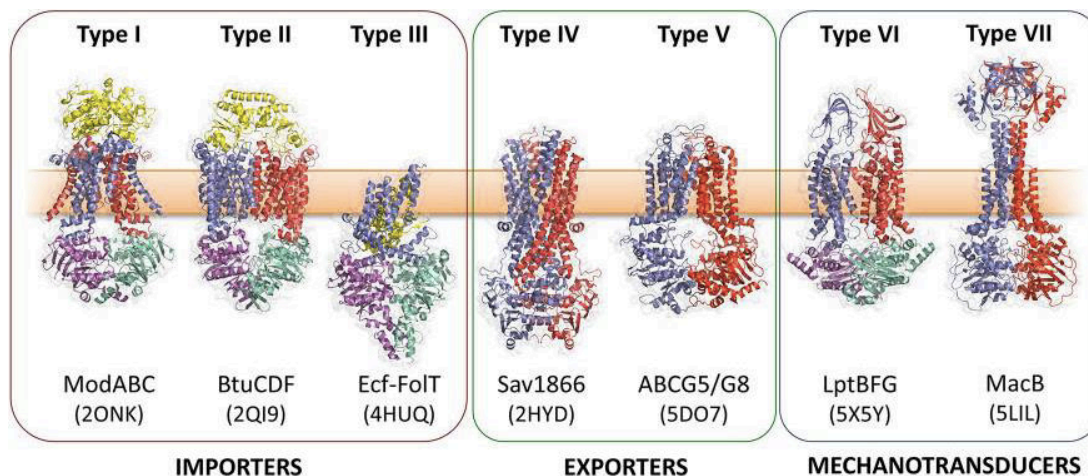


Figure 2 Seven superfamilies of ABC transporters

ABCs are here further classified based on function: types I-III are importers, types IV and V are exporters (or exporter type I or II) and types VI and VII are mechanotransducers. (Greene, Kaplan, Crow, & Koronakis, 2018)

Among the ABCs, some have narrow substrate specificity and others have wider. In particular, human, bacterial, plant and fungi ABCs that are involved in cell detoxification have broad substrate specificity (Figure 3). Some human ABC exporters confer a multidrug resistant (MDR) cellular phenotype by efflux of a wide range of drugs including e.g. anticancer agents, HIV protease inhibitors, immunosuppressive agents, pesticides, antibiotics, etc. (Gottesman, Fojo, & Bates, 2002). Bacterial ABCs translocate antibiotics and polypeptide virulence factors (Thomas & Tampé, 2018). Plants ABCs transport heavy metals and metalloids that are contaminations of agricultural soils, antibiotics, toxins produced by pathogens and anthropogenic compounds, such as herbicides and industrial waste (Kang et al., 2011). Substrate range of fungi ABC includes insecticides, fungicides, plant metabolites, antibiotics, and mycotoxins (Baral, 2017). This broad specificity of drug transport and their levels of expression determine the efficiency of cell resistance. Therefore, these proteins have been the subjects of intense studies. 19 among 48 human ABC transporters have been shown to efflux anticancer agents (Robey et al., 2018). One of the most studied ABCs is P-glycoprotein (PgP, ABCB1 or MDR1). PgP is an ABC exporter that is overexpressed in tumor cells and efflux anticancer agents.

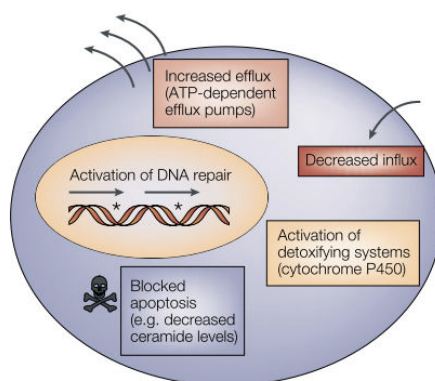


Figure 3 schematic representations of main functions leading to multidrug resistance in human cell

ABC transporters are one of factors responsible for MDR by efflux of various types of drugs. Activation of detoxifying systems, activation of DNA repair and disruptions in apoptotic signaling pathways are also main players of MDR phenotype. (Gottesman et al., 2002)

In 1992, it was suggested that PgP not only transports drugs, but also lipids (Higgins & Gottesman, 1992). Since then, many other human and bacterial ABCs have also been identified as lipid transporters and the relationship between ABCs and membrane has been focused.

I. ABC exporters

a. Cellular functions

Since ABCs are implicated in transport of tremendous range of substrates, mutations of human ABCs lead to severe genetic diseases:

- cystic fibrosis associated with cystic fibrosis transmembrane conductance regulator;
- adrenoleukodystrophy associated with ABCD1 (or ALDP);
- pseudoxanthoma elasticum associated with MRP6;
- Stargardt macular degeneration associated with ABCA4;
- Tangier disease associated with ABCA1, etc. (Wilkins, 2015).

Human ABCs are considered a promising target in drug development because of their involvements in important cellular processes, such as:

- lipid homeostasis: transport of lipids and generation of bile (Neumann, Rose-Sperling, & Hellmich, 2016);
- MDR: transport various anticancer agents such as vinca alkaloids, anthracyclines (including doxorubicin), epipodophyllotoxins, and taxanes (Gottesman et al., 2002) ;
- adaptive immune response: transport of antigen processing (Procko, Ferrin-O'Connell, Ng, & Gaudet, 2006);
- mitochondrial Fe homeostasis (Kispal, Csere, Guiard, & Lill, 1997);
- regulation of ion channels such as potassium channels and ATP-gated chloride channel (Aittoniemi et al., 2009; Bryan et al., 2007; Riordan, 2008), etc.

Functions of bacterial ABCs comprise nutrition uptake, xenobiotic protection, efflux of cellular wastes, bacterial immunity and virulence, osmotic stress, lipid transport and export of macromolecules during biogenesis, differentiation, and pathogenesis (El-Awady et al., 2017; Lubelski, Konings, & Driessen, 2007). Some bacterial ABCs also are responsible for lipid transport like MsbA (from *Escherichia coli*), TmrAB (from *Thermus thermophilus*), and LmrA (Paul D. W. Eckford & Sharom, 2010; Reuter et al., 2003; Zutz et al., 2011). Their deletions are sometimes lethal, e.g. the deletion of MsbA leads lethal accumulation of lipid A in cytoplasmic membrane (P. D W Eckford & Sharom, 2008). However, for the vast majority of ABCs, the physiological substrates are unknown. In addition, since several MDR systems are available in prokaryotic cells, the deletion of ABCs is not always lethal. In addition to the ABC primary transporters, other secondary transporters are involved in MDR: the multidrug and toxic compound extrusion (MATE) family, the small MDR (SMR) family, the major facilitator superfamily (MFS) and the resistance-nodulation-cell division (RND) family (Figure 4).

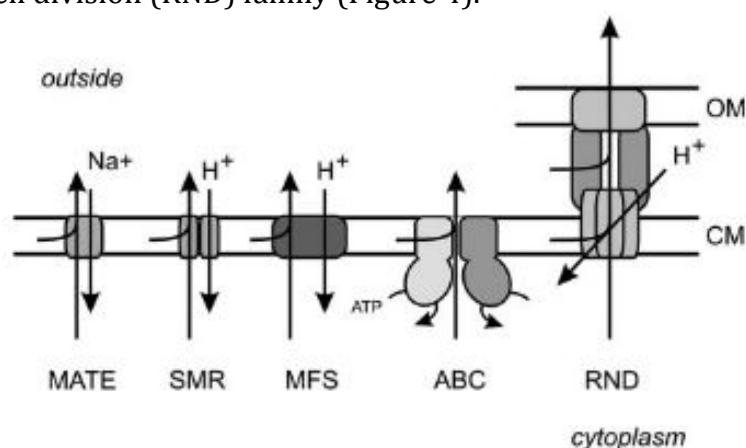


Figure 4 Schematic representations of MDR transporters in prokaryote

Different to primary ABC transporters that utilize the free energy of ATP hydrolysis, secondary transporters (MATE, SMR, MFS and RND) utilize proton or sodium motive force for drug expulsion. (Lubelski et al., 2007)

The main functions of yeast ABC are cellular detoxification and MDR as they export cytotoxic compounds and potentially toxic metabolites (Jungwirth & Kuchler, 2006). Yeast ABCs also play an important role in stress adaptation, vacuolar detoxification and regulation of mitochondrial function and lipid translocations (Prasad, Khandelwal, & Banerjee, 2016).

Plant ABCs are involved in detoxification, pathogen response, organ growth, plant nutrition, development, response to abiotic stress, and the interaction of the plant with its environment (Kang et al., 2011).

b. Classification of ABC transporters

ABCs are classified as 7 sub-families (ABCA - ABCG) based on their genomic sequence similarities. ABCA-ABCD and ABCG are transmembrane transporters while ABCE and ABCF families are soluble proteins with only NBDs. ABCE and ABCF families are implicated in completely different functions as ribosome recycling and regulation of transcription, respectively (Barthelme et al., 2011; Boël et al., 2014). The substrates and subcellular localization of each ABC family are depicted in Figure 5, the topology will be discussed below.

Human ABC-Family	A	B	C	D	G
Transporter Topology					
Lipophilic Substrates	(Phospho)lipids (A1, A3, A4, A7, A12) Sphingomyelin (A1, A3) Cholesterol (A1, A2, A5)	Phospholipids (B1, B4) Sphingolipids (B1) Bile salts (B11) Drugs (B1)	Phospholipids (C1) Bile salts (C1, C2, C3) Steroids (C1, C10) Drugs (C1, C2)	(VLC)FA (D1-D4)	Lipids (G4) Cholesterol (G1, G4, G5/G8) Steroids (G2, G5/G8) Drugs (G2)
Subcellular Localization	Plasma membrane (A1, A4, A7) Lysosome (A2, A5) Lamellar bodies (A3, A12)	Plasma membrane (B1, B4, B11)	Plasma membrane (C1, C2, C3, C10)	Peroxisome (D1-D4)	Plasma membrane (G5/G8) Endosomes (G1, G4)

Figure 5 Topology, substrates and subcellular localization of human ABC

Each corresponding ABC is specified in brackets. (Neumann et al., 2016)

Eukaryotic ABC undergoes post-translational modifications such as phosphorylation, which may regulate ABC transporter function or expression (Stolarczyk, Reiling, & Paumi, 2011).

In prokaryotes, ABCs are localized in plasma membrane and ATP is hydrolyzed at cytoplasm side. Roughly, bacterial ABCs are divided in three sub-classes according to their genetic similarities (Davidson, Dassa, Orelle, & Chen, 2008):

- Class 1 corresponds to TMDs and NBDs fused in same polypeptide chains and contains a majority of ABC exporters.
- Class 2 consists of repeated ABC domains without TMDs. The proteins from this class do not function as transporter.
- Class 3 carries TMDs and NBDs at independent polypeptide chains and contains a majority of ABC importers.

c. Topology of ABC transporters

Eukaryotic ABCs function as a full or as a 'half' transporter (Figure 5). ABCA and ABCC are full transporters with all 4 domains fused in single polypeptide chains. They can either have forward (TMD1-NBD1-TMD2-NBD2) or reverse (NBD1- TMD1- NBD2-TMD2) topologies. ABCD and ABCG are half transporters, with one NBD or one TMD. They function as a hetero- or homodimer to form a full transporter. Homodimers contain two consensus NBDs whereas heterodimers contain one degenerate ATP hydrolysis site that is not capable of ATP hydrolysis. Since the catalytically impaired function of heterodimers, the transport mechanisms of heterodimers are suggested to be different from those of homodimers. In ABCB, both full and half transporters are found. Some ABCs contain additional transmembrane domain (TMD0), the function of which is unknown. It was suggested that TMD0 is implicated in functional regulation or oligomerization (Biemans-Oldehinkel et al., 2006).

Besides, all prokaryotic ABCs are 'half transporters' (Figure 7). The most studied bacterial ABC homodimers are MsbA, Sav1866 (from *Staphylococcus aureus*), HorA (from *Lactobacillus brevis*), McjD (from *E. coli*) BmrA (from *Bacillus subtilis*) and LmrA. Some bacterial ABCs also contain one degenerative NBD, such as TmrAB, BmrCD (from *Bacillus subtilis*), LmrCD (from *Lactococcus lactis*) and TM287/28 (from *Thermotoga maritima*) heterodimers.

1. Nucleotide binding domains of ABC transporters

Nucleotide binding domains of ABCs are highly conserved subunits among ABCs. ATP molecules are bound, hydrolyzed and released at NBDs. Eukaryotic and bacterial ABCs share between 30 and 50% of sequence homology within NBDs (Wilkins, 2015). A monomer of NBD contains 2 sub-domains:

- A catalytic core domain called RecA-like domain, containing P-loop (Phosphate-binding loop) or Walker A motif (GxxGxGK (S/T), with x being any residue), a Walker B motif ($\phi\phi\phi\phi$ DE), with ϕ being hydrophobic residue), a Q-loop and an H- (or switch) loop;
- α -helical domain, containing ABC signature motif LSGGQ.

Two NBDs are organized in symmetrical head-to-tail manner with two nucleotides sandwiched at the interface (Figure 6). Walker A, ABC signature motif and H loop bind directly to ATP: Walker A binds the alpha and beta phosphates of ATP, the signature motif aligns ATP during hydrolysis and H-loop stabilizes the transition-state geometry. Meanwhile, Walker B and Q-loop coordinate magnesium and water during the hydrolysis.

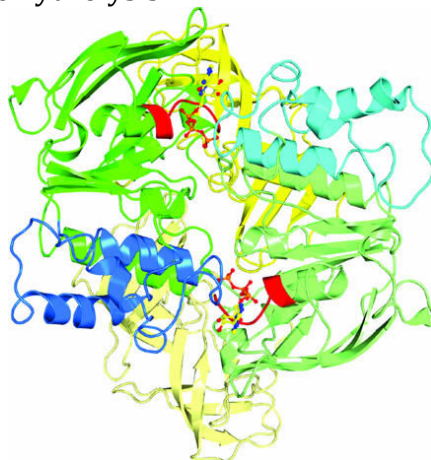


Figure 6 Structures of nucleotide-bound NBDs

Two NBDs that are dimerized in the presence of ATP are shown from MalK homodimer (PDB: 1Q12). RecA-like subdomain and α -helical subdomain are shown in green and blue, respectively. A C-terminal regulatory domain (not present in all ABC proteins) is shown in yellow. Corresponding domains in the second MalK subunit follow the same color scheme but are rendered in lighter colors. Two ATPs, represented as a ball-and-stick model, are bound between the NBDs. The Walker A motif is shown in red. (Davidson et al., 2008)

2. Transmembrane domains of ABC transporters

Transmembrane domains of ABCs are generally composed of 12 transmembrane helices for full transporter or 6 transmembrane helices for half transporters (Figure 7). For half transporters, except for ABCG families, the domain intertwining arrangement of helices 1–3 and 6 from one subunit and helices 4–5 from the opposite subunit allows to form substrate cavity. Elbow helix is positioned parallel to the water/membrane interface, possibly delimiting membrane and extramembrane domains (Zou & Mchaourab, 2009). Contrary to NBDs, TMDs are heterogeneous among ABCs (Robey et al., 2018). It has been suggested that axial rotation of transmembrane helices creates a complex network of interactions to substrates, such as cation- π interactions with aromatic residues and hydrophobic and hydrogen bonding interactions, responsible for polyspecificity of ABCs (Gutmann, Ward, Urbatsch, Chang, & van Veen, 2010).

There are only 2 cases where structures of ABC are revealed with physiological substrates: MsbA bound to lipopolysaccharide (LPS) and MRP1 bound to leukotriene C₄ (Ho et al., 2018; Johnson & Chen, 2017; Mi et al., 2017). An example of TMDs of MsbA is shown in Figure 7 (Mi et al., 2017). The cross-section of TMDs of MsbA bound to LPS (Figure 7B) and blocked in post-hydrolysis conformation in the presence of inhibitor (Figure 7C) are shown. The substrate is surrounded by transmembrane helices, which form a hydrophobic pocket and a hydrophilic cavity. Substrate is interacting with several residues of transmembrane helices that are positively charged. In post-hydrolysis conformation, the positions of helix 3 and helix 6 are notably changed, suggesting that the reorganization of transmembrane helices is responsible for release of substrates. Recent NMR studies on MsbA revealed that helix 6 is crucial in drug binding and helix 4 is responsible for the transmission of conformational changes to the NBDs upon ATP binding (Spadaccini, Kaur, Becker-Baldus, & Glaubit, 2018).

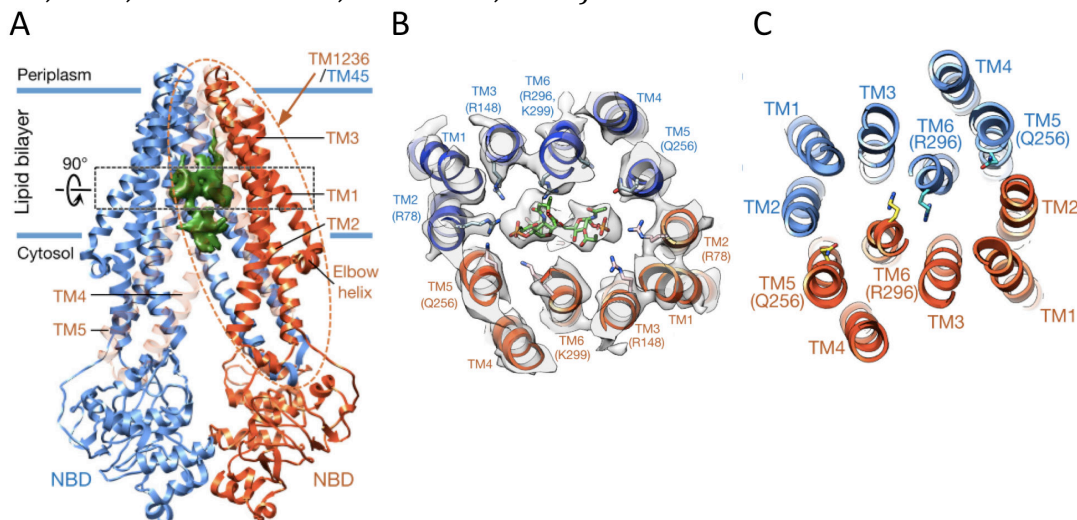


Figure 7 Cryo-EM structure of MsbA

(A) Structure of homodimeric MsbA was determined in nanodisc by cryo-EM. Two monomers are colored in blue and orange and the density of substrates, LPS is showed in green. (B) The rotated cross-section of transmembrane domains (black dotted rectangle) is shown with density of LPS. (C) The same cross-section in ADP-Vi bound form is shown (Mi et al., 2017)

d. Structures of ABC transporters

Structures of ABCs have been extensively studied at high resolution by X-ray crystallography and recently cryo-EM in detergents, in micelles of detergent/lipid and in membranes. There are two types of structure among ABC exporters (Figure 8).

The first type of exporter consists of classical structure of ABC exporters, referred to as the B-family ABC-exporter fold. The first structure of ABCs was revealed in 2001 with MsbA with incorrect analysis followed by two other incorrect structures of MsbA (Chang & Roth, 2001). Then, these structures were retracted in 2006 when Kaspar Locher's group published the structure of Sav1866 (Dawson & Locher, 2006). Since then, other ABC structures have subsequently been found with similar fold as Sav1866. The NBDs are fused to the TMDs. Half transporters have domain-swapping arrangement between the TMDs. There are different distances of separation between two NBDs in apo-conformations (Figure 9), called inward-facing conformations. The substrate cavity is open toward cytoplasmic medium where the surface cavity differs according to the distance of NBDs. Occluded conformations stand for dimerization of NBDs but without access to the cavity neither from the cytoplasmic side, nor from extracellular matrix. Outward-opened conformation indicates the dimerization of NBDs with substrate cavity opened toward extracellular matrix.

However, the amplitude of the separation is under discussion and sometimes even within the same group working on the same protein, they change their opinions (Cooper & Altenberg, 2013; Zoghbi, Cooper, & Altenberg, 2016). Recent studies in double electron electron resonance (DEER), Luminescence Resonance Energy Transfer (LRET) and electron microscopy (EM) clearly show that in apo conformations, NBDs remain separated with different distances in detergents as well as in physiologically relevant membrane mimicking systems (Cooper & Altenberg, 2013; Esser et al., 2016; Moeller et al., 2015). The large separations between NBDs (≈ 5 nm) were found by X-ray crystallography, and have long been debated whether these structures were physiologically relevant because the crystals were in the presence of detergent and protein-protein contact occurred in crystal packing by NBDs and TMDs. Studies in negatively stained EM in membrane mimicking environment showed a large spectrum of conformations of MsbA and PgP with or without ATP, suggesting a high flexibility of ABCs in membrane (Figure 10) (Moeller et al., 2015). Besides, experiment with cys-cross linking between two NBDs showed higher ATPase activity and ability for drug transport, suggesting that NBDs remain in close proximity (Loo & Clarke, 2014). Fluorescence resonance energy transfer (FRET) and LRET studies on PgP suggest that the NBDs do not separate significantly during drug transport (Verhalen, Ernst, Börsch, & Wilkens, 2012; Zoghbi et al., 2017).

The second type of exporter concerns two members of the ABCG subfamily recently solved (Figure 8). The human ABCs, ABCG5/G8 (J. Y. Lee et al., 2016) and ABCG2 (Jackson et al., 2018) have completely different fold to ABCB subfamilies with shorter transmembrane helices and intracellular loops, therefore a shorter distance between NBDs and membrane. These structures are similar to those of importers. There is no domain swapping suggesting a different mechanism of drug translocation from those of type I. Negative staining EM of NpPdr1 and NpPdr1, two full-length ABCs from plants, which belong to ABCG subfamily, also revealed shorter proteins (Pierman et al., 2017; Toussaint, Pierman, Bertin, Lévy, & Boutry, 2017).

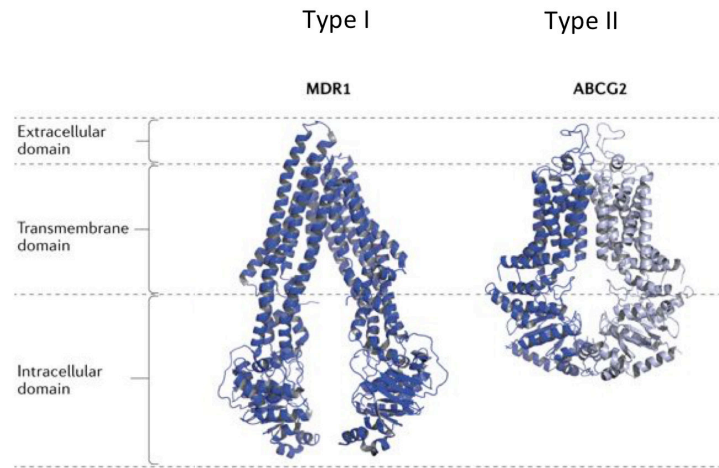


Figure 8 Two types of structures of ABC exporters

Structures of type I exporter PgP (PDB: 5KPI) and type II exporter ABCG2 (PDB: 5NJ3). Adapted from (Robey et al., 2018)

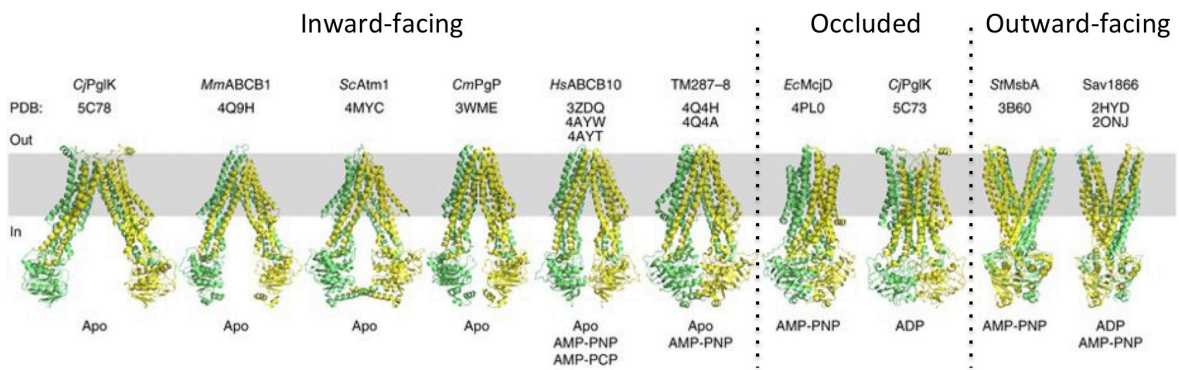


Figure 9 Several conformations of type I, B-family ABC-exporters

The name of the species and associated PDB number of each transporter are indicated on the top. Catalytic states are specified below. This figure was readapted from (Locher, 2016).

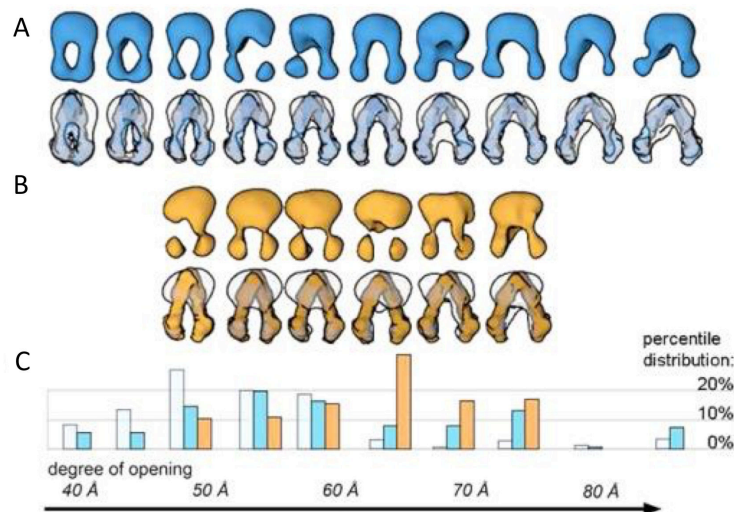


Figure 10 Large spectrums of conformations of MsbA and PgP in membrane mimicking system studied by negatively staining-EM

3D densities of MsbA (A) and PgP (B) in apo conformations are shown. (C) The recurrences of distance between NBDs for apo-MsbA (white), MsbA in the presence of ATP (blue) and apo-PgP (orange) are shown. (Moeller et al., 2015)

e. Substrate translocation mechanisms of type I exporter

Despite the numerous available structures of ABCs, the transport mechanism remains unclear. This is because structures are only snapshots and kinetic information is lacking. Several translocation models have been proposed with some conservative steps: fixation of ATP, ATP hydrolysis, release of ADP and Pi (Szöllősi, Rose-Sperling, Hellmich, & Stockner, 2018). It is worth noting that conformational changes occur without substrates by ATP hydrolysis but substrate translocation is ATP-dependent.

The first question concerns the synchronization of 2 molecules of ATP binding and hydrolysis within the same catalytic cycle. Even for ABC exporters with two functional ATP hydrolysis sites, some studies suggest that two ATP are subsequently or sequentially hydrolyzed leading to complete dissociation of NBDs (Esser et al., 2016; Higgins, 2007), while other studies suggest that ATPs are alternatively hydrolyzed, therefore NBDs remain dimerized. (P. M. Jones & George, 2004). In the case of heterodimer containing one degenerative catalytic site, structural studies suggest that the NBDs remain partially or fully in contact during catalytic cycle (Hohl et al., 2012, 2014; Mishra et al., 2014).

There are 3 main transport models for type 1 exporters. The alternative access model involves the separation of two NBDs in the apo conformation whereas NBDs remain in contact during the catalytic cycle in the outward-only model and the constant-contact model.

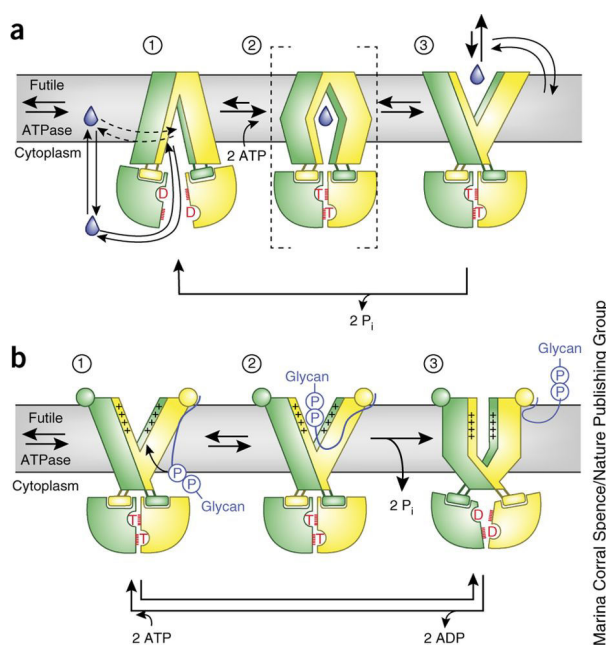


Figure 11 Two models of substrates transport

Cartoon illustrates (a) alternating access model and (b) outward-only mechanism. (Locher, 2016)

The alternating access model (ATP-switch model) is based on separated NBDs in apo inward-open conformation. The principal steps are followed:

- 1) Substrates are bound into the cavity from cytoplasm or directly from inner membrane to inward-open conformation ABCs (Aller et al., 2009; Barreto-ojeda, Corradi, Gu, & Tieleman, 2018);
- 2) ATPs are bound to NBDs ;
- 3) Conformational changes occur with dimerization of NBDs by movement of translation and rotation (see below), probably convert to occluded conformation;
- 4) Cavity opens toward extra matrix in post-hydrolysis conformation;
- 5) The rearrangement of

TMDs changes the surface of cavity, which likely leads to chemical mismatch between cavity and substrates, followed to the release of substrates; 6) ATP hydrolyses to ADP and Pi; 7) ADP and Pi are released with separation of NBDs and opening of cavity toward cytoplasm.

This mechanism has been proposed from many studies by cryo-EM, DEER and by X-ray crystallography of BmrA, MsbA, LmrA, Sav1866, Pgp (Borbat et al., 2007; Esser et al., 2016; Fribourg et al., 2014; Loo & Clarke, 2002; Moeller et al., 2015; van Veen, Margolles, Müller, Higgins, & Konings, 2000; Verhalen et al., 2017; A. Ward, Reyes, Yu, Roth, & Chang, 2007; Wen, Verhalen, Wilkens, Mchaourab, & Tajkhorshid, 2013). This mechanism is consistent with a high substrate affinity to inward-open conformation and low affinity to outward-open conformation, demonstrated for Pgp (Ramachandra et al., 1998; Zou, Bortolus, & Mchaourab, 2009). Recently, cryo-EM studies with MsbA elucidated that ATP hydrolysis occurs after substrate translocation and release (Mi et al., 2017).

Structures of different ABC revealed different degrees of separations of NBDs in terms of distance and rotation (Shintre et al., 2013). As shown in Figure 12, the positions between the nucleotide γ -phosphate (green) and the catalytic C loop (cyan) vary to one structure to another, suggesting that the dimerization of NBDs requires translational and rotational movements for alignment of catalytic sites.

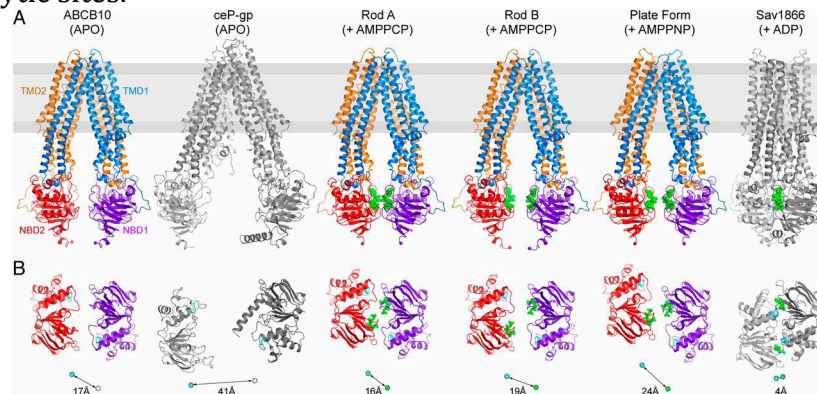


Figure 12 Rotation and translation movement for NBDs dimerization

(A) Different structures of ABCs are presented. (B) Nucleotide γ -phosphate and the C- α of the first glycine in the catalytic C loop of NBDs are presented in green and cyan colors, respectively. (Shintre et al., 2013)

In the case of small substrates, a change of orientation is not necessary during translocation. In contrast, lipids require a specific orientation, and need 180 °C rotation during the translocations. Three models have been proposed for lipid translocation mechanism (Mi et al., 2017; Neumann et al., 2016). In all models, lipids are entered by inner leaflet of membrane in inward-open conformation and lipid headgroup is positioned into the apex of the cavity. This is consistent with the structure of Pgp (PDB: 4F4C) where detergent headgroup was suggested to be fixed at the cavity with acyl chain oriented outside in the inward-open conformation (Jin, Oldham, Zhang, & Chen, 2012). In the lipid threading model, the conformational changes to outward-open cause the different surfaces and lipid headgroup slides along the surface of cavity. In the lipid gymnastics model, lipids change orientation during occluded conformation leading to translocation of lipids at outer leaflet. The trap and flip model was proposed based on cryo-EM studies of MsbA in nanodisc for transport of LPS. This model consists of lipid flipping at the same time as conformational changes to outward-open conformation.

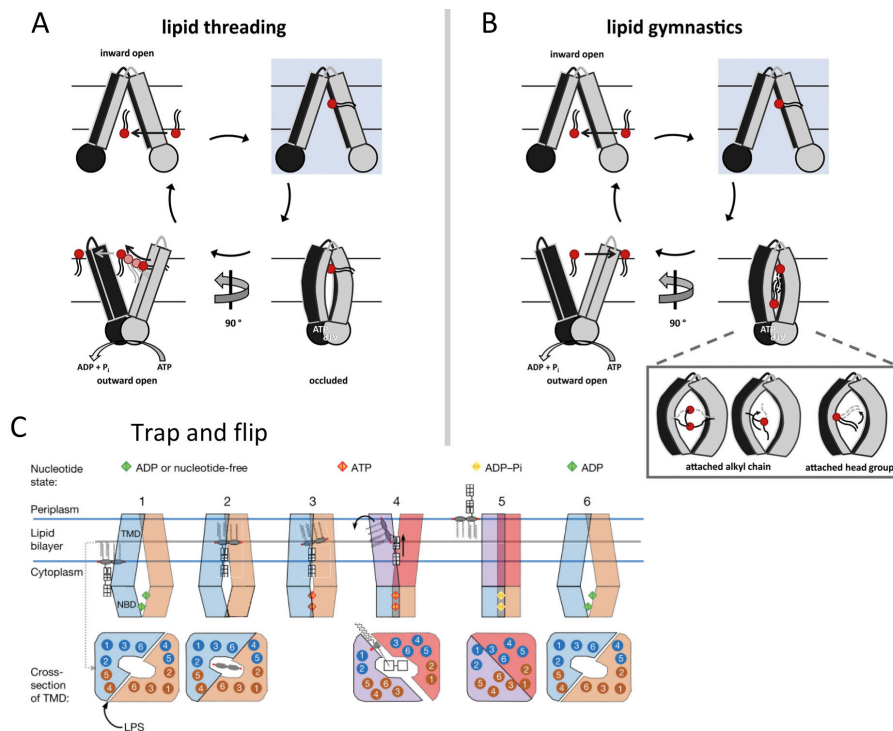


Figure 13 Lipid translocation models by alternating access models

(Mi et al., 2017; Neumann et al., 2016)

Outward-only mechanism is based on occluded and outward-open conformations (Figure 11B). This mechanism was proposed for bacterial PglK (from *Campylobacter jejuni*) for the translocation of lipid-linked oligosaccharyls (LLO) (Perez et al., 2015). The main steps are as followed: 1) Substrates are bound on the surface of ABCs in outward-opened conformation with ATP already bound to NBDs; 2) the pyrophosphate-glycan headgroup is directly transferred into the cavity by electrostatic interactions; 3) ATP hydrolyses to ADP and P_i; 4) The conformation changes to occluded conformation with release of substrate to outer leaflet.

PglK shares similar structural fold as Pgp and MsbA. However, this mechanism of transport seems unlikely at least for translocation of lipid A by MsbA because ATP pre-bound MsbA had considerably reduced affinity to lipid A (Siarheyeva & Sharom, 2009).

Constant-contact model consists of alternating ATP hydrolysis of 2 sites of catalytic sites (Figure 14). Main steps are followed:

1) One site of ATP is hydrolyzed followed with release of ADP and P_i; 2) The release of ADP induces increase of affinity for ATP in opposite ATP binding site; 3) ATP is bound and induces occlusion of both site of ATP; 4) The second ATP is hydrolyzed followed with release of ADP and P_i, and the cycle is repeated.

Functional studies in cross-linking of Pgp (Verhalen & Wilkens, 2011), LRET studies in the presence of substrates (Kaur et al., 2016; Zoghbi et al., 2017) support this model. Moreover, dynamic simulation on Sav1866 shows a stable conformation of occluded and outward-open conformations and suggests a ratio of one ATP hydrolysis/transport cycle/homodimer supporting this transport mechanism (Xu, Seelig, & Bernèche, 2017). This model is also proposed for heterodimeric ABCs (Mishra et al., 2014).

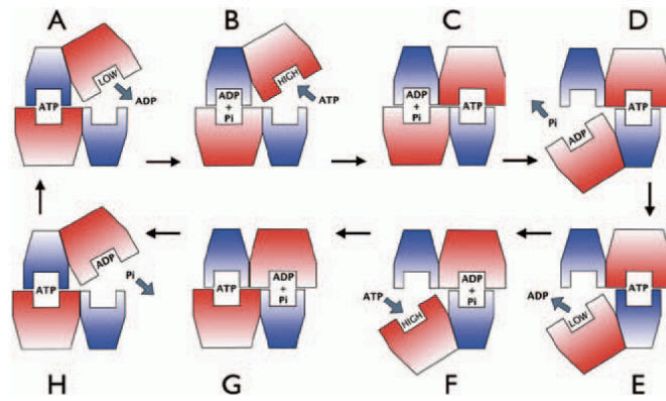


Figure 14 Schematic representations of NBDs for constant-contact model

(Peter M. Jones & George, 2013)

In addition, these different mechanisms are not mutually exclusive and may switch to different mechanism depending on substrates. LRET studies with PgP suggest that alternating access mechanism during basal ATPase activity that switches to constant-contact model in the presence of substrates (Zoghbi et al., 2017). The complication does not end here. It has been suggested that even though the substrate translocation is dependent to ATP hydrolysis, the presence of ATP leads to continuous conformational changes (Esser et al., 2016).

II. ABCs exporter and membrane

Before we discuss the interaction between ABCs and membrane, I will give a quick overview of cell membranes and their properties that can modulate integral membrane in terms of function and conformations, and vice-versa.

a. Cell membranes

1. Lipids

Membranes are made of a lipid bilayer where proteins are embedded and bound. Cellular membranes are composed of approximately thousands of different lipid species that are principally sphingolipids, sterols and glycerolipids. Lipids contain hydrophilic headgroup and hydrophobic acyl chains. This amphiphilic nature of lipids leads to assemblage to minimize the exposure of hydrophobic domains in aqueous solution. The size of lipid head-group and the length and degree of saturation of acyl chains determine the overall shape of lipids such as conical, cylindrical and inverted-conical (Figure 15, Figure 16)(Van Den Brink-Van Der Laan, Antoinette Killian, & De Kruijff, 2004). These lipids induce positive, zero and negative membrane curvature, respectively. Thus the ratio between different shapes of lipids in principle determines the membrane morphology. For example, lipid sorting may occur during cellular events involving membrane remodeling and high membrane curvature (Callan-jones, Sorre, & Bassereau, 2011). However, in most native membranes, the combination of lipids results in planar membranes.

Moreover, the lengths and the degree of saturation of the lipid acyl chains influence membrane fluidity. The more the acyl-chains are long and saturated, the more rigid the membranes are. Other lipid components such as cholesterol and hopanoid for eukaryotic and bacterial lipids, respectively increase the packing and order at short distance while increase the fluidity at large distance (Belin et al., 2018). Membrane fluidity is also increased with increasing

temperature. Phospholipid bilayers are organized in a rigid gel phase below the phase transition temperature and above, in a fluid liquid-crystalline phase.

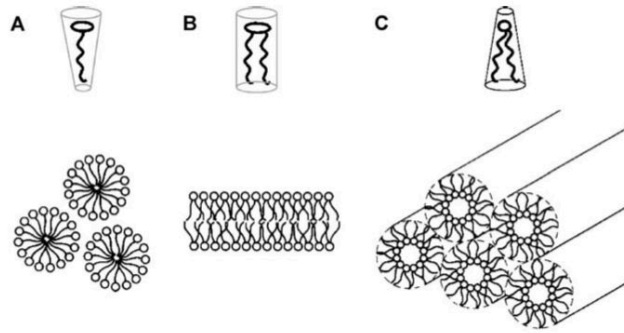


Figure 15 Overall shapes of lipids and their assembling

(A) Inverted conical shaped lipids form structures with positive curvatures such as micelles. (B) Cylindrical-shaped lipids form bilayer structures such as liquid crystalline phase. (C) Conical shaped lipids form negative curvature structures, such as hexagonal phase. (Van Den Brink-Van Der Laan et al., 2004)

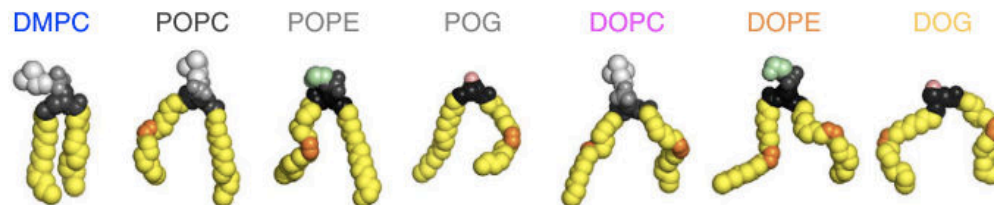


Figure 16 Overall shapes of different lipids

All-atom models of lipids are represented with different conicities. Components are represented in different colors: acyl chain in yellow, acyl chain involved in double bonds in orange; glycerol in black; phosphate in dark grey, choline in light grey; ethanolamine in green and hydroxyl in pink. (Vanni, Hirose, Barelli, Antonny, & Gautier, 2014)

2. Lipid composition in biological membrane

The ensemble lipid composition of cells seems steady. However, the local distribution of lipids is dynamic and heterogeneous between cell types, organelles and also between lipid bilayer (Figure 17)(van Meer & de Kroon, 2011). Bacterial phospholipids are mainly composed of phosphatidylethanolamine (PE), phosphatidylglycerol (PG) and cardiolipin (CL) while eukaryotic phospholipids contain extra phosphatidylserine (PS), phosphatidylcholine (PC) and phosphatidylinositol (PI). These lipids and also proteins diffuse within the membrane with certain restrictions.

In eukaryotic cells, each organelle has its proper lipid distributions such as CL that are enriched in mitochondria. Lipids segregate and form lipid domains within the membrane such as lipid rafts that are cholesterol-sphingolipid-rich regions (Simons & Sampaio, 2011). According to studies with membrane models, the lipid domain sizes vary from nanometer to micrometer ranges (Rosetti, Mangiarotti, & Wilke, 2017). The lipid composition also differs between the lipid bilayer: the inner plasma membranes are enriched of PE, PS and PC whereas the outer plasma membranes are enriched of PC, sphingomyelin or glycerolipids.

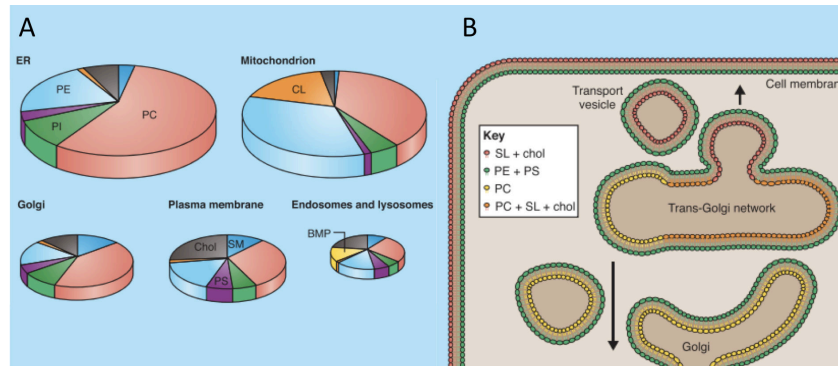


Figure 17 Lipid distributions in eukaryotic cells

(A) Lipid compositions vary according to organelles. (B) The distribution of lipids is heterogeneous within organelles and between each lipid leaflets. (van Meer & de Kroon, 2011)

3. Membrane curvature and tension

Many cellular processes such as e.g. endocytosis, exocytosis involve membrane remodeling (Figure 18). This process has been widely studied, and mechanisms have been proposed highlighting the role of lipid composition and membrane asymmetry, proteins scaffold and amphipathic helices. Although much less studied, transmembrane proteins due to their conical shapes are believed to contribute to the microscopic membrane curvature (Corradi et al., 2018). Cristae in mitochondria, vesicles from sarcoplasmic reticulum, intracellular invaginations of the plasma membrane of photosynthetic bacteria are shaped by high density of ATP synthases, Ca-ATPases and core complexes, respectively at large scale (Jungas, Ranck, Rigaud, Joliot, & Verméglio, 1999; Mühleip et al., 2016; Toyoshima, Sasabe, & Stokes, 1993).

From a physical point of view, membranes are characterized by their curvature and tension. Membrane remodeling processes require energy for membrane bending. The membrane bending is modulated by the presence of transmembrane or membrane bound proteins that change the shape and the stiffness of the membrane. For example, the bending energy of a small vesicle or a nanotube can be reduced by the enrichment of proteins that bend membrane, like e.g. dynamins or Bar proteins (Figure 18).

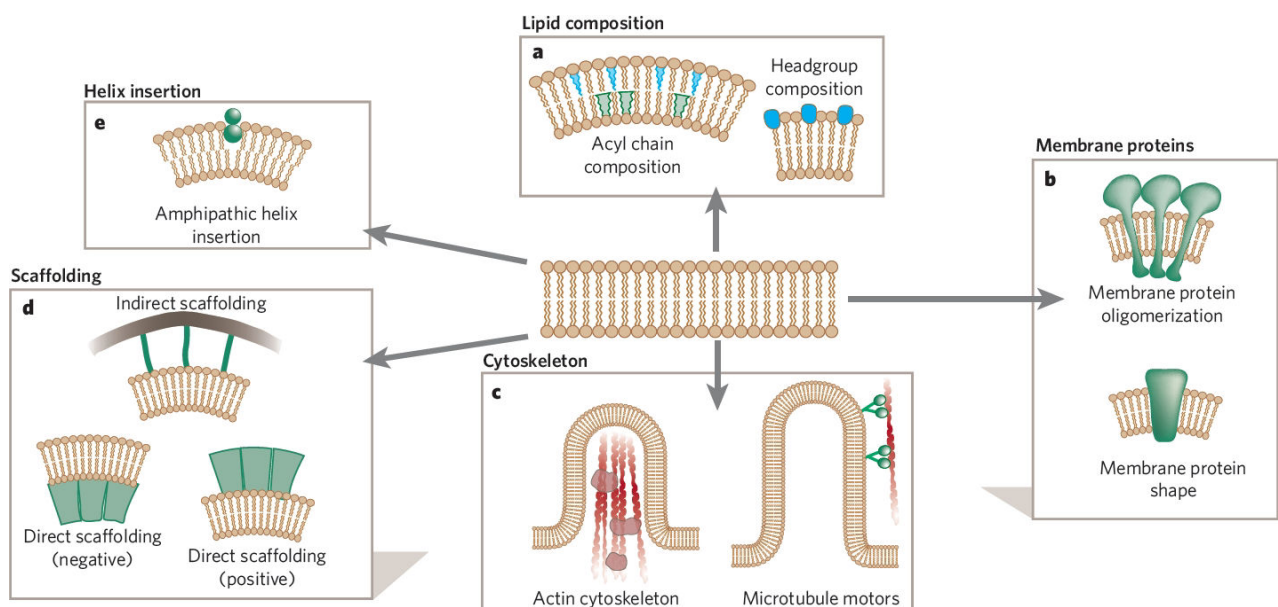


Figure 18 Cell components responsible for membrane remodeling in eukaryotic cell

(A) Lipid composition and bilayer asymmetry, (B) insertion of integral membrane proteins that have intrinsic curvature or protein oligomerizations, (C) cytoskeletal polymerization, (D) direct and indirect scaffolding, (E) and active amphipathic helix insertion into one leaflet can deform phospholipid bilayer causing positive or negative membrane curvature. (McMahon & Gallop, 2005)

Similarly, transmembrane proteins depending on their shape or “conicity” will be enriched in curved regions of membrane to minimize the bending energy (Figure 19). Consequently, if we can experimentally create membrane regions of controlled curvature, proteins will be sorted depending on their shape. This is the principle of the sorting experiments in nanotubes (see Figure 35).

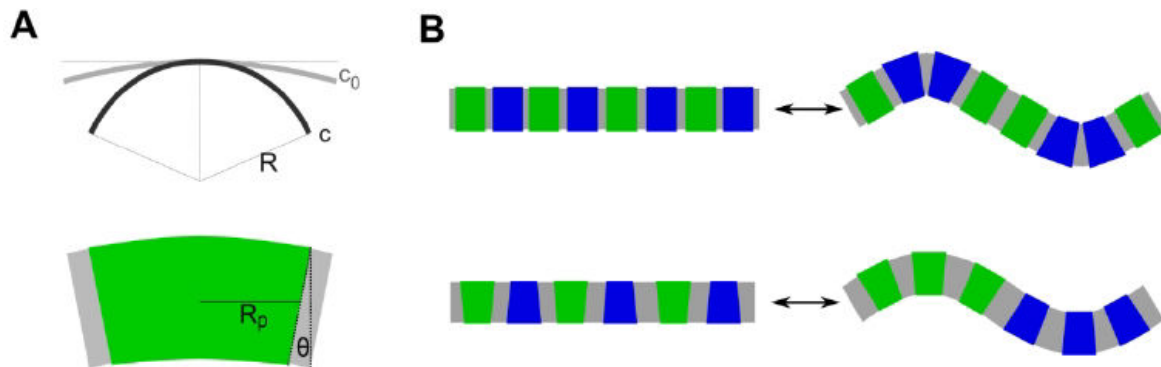


Figure 19 Model of coupling between protein distribution and membrane curvature

(A) Schematics of the coupling between transmembrane proteins and membrane shape. The upper schema depicts a cylindrical membrane deformed from resting spontaneous curvature, c_0 , to a final total curvature, $c = 1/R$. The lower schema illustrates a protein with a conical-shaped transmembrane domain with a protein-lipid interface angle, θ of 10° and protein radius $R_p = 4$ nm corresponding to a proteins curvature c_p of $1/25 \text{ nm}^{-1}$. (B) Effect of protein stiffness (upper) and shape (lower) on sorting according to curvature. In the upper schema, the rigid inclusion (green) is located in the un-curved membrane regions while the soft inclusions (blue) deform and concentrate in the highly curved regions. In the lower schema, inclusion with positive (green) and negative (blue) curvature concentrates in the corresponding regions of membrane curvature. (Sophie Aimon et al., 2014)

The other physical parameter is the microscopic membrane tension that corresponds to the stress associated with a change of membrane area. Increasing membrane microscopic tension leads to a decrease of thickness because the lipid tails are mostly incompressible, and an increase in the distance between lipid headgroups. Using single molecule tracking of proteins in GUVs, it has been shown that the motility of transmembrane proteins in lipid bilayer are modulated by membrane tension (Figure 20)(Quemeneur et al., 2014). Conical shaped proteins such as ion channel KvAP locally deform membranes while cylindrical aquaporins AQP0s do not. At low membrane tension, deformations induced by KvAP were larger and motility decreased while AQP0 was insensitive to membrane tension. At high membrane tension, deformations were reduced and motility of KvAP reached motility of non-conical shaped proteins.

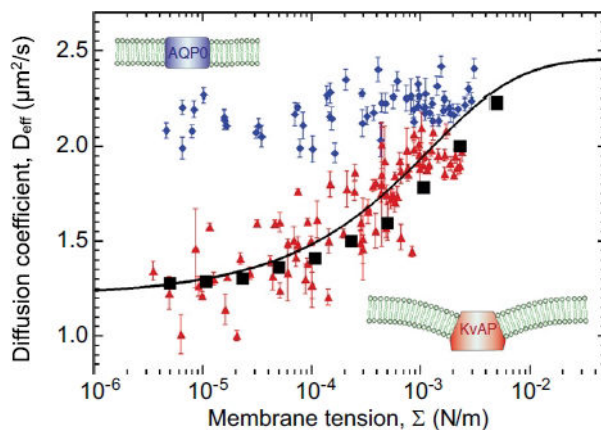


Figure 20 Protein lateral mobility in fluctuating membranes

Diffusion coefficients (D_{eff}) are presented as a function of membrane tension Σ for AQP0 (diamond) and KvAP (triangles). (Quemeneur et al., 2014)

4. Interaction between protein and membrane

Interaction between protein and lipids can be viewed as molecular interactions such as hydrophobic effects, hydrogen bonding or charge interactions, or in physical terms such as lipid fluidity, membrane curvature, thickness and tension. The interplay between the lipid composition and function of transmembrane protein is more and more documented (Phillips, Ursell, Wiggins, & Sens, 2009). In contrast, information on how physical membrane properties affect protein is lacking.

First, lipids that are strongly bound and resolved in crystal structures of transmembrane proteins are defined as structural lipids, and are considered as structural component of protein (Pyle et al., 2018). If these lipids are removed from proteins, e.g. during purification step, proteins tend to aggregate. Second, the first shell of lipid molecules that interacts with the protein are called annular lipids (A. G. Lee, 2003; Palsdottir & Hunte, 2004). Annular lipids are not steady and continuously exchanging with bulk lipids. As consequences, annular lipids remain in the shell for a short period of time. However, membrane proteins have their unique annular lipid composition (Corradi et al., 2018), suggesting a specific sorting of annular lipids related to the presence of protein.

Hydrophobic matching between protein and membrane is also an important factor for protein function (Andersen & Koeppe, 2007; Brown, 2012). The thickness of membrane depends on the length of lipid acyl chains. Depending on the size of hydrophobic core of transmembrane protein, the membrane undergoes a deformation or mutually, the thickness of bilayer can affect the conformation or distortion of protein (Figure 21). Therefore, hydrophobic match also induce depletion or enrichment of lipids surrounding the protein (Corradi et al., 2018). It has been shown that the activity of some transmembrane proteins e.g. Ca^{2+} -ATPase and P-type ATPases depends on the length of acyl chains (Pignataro et al., 2015; Starling, East, & Lee, 1993). Moreover, hydrophobic mismatch can induce protein clustering in order to minimize the hydrophobic mismatch between proteins and the surrounding lipids (Schmidt & Weiss, 2010).

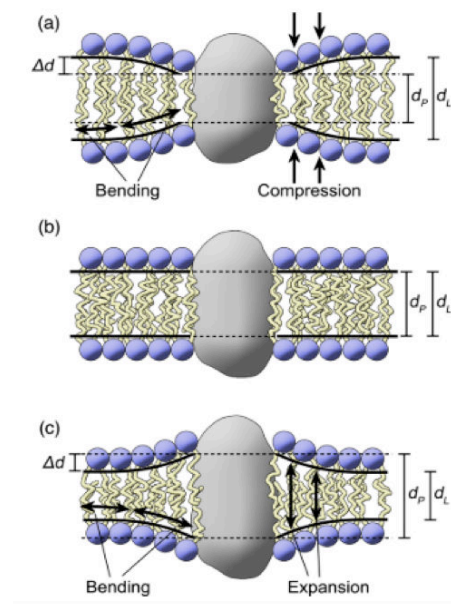


Figure 21 Hydrophobic mismatch

Membrane thickness (d_l) depends on hydrophobic surface of protein (d_p) with negative (a), zero (b) and positive (c) mismatch. Hydrophobic coupling involves local compression (a) or expansion (c) (Δd) of the bilayer at protein-lipid interface. (Brown, 2012)

Finally, lipid charge can indirectly influence the function of protein by local concentration of certain charged ions. The presence of negative charges in lipid headgroup increases the negative charge on the membrane surface and may lead to repulsion and attraction of negatively charged and positively charged ions and molecules, respectively (Y. Wang, Botelho, Martinez, & Brown, 2002).

b. Function of ABC transporters and membrane

The function of ABCs is studied through substrate transport and ATP hydrolysis measurement. Function of ABCs is strongly affected by membrane properties. The complication on clarifying the role of lipids/membrane to ABCs is followed: (i) ABCs translocate lipids and lipid-like molecules that partition into the lipid bilayer; (ii) some detergents are putative substrates; (iii) their physiological substrates are often unknown; (iv) ABCs have strong basal activities. Therefore, it is difficult to relate the stimulation or inhibition effects of lipids to function whether it is directly affected as substrates or specific interaction between lipids and protein or indirectly affected by physical membrane properties.

Background on the function of ABCs

The affinity for ATP is low with K_d values above 1 mM ATP (Figure 22). This low K_d is specific to ABCs compared to P-type ATPases with K_d at μM .

The function of ABCs can be fully inhibited by commercially available inhibitors: orthovanadate (Vi), AMP-PNP and ATP- γ -S that lock NBDs in close contact.

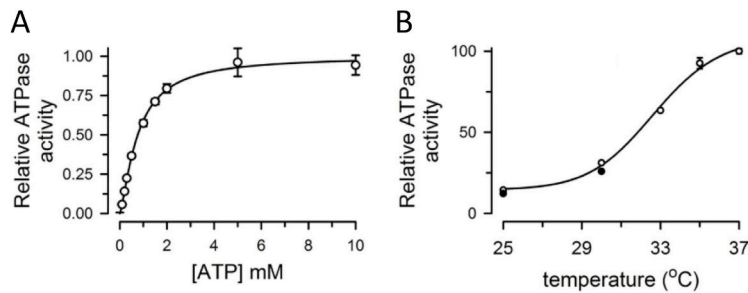


Figure 22 ATPase activity of MsbA according to ATP concentration and temperature.

This figure has been readapted from (Cooper & Altenberg, 2013)

Detergent

Once ABCs are purified in detergent, measurement of ATPase activity is often the first step of the biochemical characterization. Rates of ATPase hydrolysis are extremely variable among ABCs and even for the same ABC; activity varies from nmole to μ mole ATP/mg protein/min. It is not clear if this large range is related to difference in ABCs or to the experimental conditions including proper expression and purification. Moreover, detergents are putative substrates that can stimulate or inhibit ATP hydrolysis. Thus an “absolute” value of ATPase activity in detergent is usually not measurable and studies are often based on comparison of experimental conditions.

For example, purification of LmrA in Fos-choline-16 showed substrate stimulated ATPase activity whereas LmrA purified in n-dodecyl- β -d-maltoside (DDM) was not (Infed, Hanekop, Driessen, Smits, & Schmitt, 2011). Surprisingly, once reconstituted in membrane, an opposite behavior was observed; substrate stimulation was only observed with LmrA purified in DDM. This was also the case for ABCG1, purification with DDM led active protein after reconstitution whereas purification with protein Fos-choline-14 was not (Hirayama, Kimura, Kioka, Matsuo, & Ueda, 2013). PgP and ABCG1 showed low or no activities in detergent whereas activity was restored once reconstituted in membrane (Ambudkar, 1995).

Some detergents are suggested as substrates. Triton-X 100 was reported to be substrate of PgP (Beck et al., 2013; Li-Blatter, Nervi, & Seelig, 2009; Loo & Clarke, 2017) that stimulated or inhibited ATPase activity in detergent concentration dependent manner. Activity was stimulated 60% at 5 μ M of Triton X-100, and then inhibited progressively above 30 μ M, until 40% of activity was inhibited in membrane. Moreover, studies in mass spectroscopy (MS) suggested that PgP purified in DDM possibly fixed one to two detergent molecules in the cavity (Marcoux et al., 2013).

Another reason could be related to structural lipids, important for protein function, that are washed out with some detergents. Indeed, the delipidation of protein led to deactivation of protein function for TmrAB, MsbA and PgP (Bechara et al., 2015; Doige, Yu, & Sharom, 1993; Kaur et al., 2015).

Lipids

The functional effect of lipids was investigated either by ability to restore activity after delipidation of protein, or by reconstituting proteins in membrane models.

Although delipidation of PgP led to complete loss of ATPase activity, the addition of lipids restored ATPase activity (Doige et al., 1993). This suggests that the loss of activity in some cases does not involve protein denaturation. The ATPase activity was restored efficiently in the order of PC > PE > PS > PI. PgP showed a strong preference for short or unsaturated fluid lipids over longer and saturated lipids. In the case of McjD, the basal ATPase activity was also restored with

various lipids, in the order of PE, *E. coli* polar lipids > PG (Mehmood et al., 2016). The presence of substrates stimulated the activity in the order *E. coli* polar lipids > PE, PG. Since *E. coli* polar lipids are mainly composed of PE and PG, a synergistic role of PE and PG in ATPase activity and in protein stability was suggested.

ATPase activities of reconstituted ABCs were investigated in different membrane models such as liposomes and nanodisc (see Membrane models). First, ABC transporters often show a lower ATPase activity in detergents than in proteoliposomes (Dawson & Locher, 2006). For example, the activity of MsbA was 10 times higher in nanodisc than in detergent (Zoghbi et al., 2016). Second, PE has been reported to be required for the transport activity of HorA (Gustot, Smriti, Ruysschaert, Mchaourab, & Govaerts, 2010). Especially, the ATPase activity was higher in PC than in PE but the transport only occurred in PE. TAP1/TAP2 also revealed peptide transport activity dependent to lipid composition in order: *E. coli* = *E. coli*/PC lipids > PE > PC/PI 9/1 w/w > PC/PE 9/1 w/w (Schölz et al., 2011).

All together, *E. coli* and PE lipids seem to provide optimal activity for both eukaryotic and bacterial ABC exporters.

Substrate-membrane repartition

Amphiphilic substrates are partitioned between the aqueous and the lipidic membrane phase. For many substrates, the concentration in membrane is high and can reach several mM even if μ M are present in the aqueous medium. This large concentration of substrates interacts with proteins but also can modify the membrane properties.

The substrate binding to PgP was investigated by fluorescence quenching in membrane. This experiment revealed that substrates had higher partitioning into unsaturated acyl chain bilayers, Egg PC (EPC) than saturated lipids such as DMPC and DPPC (Romsicki & Sharom, 1999). Tryptophan fluorescence quenching of PgP showed that binding affinity of substrates correlated to lipid-water partition coefficient, suggesting that some drugs are recruited to proteins from the inner leaflet.

Drug repartition coefficient increased with increasing temperature and substrates preferentially partition into the liquid crystalline phase of a lipid bilayer compared to the gel phase (Clay & Sharom, 2013). The length of acyl chain also modified drug affinity to Pgp (Sharom, 2014). Higher drug transport rates were observed in the liquid crystalline phase than in the gel phase but it is difficult to distinguish the contribution to the stimulation of substrate transport among lipid phase, temperature and substrate repartition and affinity.

Lipids as substrates

To add another level of complexity, lipids are substrates of ABCs. Therefore, the presence of ABCs can affect their lipid environment (Klappe, Hummel, Hoekstra, & Kok, 2009). The presence of ABCA1 in the plasma membrane results a redistribution of cholesterol, sphingomyelin and caveolin (Landry et al., 2006). The transfection of PgP into kidney epithelial cells stimulated the transport of platelet-activating factor, a natural short-chain PC, across the plasma membrane (Ernest & Bello-reuss, 1999). A possible co-localization of ABCs and lipid raft domain, which is enriched in cholesterol and sphingolipids, is under debate. It was suggested that lipids and lipid rafts act as modulators of localization and function of ABCs (Klappe et al., 2009). But related to complexity in raft isolation procedure, e.g. use of detergent, it is difficult to draw a clear conclusion.

c. Conformation of ABCs and their surrounding environment

Here, differences of conformations found in detergent, in membrane and in the presence of substrates are compared.

LRET and FRET studies on MsbA and PgP showed that the distance between NBDs are smaller in nanodisc than in detergent or in crystal structures in detergent (Aller et al., 2009; Jin et al., 2012; A. B. Ward et al., 2013; Zoghbi et al., 2017, 2016). Besides, DEER studies on MsbA suggest that conformations were similar between detergents and liposomes (Borbat et al., 2007; Zou et al., 2009).

Moreover, LRET and FRET studies with PgP showed a closer distance of NBDs in the presence of substrate verapamil than in apo conformation in membrane (Verhalen et al., 2012; Zoghbi et al., 2017). Given the fact that the activity is stimulated in the presence of verapamil, it was suggested that verapamil stimulates the activity by putting two NBDs closer.

Within the membrane, conformational changes occur depending on lipids composition. Attenuated Total Reflection-Fourier Transform Infrared Spectroscopy data on HorA showed a different conformation between PC and PE (Gustot et al., 2010) at the level of TMD4. As substrate translocation only occurred with PE, it was suggested that lipids are key determinants of conformation and function of ABCs.

d. Annular and structural lipids

Native mass spectrometry studies showed that TmrAB purified in DDM from *E. coli* retained endogenous lipids (Bechara et al., 2015). Further delipidation without protein denaturation revealed annular lipids composed of minimum 5 PG lipids and PE lipids. The majority of annular lipids had acyl chain lengths between C16 to C18 and several unsaturations.

Molecular dynamic simulations of McjD in the mixture of PE, PG and CL showed an enrichment of negatively charged PG and CL on the protein surface with higher quantity of PG than CL (Figure 23A)(Mehmood et al., 2016). Moreover, the lipid enrichment was asymmetrical between the leaflets due to asymmetrical distribution of charged amino acids of the protein (Figure 23B). MD simulation of PgP showed an enrichment of polyunsaturated lipids and depletion of fully saturated and cholesterol in lower leaflet surrounding the protein (Figure 23C).

Overall, this suggests that ABCs show a preference to negatively charged, especially PG and poly-unsaturated lipids in their surrounding environment.

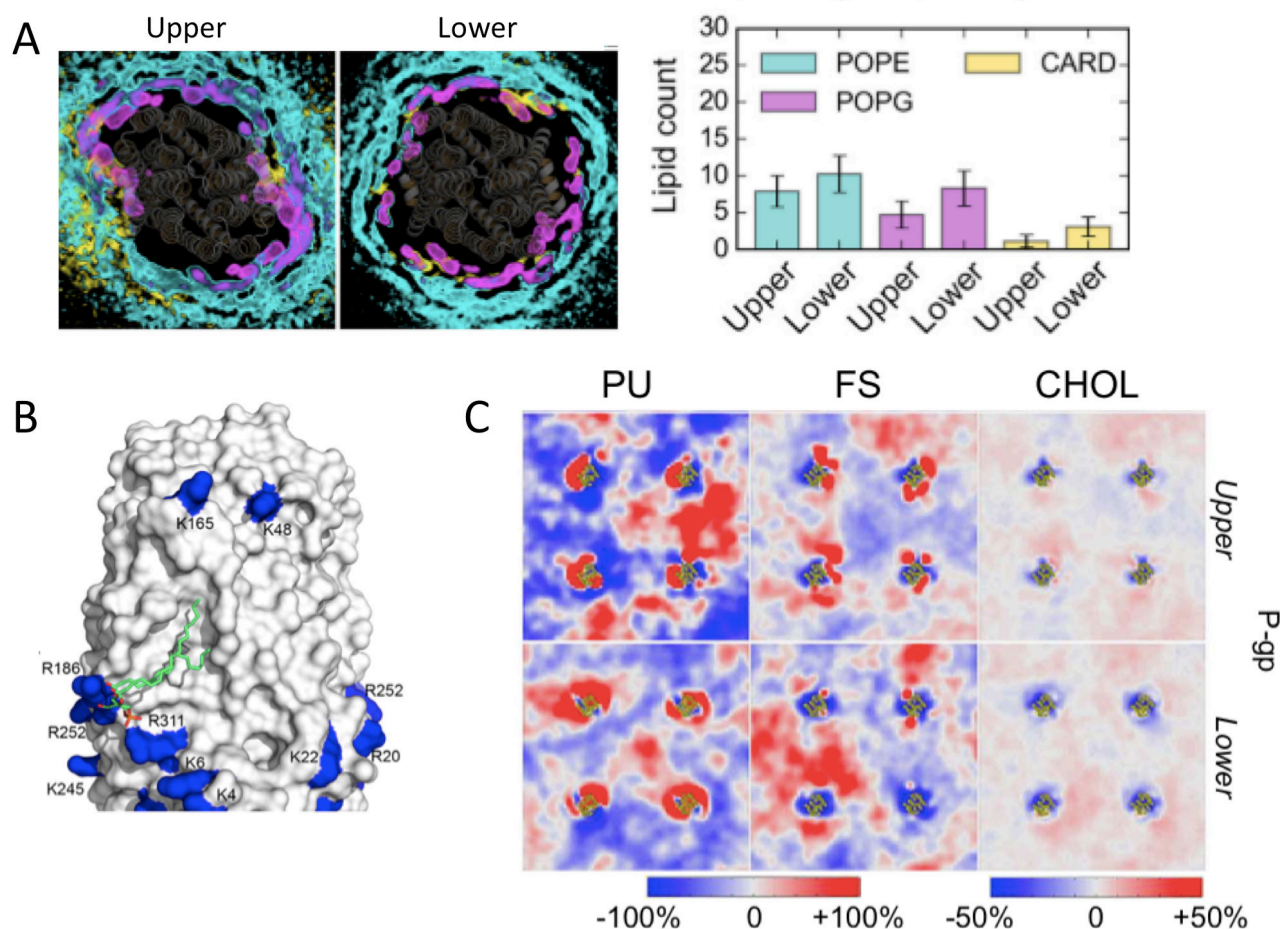


Figure 23 Lipid densities surrounding McjD and PgP by MD.

Lipid densities surrounding McjD (A) was investigated by molecular dynamics simulation in upper and lower membrane leaflet. (B) McjD has an asymmetric distribution of positively charged residues (blue) at the upper and lower leaflets. (C) 4 molecules of PgP in fixed position were shown for upper and lower leaflet. PU, FS and CHOL stands for poly-unsaturated, fully saturated, and cholesterol classes, respectively. (Corradi et al., 2018; Mehmood et al., 2016)

e. Membrane curvature and thickness

Molecular dynamic simulation revealed different membrane curvature and thickness surrounding PgP (Corradi et al., 2018). Mean membrane curvature K_M is an indication of the extent of membrane bending. Overall, PgP had thin and convex membrane surrounding the protein. In outer leaflet, the membrane was thicker surrounding the protein that is consistent with convex surface. In contrast, lower membrane was thinner surrounding the protein.

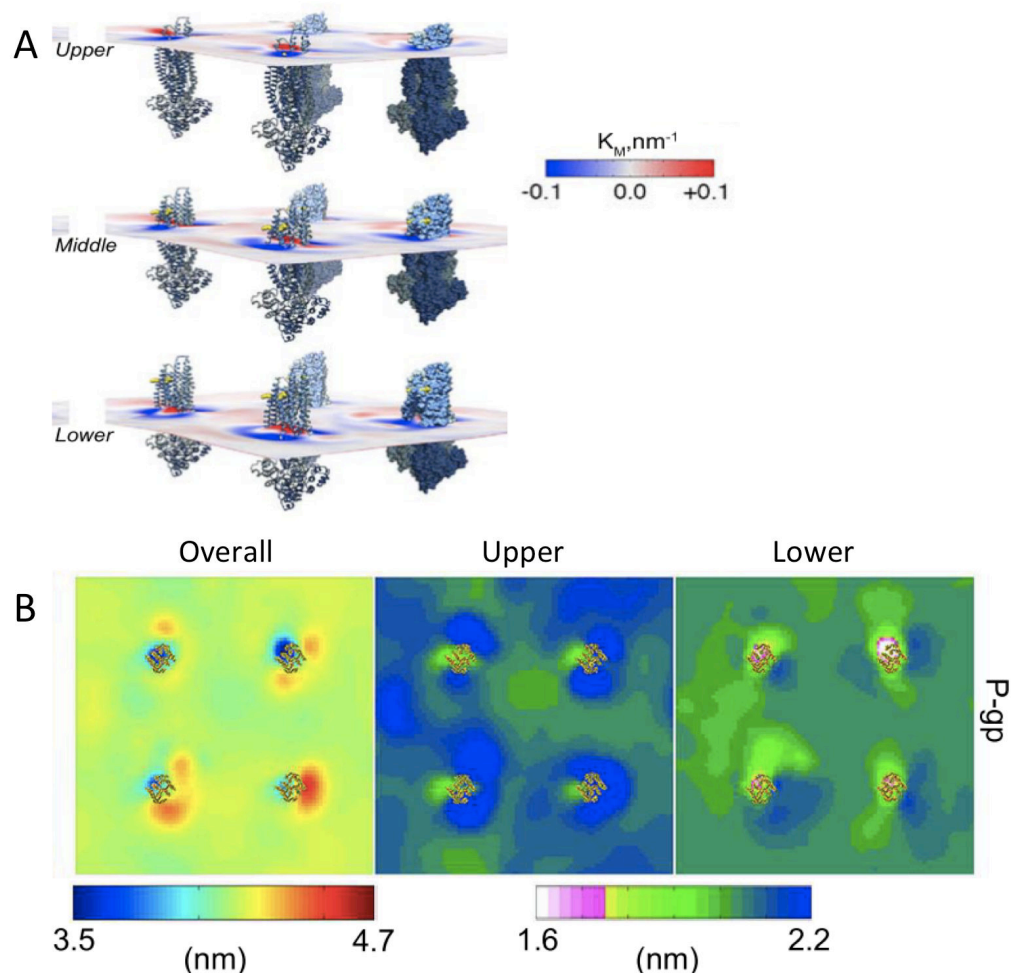


Figure 24 Membrane curvature and thickness surrounding PgP by MD

Mean membrane curvature (K_M) (A) and thickness (B) were investigated by MD surrounding 4 PgP in fixed position. (Corradi et al., 2018)

f. Oligomerization of ABC transporters

Oligomerization higher than the putative monomeric state was proposed for some ABC transporters, including ABCA1, ABCA3, ABCD1, ABCD2 and ABCG2.

ABCD1 and ABCD2 were suggested to form tetramers during catalytic cycle in the peroxisomal membrane even though the functional role of this tetramerization remains unknown (Geillon et al., 2017). In contrary, *in vivo* studies on ABCA1 and ABCA3 showed that these proteins form both monomeric and oligomeric states that coexist during the catalytic cycle. Especially, single molecule studies on full-transporter ABCA1 responsible for generation of high-density lipoprotein (HDL) showed that ABCA1 oligomerized in dimer in apo conformation, then dissociated to monomer after substrate translocation (Figure 25)(Nagata, Nakada, Kasai, Kusumi, & Ueda, 2013). In regard of ABCG2, phosphorylation affected the oligomerization and plasma membrane localization (Xie et al., 2008).

However, how oligomerization of ABCs affects their functions is still under debate and it is possible that monomeric and oligomeric states coexist. Oligomerization state may influence the substrate binding affinity and regulate its function.

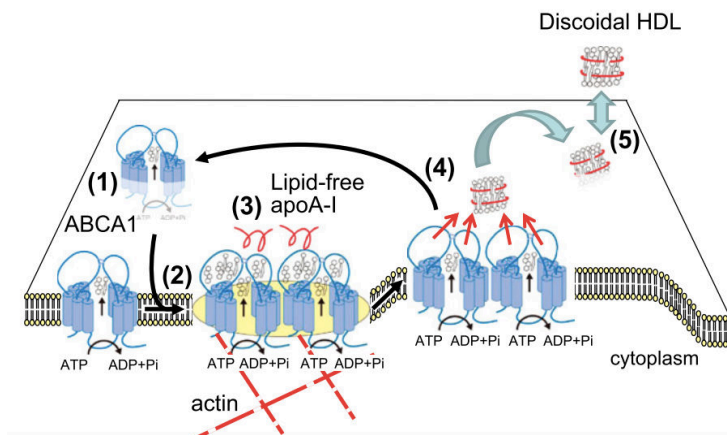


Figure 25 Oligomerization mechanism proposed for ABCA1

(1) ABCA1 freely diffuses in membrane (2) until it forms dimers and immobilized by tethering to actin cytoskeletons. (3) Lipid-free apoA-I binds to the ABCA1 dimer. (4) Lipids are translocated and ABCA1 dimer dissociates into monomers. (Nagata et al., 2013)

In conclusion, functional properties of ABCs have been extensively studied, but there are many variations among them. Even with the same protein, the activity is not the same from one article to another (Kawai, Caaveiro, Abe, Katagiri, & Tsumoto, 2011; Zoghbi et al., 2016). This is due to the complex relationship between ABC and lipids but also linked to the system where the functional assays are carried out, i.e. the presence of detergent, different lipids, substrates and different reconstitution systems. In addition, there is a clear lack of studies on the physical properties of membranes on ABCs.

III. Dynamics of ABC exporters

A complete understanding of the functional mechanism requires a detailed description of the dynamics. Several dynamics studies have been performed for ABCs in different states (in detergent, in detergent/lipid micelles and in membrane) with different techniques: electron paramagnetic resonance, nuclear magnetic resonance (NMR), fluorescence and luminescence studies. The results are not always in agreement that may be related to different membrane systems, transporters and other conditions as variable substrates.

Altenberg and coworkers studied dynamics of NBDs by LRET technique. MsbA in liposomes had completely separated NBDs following ATP hydrolysis, therefore supporting alternating access model (Cooper & Altenberg, 2013). Few years later, the same group revealed that MsbA reconstituted in nanodisc has partially separated NBDs with 2 main populations, supporting constant-contact model (Zoghbi et al., 2016) (Figure 26 A, B). In addition, NBD were more opened in detergent (≈ 50 Å), than in nanodisc (≈ 36 Å), suggesting that the lipid bilayer modulates the conformations of MsbA.

They have also performed LRET studies on PgP in nanodisc at equivalent residues to MsbA at the NBDs (Figure 26 C, D). They suggest that NBDs also remain close to each other (Zoghbi et al., 2017). Especially, the presence of substrates led to closer NBDs of PgP with equilibrium dynamics shifted to ≈ 33 Å. As the activity of PgP is higher in the presence of substrates, they suggest that the distance between NBDs determines the activity.

Wilkins and coworkers performed FRET studies on PgP in liposomes (Verhalen et al., 2012) (Figure 27). They fluorescently labeled NBDs and recorded fluctuation of fluorescence in real time. NBDs remained in close contact during substrate translocation than in apo-conformation

with 4 main conformations. The total catalytic cycle time is suggested to be several tens of msec at 37 °C.

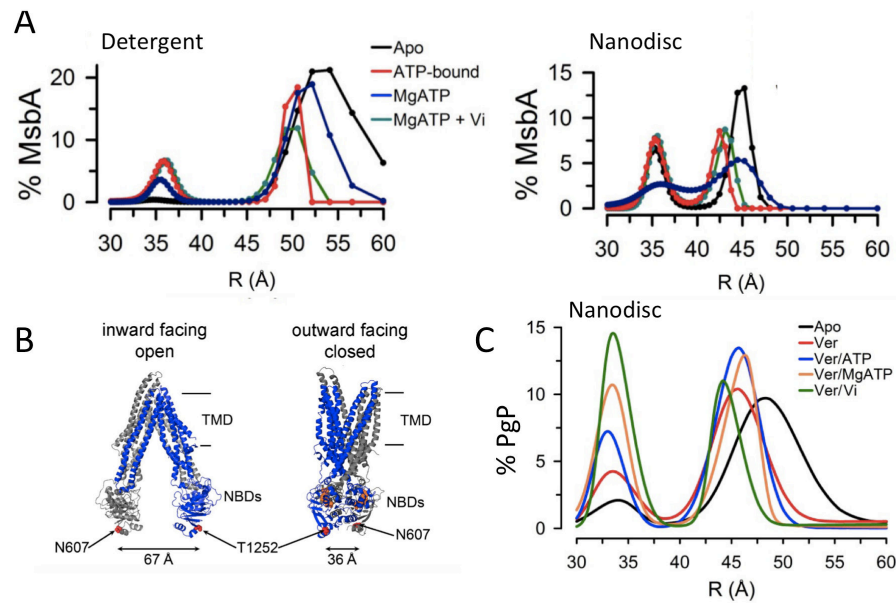


Figure 26 LRET results on MsbA and PgP

(A) The distance between NBDs of MsbA was investigated in detergent and in nanodisc in different conformational states. (B) Structure in apo conformation (PDB: 4Q9H) and model in post-hydrolysis conformation of PgP were used for prediction of distance for PgP N609/T1252. MsbA was also labeled at equivalent residue. (C) The distance between NBDs of PgP was investigated in nanodisc. Figures were readapted from (Zoghbi et al., 2017, 2016).

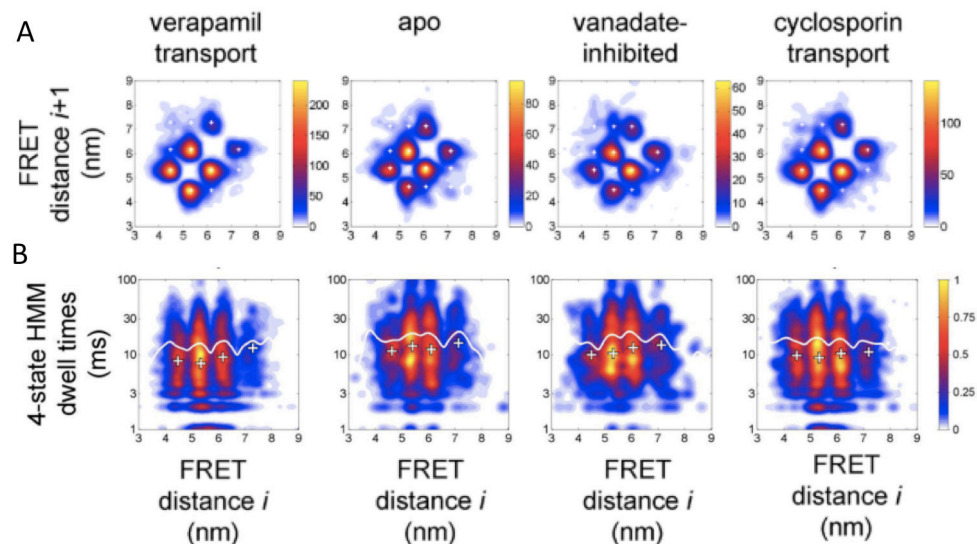


Figure 27 smFRET results of PgP

(A) FRET transition density plots sequential FRET states S_i and S_{i+1} suggests 4 predominant conformations. (C) Dwell time distributions (white curve) for each assigned steps are all superior to 10 ms, suggesting that a total catalytic cycle is several tens of msec. (Zarrabi, Ernst, Verhalen, Wilkens, & Borsch, 2014)

DEER studies on PgP in lipid/detergent micelles revealed the distance distributions that are representative of inward-facing and outward-facing conformations, supporting alternating access model (Figure 28). Contrary to LRET and FRET experiments, the extensive conformational movements were only observed in the presence of inhibitor. In addition, they have found an

asymmetric ATP hydrolysis despite their intact ATP hydrolysis motifs. They suggest that the hydrolysis of one ATP leads to occluded conformation, and then the hydrolysis of two ATPs lead to outward-open conformations.

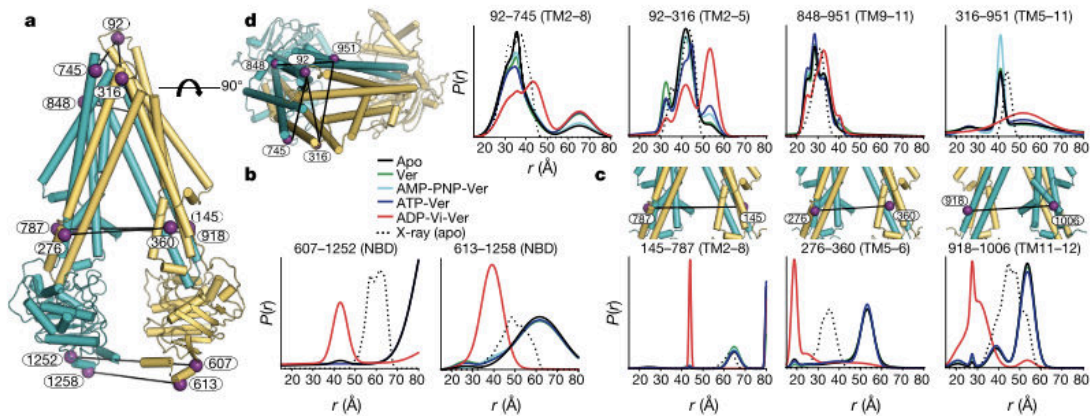


Figure 28 DEER experiment on PgP

(a, c, d) Structure of apo-PgP crystal structure (PDB: 4M1M) with position of spin label pairs. Distance distribution was studied in different conditions (b) for each spin pairs. (Verhalen et al., 2017)

It is possible that ABCs have their own characteristics or different mechanisms depending on their surrounding environments or substrates. Overall, there is clearly complex interplay between protein function, conformations, dynamics and membrane properties.

IV. Reconstitution of ABC transporters in membrane models

a. Membrane models

Native membranes are made of various lipids, transmembrane proteins and membrane bound proteins. To overcome this complexity, simplified *in vitro* membrane models have been developed giving access to specific membrane parameters (Figure 29)(Parmar, Lousa, Muench, Goldman, & Postis, 2016; Shen, Lithgow, & Martin, 2013; Skrzypek, Iqbal, & Callaghan, 2018). These simplified systems allow first of all determining unambiguously the putative function of the protein in a system less complex than the cell. Second, the function can be studied by modulating and controlling the accessible parameters e.g. the lipid composition, the protein density in the membrane, the presence of soluble or membrane cofactors and the composition of the internal and external environment.

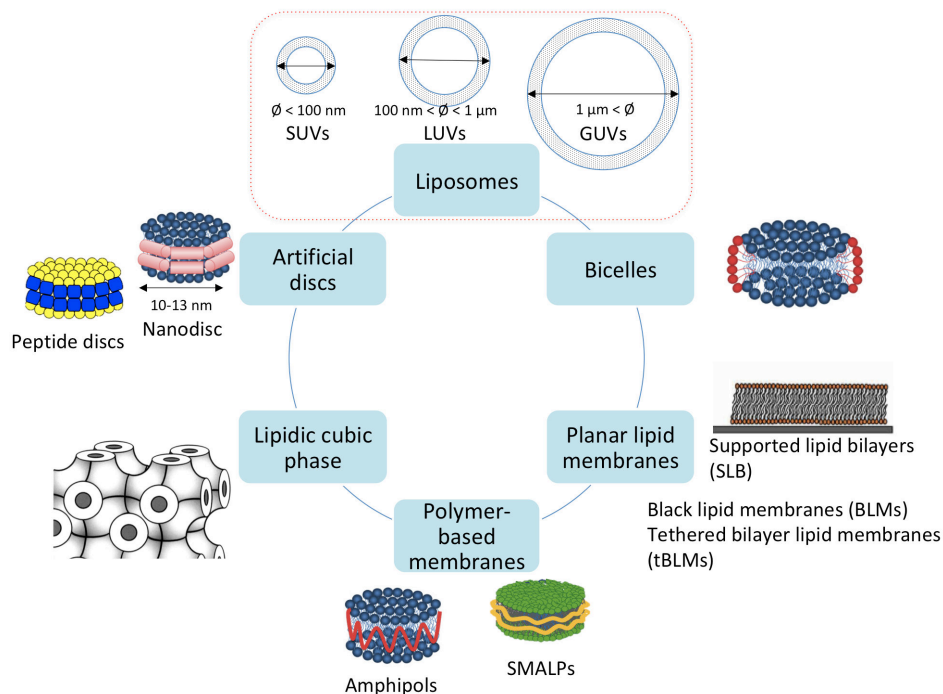


Figure 29 Membrane models

Figure is readapted from (Deleu, Brasseur, & Dufre, 2008; Dörr et al., 2014; Jamshad et al., 2011; Landau & Rosenbusch, 1996; Ujwal & Bowie, 2011). Red box indicates membrane system used during the thesis.

The first membrane state that is extensively used is micelles of detergent. The latter provides an amphiphilic environment suitable to maintain the integrity of membrane proteins. This allows studying both function and structure of membrane proteins, as is the case with all purified ABCs. Functional characterizations include measurements of ATP hydrolysis, substrates binding, inhibition, and oligomerization states. Structural analysis include structure determination by X-ray crystallography, cryo-EM, DEER, LRET etc. The function of ABC in detergent is extremely variable, e.g. ATPase hydrolysis are in the range of nmole to μ mole ATP/mg/min (e.g. Ntpdr5/ABCG5 (Toussaint et al., 2017); Npdr1 (Pierman et al., 2017), BmrA (Ravaud et al., 2006)). However, it is not clear if this variability is related to proteins or if detergents are stimulating or inhibiting as amphiphilic substrates for ABCs.

ABCs have been also studied in a membrane bilayer, in liposomes or nanodiscs, or in different membrane mimicking environments, amphipols, SMALs, amphiphilic peptides...

ABCs have been reconstituted in proteoliposomes that are closed vesicles with define external and internal media. According to the size of proteoliposomes, liposomes are called small, large and giant unilamellar vesicles, SUVs, LUVs and GUVs, respectively. SUVs are smaller than 100 nm of diameter, LUVs are between 100 nm and 1 μ m, and GUVs are larger than 1 μ m. Proteoliposomes have been used to study the function of ABC transporters, ATP hydrolysis, interaction with substrates and inhibitors, lipid protein or protein-protein interaction. In some cases when substrates are soluble, translocations have been also studied (described in more details below).

Polymer-based membrane and artificial discs are emerging *in vitro* membrane system (Jamshad et al., 2011). They can be considered as intermediate states between the solubilized state in detergent and the reconstituted state in vesicle. With these models, membrane proteins associated with polymers form soluble particles in the absence of detergent. This facilitates several biophysical approaches for which the size of liposomes is a limitation like smFRET, LRET, DEER, cryo-EM. Nanodiscs are made of membrane scaffold protein that are genetically engineered from apolipoprotein A-I (Sayaka Inagakia, Rodolfo Ghirlandob, 2014). The main

interest of nanodisc is that nanodisc encloses a small patch of lipid bilayer and it thus allows studying proteins in a lipid bilayer. Nanodiscs are homogeneous objects of small and defined size from 10 to 20 nm depending on the membrane scaffold protein constructs. Proteins are accessible from both sides of nanodiscs that is an advantage compared to proteoliposomes since all proteins are accessible to effectors. However, transport of substrates or formation of an ionic gradient cannot be followed. Nanodiscs have been successfully used for functional studies of bacterial and eukaryotic ABCs (Eggensperger, Fiset, Parcej, Schäfer, & Tampé, 2014; Ritchie, Kwon, & Atkins, 2011; Zoghbi et al., 2017, 2016) and structural studies, especially by cryo-EM (Mi et al., 2017; Taylor et al., 2017). ABCs have high ATPase activities in nanodiscs. Except in the report of Altenberg 2017 where two steps of purification have been used to get homogeneous population of nanodiscs, in other functional studies, nanodisc preparations usually show a very broad peak in FPLC and likely also contain membrane fragments, proteins aggregate and free proteins vesicles.

Amphipols are short polymers that form an amphiphilic belt around proteins and stabilize membrane proteins in the absence of detergent. They have been extensively used for functional and structural studies of membrane proteins (Popot, 2010). A limitation is that proteins are not in a lipid bilayer environment. Recently, MsbA was reconstituted in amphipols for functional studies (Ho et al., 2018). Styrene maleic acid are recent lipid particle system (SMALPs) (Morrison et al., 2016) that have membrane solubilizing properties but do not form micelles. It is claimed that proteins are extracted from native cells with their endogenous lipids. Several ABCs have been studied in SMALPs, including BmrA and showed higher ATPase activities and stabilities than in detergent (Gulati et al., 2014). A main drawback is the precipitation of SMALP in the presence of Mg²⁺ preventing ATPase hydrolysis measurements.

As described in the results, we have studied BmrA solubilized in micelles of detergent, micelles of lipid/detergent and proteoliposomes. This allowed us to access to physico-chemical parameters of the membrane: lipid composition, membrane curvature and protein density. We did not differentiate between SUVs and LUVs for a matter of practicality. All liposomes smaller than 500 nm in diameter were referred as SUVs.

b. Reconstitution into SUVs

1. Reconstitution methods

Several reconstitution methods have been developed since the 1980s (see reviews Geertsma, Nik Mahmood, Schuurman-Wolters, & Poolman, 2008; J. L. Rigaud, Pitard, & Levy, 1995). The most commonly used method consists of adding solubilized lipids to purified proteins in detergents, then removing detergents to form lipid bilayers in which the proteins are incorporated (Figure 30). During this process, slow detergent removal leads to large vesicles because micelle fusion, lipid exchange and post-vesiculation are not spontaneous procedures.

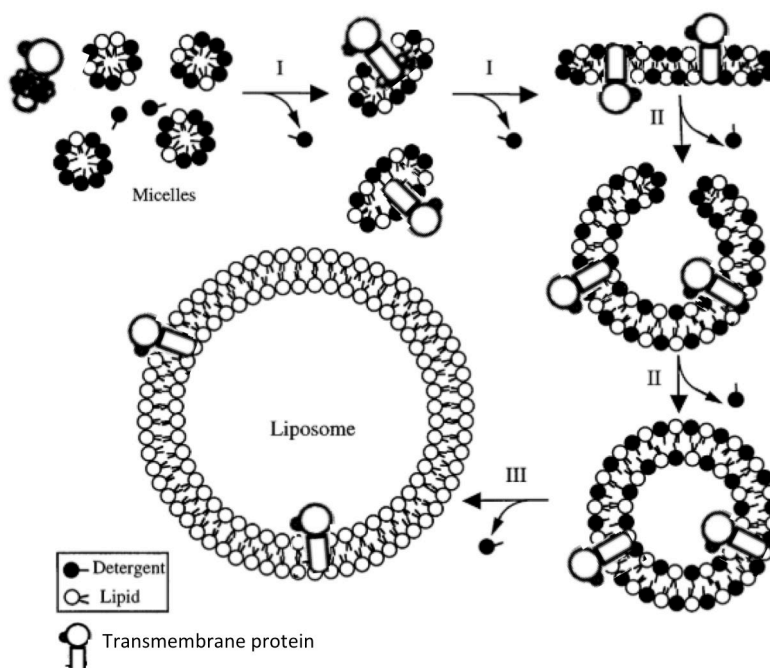


Figure 30 Schematic representation of detergent mediated proteoliposome formation.

Detergent removal from mixture of totally solubilized lipids and protein in detergent leads to reconstitution of protein in liposome. The orientation of protein is not controlled. There are three steps of formation of proteoliposomes as detergents are eliminated: (i) micellar equilibration consists of fusion and lipid exchange between micelles of lipid/detergent, resulting on formation of bilayers to minimize exposure of hydrophobic regions of lipids and proteins to the aqueous solutions; (ii) vesiculation consists of bilayer closure; (iii) post-vesiculation is complete detergent elimination (J.-L. Rigaud & Levy, 2003; J. L. Rigaud et al., 1995)

2. Detergent removal

Several detergent removal methods have been reported based on the physico-chemical properties of detergents and each of them with advantages and disadvantages (Figure 31). Not all have been used with ABCs.

The simplest is dialysis, which removes detergent using the gradient of detergent monomers between the inside of the dialysis bag containing lipid/protein/detergent mixture and the external medium. The interest is the simplicity of application, that it works well with detergents with high critical micelle concentration (cmc) (high gradient) like octylglucoside (OG) (cmc 17 mM), the disadvantage is the excessive duration of several weeks for detergent with low cmc like DDM (cmc 0.2 mM). Reconstitution can also be done by diluting the mixture at concentration below the cmc of detergent. It is simple, fast, but often leads to heterogeneous systems with residual detergent in the membranes and is intended for detergents with high cmc to avoid too strong dilution. Since ABCs are poorly stable in high cmc detergents, these methods have not been often used.

Method	Method Description	Notes
Dilution	Detergent free dilution buffer is added to lower the detergent concentration. PLs form when [detergent]<CMC	<i>Advantages:</i> <ul style="list-style-type: none"> detergent removal rate may be controlled may monitor the PL formation <i>Disadvantages:</i> <ul style="list-style-type: none"> cannot remove all detergent heterogeneous and dilute samples
Gel filtration	Separates monomer and mixed micelles from PLs based on the difference in size. Elution in a detergent free buffer	<i>Advantages:</i> <ul style="list-style-type: none"> fast, simple, efficient and reproducible <i>Disadvantages:</i> <ul style="list-style-type: none"> dilute sample may lose lipids in the resin
Dialysis	The lipid/detergent/protein mix is dialysed against detergent-free buffer in a dialysis bag	<i>Advantages:</i> <ul style="list-style-type: none"> gentle process suitable for labile or unstable molecules in liposomes inexpensive and simple <i>Disadvantages:</i> <ul style="list-style-type: none"> no control over detergent removal rate poor reproducibility and long time scale
Adsorption to polystyrene beads	A physical adsorption method. The hydrophobic detergent tails bind to the hydrophobic surface of the beads. Polystyrene beads are removed by filtration, centrifugation or gravity	<i>Advantages:</i> <ul style="list-style-type: none"> fast (minutes-hours) control of detergent removal rate <i>Disadvantages:</i> <ul style="list-style-type: none"> minor loss of lipids

Figure 31 Detergent elimination methods

(Skrzypek et al., 2018)

The other methods use hydrophobic adsorption on Amberlite resins in column or by cyclodextrin molecules in solution; the latter case has not been yet used with ABCs. In the first case, the elimination is carried out by passing the mixture through a column filled with beads, only the detergent monomers enter the pores of the beads and the micelle/monomer equilibrium is displaced along the column, leading to the formation of proteoliposomes. Elimination is fast and leads to vesicles that are heterogeneous in size and shape. This has been used e.g. for the reconstitution of Pgp for further analysis by smFRET (Verhalen et al., 2012) or LRET (Cooper & Altenberg, 2013).

Finally, the most widely used method for membrane protein in general as for ABCs is the use of polystyrene beads, known as BioBeads, which was characterized in detail in the 1990s and which leads to the most efficient reconstituted systems (J.-L. Rigaud & Levy, 2003; J. L. Rigaud et al., 1995). BioBeads are porous beads that adsorb detergents by hydrophobic interaction. All detergents, whatever their cmc, can in principle be adsorbed: about thirty detergents have been successfully tested in the laboratory. This property is crucial because the choice of detergent is very often determined upstream of the reconstitution by the stability of the protein. Thus, BioBeads are capable of eliminating detergents at high cmc (Hecameg cmc 20 mM up to very low cmc lauryl Maltose Neopentyl Glycol cmc 10 μ M)(Figure 32)(J.-L. Rigaud, Lévy, G, & Lambert, 1998). Measurements made with radioactive detergents have shown that the residual detergent in the bilayers is less than 1 detergent molecule per 100 lipids. The consequence is a low passive ionic permeability of the membranes, crucial for substrate transport studies.

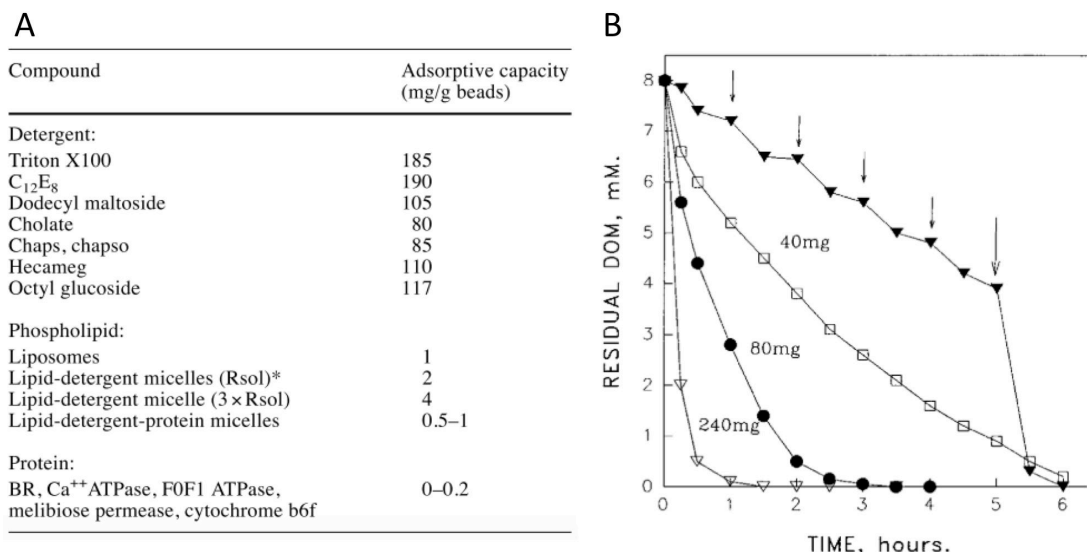


Figure 32 Adsorption characteristics of BioBeads

(A) The adsorption capacity of detergents, phospholipids and proteins by BioBeads was characterized. (B) The dodecyl maltoside (DOM) absorption kinetics of SM2 BioBeads is shown. At time zero, different amounts of BioBeads were added to 1 ml containing 5 mM phospholipids and 8 mM DOM supplemented with a radioactive detergent. The amounts of detergent have been monitored over time. The black arrows indicate five successive additions of 10 mg beads. (Lambert, Lévy, Ranck, Leblanc, & Rigaud, 1998; J.-L. Rigaud et al., 1998)

Due to pore size, protein adsorption is zero and negligible for lipids (less than 1 mg lipid per gram of BioBeads). The adsorption rate depends on the temperature and decreases by a factor of 2 every 12 °C of decrease. Thus proteoliposomes can be formed at 4 °C or 60 °C.

An important characteristic is that the adsorption rate depends only on the BioBeads/detergent ratio (Figure 32 B). Adsorption curves that are available for several detergents, e.g. for Triton X 100 (Lévy, Bluzat, Seigneuret, & Rigaud, 1990) and depend on the amount of BioBeads. These curves can be extrapolated for other experimental conditions (volume, concentration of detergent, lipid), if the BioBeads/detergent ratio is maintained.

Finally, elimination with BioBeads leads to vesicles with sizes ranging from 20 to 500 nm, depending on the type of lipid and the rate of removal. In all reported cases, vesicles are unilamellar, a crucial criterion for the study of reconstituted systems.

Once reconstituted the proteoliposomes are stable for generally 1- 2 days, however the function may be less stable depending on proteins.

As examples, bacterial homodimeric or heterodimeric ABC transporters (e.g. BmrA (Steinfels et al., 2004), BmrCD (Geertsma et al., 2008; Mishra et al., 2014), MsbA (P. D W Eckford & Sharom, 2008), LmrA (Reuter et al., 2003)), yeast ABC (Pdr11P (Laub et al., 2017)), human ABCs (Pgp (Zoghbi et al., 2017), TAP 1/TAP2 (Eggensperger et al., 2014)) have been reconstituted by detergent removal using BioBeads.

3. Characteristics of proteoliposomes for accurate quantitative measurements

In general, we consider that if lipid/protein/detergent are mixed and detergent eliminated, then proteins are reconstituted in membranes but not necessarily in vesicles. This often allows a biochemical characterization to begin.

However, if accurate quantitative measurements are to be made, for example to determine stoichiometry of substrate/protein, ATP hydrolysis rate, etc. the reconstituted systems must satisfy the following criteria:

- **Incorporation:** the rate of proteins incorporated in vesicles and that of unincorporated and aggregated proteins must be known. To measure the incorporation rate, one often uses the separation of products: proteoliposomes, aggregated proteins, and liposomes without proteins according to their density by centrifugation through a gradient (or of layers) of sucrose. Incorporation is usually measured in studies with ABCs at least for one experimental condition but often not for all conditions in the study.
- **Orientation:** it is essential to know if the functional site of protein is accessible to substrates, inhibitors for interpretation of measurements. It is rare that 100% of proteins are oriented in physiological orientation and most often proteins are oriented around 50/50 inside-in/inside-out. The orientation depends on the reconstitution method and the type of protein (see direct incorporation). Orientation is often measured by comparing proteins in liposomes and proteins after solubilization of proteoliposomes, e.g. after proteolytic digestion, specific inhibition, etc. In most studies with ABC transporters, except e.g. in (Gustot et al., 2010), orientation of incorporated ABCs is not measured.
- **Lamellarity of proteoliposomes:** if proteins are incorporated into multilamellar vesicles, some proteins are inaccessible to externally added substrates or nucleotides. In this case, functional measurements are underestimated. Cryo-EM is the most powerful method to visualize vesicles. This parameter has been reported only for the proteoliposomes of BmrCD (Galián et al., 2011).
- **Homogeneous distribution of proteins in vesicles:** proteins are often considered to be distributed throughout the liposome population, which is not always the case (Lévy, Gulik, Bluzat, & Rigaud, 1992). The consequence may be heterogeneous protein/protein interactions in the liposome population. Population heterogeneity is visible by sucrose gradient sedimentation where several bands appear.
- **Low passive membrane permeability:** this criterion is indispensable for the substrate transport studies. This depends on the quality of the lipid mixture (presence of lyso-lipid) and residual detergent, which can increase passive permeability. It is accepted that during ATP hydrolysis assays, if detergent is fully removed, membranes are impermeable for ATP and soluble substrates.

According to the literature, in the vast majority of reconstitution of ABC transporters, proteoliposomes have not been extensively characterized.

4. Reconstitution by direct incorporation into pre-formed liposomes.

The so-called direct incorporation consists in destabilizing preformed liposomes by under-solubilizing concentrations of detergent to create defects in the membrane, to then allow the insertion of membrane proteins (Figure 33). Proteins in detergents are incorporated by their most hydrophobic domain, leaving the extramembrane domain pointing outward. The consequence is a unique orientation of the proteins in the vesicles. The defects are specifically created by sugar-based detergents, like DDM, OG. In the case of ABC transporters, proteins are incorporated with the NBDs pointing outward, i.e. in an inside-out conformation, and accessible to ATP or substrates added in the external medium.



Figure 33 Schematic representation of direct incorporation method

Transmembrane proteins are added to pre-formed SUVs in the presence of sub-solubilizing concentration of detergent. Proteins are inserted by their hydrophobic domain to liposome. (J.-L. Rigaud & Levy, 2003)

Another mechanism of direct incorporation was found by Rigaud and co-workers (reviewed in (J. L. Rigaud et al., 1995)). It consists of the transfer of proteins into a mixture of 60-70% liposomes saturated with Triton X-100 and 30% solubilized lipid/detergent micelles. However, the transfer was not total leading to heterogeneous population of proteoliposomes.

It is worth noting that direct incorporation methods are successful for well-defined lipid/detergent ratio, i.e. 1/1 DDM/lipid or 1.3 OG/lipid mole ratios.

For many ABCs, reconstitutions were performed by direct incorporations. However, detailed analysis of the literature revealed that in most cases, the accurate conditions of incorporations were not correctly considered, resulting to uncertainty on protein orientation (see e.g. (Herget et al., 2009; Zou et al., 2009)).

c. Reconstitution into GUVs

The size of GUVs is similar to that of eukaryotic cells, therefore considered as cell mimicking membrane system. GUVs are usually grown by swelling of lipid/protein film and this approach has been developed since many years to study ion channel by electrophysiology approaches. However, since few years now, physicists have developed new approaches to form GUVs more homogeneous in size and lamellarity and suitable for physical measurements. The size of GUVs allows micromanipulation of liposomes with optical tweezers or micropipettes, and can be observed directly by optical/fluorescence microscopy (S Aimon, 2011). Compared to SUVs, GUVs allow to investigate membrane properties such as phase separation, lipid mobility, membrane bending and lipid microdomains... (Baumgart et al., 2007; Bhatia et al., 2015; Cheniour, Brewer, Bagatolli, Marcillat, & Granjon, 2017; Dietrich et al., 2001; Girard et al., 2004; Kahya, Scherfeld, Bacia, Poolman, & Schwille, 2003). When coupled to appropriate set-up, membrane tension and curvature can also be modified and controlled. Membrane bound proteins associated to biological functions, adhesion, fusions, fissions, cell division and interaction between peptides and many others were investigated (Levental & Levental, 2015; Römer et al., 2010; Terasawa, Nishimura, Suzuki, Matsuura, & Yomo, 2012).

As shown in Figure 34, several methods allow reconstitution of transmembrane proteins into GUVs, reviewed in (Jørgensen, Kemmer, & Pomorski, 2017). Four ABCs have been reconstituted in GUVs: (i) Human PgP was reconstituted by gel swelling method (Kim, Kim, & Lee, 2015); (ii) BmrCD reconstituted by fusion of proteoliposomes (Dezi et al., 2011); (iii) OppA, an ABC importer, was reconstituted by direct incorporation (Doeven et al., 2005); and hamster Pgp was reconstituted by electroformation method (Park & Majd, 2018). It is worth noting that in all cases, the presence of ABCs in GUVs was not directly assessed by fluorescence of proteins but indirectly shown by substrate transport, ATPase activity or membrane permeability. This is important

since, as shown e.g. in results, GUVs are fragile vesicles, can be permeable to ATP or coexist with small proteoliposomes, complicating the interpretation of the measurements.

Approach	Advantages	Disadvantages
Spontaneous swelling (1a)	Simple procedure Physiological buffer composition Physiological lipid composition	Requirement of charged lipids or sugar solution Heterogeneous vesicle population ^a Slow procedure Dehydration necessary
Electroformation (1b)	Rapid procedure Homogeneous vesicle population Narrow lipid composition	Special equipment requirement Possible oxidation of polyunsaturated lipids Charged lipids compromise GUV formation Dehydration necessary
Peptide-induced fusion (2)	Homogeneous vesicle population	Laborious procedure Incorporation of peptide molecules Limited insertion of protein
Direct reconstitution (3)	Rapid procedure	Detergent removal Protein aggregation Careful protocol optimization
Detergent-mediated reconstitution (3)	Rapid procedure Physiological buffer composition	Detergent removal Careful protocol optimization
Spontaneous fusion (4)	Simple procedure Homogeneous vesicle population	Slow process Low efficiency and yield
Droplet transfer method (5)	Asymmetric leaflet lipid distribution Controlled protein orientation Physiological buffer composition	Careful protocol optimization Precludes lipids with poor solubility in oil Oil can be present
Microfluidic jetting (6)	Asymmetric leaflet lipid distribution Controlled protein orientation Physiological buffer composition	Technically challenging Small sample sizes

Figure 34 Reconstitution methods of integral membrane protein in GUVs

(Jørgensen et al., 2017)

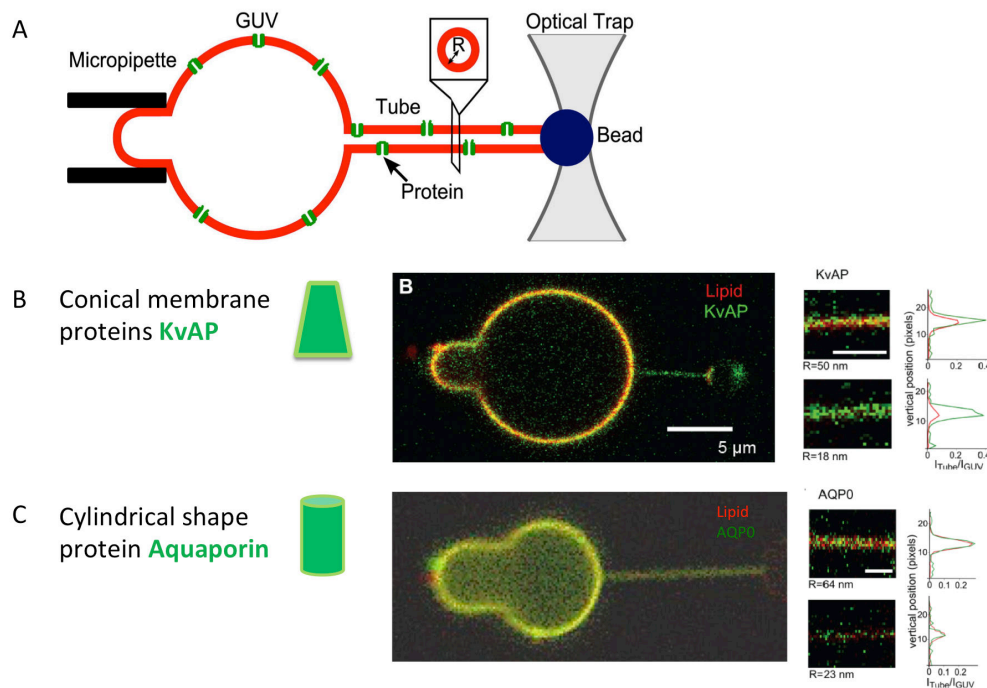


Figure 35 Sorting in curved membrane according to shape of protein

(A) Schema of nanotube pulling experiment from GUVs. Fluorescently labeled protein is reconstituted in GUVs. A curved membrane, nanotube, is pulled with micropipette and optical trap from GUVs. Membrane tension and curvature (radius of nanotube) are controlled by micropipette aspiration. The shape of protein determined protein enrichment factor, sorting, in nanotube; conical KvAP were enriched in curved membrane (B) whereas cylindrical Aquaporins were not (C). The sorting value was calculated based on the fluorescence of protein in nanotube/GUVs normalized by same lipid fluorescence. (S Aimon, 2011)

P. Bassereau and coworker have designed a setup to investigate the spatio-temporal distribution of transmembrane proteins in curved membrane (S Aimon, 2011). The principle of the experiment consists in pulling lipid nanotubes from GUVs where membrane tension can be changed. Thus membrane curvature in nanotube can be changed and controlled with different diameters at different membrane tension (Figure 35 A). In practice, GUV is held by micropipettes, in which the aspiration pressure regulates the membrane tension. GUV, containing biotinylated lipids, is moved to touch optical trapped bead, which is streptavidin-functionalized. Moving the GUV backwards via the micropipette pulls the nanotube. By modulating the tension, the radius of nanotube can be controlled in the range of 7 – 100 nm.

This approach has been successfully utilized to study the distribution of KvAP and AQP0, two transmembrane proteins with same lateral size. Protein enrichment in the nanotube “sorting” was quantified by measuring the fluorescence intensities of proteins in the nanotube compared to GUVs. The fluorescence intensities of protein were normalized by the lipid fluorescence intensities:

$$S = (I_{\text{protein Tube}} / I_{\text{lipid Tube}}) / (I_{\text{protein GUV}} / I_{\text{lipid GUV}})$$

The distribution AQP0 proteins, that have a cylindrical shape, was not influenced by membrane curvature with $S = 1.1 \pm 0.4$ in the range of 15 nm and 35 nm radius of nanotube (Figure 35 C). While KvAP proteins, that have a conical shape, were enriched in curved membrane with average $S = 3.5$ in the range of 15 nm and 35 nm radius of nanotube (Figure 35 B). Even in large nanotube ($r = 50$ nm), KvAP were already enriched with $S = 1.6 \pm 0.1$ and by increasing the membrane curvature to 18 nm radius, KvAP enrichment increased to $S = 4 \pm 0.8$. Combining experimental sorting value with thermodynamic sorting model, spontaneous curvature, C_p , for each protein was measured. For KvAP, $C_p = 0.04 \text{ nm}^{-1}$ was calculated and AQP0 has zero spontaneous. These experiments were performed at different membrane tensions.

So far, this approach was investigated for proteins with fixed conformation. Now, the associated question is how a protein with large conformational changes such as ABCs will be distributed in a curved membrane during the catalytic cycle.

V. BmrA, an homodimeric ABC from *B. subtilis*

BmrA is an ABC exporter (~65 kDa) from *B. subtilis*. It is a half-transporter that functions as a homodimer (Dalmas et al., 2005). This transporter shares 32% and 35% sequence identity for each half of human PgP and an additional 21% and 19% of conservative substitutions, respectively. BmrA also shares 33% of sequence identity with MsbA from *E. coli* with additional 23% of conservative substitutions. As shown in Figure 36, BmrA shares common substrates as PgP and MsbA including antibiotics, anticancer agents, suggesting a common transport mechanism. The structure of BmrA is unknown. J.M. Jault (IBCP, Lyon) provided a model of BmrA based on structure of MsbA (PDB: 3B5W) (Figure 37). BmrA contains 14 positively charged amino acids per monomer, 12 of those are positioned in inner leaflets.

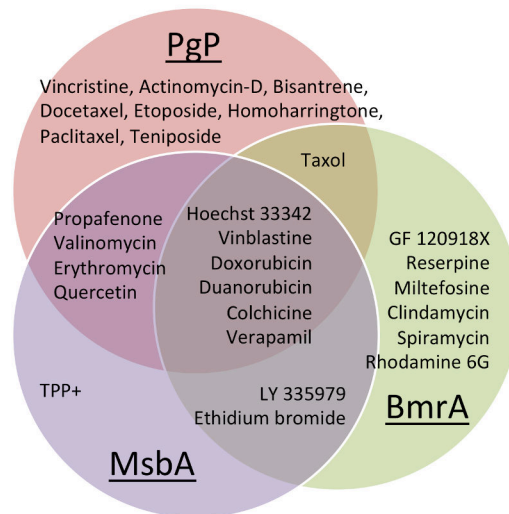


Figure 36 Common drug substrates between PgP, BmrA and MsbA

(Reyes, Ward, Yu, & Chang, 2006; Siarheyeva & Sharom, 2009; Steinfels et al., 2004; Y. H. Wang, Li, Yang, & Yang, 2005)

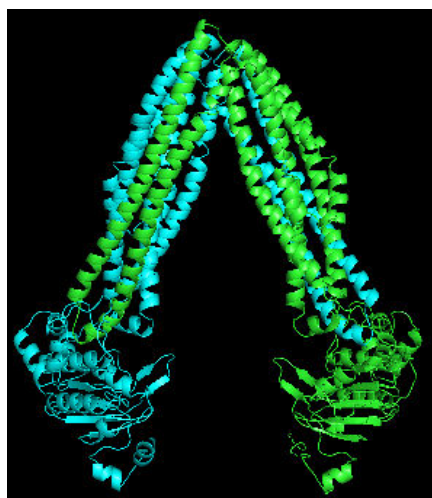


Figure 37 Model of BmrA

This model was constructed based on structure of MsbA (PDB: 3B5W). BmrA is a homodimer and each monomer is represented in green and blue colors.

However, its physiological substrate and its function in *B. subtilis* are unknown (C Orelle et al., 2008; Cédric Orelle, Dalmas, Gros, Di Pietro, & Jault, 2003; Ravaud et al., 2006; Steinfels et al., 2004). BmrA is dispensable for the normal growth of *B. subtilis*, as for many bacterial MDR transporters (Neyfakh, 1997). It was shown that BmrA was overexpressed in cervimycin C (CmC)-resistant clones of *B. subtilis*, conferring a resistance against CmC (Krügel et al., 2010), which is an antibiotic complex produced by *Streptomyces tendae*.

BmrA's ATPase activity is considered one of the highest among ABCs with MsbA. It was reported that ATPase activity increased 10 times after reconstitution in liposome than in detergent (Steinfels et al., 2004). ATPase activity V_{max} was 7 $\mu\text{mol}/\text{min}/\text{mg}$ of protein at 37 °C in *E. coli* extract liposome.

a. Dynamics and structural studies of BmrA

Dynamics and structural studies of BmrA have been investigated by hydrogen/deuterium exchange (HDX) coupled to MS and cryo-EM.

HDX and trypsin digestion of BmrA showed significant conformational changes during catalytic cycle in membrane or in detergent (Mehmood, Domene, Forest, & Jault, 2012). In addition, a high flexibility of two intracellular domains (ICDs) was shown. Local HDX results suggest that in the resting state, BmrA undergoes different conformations.

Structural studies of apo-BmrA in bilayer were investigated by cryo-EM at high protein density (Chami et al., 2002; Fribourg et al., 2014). BmrA assembled in highly curved, ring-like assemblies that are homogenous in shape and in size at detergent/lipid below 1 molar ratio (Figure 38 A, B, D). Rings made of 24 homodimers of apo-BmrA in membrane were observed. Further detergent removal led to the coalescence of rings to form non-crystalline tube-like structures. 3D model revealed a separation between NBDs at high protein density. Other than rings, membrane sheets were observed within the same lipid composition. Further analysis suggested at least 2 different apo conformations with different distances of separation between NBDs (Figure 38 C-E).

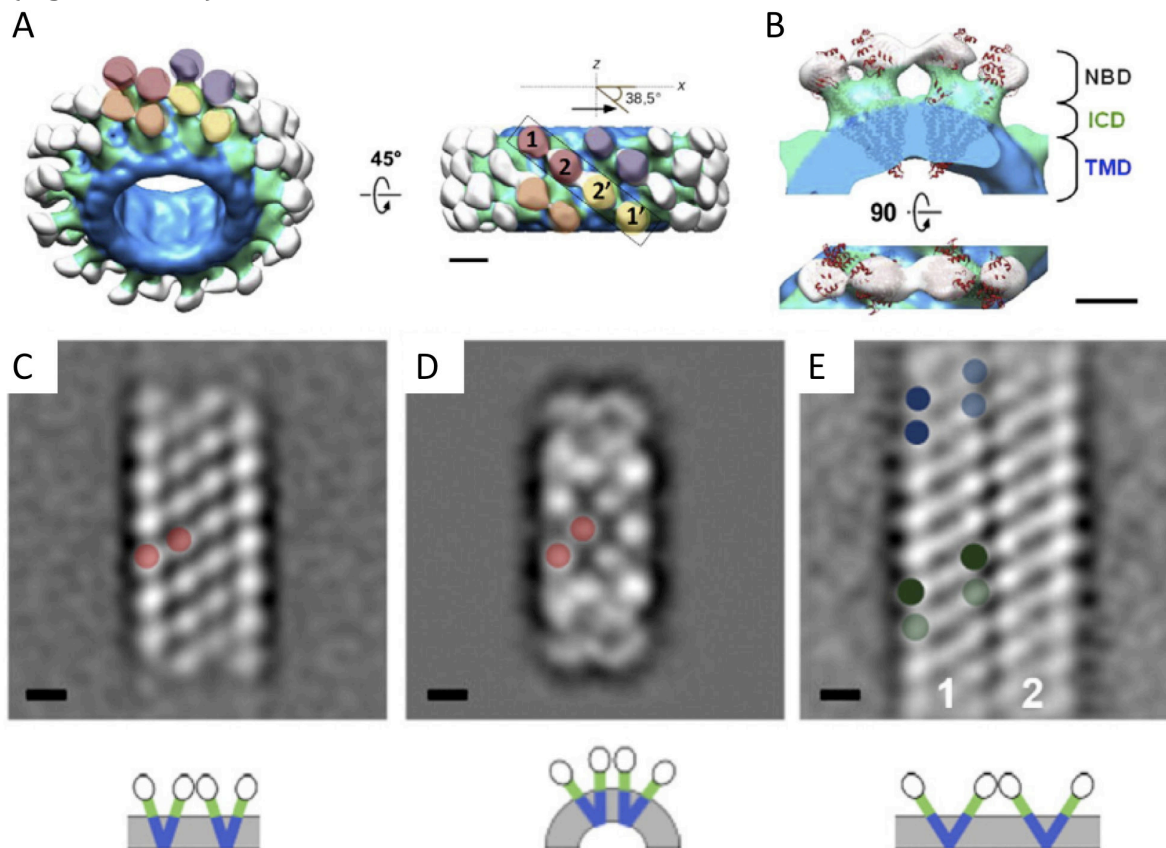


Figure 38 Structural studies of apo-BmrA by cryo-EM

(A) 3D model of rings shows arrangement of BmrA homodimers in different colors. (B) Sub-domains of BmrA, NBDs, ICDs and TMDs are indicated. (C) Average image of thin membrane sheets show similar arrangement of NBDs than rings (red circles indicates NBDs of same homodimer). (D) Representative side view of rings shows the arrangement of the homodimer of BmrA (red circles). (E) Average image of large membrane sheets shows larger separation between NBDs than ring and thin membrane sheets. Scale bar indicates 5 nm. (Fribourg et al., 2014)

b. Interplay between BmrA and membrane at high protein density

This is a summary of the results of my Master 2 derived from the reconstitution of BmrA at high protein density and analyzed by EM. Results provided evidences of interplay between BmrA and the morphology of the surrounding membranes. This coupling is modulated by lipid composition and by protein conformational state.

The reconstitution of BmrA in different lipid compositions led to 3 main membrane morphologies: rings, ribbons and tubes (Figure 39). These 3 morphologies coexisted but the proportion varied according to parameters of reconstitution. Mainly, the proportion was modulated by lipid composition. For example, rings were more homogeneous in the case of reconstitution in the presence of saturated chain lipids DMPC, tubes were homogeneous in the presence of *E. coli* extract lipids in lipid/protein ratio 2 w/w and ribbons were formed in the presence of EPC/EPA lipids. Especially, ribbons were preferentially formed at low lipid/protein ratio in the presence of negatively charged lipids. There is thus lipid specificity on the morphology of membranes reconstituted with apo-BmrA, probably related to conformation of BmrA.

These assemblies are not induced due to hydrophobic mismatch. For example, rings are formed in different lengths of lipid chains and also in a lipid chain mixture (EPC, *E. coli*). Besides, it is possible that protein-protein interaction occurs, which leads to specific assemblies and membrane curvature.

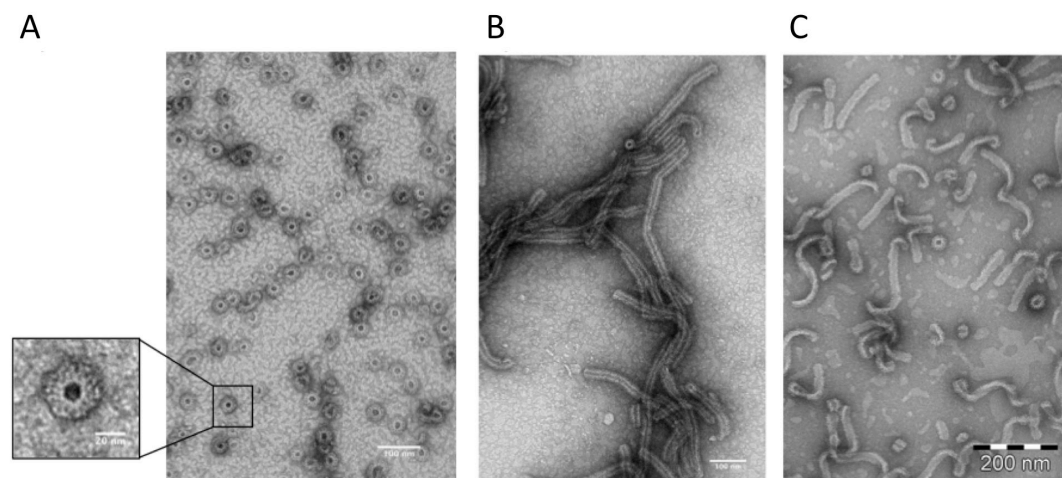


Figure 39 Principal BmrA/membrane assemblies.

Negative staining EM images shows rings (A), tubes (B) and (C) ribbons BmrA/membrane assemblies that were reconstituted in DMPC, *E. coli* lipids and EPC/EPA 9/1 w/w, respectively.

The addition of ATP and Vi to apo BmrA rings assemblies resulted in the flattening of the membrane (Figure 40). This a first evidence for the coupling between the catalytic state of an ABC transporter and it surrounding membrane.

Moreover, Vi-trapped BmrA are reconstituted in vesicles that are less curved than in rings, ribbons and tubes (Figure 41). Within the vesicles, protein domain formation was observed (Figure 41B, D).

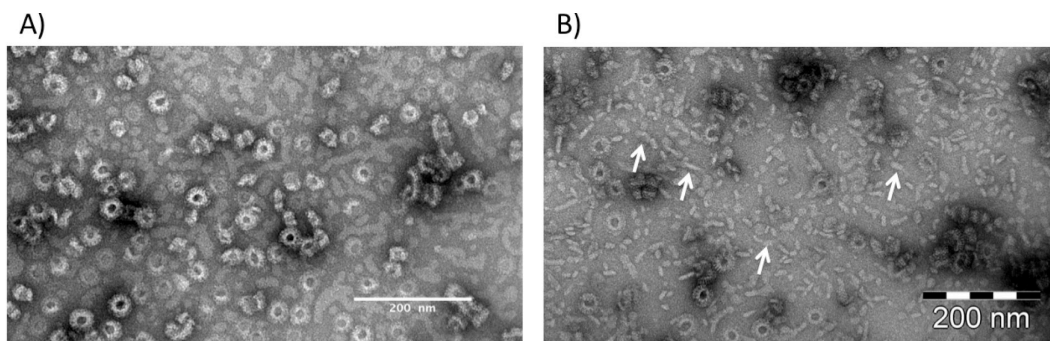


Figure 40 Membrane morphology modification.

(A) The addition of ATP and vanadate to apo-BmrA in rings induces the appearance of flat membrane fragments (B, white arrows).

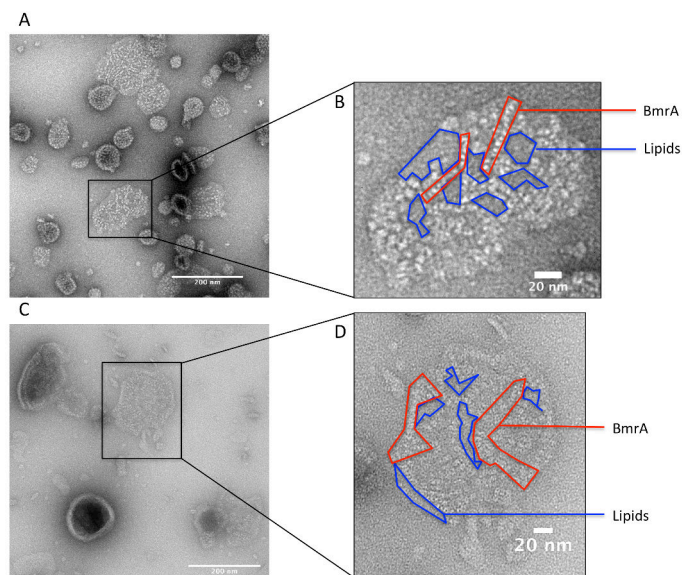


Figure 41 Protein domain formation in post-hydrolysis conformation.

Vi-trapped BmrA was reconstituted in EPC/EPA (A, B) and DMPC (C, D), respectively. (B, D) Formations of protein and lipid domains are shown in red and in blue, respectively.

Substrates bind to the transmembrane cavity and may modulate conformations of BmrA. Two BmrA substrates, doxorubicin and H33342 with different dissociation constants (22.1 μM and 9.5 μM , respectively) were selected and added to apo-BmrA-EPC/EPA in ribbons assemblies (Steinfels et al., 2004).

The presence of substrates induced in membrane twisting with greater curvature than in apo-conformation (Figure 42 B, C). Either, substrate binding can induce conformational changes of BmrA, nor the repartition of substrates in membrane may influence membrane morphology.

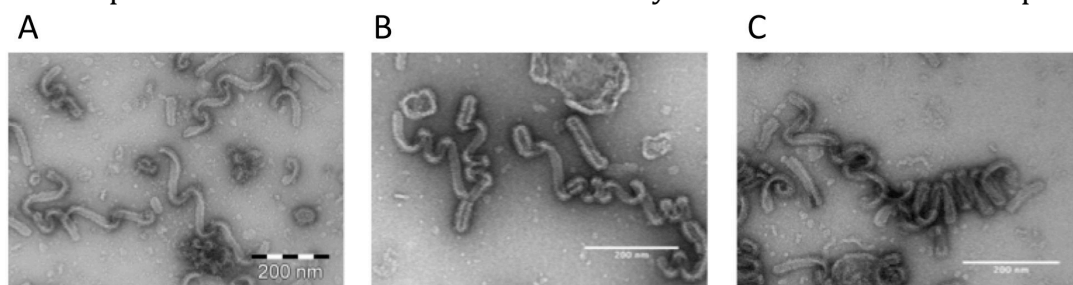


Figure 42 The presence of substrates induces membrane twisting

In apo-BmrA in ribbon shape (A), 30 μM of doxorubicin (B) and H33342(C) were added and analyzed in negative staining by EM.

c. Aims of the thesis

As explained in the introduction, there is a huge amount of data on the structure and function of ABCs. This is a field in which the results appear contradictory, even if they are carried out by the same authors. This shows that ABCs are extremely sensitive to their environment and there are probably several transport mechanisms.

In this thesis, we wanted to focus on the importance of the membrane in the function and spatial organization of a bacterial ABC. We chose BmrA, a bacterial ABC available in quantity that we studied in different membrane systems whose physico-chemical properties were modulated and controlled.

We addressed the following questions:

- 1) What are the quantitative contributions of the lipid composition and the membrane curvature to the function of BmrA?
- 2) How membrane properties modulate the spatial assembly of BmrA during the catalytic cycle?

We explored coupling in more detail in diluted condition to avoid protein-protein interaction. We combined several complementary strategies of membrane biochemistry and biophysics and single-molecule biophysics, in collaboration with physicist groups (Figure 43).

Firstly, the function of BmrA in relation to its environment was studied. We compared ATP hydrolysis activity of BmrA in pure detergent micelles, detergent/lipid mixed micelles and membranes. We took advantage of the team's expertise in the reconstitution of a transmembrane protein to control and modulate membrane environments: lipid composition, liposome sizes and protein density. In addition, we characterized the reconstitution systems in terms of protein orientation, protein incorporation rate, and lamellarity of liposomes to compare the effect of membrane on the function of BmrA.

Secondly, we studied the effects of membrane curvature and tension on the transmembrane part of BmrA in collaboration with P. Bassereau (Institut Curie, Paris). We used nanotube-pulling experiments with GUV where membrane curvature and tension were controlled. We studied the distribution of BmrA in apo-, post-hydrolysis conformations and during catalytic cycle in curved membrane.

Finally, the dynamics of NBDs of BmrA was studied according to its membrane environment in collaboration with E. Margeat (CBS, Montpellier) and M. Dahan (Institut Curie, Paris). FRET technique was used to delineate the distance between the two NBDs. Optimization of labeling with fluorescent dyes was performed with WT as well as mutants at single cysteine residue at the NBDs. Ensemble FRET was studied by fluorescence spectroscopy and by measuring donor's lifetime by FCS. Single-molecule FRET studies were carried out in parallel by FCCS in detergent and in liposomes.

Feedback between BmrA and its surrounding environment

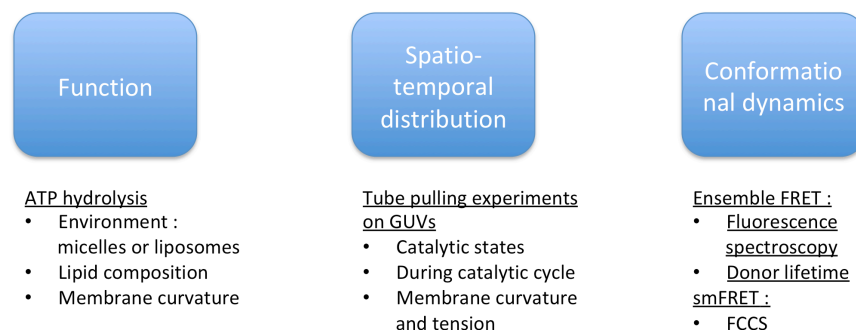


Figure 43 Strategies to study interplay between BmrA and its surrounding environment.

Material and methods

I. Expression and purification of BmrA

BmrA purification was carried out as previously reported (Steinfels et al., 2002, 2004; Wiseman et al., 2014). John Manzi (UMR168) optimized expression and purification of BmrA with some modifications. I purified BmrA along the thesis.

a. Expression

1. Plasmid

Jean-Michel Jault (IBCP, Lyon) provided plasmid pET23b+ containing BmrA WT. Plasmids of mutants were designed by me and constructed by Eurofin (Germany) from WT plasmid:

- M1: C436S;
- M2: C436S / T444C;
- M3: C436S / T559C.

2. Transformation

Artificial transformation was carried out by electroporation with *E. coli* (C41(DE3)) competent cells. C41(DE3) is a derivate of BL21(DE3) cell.

3. Culture medium

Cells were grown in 2x YT media containing: 16 mg/ml Tryptone, 10 mg/ml Yeast Extract and 5.0 mg/ml NaCl.

4. Expression

All procedures were carried out in sterile condition. C41(DE3) cells (50 µl) were thawed on ice. DNA (1 µg) was added in cells and transferred to precooled electroporation cuvette. Electroporation was performed at 3 Kv, 1.5 V. LB (1 mL) was added into electroporation cuvette and was gently mixed with cells with pipette. Cells were transferred to 1.5 mL eppendorf tube to grow for 1 h at 37 °C. Cells were again transferred to 150 ml of 2x YT medium supplemented with 0.1 mg/ml of ampicillin and were grown overnight at 25 °C. Bacteria (100 ml) were transferred in 4 L of 2TY medium supplemented with 0.1 mg/ml of ampicillin. Bacteria were grown at 25 °C until O.D._{600 nm} reached 0.6 - 0.8. Protein expression was induced with 0.7 mM of IPTG for 4 h at 25 °C. To collect cells, culture was centrifuged at 8,000 rpm with SLA3000 rotor for 10 min at 4 °C. Supernatant was discarded and cell pellet was washed and centrifuged in 80 ml of PBS. Cell pellet was resuspended in 100 ml of buffer: 50 mM Tris pH 8.0, 5 mM MgCl₂, 1 mM phenylmethylsulfonyl fluoride (PMSF, a serine protease inhibitor), 4 complete EDTA-free protease inhibitor cocktail tablets (Sigma) and stored at -20 °C.

b. Membrane preparation

Transformed cells were thawed at 4 °C in the presence of lysozyme and DNase. Cells were broken using constant systems cell disruptor, 1 pass at 2400 bar at 4 °C. EDTA was added to 10 mM final concentration. Solutions were centrifuged for 5 min at 8,000 rpm to compress foam from lysis. Supernatant was collected and centrifuged at 30,000 x g for 1 h at 4 °C in order to

separate between lysed and non-lysed cells. Supernatant was collected and ultra-centrifuged for 1 h at 100,000 x g at 4 °C (37,000 rpm with 70Ti rotor) to collect membrane. Supernatant was discarded and membrane pellet was resuspended in 10 ml of 20 mM Tris pH 8.0, 300 mM of sucrose. Concentration of membranes was measured by Bradford method in 0.02% SDS buffer. Next, 25 mg of membrane was aliquoted, frozen with liquid nitrogen and stored at -80 °C. In general, 550 mg of membrane were obtained from 4 L of culture. Protein expression was analyzed by 12% SDS-PAGE gel (Figure 44).

Expression and membrane preparation of mutants were performed with the same protocol as WT (Figure 44). No difference of expression rate was observed on SDS-PAGE gel between WT and mutants.

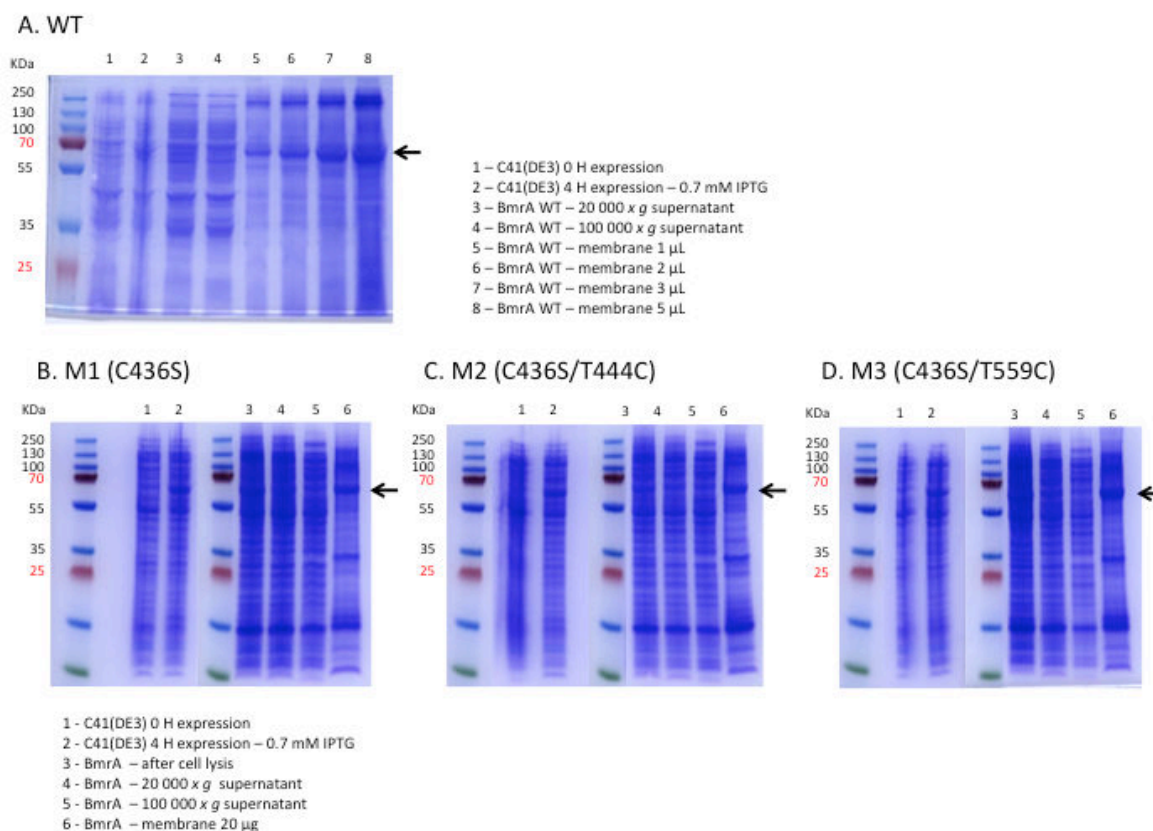


Figure 44 Overexpression of BmrA in membrane.

BmrA WT (A) and mutants (B-D) were overexpressed in C41(DE3) competent cells. Cells were transformed and grown in 2x YT media supplemented with 0.1 mg/ml of ampicillin. Once O.D.600 nm was reached to 0.6 – 0.8, protein expressions were induced with 0.7 mM of IPTG for 4 h at 25 °C. Cells were collected and lysed using constant system disruptor. Membranes were collected and expression levels of BmrA (black arrows) were analyzed on 12% SDS-PAGE gel stained with Coomassie blue.

c. Purification of BmrA

BmrA was purified in DDM 0.05%. According to activities of BmrA measured in Triton X-100 and LMNG, BmrA was also stable and could likely be purified with these other detergents (see ATPase activity depends on the type of detergent) (Wiseman et al., 2014). BmrA was purified by affinity chromatography using hexahistidine tag present at its C-ter.

DDM was freshly prepared (3 mL of 10%). Membrane containing overexpressed BmrA (25 mg) was added in 24 ml of solubilization buffer A. Membrane was solubilized for 1 h at 4 °C on spinning wheel. Solution was ultra-centrifuged at 50,000 rpm for 30 min at 4 °C with 70Ti rotor.

Supernatant containing solubilized proteins was collected, added to 1 ml of pre-washed Ni-NTA agarose beads (50 ml of milliQ water, 10 ml of buffer B) and incubated for 2 h at 4 °C on spinning wheel. Ni-NTA resin was washed with buffer B, 5 ml in batch and 10 ml over the column. Buffer C (3 ml) was added over the column to eliminate β -mercaptoethanol. Fractions of elution buffer D (500 μ l) were added over the column and solutions containing BmrA were collected. Each step of purification was analyzed on 12% SDS-PAGE gel. Oligomeric state of purified BmrA was analyzed with a gradient 4-12% blue native gel, stained with Coomassie blue (Figure 45). Concentration of proteins was measured by Bradford method. Protein were aliquoted, frozen with liquid nitrogen and stored at -80 °C. In general, approximately 550 μ g of BmrA was purified with 25 mg of membrane.

Mutants were also purified as WT.

Buffers:

Solubilization buffer A:

100 mM Tris, pH 8.0, 200 mM NaCl, 10% glycerol, 20 mM imidazole, 1% DDM, 1 mM PMSF, 1x protease inhibitor tablet

Buffer B:

100 mM Tris, pH 8.0, 100 mM NaCl, 20 mM imidazole, pH 8.0, 10% glycerol, 5 mM β -mercaptoethanol, 0.05% DDM

Buffer C:

100 mM Tris, pH 8.0, 100 mM NaCl, 20 mM imidazole, pH 8.0, 10% glycerol, 0.05% DDM

Elution buffer D:

50 mM Tris, pH 8.0, 100 mM NaCl, 250 mM imidazole, pH 8.0, 10% glycerol, 0.05% DDM

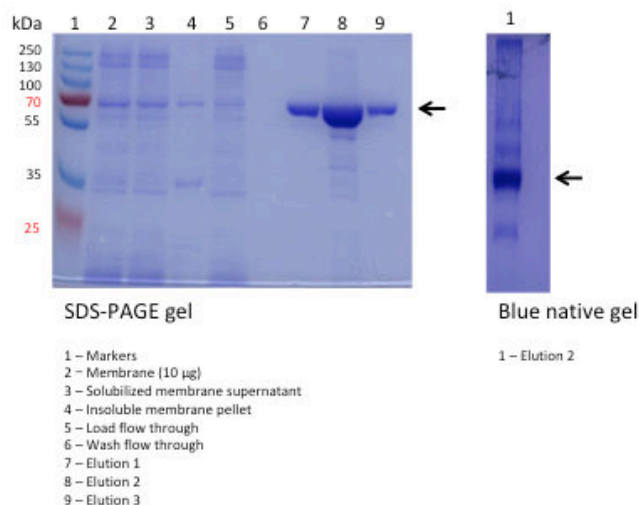


Figure 45 Example of purification of BmrA.

Membrane overexpressing BmrA was solubilized in DDM 1% for 1 h at 4 °C on the spinning wheel. Solubilized membrane proteins were collected by ultracentrifugation and incubated with Ni-NTA agarose beads for 2 h at 4 °C. Agarose beads were washed with 15 ml of buffer and BmrA was eluted. Purification of BmrA (black arrows) was analyzed on 12% SDS-PAGE gel and purified BmrA on gradient 4 - 12% blue native gel, stained with Coomassie blue.

II. Labeling of BmrA with fluorescent dyes

a. Labeling by thiol-maleimide reaction

This method consists to label purified protein in detergent and wash unbound dyes by affinity chromatography (Figure 46). BmrA was labeled at a single Cys residue with fluorescent maleimide dyes: C436 for WT, T444C for M2 and T559C for M3. Thiol-maleimide reaction was performed at pH 7 and total washing volume was minimized to avoid possible delipidation.

We carried out different methods of labeling with purified BmrA in detergent, in native membrane, in proteoliposomes and in BmrA bound to Ni-NTA resin. We decided to perform labeling with purified protein in detergent due to better reproducibility, labeling rate and activity of the protein.

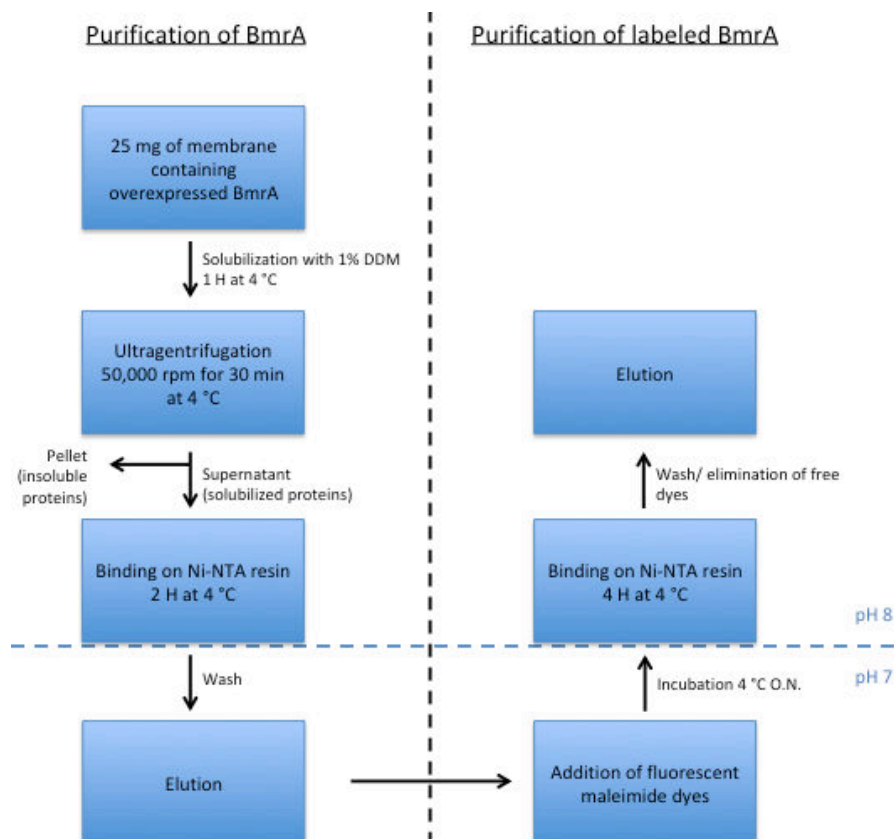


Figure 46 Schema of purification of BmrA and labeled BmrA

b. Preparation of fluorescent dyes

Dyes were dissolved in DMSO at 10 mM, aliquoted under argon gas and stored at -20 °C. Cy3B maleimide dyes were stored at -80 °C.

Fluorescent dye	ϵ_{\max} (cm ⁻¹ M ⁻¹)	λ Ex/Em (nm)	MW	Company
Alexa Fluor™ 488 C5 Maleimide	72,000	493/516	720.7	Sigma
Alexa Fluor 647 C2 Maleimide	265,000	651/671	~1250	Sigma
Atto610	150,000	616/633	613	ATTO-TEC

maleimide				
Cy3B maleimide	130,000	559/570	796	GE Life Sciences
Dy547P1 maleimide	150,000	551/565	804.9	Dyomics
Dy647P1 maleimide	250,000	653/672	831	Dyomics
Sulfo-Cyanine3 maleimide	162,000	548/563	777	Lumiprobe
Sulfo- Cyanine5 maleimide	271,000	646/662	803	Lumiprobe

Table 1 List of fluorescent dyes

c. Purification of labeled BmrA

pH of buffer was changed to pH 7 to optimize thiol-maleimide reaction and then to pH 8 for binding of BmrA on Ni-NTA resin. Total washing volume was adjusted to wash free dyes and to preserve protein's activity.

First steps of purification were the same as classic purification until incubation of protein with Ni-NTA resin. Ni-NTA resin was washed with 5 ml in batch and 4 ml over the column with buffer E. Elution buffer G was added by 250 µl fractions over the column and all fractions containing BmrA were collected (1.25 ml). Concentration of protein was measured by Bradford method. Fluorescent dye was added to dye/protein 10-20 mol/mol (see Optimization of ratio of two fluorescent dyes) and incubated at 4 °C, overnight on spinning wheel. Protein was diluted in buffer F to 15 ml final volume to decrease the concentration of imidazole to 20 mM. Protein was added to 0.4 ml of pre-washed Ni-NTA agarose (25 ml of milliQ water, 5 ml of buffer E). Ni-NTA resin was washed with 1 ml in batch and 5 ml over the column with buffer C. Protein was eluted with fractions of 100 µl of elution buffer D. Each step of purification was analyzed on 12% SDS-PAGE gel by fluorescence and stained by Coomassie blue (Figure 47). Labeled BmrA was purified (black arrow) without free dyes (red arrow).

Concentration of protein was measured by Bradford method and concentration of fluorescent dyes was measured by absorbance by Beer-Lambert law. Rate of labeling was calculated by ratio of concentration of dye to protein. Proteins were aliquoted, frozen with liquid nitrogen and stored at -80 °C. In general, approximately 300 µg of labeled proteins were obtained with 625 µg of proteins.

Rates of labeling between WT and M2 were similar whereas the labeling of M3 was different.

Supplementary buffers:

Buffer E:

100 mM Tris, pH 7.0, 100 mM NaCl, 20 mM imidazole, pH 7.0, 10% glycerol, 0.05% DDM

Buffer F:

100 mM Tris, pH 8.0, 100 mM NaCl, 10% glycerol, 0.05% DDM

Elution buffer G:

50 mM Tris, pH 7.0, 100 mM NaCl, 250 mM imidazole, pH 7.0, 10% glycerol, 0.05% DDM

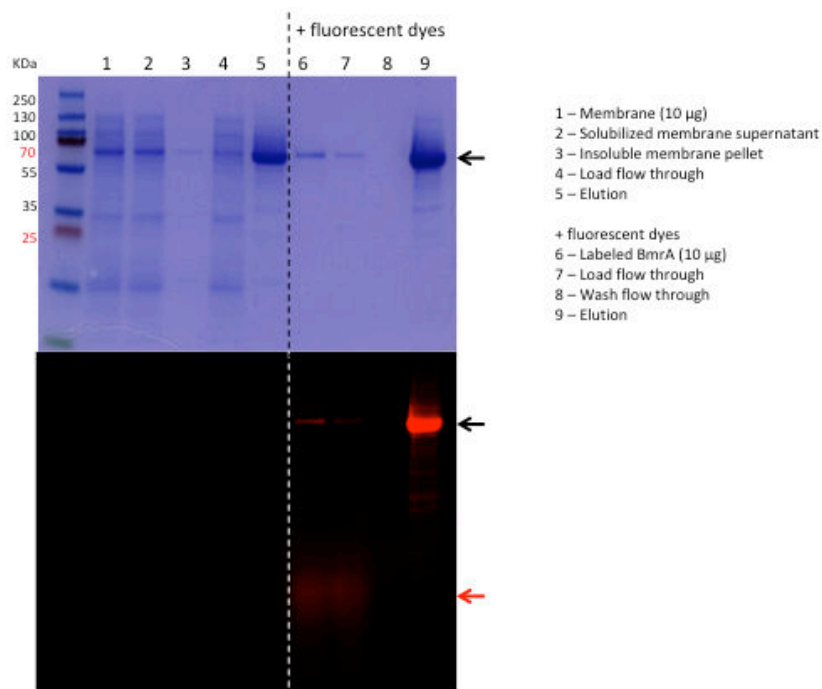


Figure 47 Example of purification of labeled BmrA.

Dy647P1 maleimide dyes were added to purified BmrA to dye/protein 10 mol/mol in buffer pH 7 and incubated over night at 4 °C on spinning wheel. Free dyes were washed 30 times resin volume by affinity chromatography. Labeled BmrA (black arrows) was eluted and analyzed on 12% SDS-PAGE gel by fluorescence and stained with Coomassie blue. All free dyes (red arrow) were washed out in purified labeled-BmrA.

III. Method and characterization of reconstitution of BmrA in proteoliposome

BmrA was reconstituted from micelles of protein/lipid/detergent followed by detergent removal by BioBeads (Figure 48-1). BmrA was also reconstituted by direct incorporation into liposomes destabilized by sub-solubilizing concentration of sugar-based detergent, e.g. DDM, (Figure 48-2). Detergent was further removed by BioBeads.

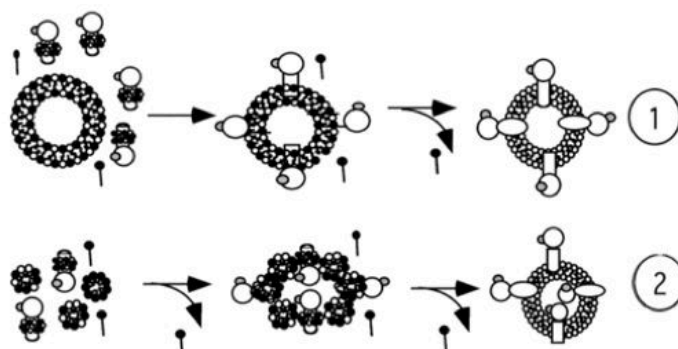


Figure 48 Schema of different strategies of reconstitution

(1) Direct incorporation method of transmembrane protein into preformed unilamellar vesicles in the presence of detergent. (2) Transmembrane proteins reconstituted from micelles of lipids/detergents/proteins by detergent removal. Detergents were removed by BioBeads. (Rigaud et al, 2003, method and enzymology)

a. Preparation of lipids

Lipids were purchased from Avanti Polar Lipids in chloroform and kept at -80 or -20 °C under argon gas. Fluorescent Texas Red DHPE was purchased from Thermo Fisher in powder, solubilized in chloroform and kept at -20 °C under argon gas.

In general, liposomes were prepared from resuspension of dried film in water at 10 mg/ml, sonicated for 30 s (tip sonicator), aliquoted and kept at -20 °C. For small volume and fluorescent lipids, dried film was solubilized in buffer containing Triton X-100/lipid 2.5 w/w, for 30 min at room temperature under magnetic stirrer agitation.

Name of lipid	Average MW and comments	Utilization
Brain PS (L- α -phosphatidylserine)	825	Functional assay
DOPC (1,2-dioleoyl-sn-glycero-3-phosphocholine)	786.1	Functional assay
DOPE (1,2-dioleoyl-sn-glycero-3-phosphoethanolamine)	744	Functional assay
DOPG (1,2-dioleoyl-sn-glycero-3-phospho-(1'-rac-glycerol))	797	Functional assay
DSPE-PEG(2000)	2780.4	GUVs growth
DSPE-PEG(2000) Biotin (1,2-distearoyl-sn-glycero-3-phosphoethanolamine-N-[biotinyl(polyethylene glycol)-2000])	3016.8	GUVs growth
<i>E. coli</i> Cardiolipin (<i>E. coli</i> CA)	1430	Functional assay
<i>E. coli</i> PG (L- α -phosphatidylglycerol (<i>E. coli</i> PG))	761.1	Functional assay
<i>E. coli</i> , polar extract	Phosphatidylethanolamine 67% w/w Phosphatidylglycerol 23,2 % w/w Cardiolipin 9,8 % w/w	Functional assay, FRET
EPA (Egg Phosphatidic Acid)	706.2	Functional assay, GUVs growth FRET
EPC (Egg Phosphatidylcholine)	770.1	Functional assay, GUVs growth, FRET
EPE (Egg Phosphatidylethanolamine)	746.6	Functional assay
Texas Red™ DHPE	1381.9	GUVs growth,

(Texas Red™ 1,2-Dihexadecanoyl-sn-Glycero-3-Phosphoethanolamine, Triethylammonium Salt)	(Excitation/emission maxima ~595/615 nm)	Floatation
---	--	------------

Table 2 List of lipids

b. Preparation of detergent

Detergents was purchased from Anatrace in powder and stored at -20 °C. Triton X-100 was purchased in 10 % solution and kept under argon at -20 °C. Detergents were solubilized in water and kept at 4 °C for a month.

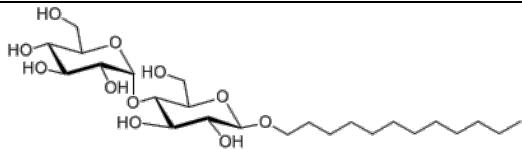
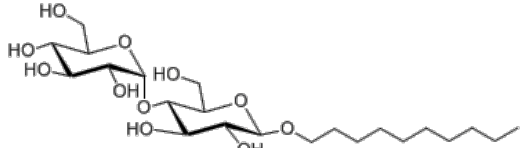
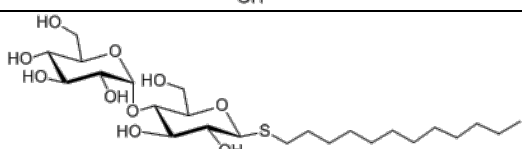
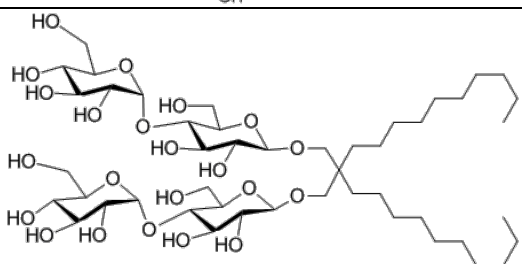
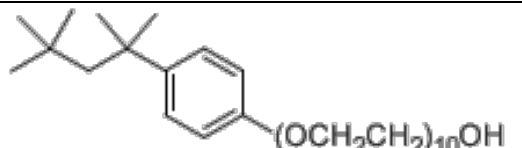
Detergent	Chemical structure	MW and comments
DDM (n-Dodecyl-β-D-maltopyranoside)		MW: 510.6 CMC: (H2O) ~ 0.17 mM (0.0087%)
DM (n-Decyl-β-D-maltopyranoside)		MW: 482.6 CMC: (H2O) ~ 1.8 mM (0.087%)
DOTM (n-dodecyl-β-D-thiomaltopyranoside)		MW: 526.6 CMC: (H2O) ~ 0.05 mM (0.0026%)
LMNG (Lauryl Maltose Neopentyl Glycol)		MW: 1005.19 CMC: (H2O) ~ 0.01 mM (0.001%)
Triton X-100 (Anapoe-X-100)		MW: 647.0 CMC: (H2O) ~ 0.23 mM (0.015%)

Table 3 List of detergents

c. Reconstitution by detergent removal

BmrA reconstitution carried out as previously reported method (J.-L. Rigaud & Levy, 2003; J. L. Rigaud et al., 1995; Steinfels et al., 2004).

1. Preparation of BioBeads

BioBeads were washed in batch. BioBeads (5 g) were added to 25 ml of methanol and slowly stirred for 40 min. Methanol was discarded and beads were washed 3 times for 10 min

with excess of water (at least 25 ml each time). Beads were stored in water at 4 °C. Washing procedure was repeated every month.

2. Reconstitution from micelles of lipid/detergent/protein

Lipid solubilization

Lipids were solubilized in 2-4 mg/ml in buffer 50 mM MOPS pH 7.5, 150 mM NaCl, 1 mM MgCl₂. Lipids were solubilized at Triton X-100/lipid 2.5 w/w ratio for 15 min or in DDM/lipid 3 w/w ratio over night at 20 °C. Desired amount of protein was added to solubilized lipids and incubated for 15 min at 20 °C. For single molecule experiment, protein was diluted in buffer 50 mM MOPS pH 7.5, 150 mM NaCl, 0.05% DDM before addition.

Detergent removal

BioBeads were added 3 times sequentially: BioBead/detergent 10 w/w for 2 h, 10 w/w for 1 h, 20 w/w for 1 h at 20 °C.

Detergent removal to form small liposomes ($\emptyset \approx 30$ nm)

BioBeads were added to BioBeads/detergent 40 w/w for 4 h at 4 °C or 30 w/w for 2 h, 30 w/w for 1 h, 60 w/w for 1 h at 4 °C.

3. Direct incorporation reconstitution

Sugar based-detergent was added at Rsat (detergent/lipid ratio of lamellar-to-micellar transition) to preformed unilamellar liposomes that perturbed the membrane but not enough for solubilization (Figure 48 1). Addition of transmembrane protein allowed incorporation by its hydrophobic domain. BmrA was reconstituted with NBDs outside of liposomes, i.e. inside-out orientation.

Experiment was performed at 20 °C under magnetic stirrer agitation. Concentration of DDM was calculated according to:

Concentration of DDM = Rsat*concentration of lipids + cmc (molar concentration)
Rsat of DDM was 1 (mol/mol). (Lambert et al., 1998)

Usually, 2 mg/ml, i.e. 2.6 mM of lipids were used for direct incorporation:

Concentration of DDM = 2.6 mM + 0.2 mM = 2.8 mM

Liposomes were incubated overnight for *E. coli* and 2 h for EPC/EPA. Protein was incubated and stirred for 15 min. BioBeads were added at BioBead/detergent 20 w/w for 4 h.

d. Protein orientation

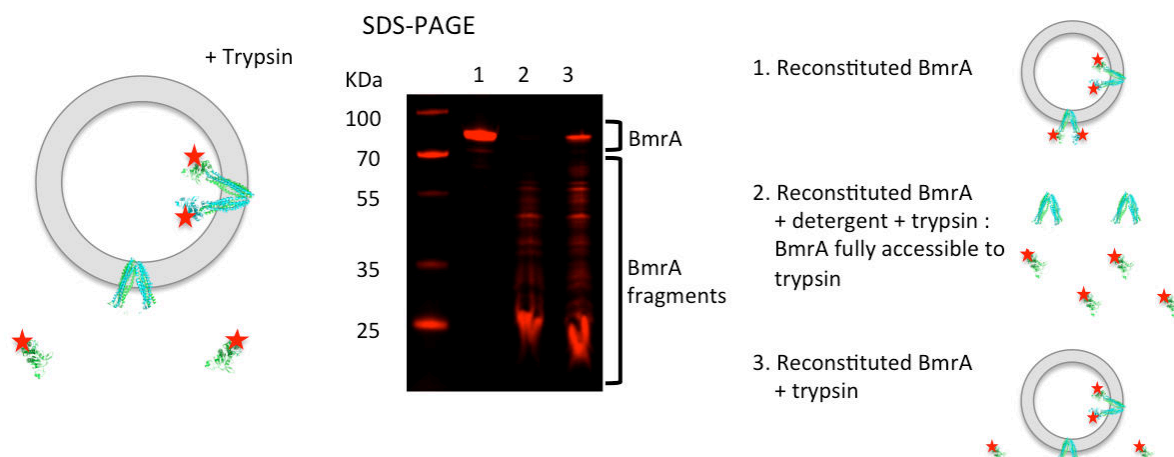


Figure 49 Characterization of protein orientation in liposomes by proteolysis

Fluorescently labeled BmrA was reconstituted in liposomes and same (weight) concentration of trypsin was added. The solution was incubated for 30 min at 20 °C under magnetic stirrer agitation. Adding 1 mM of PMSF stopped the reaction. Then, the proportion of digested proteins compared to total proteins was measured the fluorescence on SDS-PAGE gel 12%.

1. Preparation of trypsin

Trypsin (sigma) was dissolved in 1 M HCl and stored at -20 °C. Trypsin was diluted in buffer before use.

2. Preparation of PMSF

PMSF power was solubilized in isopropanol at 100 mM and stored at -20 °C.

3. Proteolysis

Alexa488- or Atto610-labeled BmrA was reconstituted in liposomes. Same concentration (weight) of trypsin as proteins was added. For example, 4 µg/ml of trypsin was added to 4 µg/ml of protein in 40 µl total volume. Solution was incubated at 20 °C for 30 min under magnetic stirrer agitation. Reaction was stopped with 1 mM PMSF and kept on ice. Fluorescence of protein 0.1-0.05 µg was measured on SDS-PAGE gel by ChemiDoc™ MP Imaging System. Percentage of orientation was calculated by fluorescence of digested proteins compare to total proteins.

e. Protein incorporation

Flotation separates liposomes, proteoliposomes and aggregated proteins based on their densities (Figure 50). Aggregated proteins were positioned at 30% whereas the proteoliposomes were positioned at 5 to 20% of sucrose according to lipid/protein ratio. After centrifugation, fluorescence of proteins and liposomes were analyzed on SDS-PAGE gel.

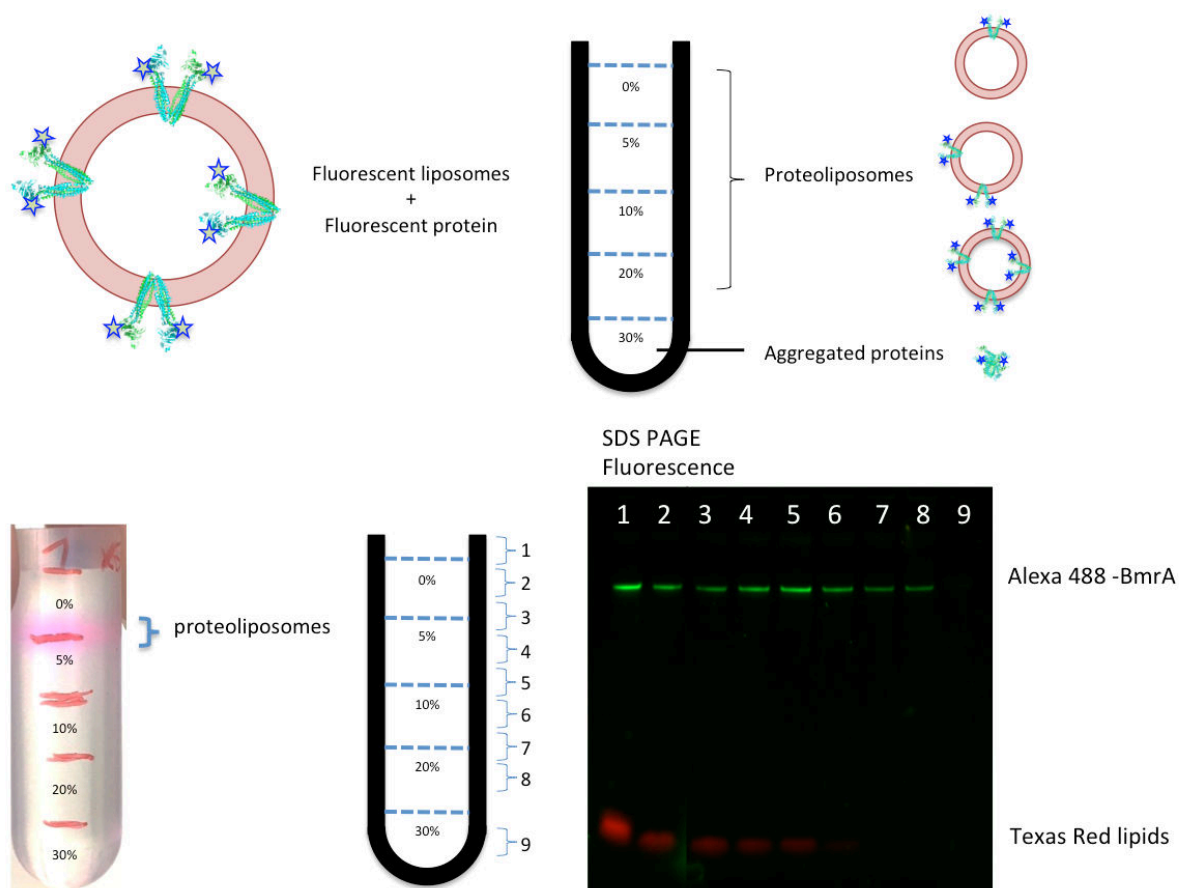


Figure 50 Incorporation rate measured by flotation

Alexa488 labeled BmrA was reconstituted into fluorescent liposomes. Proteoliposomes were mixed with 30% sucrose and sucrose was gently added into the centrifuge tube. After 16 h of centrifugation at 100 000 x g with swing-out rotor, and fluorescence of proteins and lipids were analyzed on 12% SDS-PAGE gel.

Final volume of flotation was adjusted according to size of centrifuge tube and number of sucrose steps. In our case, 2.5 ml sized centrifuge tube (Ref.347357, Beckman coulter) was used with 4 sucrose steps. Therefore, final volume was adjusted to 2.3 ml. Sucrose (20%, 10% and 5%) was prepared in buffer 50 mM MOPS pH 7.5, 150 mM NaCl. In parallel, 575µl of 30% of sucrose containing 100 µl of 3 mg/ml proteoliposomes were prepared. Sucrose flotation step was prepared by adding 30%, 20%, 10% and 5% of sucrose (575 µl each) respectively in centrifuge. Centrifugation was performed with swing-out rotor (TLS-55 rotor) at 100, 000 x g for 16 h or at 150,000 x g for 4 h at 4 °C. Fractions were collected from the top and fluorescence of liposomes and proteins were analyzed on 12% SDS-PAGE gel. Incorporation rate was calculated: 1- (fluorescence of protein at 30% / fluorescence of total proteins).

f. Size of liposomes by dynamic light scattering (DLS)

Size of liposomes (0.5 – 2 mg/ml) was measured by Nano Z-S ZETA SIZER (MALVERN) with ZEN-0040 cuvette. Parameters for Zetasizer software were set as “phospholipids vesicles” as materials (refraction index: 1.490) and “water” as dispersant at 20 °C.

g. Size and lamellarity of liposomes by cryo-electron microscopy

Aur lie Di Cicco performed cryo-electron microscopy. Holey formvar lacey grids (Ted pella) were glow discharged for 30 s under vacuum. Then, 4  l of samples (usually 1 mg/ml of liposomes) were deposited during 30 s on the grid and flash frozen by automatic plunge freezer EM GP2 (Leica) in liquid ethane. Images were taken on a Tecnai 20 electron microscopy operating at 200 KV (LaB6) with a CMOS TVIPS (4k) camera. Images were taken under low dose conditions and were defocused from -1 to -3  m.

IV. Reconstitution of BmrA into GUVs

GUVs were grown by fusion of small proteoliposomes to GUVs or by swelling of partially dried lipid/protein proteoliposomes by alternating current electric field (Figure 50). GUVs were observed by confocal microscopy as previously reported for KvAP (Garten, Aimon, Bassereau, & Toombes, 2015).

a. Fusion of small proteoliposomes to GUVs

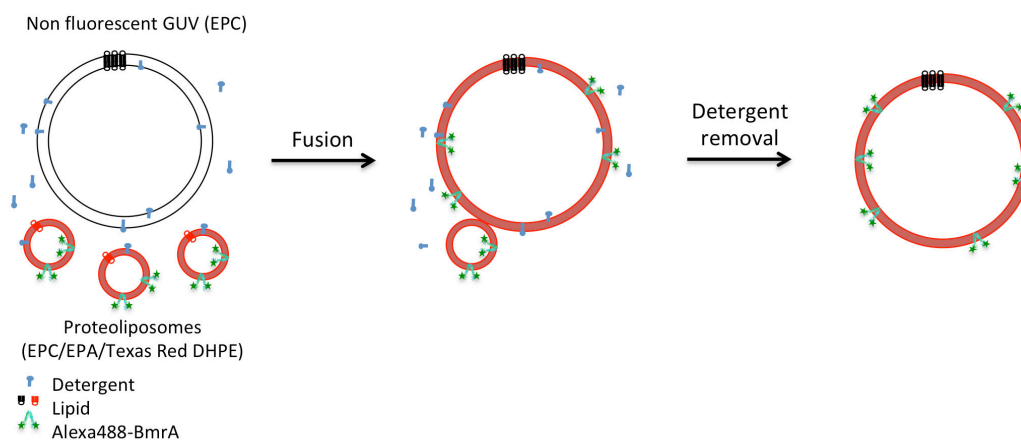


Figure 51 Principle of fusion of proteoliposomes to GUVs

GUVs are incubated with fluorescently labeled proteoliposomes in the presence of sub-solubilizing concentration of detergent. Proteoliposomes are fused to GUVs and detergents are removed.

Growth of GUVs in the presence of DOTM

Non fluorescent GUVs (EPC) were grown in the presence of 75  M DOTM on ITO slides by electroformation at 10 Hz, 1.1 V for 3 h 30 at room temperature in sucrose 400 mM.

Fusion of fluorescent small proteoliposome to GUVs

Proteoliposomes (EPC/EPA/Texas Red DHPE 9/1/0.5 w/w/w) were incubated in the presence of 75  M DOTM or 0.2 - 0.4 Triton X-100/lipid mol/mol in 100 mM MOPS pH7, 200 mM NaCl. Then, GUVs were added to proteoliposomes at 1 v/v and incubated over night at room temperature in the dark. BioBeads were added at BB/ detergent 20 w/w at room temperature for 30 min for detergent removal.

b. Incorporation of BmrA in GUVs by electroformation

Reconstitution of proteoliposomes

Proteoliposomes were reconstituted from micelles of protein/lipid/detergent. Reconstitution was performed at 3 mg/ml of EPC/EPA/DSPE-PEG2000/DSPE-PEG2000-biotin, Texas Red DHPE (89/8.9/1/0.01/0.1 mol) with lipid/protein ratio 10 w/w of Alexa488-BmrA. The presence of PEG lipids prevented sticking GUVs each other. After reconstitution, buffer was exchanged to 5 mM MOPS pH 7.5, 5 mM trehalose, 20 mM NaCl with pre-equilibrated PD SpinTrap G-25. Buffer was exchanged to low salt buffer after reconstitution because GUVs did not grow in reconstitution buffer. Proteoliposomes were aliquoted, frozen with liquid nitrogen and stored at -80 °C.

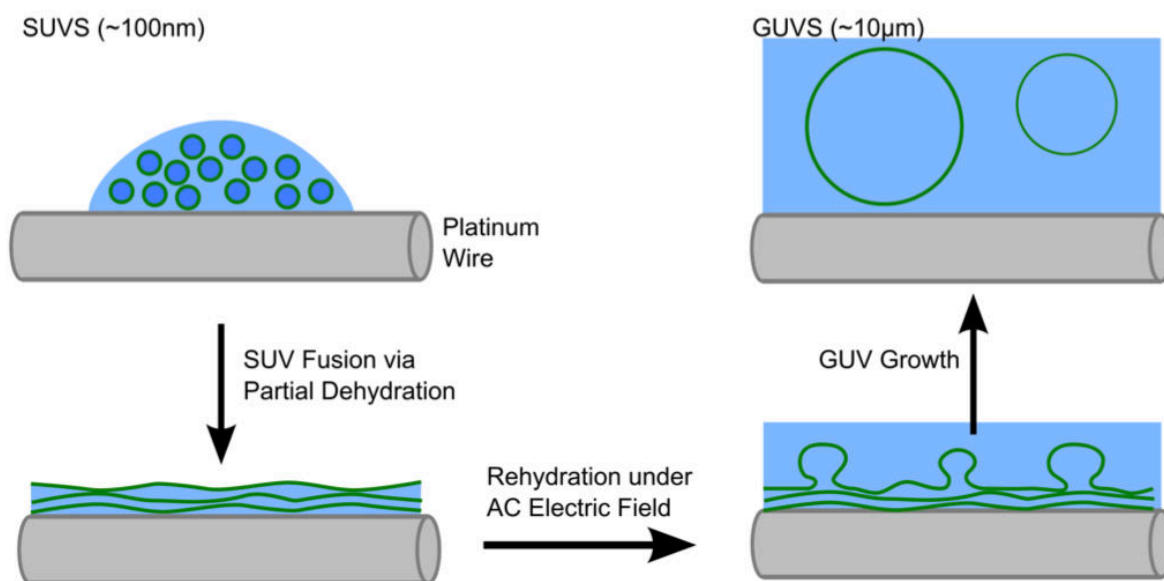


Figure 52 Principle of reconstitution of transmembrane proteins into GUVs

Small drop containing proteoliposomes was partially dried on platinum wire. After rehydration, GUVs were grown from lipid/protein film under electric field.

Electroformation of GUVs on platinum wire:

All processes were carried out at 4 °C. Proteoliposomes were mixed with liposomes at 1/1 v/v prepared by sonication in bath. Concentration of trehalose was adjusted to 3.5 mM. Electroformation chamber was assembled and glow discharged for 30 s with less than 3 mA. The mixture was deposited by separate drops on platinum wire and dried for 1 h in air. Drops should not be fused. Drying time was the key step for GUVs growth: if the mixture were completely dry, proteins were aggregated and GUVs devoid of proteins were grown; and if it was not dried enough, proteoliposomes were washed out during addition of growing buffer. GUVs were grown in buffer 5 mM MOPS pH 7.5, 20 mM NaCl, 255 mM sucrose for 4-5 h at 350 mV at 500 Hz. GUVs were collected by pipetting on the surface of platinum wire.

V. ATPase hydrolysis measurement

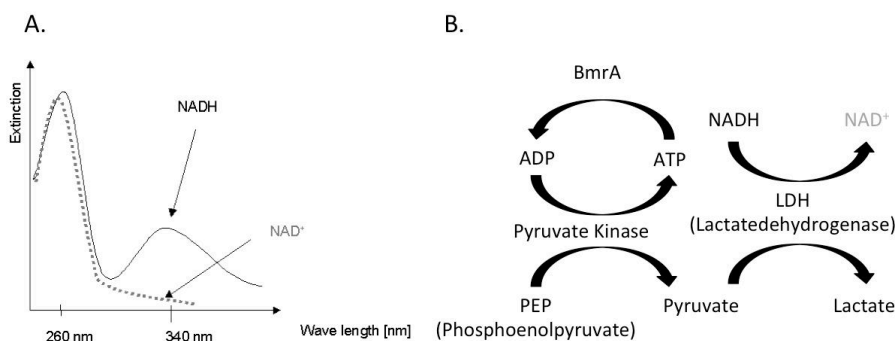


Figure 53 Principle of ATPase activity measurement coupled with oxidation of NADH.

(A) NADH is absorbed at 340 nm whereas NAD⁺ is not. (<http://biochem4.biochem.okstate.edu>) (B) ATPase activity can be measured by absorbance changes of NADH/NAD⁺ at 340 nm coupled to different enzymes.

ATPase hydrolysis was carried out by absorbance changes of NADH/NAD⁺ ratio at 340 nm (Figure 53A) that is inversely proportional to ATP hydrolysis with mixture of enzymes (Figure 53B). During the measurement, concentration of ATP was maintained (De La Cruz & Ostap, 2009).

a. Preparation of ATP

ATP (100 mM) (sigma) was prepared in 100 mM Hepes pH 8. pH was adjusted to pH 7.5 with KOH and stored at -20 °C.

b. Preparation of ADP

ADP (100 mM) (sigma) was dissolved in water, pH was adjusted to pH 7 with KOH and stored at -20 °C.

c. Preparation of orthovanadate

Orthovanadate (100 mM) (sigma) was prepared in water. pH was adjusted to 10 with HCl by repeating boiling for 5 min, cooling down and pH readjusting steps until pH was stable. The exact concentration of orthovanadate was measured by absorbance using the molar extinction coefficient ($\epsilon_M = 3,550$ at 260 nm). Solution was aliquoted and stored at -20 °C. Orthovanadate was boiled at least 5 min before use.

d. Preparation of AMP-PNP

AMP-PNP (100 mM) (sigma) was prepared in buffer of experiment (pH 7.5) and stored at -80 °C.

e. Preparation of ATP- γ -S

ATP- γ -S (100 mM)(sigma) was freshly prepared in buffer and kept at 4 °C.

f. Preparation of cocktail of enzymes:

- L-Lactate dehydrogenase (LDH) (sigma) was stored at 3300 units/ml in -20 °C in 50% glycerol
- Pyruvate kinase (PK) (sigma) was stored at 10000 U/ml at -20 °C in 50% glycerol
- Phosphoenolpyruvate (PEP) (sigma) was stored at 100 mM at -20 °C in water
- NADH (50 mg) (sigma) was aliquoted to 1 mmole, lyophilized and stored in dark at room temperature.

g. Preparation of 5X cocktail of enzymes:

Solution was prepared freshly, kept on ice in dark. NADH (2 tubes), 6 µl of LDH 3300 units/ml, 10 µl of pyruvate kinase 10000 U/ml and 5 µl of 100 mM of PEP were added in 200 µl total of buffer (50 mM MOPS pH 7.5, 150 mM NaCl) to get final concentration of:

- 2 mmoles of NADH
- 100 units/ml of LDH
- 500 units/ml of PK
- 2.5 mM of PEP

h. ATPase activity measurement

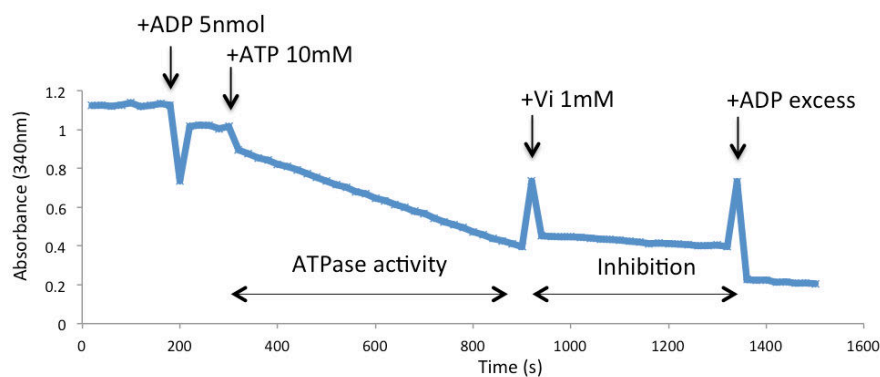


Figure 54 Example of ATPase activity measurement

Proteins ($\approx 0.5 \mu\text{g}$) were incubated for 4 min at desired temperature. ADP (5 nmol) was added to control the quality of reaction. ATPase activity was measured for 4 min at desired concentration of ATP. Rate of inhibition was calculated by measuring the activity after addition of inhibitor.

ATPase activity was measured in 50 mM MOPS pH 7.5, 150 mM NaCl, 10 mM of MgCl_2 with 1X cocktail and $0.5 \mu\text{g}$ of protein at 20 °C or 37 °C in 100 µl total volume. Absorbance of NADH was measured by spectrometer (Cary Win 60 UV – Vis, Agilent Technologies) at 340 nm every 15 s with quartz cuvette (N.105-254-15-40, Hellma Analytics, 3 x 3 mm). Proteins were incubated for 4 min at desired temperature. Addition of 1 µl of 5 mM ADP confirmed the quality of reaction. ATP was added and absorbance was recorded for 4 min but first minute of reaction was ignored for ATPase activity calculation. Rate of inhibition was measured by adding 1 mM of orthovanadate, 10 mM of AMP-PNP or 5 mM of ATP- δ -S. ATPase activity was calculated by quantity of NADH oxidized (equivalent to quantity of ATP hydrolyzed), per min and per mg of protein.

VI. Ensemble FRET measurement by fluorescence spectroscopy

a. Fluorescence spectroscopy

Ensemble FRET signal was measured on Cary Elipse Fluorescence Spectrophotometer (Agilent Technologies) with spectrometer quartz cuvette (N.105-250-15-40, Hellma Analytics, 10 x 2 mm). Emission spectrum was performed with an excitation wavelength lower than maximal excitation wavelength in order to avoid light scattering of liposomes (Figure 55A) and all parameters were kept the same (excitation wavelength, excitation and emission slits). Final concentration of each fluorescent dyes were adjusted to 200 nM. Baseline was corrected in buffer for each measurement. Experiment was performed after 3 min of incubation after addition of ATP or inhibitors at 20 °C.

In detergent

BmrA was diluted to 200 nM in buffer 50 mM MOPS pH7.5, 150 mM NaCl, 0.05% DDM, 10 mM of MgCl₂. ATP (10 mM) and inhibitors (10 mM of AMP-PNP, 1 mM of orthovanadate or 5 mM of ATP-γ-S) were added.

Proteoliposomes

Reconstitution was performed with EPC/EPA (90/10 w/w) or *E. coli* lipid polar extract at 1-2 mg/ml from micelles of lipid/detergent/protein (approximately lipid/protein ratio of 100 w/w). Buffer for FRET measurement contained 10 mM and 1.5 mM of MgCl₂ for EPC/EPA and *E. coli* lipids, respectively since *E. coli* liposomes tend to aggregate at 10 mM of MgCl₂. ATP was added as same concentration as MgCl₂. For inhibition, 1 mM of orthovanadate, 10 mM of AMP-PNP or 5 mM of ATP-γ-S were added.

b. Fluorescence spectroscopy analysis

F_{FRET} was calculated as described in (Clegg, 1992).

First, emission spectrum was recorded with excitation wavelength that was 20 nm lower than the maximal excitation wavelength. This allowed avoiding light scattering of liposomes (Figure 55A).

Second, F_{FRET} was corrected for excitation and emission cross-talks (Figure 55B) by measuring a sample containing donor only and a sample containing acceptor only, in the same condition of FRET measurement. Ratio R1 (leakage of the donor emission at the acceptor emission wavelength) and R2 (direct excitation of acceptor at the donor excitation wavelength) were calculated by ratio of area A1 and A2. Wavelengths for calculation of area were selected \pm 10 nm from the maximum emission and remained the same during analysis. Area between two wavelengths was calculated by Matlab using trapz function: Area = trapz(...,dim). F_{FRET} was calculated as:

$$F_{\text{FRET}} = A2 - A1/R1 - A3/R2 \quad (\text{Figure 55B})$$

Third, extinction coefficient of selected wavelength ϵ_n was calculated (Figure 55C). ϵ_n was calculated by the ratio of absorbance between maximal and selected wavelengths:

$$\varepsilon_n = \varepsilon_{\max} / A_{\max} \times A_n$$

Finally, FRET efficiency E_{FRET} was calculated by following formula:

$$E_{\text{FRET}} = (F_{\text{FRET}} \times \varepsilon_A) / (F_A \times \varepsilon_D \times d)$$

With ε , extinction coefficient and d , efficiency of labeling of the donor.

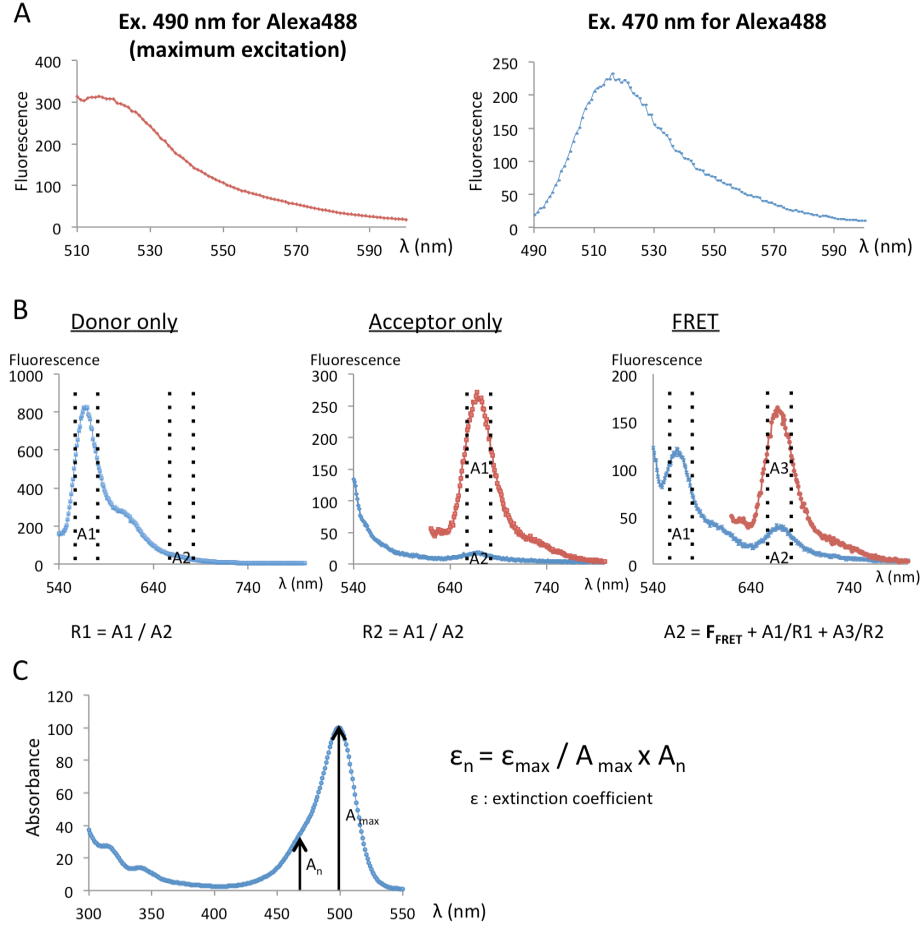


Figure 55 Analysis of E_{FRET} by fluorimeter.

(A) Emission spectrum was measured with an excitation wavelength lower than maximal excitation wavelength in order to avoid light scattering of liposomes. (B) F_{FRET} signal was corrected for excitation and emission cross-talks. (C) Extinction coefficient of selected wavelength ε_n was calculated by ratio of absorbance A_{\max} and A_n .

VII. Fluorescence Cross-Correlation Spectroscopy

Experiments were performed with home-built inverted confocal PIE-MFD microscope (Emmanuel Margeat, CBS) (Olofsson & Margeat, 2013) at 20 °C. 50 μl of solutions were loaded into 384-well plates (Greiner Bio One).

Fluorescent dye	Laser	Excitation Filter	Emission filter
Alexa 488	SC450-4-20MhZ	488/10	535/50
Sulfo-Cy3	SC450-4-20MhZ	532/10	590/75
Atto 610	SC450-4-20MhZ	574/10	630/60
Sulfo-Cy5	SC450-4-20MhZ	633/10	675/50

Table 4 List of laser and filter according to fluorescent dyes.

a. Measurement of fluorescent lifetime

1. Ensemble FRET by FCCS

Laser power was approximately 2.5 μ W.

In detergent

BmrA was diluted to 200 μ M concentrations in buffer 50 mM MOPS pH7.5, 150 mM NaCl, 0.05% DDM, 10 mM of $MgCl_2$.

In Proteoliposome

Lipid/protein ratio was varied from 40 to 400 w/w. Buffer contained 10 mM and 1.5 mM of $MgCl_2$ for EPC/EPA and *E. coli* lipids, respectively.

Equimolar concentration of ATP was added as $MgCl_2$. For inhibition, 1 mM of orthovanadate or 10 mM of AMP-PNP or 5 mM of ATP- γ -S were added.

2. Analysis of ensemble FRET

Data analysis was performed with software FitMachine. Lifetime was considered bi-exponential.

b. Single-molecule FRET

1. Single-Molecule FRET by FCCS

SmFRET was measured in similar condition as ensemble FRET measurement with different concentration of proteins. Laser power was 10 - 15 μ W.

In detergent

BmrA was diluted to 50 pM.

In detergent/lipid

BmrA (100 pM) in 50 mM MOPS pH7.5, 150 mM NaCl, 0.05% DDM, 10 mM of $MgCl_2$ was added to 100 μ M of solubilized lipids in 50 mM MOPS pH7.5, 150 mM NaCl, 0.02% triton X-100, 10 mM of $MgCl_2$.

In Proteoliposome

Proteoliposomes were reconstituted at lipid/protein ratio 40 000 w/w (\approx 0.05 homodimer per liposome) to obtain 1 homodimer per liposome.

2. Analysis Single-Molecule FRET

Analysis were performed by the Software Package for Multiparameter Fluorescence Spectroscopy, Full Correlation and Multiparameter Fluorescence Imaging developed in C.A.M. Seidel lab (<http://www.mpc.uni-duesseldorf.de/seidel/>). 3 programs were used, successively:

- PARIS: Paris program was used for data processing to eliminate backgrounds, aggregations, and select bursts of single molecule fluorescent signals. For each single molecule, the FRET efficiency and stoichiometry parameters were calculated, as well as the donor, acceptor fluorescence lifetimes.

- Margarita: Margarita visualized data from PARIS in 2D histograms. Three parameters were considered to select dual-labeled protein:
 - TGX-TRR: difference in mean arrival time between photons after green excitation (that is donor and FRET photons) and photons after red excitation
 - Tau (Yellow): lifetime of the acceptor upon direct excitation
 - S (prompt)/S (total): Stoichiometry
 For example, criteria for BmrA sulfo-Cy3/sulfo-Cy5 couples were:
 - $-1.5 < \text{TGX-TRR} < 1.5$ to eliminate photobleaching events
 - $0.65 \text{ ns} < \text{Tau (Yellow)} < 3 \text{ ns}$ for the removal of donor-only labeled molecules
 - $0.47 < \text{S (prompt)/S (total)} < 1$ for the removal of acceptor-only labeled molecules
- OriginLab: OriginLab was used to fit the histograms using Gaussian distributions.

Results

I. ATP hydrolysis of BmrA in micelles and reconstituted in membranes.

To study the function of BmrA, we measured ATP hydrolysis with a coupled enzyme assay that is commonly used for ABC transporters. We did not measure the drug transport. This is often the case for ABC transporters since substrates are mostly amphiphilic molecules that partition into the membrane and do not accumulate in the internal volume (Figure 56B). Substrate transport was studied with BmrA-overexpressed inverted *E. coli* membrane vesicles (Cao et al., 2009; Steinfels et al., 2004). In this case, vesicles are often multilamellar; substrates can be therefore accumulated in encapsulated liposomes. In our studies, activities are measured with unilamellar vesicles (see Figure 70). We measured V_{max} of BmrA at 10 mM of ATP at 37 °C, K_d is 1.5 mM (Steinfels et al., 2004). In most studies of ABC transporters, substrates are studied through their stimulating or inhibiting effect of ATPase activities. However, as seen below, substrates had negligible effects on BmrA.

ATP activities are reported as $\mu\text{mole of ATP/mg/min}$, as usually reported for ABCs, rather than as e.g. turnovers since the number of molecule of ATP per catalytic cycle is likely 2 but still under debate. In some experiments where activities were slightly different from our standard values due to experimental variations in temperature or quality of the coupled enzymes assay, results are depicted in % of the maximum ATPase hydrolysis of *E. coli* proteoliposomes always used as control.

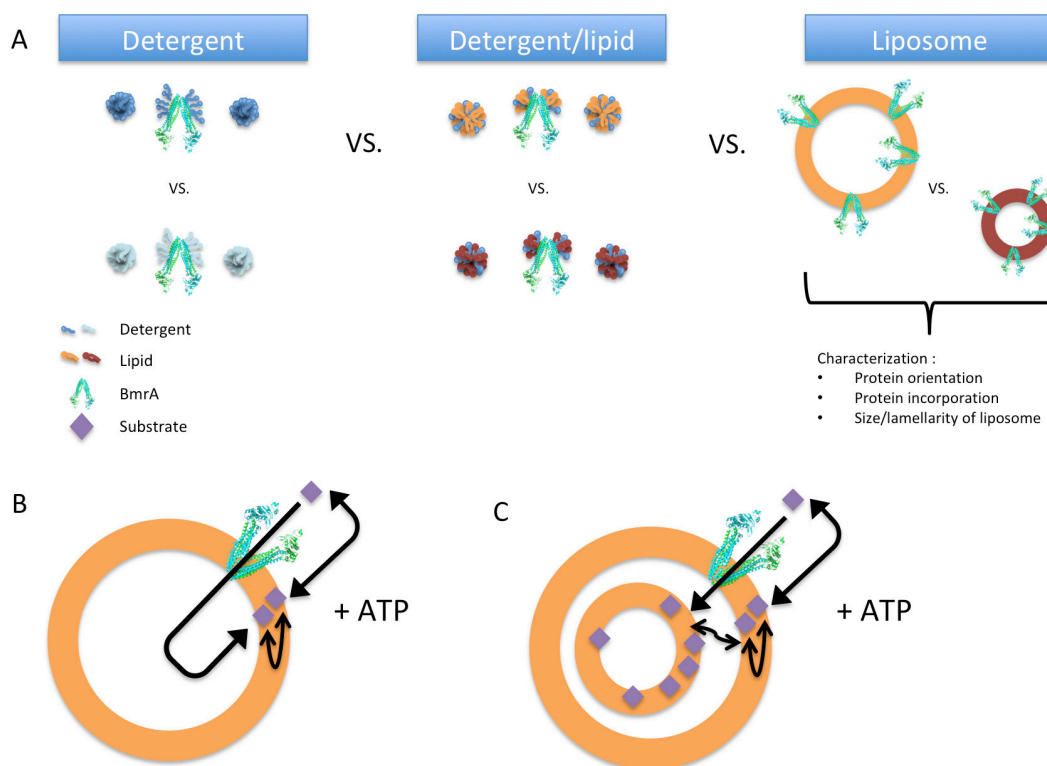


Figure 56 Functional analysis of BmrA according to its surrounding environment.

(A) ATP hydrolysis was studied in micelles of detergent, detergent/lipid mixture and membrane. (B) Substrate transport is often complicated to follow since substrates due to their amphiphilicity do not accumulate in the internal volume of the liposomes but are distributed in the membrane. (C) BmrA substrate transport can be measured with e.g. multilamellar inverted vesicles as with purified inner membrane vesicles of *E. coli*. In this case, the substrates were accumulated in liposomes that were inside.

a. Experimental conditions

1. Inhibition rate of different inhibitors

We selected three inhibitors that were often used to inhibit ATPase activity of ABCs and studied their inhibition rate. AMP-PNP and ATP- γ -S are non-hydrolysable derivative of ATP molecules that inhibit ABCs reversibly in pre-hydrolysis conformation. Addition of ATP molecules in the medium is not required to inhibit proteins with these two inhibitors. Orthovanadate inhibits irreversibly ABCs in the presence of ATP. Orthovanadate forms a complex with Mg and ADP during the first catalytic turnover, which blocks the protein in post-hydrolysis conformation by preventing release of ADP molecules.

ATPase activity was inhibited at approximately 85% for AMP-PNP and 93% for ATP- γ -S (Figure 57). Since ATP hydrolysis inhibition with non-hydrolysable analogs has been measured in the presence of ATP, it is likely that inhibition is complete in the absence of ATP, as e.g. in experiments with GUVs (see Figure 91). The inhibition rate of orthovanadate was 84% that is lower than reported (Steinfels et al., 2004). This may be due to interference of orthovanadate with coupled enzyme assays during activity measurement (J.M. Jault, pers. comm.). Indeed, we found evidence that vanadate effectively inhibited proteins in GUVs experiments (see Sorting of BmrA according to its catalytic state).

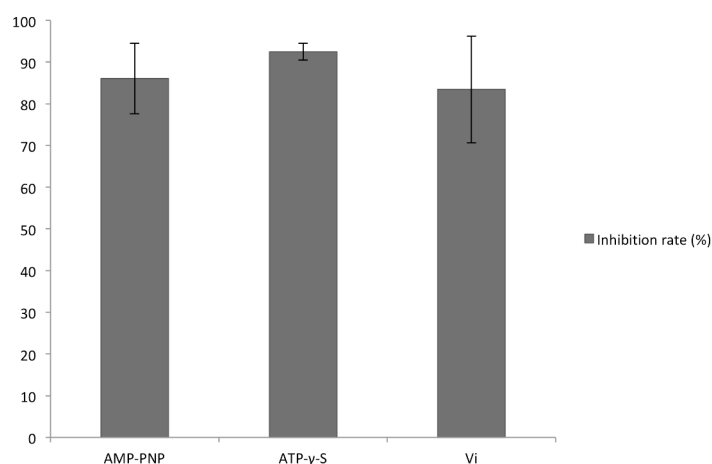


Figure 57 Inhibition rate of different inhibitors.

Inhibition rate was calculated by comparing between ATP hydrolysis before and after addition of 10 mM of AMP-PNP, 5 mM of ATP- γ -S or 1 mM of orthovanadate in the presence of 10 mM of ATP.

2. Effect of substrate on ATPase activity

Effect of vinblastine and verapamil, 2 substrates that were reported to modify ATP activity of BmrA (Steinfels et al., 2004) on ATP hydrolysis, was investigated with BmrA reconstituted in *E. coli* proteoliposomes. Here, we measured the activity at 1.5 mM ATP corresponding to the K_d for ATP and not at V_{max} , to be able to observe a stimulation or inhibition of the activity.

Weak or no substrate effect on ATPase activity was observed in the range of 0.5 – 500 μ M except for 500 μ M of vinblastine (Figure 58). Since the lipid concentration was approximately 500 μ M and since substrates partition in favor of the membrane, it is likely that the concentration of substrate in membrane is larger than the concentration of lipids. Although DLS showed that

the liposome size did not change in the presence of 500 μM of substrates, we did not increase the concentration of the substrates above 500 μM .

This result is slightly different with what has been published in (Steinfels et al., 2004). A low and maximum of 20% stimulation and inhibition effects were observed at low (10 - 20 μM) and high (30 - 80 μM) substrate concentrations, respectively for reserpine, verapamil and vinblastine. It is worth noting that physiological substrates for BmrA are unknown.

Since the effect of these substrates was weak, we performed the following ATPase activity measurements without substrates.

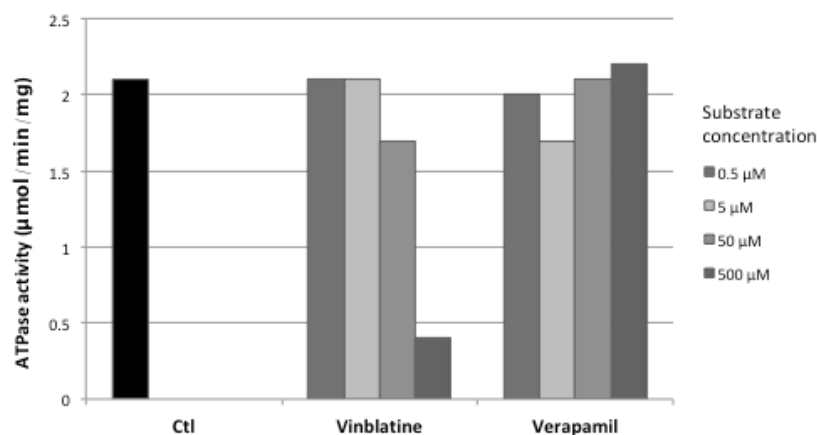


Figure 58 Substrate effects on ATPase activity.

ATPase activities of BmrA reconstituted in *E. coli* proteoliposomes were measured with different concentrations of vinblastine and verapamil at 1.5 mM ATP.

b. ATPase activity of BmrA in micelles of detergent and detergent/lipid

1. ATPase activity depends on the type of detergent

We studied the activity of BmrA solubilized in micelles of different detergents at concentrations above cmc. We calculated the concentration of micelles of detergent to confirm that BmrA was in less than one homodimer/micelle to avoid any protein/protein interaction:

$$[\text{Detergent}]_{\text{micelle}} = ([\text{Detergent}] - \text{cmc}) / \text{Aggregation number of micelle}$$

where aggregation number means number of detergents per micelle. Aggregation numbers of DDM and Triton X-100 were approximately 100 and 115, respectively.

0.5 μM of BmrA homodimer was diluted in approximately 80 μM and 60 μM of micelles of DDM and Triton X-100, respectively. Aggregation number of LMNG is not known. Given that the number of aggregations increases with the decrease in cmc, the aggregation number of LMNG should be higher than that of DDM but it is likely that the concentrations of LMNG micelles remained well above the concentration of homodimers of BmrA. In all cases, BmrA is diluted at less than one homodimer/micelle of detergent.

BmrA was highly active in all 3 detergents (Figure 59) and ATPase activity could be completely inhibited by ATP- γ -S. However, ATPase activities were similar in Triton X-100 or LMNG and 3 times slower in DDM. It is worth noting that we cannot determine whether Triton X-100 and LMNG stimulate or DDM inhibits the activity.

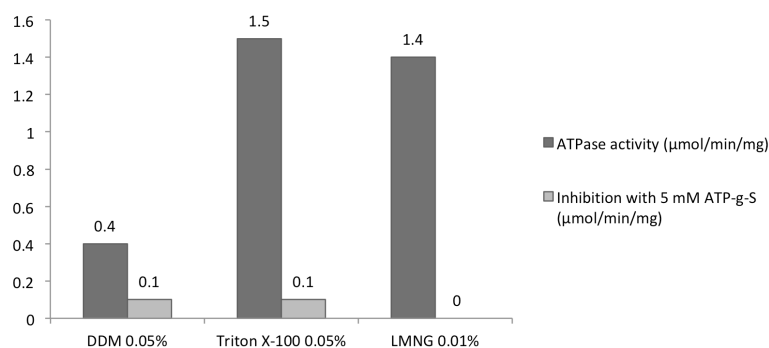


Figure 59 ATPase activity of BmrA solubilized in different detergents.

BmrA WT was purified in 0.05% DDM and diluted in 0.05% Triton X-100 or in 0.01% LMNG in 50 mM MOPS pH 7.5, 150 mM NaCl, 10 mM MgCl₂. Cmc's of DDM, Triton X-100 and LMNG are 0.009%, 0.015% and 0.09%, respectively. Sample was preincubated for 4 min at 37 °C. ATPase activity measurement was initiated by adding 10 mM of ATP at 37 °C. Then, 5 mM of ATP-γ-S was added to inhibit ATP hydrolysis.

2. No lipid specificity on ATPase activity in micelles of detergent/lipid

ATPase activity stimulation in the presence of lipids

We next kept BmrA solubilized in micelles of DDM or Triton X-100 but we doped the micelles with different lipids. We used a mixture of neutral phosphatidylcholine lipids, i.e. Egg PC and 10% of negatively charged lipid, PG.

The presence of lipids increased approximately by 35% the activity of BmrA solubilized in DDM or in Triton X-100 (Figure 60). In the range of 0.03 – 0.1% of Triton X-100, no significant difference of activity was observed. Same results were observed after resolubilizing previously reconstituted BmrA in EPC/PG liposomes (data not shown).

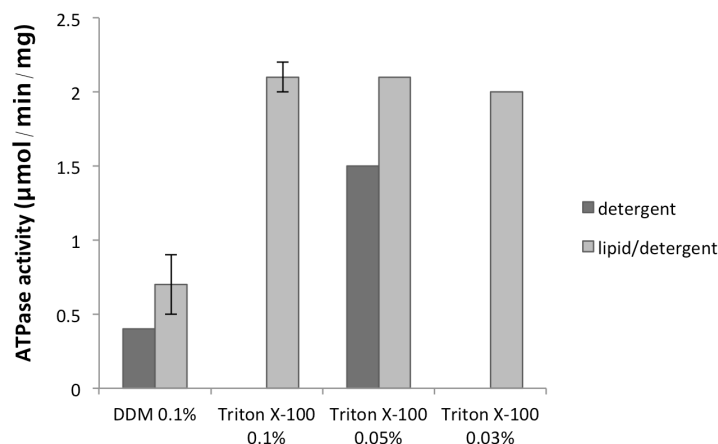


Figure 60 ATPase activity in lipid/detergent micelles.

ATPase activity of BmrA was studied in detergent/lipid micelles with different concentration of detergents. 0.8 μM of BmrA was diluted in 500 μM of EPC/PG (9/1 w/w) solubilized with DDM or with Triton X-100.

ATPase activity according to lipid composition

We next compared the activity of BmrA solubilized in micelles of TX 100 and with EPC/PG lipid mixture or *E. coli* polar lipid extract, two completely different lipid mixtures in both lipid composition and charges.

ATPase activities were stimulated approximately 35% compared to micelles of detergent for both lipid composition (Table 5) but no difference of activity between two lipid compositions was observed.

37 °C 10 mM ATP	ATPase activity ($\mu\text{mol}/\text{min}/\text{mg}$)
<i>E. coli</i> extract lipids /Triton X-100	2.3 ± 0.2
EPC/PG (9/1 w/w) /Triton X-100	2.1 ± 0.1

Table 5 ATPase activity according to lipid composition in micelles of lipid/detergent.

BmrA in DDM 0.05% was added to solubilize *E. coli* lipids or EPC/PG (0.4 mg/ml) in Triton X-100 (0.1%) and ATPase activity was measured.

c. Functional analysis according to lipid composition in membrane

1. Lipid specificity of ATPase activity in membrane

As described in the following experiments, BmrA has been reconstituted in membrane made of various lipid mixtures. As shown below and as reported for most transmembrane proteins, functional reconstitutions can be successfully obtained with non-native lipids. BmrA is a transmembrane protein from the plasma membrane of *B. subtilis*. The closest lipid composition commercially available is *E. coli* polar lipid extract. However, we also used lipids from other sources including from eukaryotes like Egg PC or Brain PS that were either at lower cost than bacterial ones or available. Indeed, these lipids were useful to reveal some properties of lipid/BmrA interactions.

We used *E. coli* polar lipid extract and Egg PC, Egg PA, Brain PS, Cardiolipin (*E. coli*), PG (*E. coli*) and DOPC, DOPG, DOPE synthetic lipids with double acyl chains with a single unsaturation.

BmrA was reconstituted in proteoliposomes made of EPC/PG (9/1 w/w) or of *E. coli* polar lipid extract where no difference of activities was observed in micelles of detergent/lipid.

Activities were increased 1.5 and 3 folds, in EPC/PG and *E. coli* proteoliposomes, respectively, compared to micelles of lipid/detergent (Figure 61). Moreover, ATPase activities were significantly different depending on lipid composition with the highest activity in *E. coli* proteoliposomes.

We cannot distinguish whether the increase in activity is related to detergent elimination and/or lipid stimulation. However, since the detergent is completely eliminated in the membrane, the difference in activity between both lipid mixtures can be attributed to the lipids contributions. The highest activity was measured in *E. coli* polar lipid extract composed of approximately 67% of PE, 23% of PG and 10% of CL.

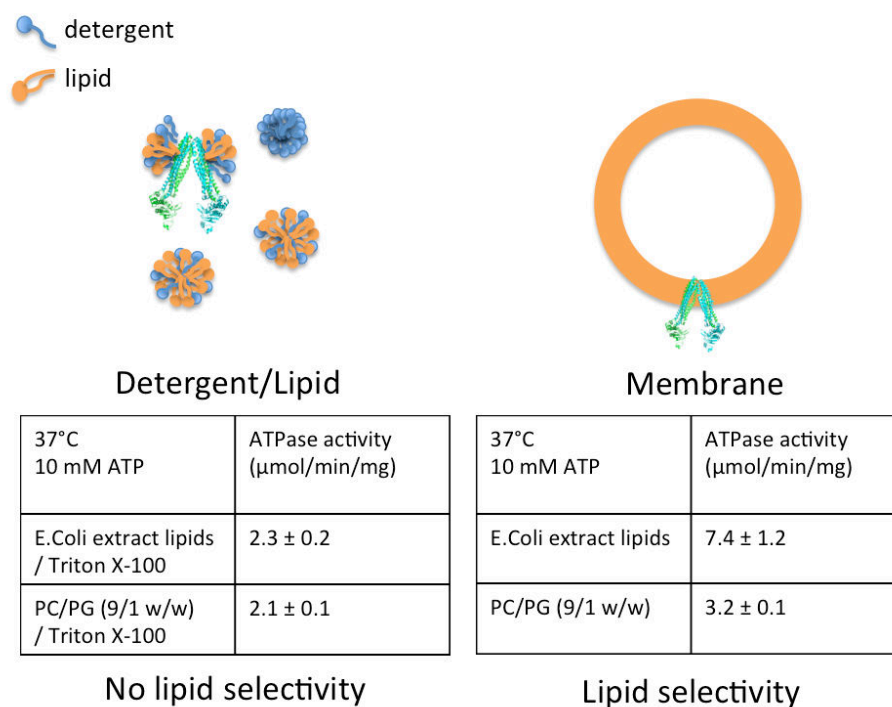


Figure 61 Lipid specificity on ATPase hydrolysis in reconstituted system.

Activities of micelles of detergent were measured as previous experiment (see Figure 60).

We next studied whether specific lipids of *E. coli* lipids were responsible for such stimulation of ATPase hydrolysis.

2. ATPase activity depending on negatively charged lipids

BmrA was reconstituted in PE vesicles, which is the major lipid component of *E. coli* lipids and with increasing amounts of negatively charged lipids, CL or PG. Activity was stimulated 2 and 3 folds in the presence of both negatively charged lipids respectively (Figure 62). A minimum of 10% negatively charged lipids is needed to observed an increase of activity but 10 % was also enough to reach the maximum of stimulation. Since CL lipids have 2 negative charges while PG has one, activity stimulation does not depend on the number of charge but rather on lipid specificity. Interestingly, a mixture of EPE and 10% of PG was enough to reach 89% of activity of *E. coli* liposome.

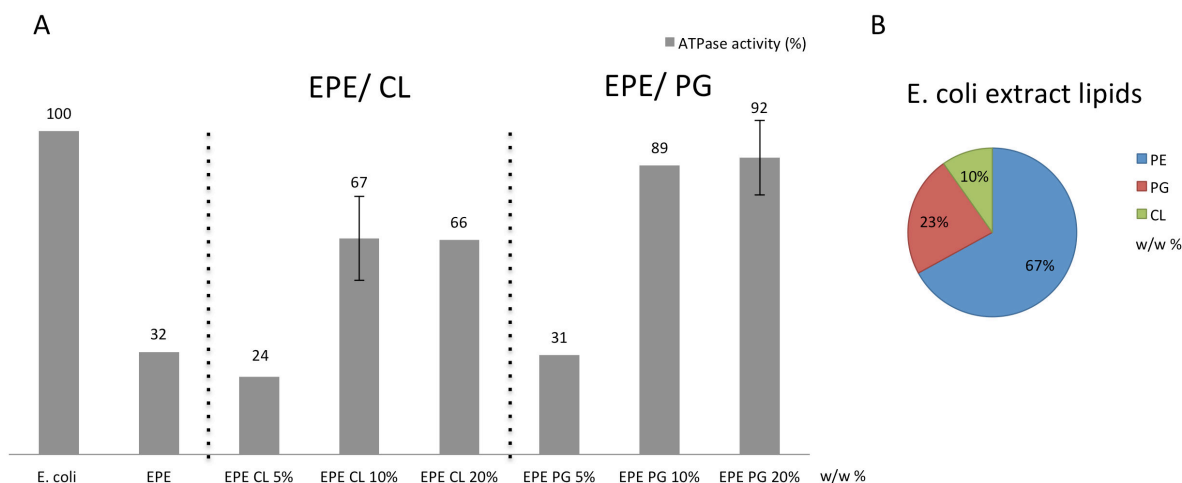


Figure 62 Increase of ATPase activity with increasing amount of negatively charged lipids in PE vesicles.

(A) The amount of negatively charged lipids CL and PG were varied in EPE vesicles. ATPase activities were normalized with respect to that obtained in *E. coli* liposomes because for an unknown reason all activities were higher at that period. (B) Lipid composition of *E. coli* polar extract lipids.

3. ATPase activity in PC vesicles

We also studied ATPase activity with another lipid head group subtype, i.e. phosphatidylcholine. Interestingly, bacterial BmrA still remained highly active in EPC vesicles that are not present in *E. coli* or *B. subtilis* membranes (Figure 63). The effect of 3-fold stimulation of negatively charged lipids was also observed. Moreover, 10% of other negatively charged lipids such as EPA and bPS, two negatively charged eukaryotic lipids also increased ATPase activity (Figure 63B). However, the activities were lower in EPC than EPE liposomes. Addition of 20% and more of EPE lipids in EPC also increased the ATPase hydrolysis. However, EPE led to a maximum of 1.5-folds increase of activity compared to the 3-folds increase by negatively charged lipids.

When compared to the highest activity reported for the *E. coli* lipid proteoliposomes, these results suggest a synergistic stimulation on ATPase activity of PE lipids and negatively charged lipids, especially PG lipids when present in *E. coli* lipid mixtures.

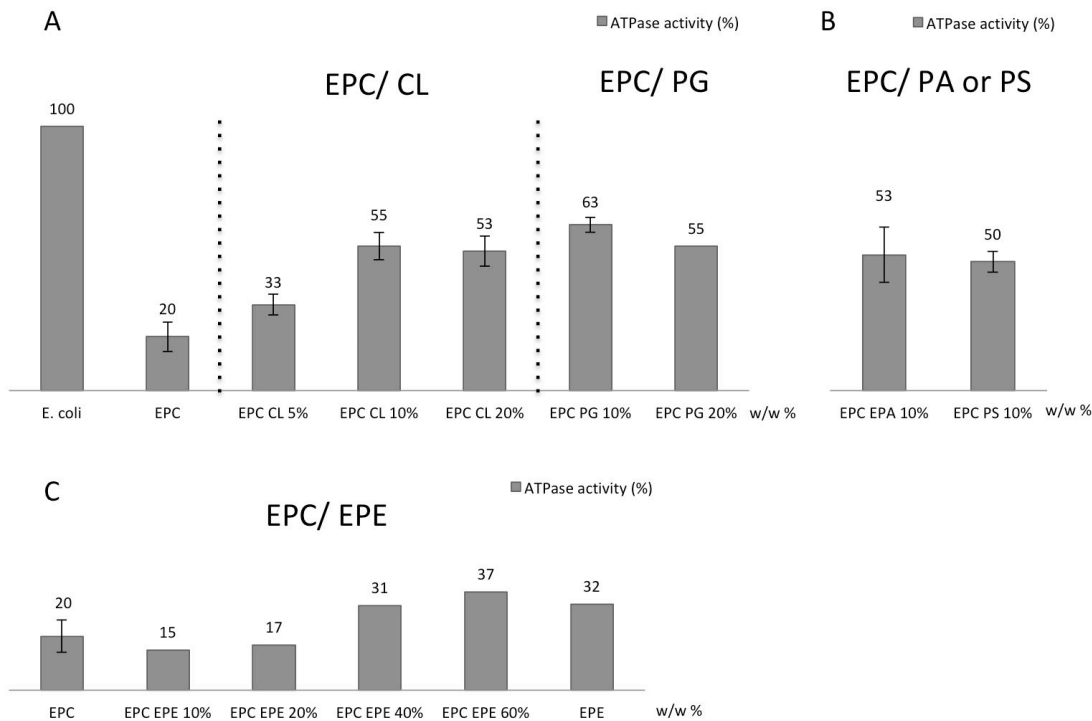


Figure 63 ATPase activity in PC vesicles with increasing amount of negatively charged lipids.

BmrA was reconstituted in EPC vesicles with different amount of negatively charged lipids CL, PG, EPA or PS (A, B) or with neutral lipids EPE (C). ATPase activities were measured and normalized to activity obtained in *E. coli* liposomes.

d. Complete characterization of reconstituted proteoliposomes

We studied in more details the characteristics of BmrA proteoliposomes that may influence the ATPase activity measurement (Figure 10):

- Protein orientation: as liposomes are impermeable to ATP, only proteins with NBDs oriented outside of proteoliposomes, i.e. inside-out orientation are accessible to ATP;
- Incorporation of protein: only protein incorporated in liposomes are fully active;
- Unilamellarity of liposome: if liposomes are multilamellar, only proteins in the external liposomes are accessible to ATP.

We analyzed proteoliposomes made of *E. coli* polar lipid extract and EPC/EPA (9/1) where ATPase activity were significantly different and characterized these factors.

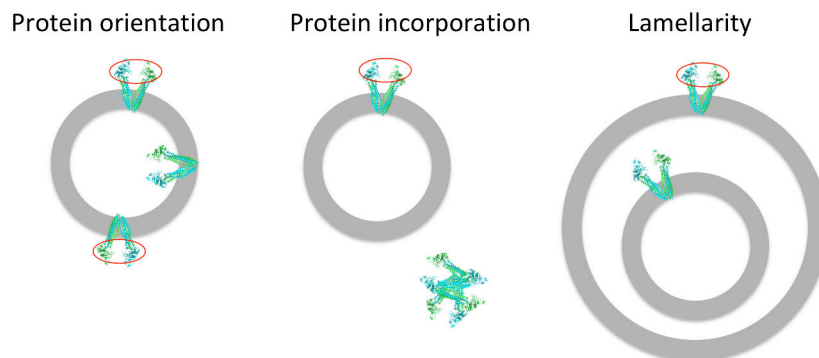


Figure 64 Characterization of reconstituted system.

The factors that influence accessibility of ATP to NBDs were studied: protein orientation, protein incorporation rate and lamellarity of liposomes. Only proteins with the red circle are accessible to ATP or active.

1. Protein orientation

Protein orientation was studied by trypsin digestion of fluorescently labeled BmrA with Alexa488 or Atto610 labeled BmrA at C436 present in NBDs. Trypsin was added to reconstituted system and only NBDs pointing outward proteoliposomes were digested by trypsin. Since one fluorescent probe is labeled per NBD, the percentage of inside-out proteins can be derived from fluorescence in SDS-PAGE gels (Figure 65).

Optimization of trypsin concentration in proteoliposomes

Optimal trypsin concentration was determined for the complete digestion of BmrA solubilized in Triton X100 and then applied to proteoliposomes. BmrA was fully digested at 0.2 w/w protein/trypsin when solubilized in micelles of lipid/detergent (Figure 65, lane 9). At same trypsin concentration, BmrA in proteoliposomes show 22 % of remaining fluorescent protein signal at 65 KDa demonstrating that BmrA was incorporated 78/22 inside-in/inside-out in the population of proteoliposomes. (Figure 65, lane 10). This experiment also shows that the proteoliposomes were impermeable to trypsin.

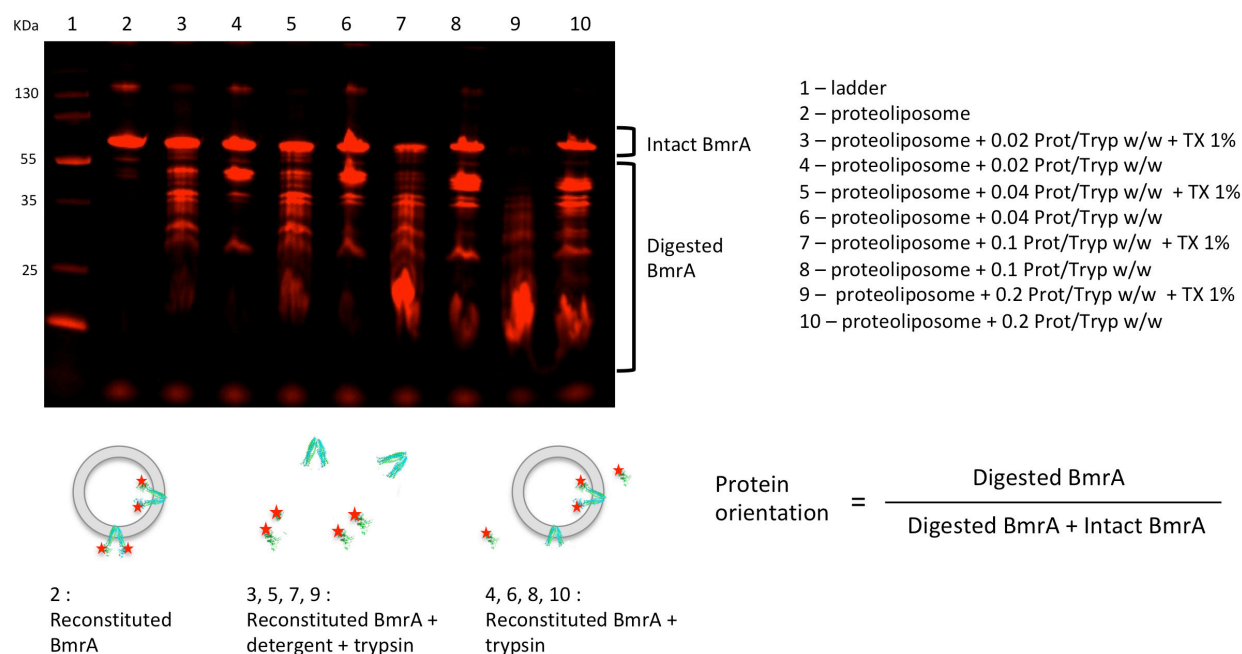


Figure 65 Optimization of trypsin concentration for BmrA digestion in reconstituted system.

Atto610-BmrA was reconstituted in EPC/EPA (9/1 w/w). Proteoliposomes were incubated with increasing concentration of trypsin (0.02 – 0.2 BmrA/trypsin w/w) for 30 min at 20 °C under magnetic stirrer agitation. In the same conditions, Triton X-100 (1%) was added as a control where proteoliposomes were solubilized with all proteins accessible for digestion. BmrA (0.1 µg) was analyzed on 12% SDS-PAGE gel.

Orientation of BmrA according to lipid compositions and reconstitution methods

So far, proteoliposomes were reconstituted from micelles of proteins/ lipids/detergents. Proteins are generally oriented 50/50 inside-in/inside-out although we also demonstrated that BmrA was more asymmetrically oriented. A 100% orientation is usually obtained by a method of direct incorporation of proteins into preformed liposomes destabilized by subsolubilizing concentrations of detergent. Proteins are inserted through their hydrophobic domain leaving their more hydrophilic domain pointing outward the membrane. In the case of BmrA it is expected that BmrA would incorporate inside-out leaving the NBDs pointing outward.

We performed both types of reconstitution of Atto610-BmrA in EPC/EPA (9/1 w/w) and *E. coli* lipids and compared orientations. As expected, direct incorporation increased the final % of inside-out orientation (Figure 66C). However, direct incorporation required more reconstitution steps and with lower reproducibility. In addition, cryo-EM images show that sizes and lamellarity of *E. coli* proteoliposomes were heterogeneous likely because preformed liposomes were fused during the first step of incubation with detergent. Moreover, reconstitution from solubilized protein/detergent/lipid mixtures led to non-symmetrical incorporation with 75% inside-out orientation. Therefore, we performed reconstitutions from micelles of detergent/lipid/protein for further studies.

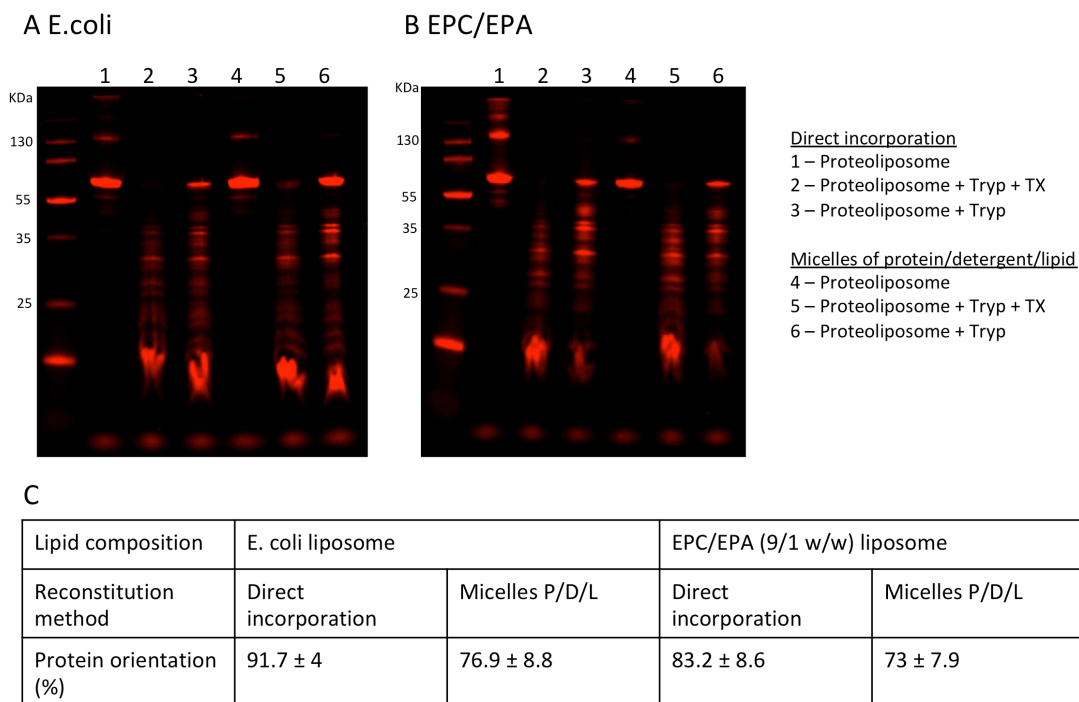


Figure 66 Orientation of BmrA according to lipids composition and reconstitution methods.

(A, B) Atto610-BmrA was reconstituted in *E. coli* or EPC/EPA proteoliposomes by direct incorporation method or from micelles of protein/detergent/lipids. Proteoliposomes were incubated with trypsin at 1 protein/trypsin w/w for 30 min at 20 °C. Protein orientation rates were analyzed as in Fig. 11 (C). Experiments were repeated at least 3 times.

Different trypsin digestion in post-hydrolysis conformation

We compared trypsin digestion of BmrA in apo conformation and after addition of ATP-Vi in post-hydrolysis conformation.

Proteolysis of ATP-Vi BmrA by trypsin was less efficient compared to apo-conformation in both micelles of detergent/lipid or in reconstituted system. This result suggests that conformational change occurs in the NBDs in the presence of ATP and Vi that reduced the accessibility of trypsin to C436 in NBDs.

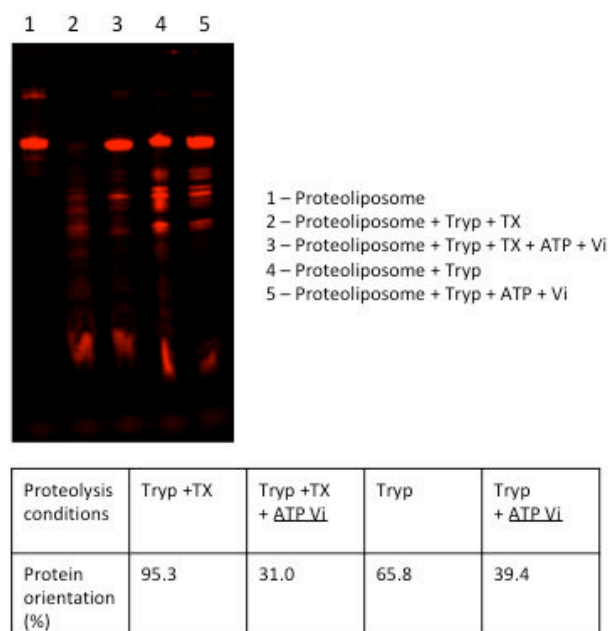


Figure 67 Different accessibilities of trypsin to C436 in apo and ATP-Vi states

(A) Apo Atto610-BmrA was reconstituted in *E. coli* liposomes. After reconstitution, some sample was incubated with 1 mM of orthovanadate and 1 mM of ATP for 10 min at room temperature.

2. Protein incorporation

Proteins incorporated in liposomes are fully active while aggregated proteins are likely inactive. We measured the yield of protein incorporation in proteoliposomes by flotation by separating proteoliposomes, liposomes devoid of proteins and aggregated proteins. Aggregated proteins are positioned at 30% of sucrose while proteoliposomes are positioned at 5 - 20% of sucrose depending on protein density in the liposomes.

Protein incorporation yields in EPC/EPA and E. coli liposomes

In both lipid compositions, 98% of BmrA was incorporated. The repartition of BmrA among the population of liposomes is homogenous in EPC/EPA (Figure 68 B, fraction 1) and broader in *E. coli* proteoliposomes (Figure 68 A, fractions 2, 3). Reconstitution with *E. coli* lipid led to proteoliposomes with a lipid/protein ratio higher than the initial solubilized LPR, coexisting with protein-free liposomes.

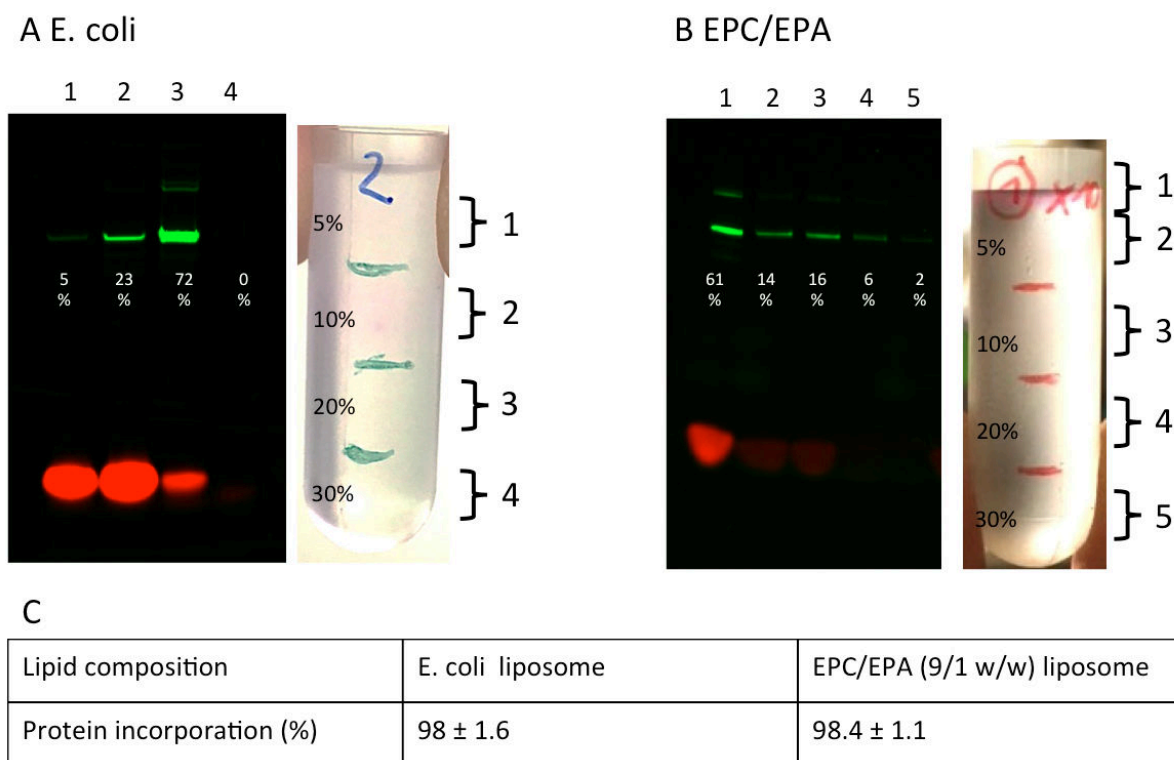


Figure 68 Protein incorporation rate in *E. coli* and EPC/EPA liposomes.

Alexa488-BmrA was reconstituted from micelles of lipid/detergent/protein, at lipid/protein 200 w/w in *E. coli* and EPC/EPA (9/1 w/w). For both lipid compositions, 0.5% w of Texas Red DHPE lipids were introduced as lipid marker. Flotation was performed with 300 μ g of liposomes. Fractions were collected and presence of liposomes and proteins were analyzed on 12% SDS-PAGE gel by fluorescence (A, B). (C) Average incorporation rate was calculated by the formula $PI = \frac{1 - \text{Intensity of fluorescence of protein in the 30\% sucrose fraction}}{1 - \text{Intensity of fluorescence of protein in the 5\% sucrose fraction}}$.

ATPase activity does not depend on protein density

We studied whether protein density in vesicles influences ATPase activity of BmrA by measuring ATP hydrolysis in proteoliposomes reconstituted at different lipid/protein ratio.

As shown in Figure 69, protein density did not affect ATPase activity of BmrA in both lipid compositions. This suggests the absence of protein/protein functional interactions in vesicles. This result also demonstrates that the reconstitution is as efficient whatever lipid/protein ratio, i.e. that orientation of protein, protein incorporation yields and lamellarity of liposomes are the same in the range of 20 – 300 of lipid/protein w/w ratio.

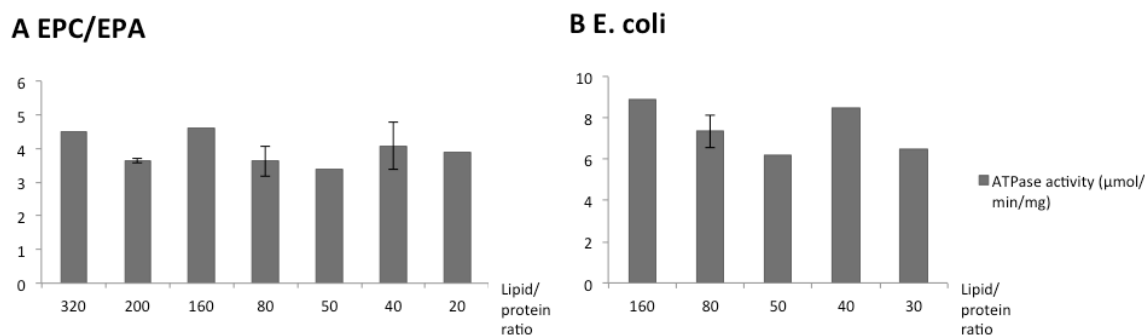


Figure 69 ATPase activity according to lipid/protein ratio.

3. Unilamellarity and sizes of liposomes

Lamellarity and sizes of liposomes were investigated by cryo-electron microscopy. BmrA was reconstituted in EPC/EPA (9/1 w/w) and *E. coli* proteoliposomes and then reconstitutions were imaged by cryo-EM.

In both cases, 100% of proteoliposomes were unilamellar (Figure 70 A, B). Besides, the size of *E. coli* proteoliposomes was homogeneous with approximately 60 nm of diameter while those of EPC/EPA were heterogeneous with small 20 nm (white arrows) and larger up to 150 nm diameters. The sizes of proteoliposomes were investigated in more detail in next chapter, Liposome size.

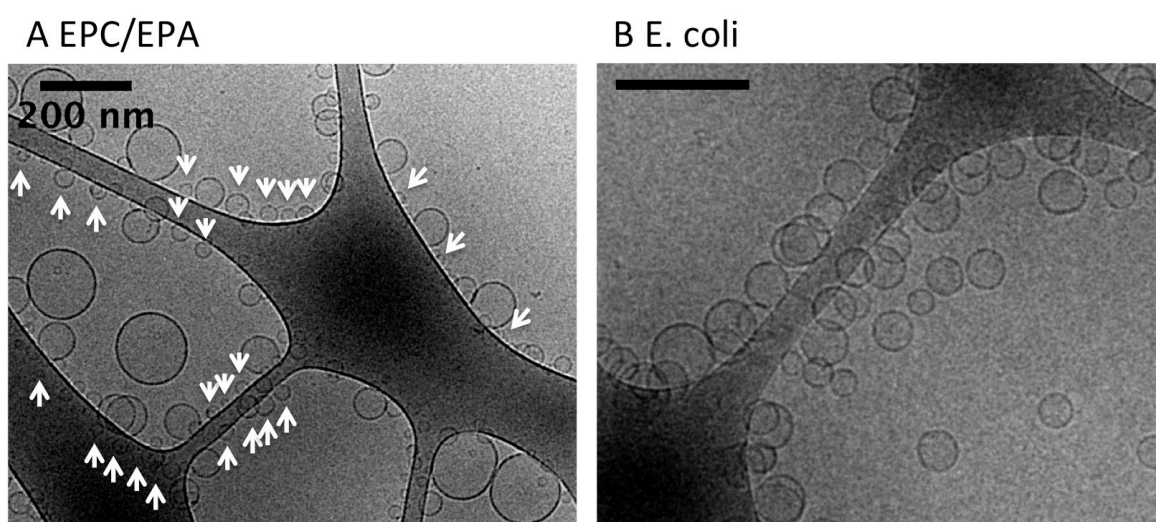


Figure 70 Unilamellarity and size of liposomes studied by cryo-EM.

(A, B) Images of EPC/EPA (9/1 w/w) and *E. coli* proteoliposomes by cryo-EM show unilamellar liposomes. White arrows indicate proteoliposomes smaller than 20 nm of diameter.

e. Characteristics of EPC/EPA and *E. coli* proteoliposomes

Lipid composition	ATPase activity ($\mu\text{mol}/\text{min}/\text{mg}$)	Protein orientation (%)	Protein incorporation (%)	Size of liposome (diameter in nm)
EPC / EPA (9/1 w/w)	3.9 ± 0.8	74 ± 2	98 ± 1	Heterogeneous $\approx 20 + 150$
<i>E. coli</i> lipid extract	7.4 ± 1.2	77 ± 9	98 ± 2	Homogenous ≈ 60

Table 6 ATPase activity measurement between EPC/EPA and *E. coli* proteoliposomes

f. Conclusion

In this chapter, ATPase hydrolysis of BmrA was investigated according to its surrounding membrane environment. In micelles of detergent, ATPase activity depends on the type of detergent, is stimulated by the addition of lipids but without lipid specificity. In reconstituted membranes, the activity significantly increases up to 15 folds depending on the lipid composition. Negatively charged lipids such as CL, PG, PA and PS stimulated the activity. ATPase activity was the highest in PE based vesicles, E. coli and PG/PE 1/9 w/w liposomes. Proteins were also active in PC vesicles, with similar stimulation by negatively charged lipids. These data suggest that in E. coli or B. subtilis native membranes, both PE and negatively charged PG lipids contribute to the high ATP hydrolysis of BmrA.

We also have compared ATPase activity in EPC/EPA and E. coli liposomes with fully characterized reconstituted systems in terms of protein incorporation and orientations, size and lamellarity of liposomes. With all characteristics similar, ATPase activity was significantly higher in E. coli than EPC/EPA proteoliposomes. However, E. coli proteoliposomes were significantly smaller than EPC/EPA liposomes questioning if membrane curvature of proteoliposomes may influence ATP hydrolysis.

II. Functional analysis according to membrane curvature

The variation in proteoliposome size changes membrane curvature and tension. Membrane curvature can be measured by DLS or cryo-EM. Membrane tension is not accessible in small liposomes but can be measured in experiment in GUVs (see Sorting and spatio-temporal distribution of BmrA in curved membrane according to its catalytic states). Cryo-EM imaging was performed by A. Di Cicco, I prepared the liposomes and analyzed the data.

a. Liposome size

1. Comparison between DLS and cryo-EM images

By comparing the size distribution of liposomes by the DLS with cryo-EM images, we found that measurements with cryo-EM images were more accurate. For example, the EPC/EPA liposomes measured by DLS show a broad distribution of sizes between 25 and 110 nm of radius with a maximum peak at 50 nm of radius as shown in Figure 71A. The distribution shows a shoulder (red arrow), suggesting a heterogeneous population. The same EPC/EPA liposomes in the cryo-EM images show that all liposomes were unilamellar (see Unilamellarity and sizes of liposomes). In addition, the size distribution revealed 2 distinct populations with small liposomes ($20\text{ nm} < \varnothing < 40\text{ nm}$) and liposomes between 50 - 80 nm radii. DLS measurements were more consistent with homogeneous populations of liposomes such as *E. coli* liposomes even if % of large liposomes were overestimated (Figure 71 C, D).

For the following experiments, we used cryo-EM images for accurate distribution of populations and DLS for a first comparison between vesicles.

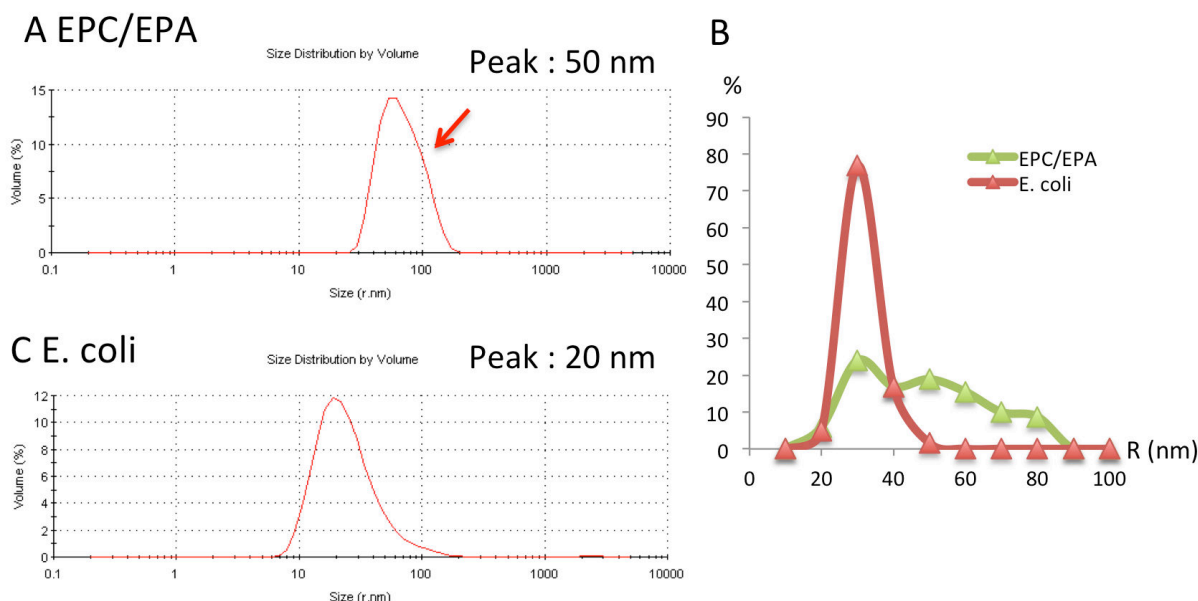


Figure 71 Comparison of size distribution between DLS and cryo-EM images.

Size distributions were studied by DLS (A, B) or based on cryo-EM images (see Figure 70) with approximately 1600 vesicles. Small liposomes $< 20\text{ nm}$ in radius are slightly underestimated in cryo-EM measurements.

2. Measurement of sizes of liposomes from Cryo-EM images

To get better statistics on size distribution of liposomes by cryo-EM images, C. Caporal (UMR168) wrote a program based on contour measurements. The program consists of applying a canny edge detector and a circle Hough transforms detection using OpenCV. The software threshold parameters were set manually by the user for each image.

As shown in Figure 72, the program detects well homogeneous liposome populations. However, the program slightly underestimates small liposomes coexisting with larger vesicles (Figure 72B). In all cases, the measurements were much more accurate than in DLS.

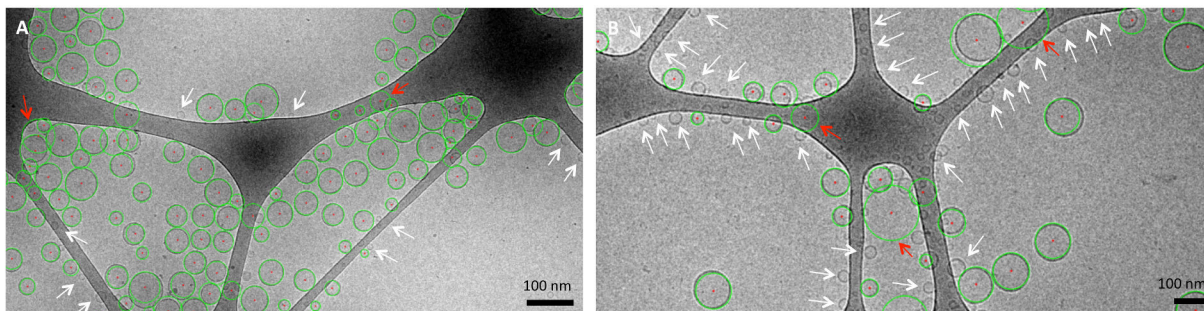


Figure 72 Detection of liposomes on cryo-EM images for homogeneous and heterogeneous sizes.

The quality of detection of liposomes was compared between homogenous (A) and heterogeneous (B) populations of liposomes. White arrows indicate liposomes that are not detected and red arrows indicate detection of liposomes that do not exist.

We carried out studies on liposome size in the absence of proteins because: (i) we would have consumed a lot of protein; (ii) liposome size was independent of the presence of low protein density protein, e.g. at 40 lipid/protein w/w where ATP hydrolysis assays are performed (Figure 73). This result also suggests that proteins have a negligible effect on the mechanism of proteoliposomes formation at low protein density.

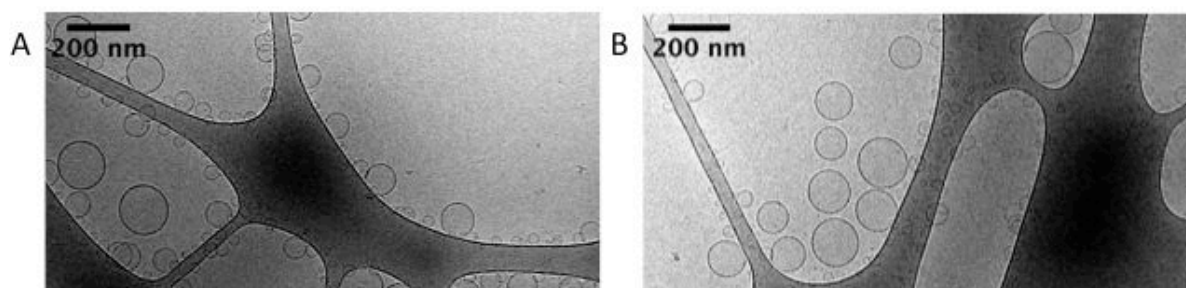


Figure 73 Same population of liposomes and proteoliposomes at low lipid/protein ratio.

EPC/EPA vesicles were reconstituted without (A) and with (B) BmrA. No difference on liposome sizes was observed between in the presence (A) or the absence (B) of BmrA in EPC/EPA 9/1 w/w.

Overall, we observed 3 major types of liposome populations (Figure 74):

- Homogenous population of small liposomes ($\varnothing \approx 20-60$ nm);
- Broad and homogenous population of liposomes ($\varnothing \approx 60-150$ nm);
- Heterogeneous population with mixture of small and large liposomes.

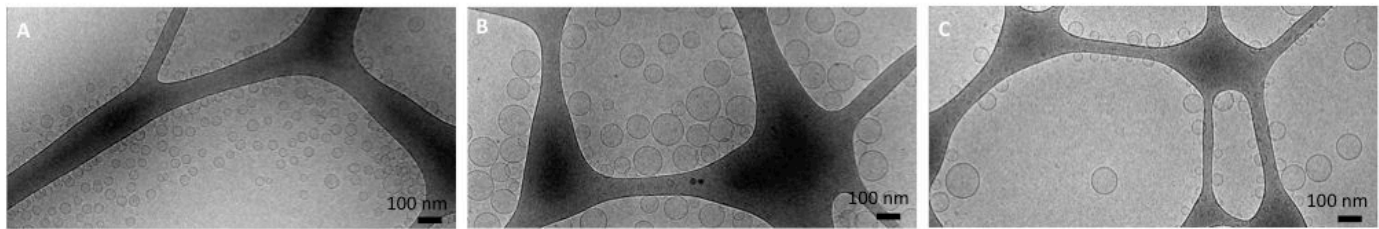


Figure 74 Different populations of liposomes reconstituted by detergent removal.

Three major populations of liposomes were observed: (A) homogenous population of small liposomes, (B) broad and homogenous population of liposomes and (C) heterogeneous population of small and large liposomes.

We observed different population of liposomes depending on the lipid compositions:

- *E. coli* liposomes were small and homogeneous (60 nm in diameter) (Figure 75). Similar but slightly smaller population of liposomes was produced with EPE/PG 80/20 w/w (50 nm in diameter).
- EPC liposomes were large and homogeneous (100-150 nm diameter) (Figure 76).
- Incorporation of EPE in EPC membranes decreased the size of liposomes with increasing amount of EPE but population of vesicles remains homogeneous (Figure 76).
- Incorporation of negatively charged lipids such as EPG or EPA led to the formation of small liposomes coexisting with large liposomes (Figure 77).
- Incorporation of negatively charged brain-PS in EPC showed an opposite behaviour to that of EPC/EPA or EPC/PG. Small liposomes were not observed and the population of liposomes remained homogeneous and large.

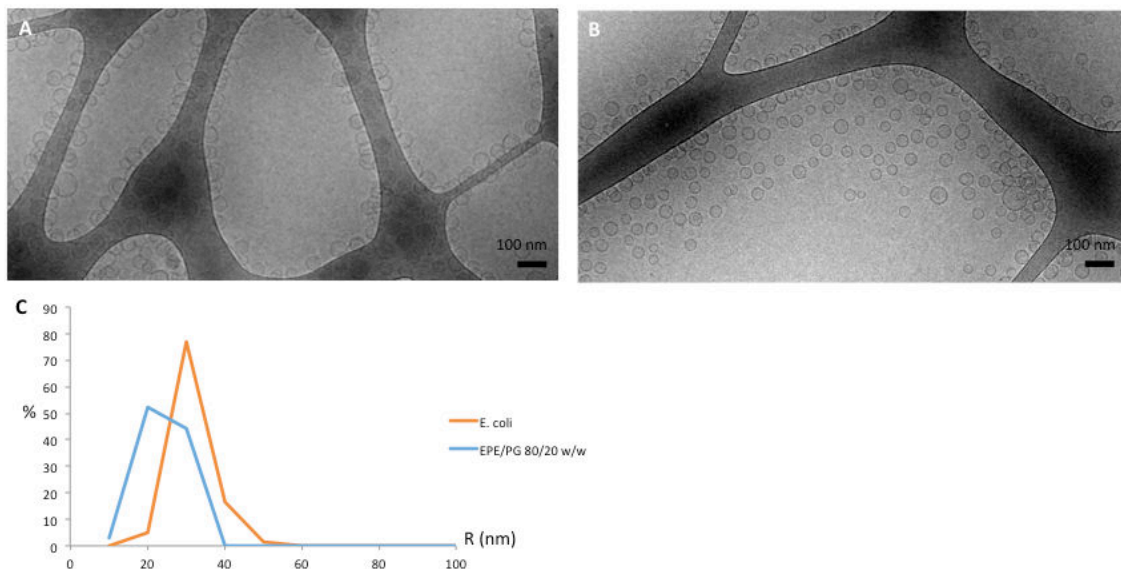


Figure 75 Homogenous small liposomes made of *E. coli* lipid extract or EPE/PG 8/2 w/w lipid mixture.

(C) Approximately 1600 liposomes were analyzed.

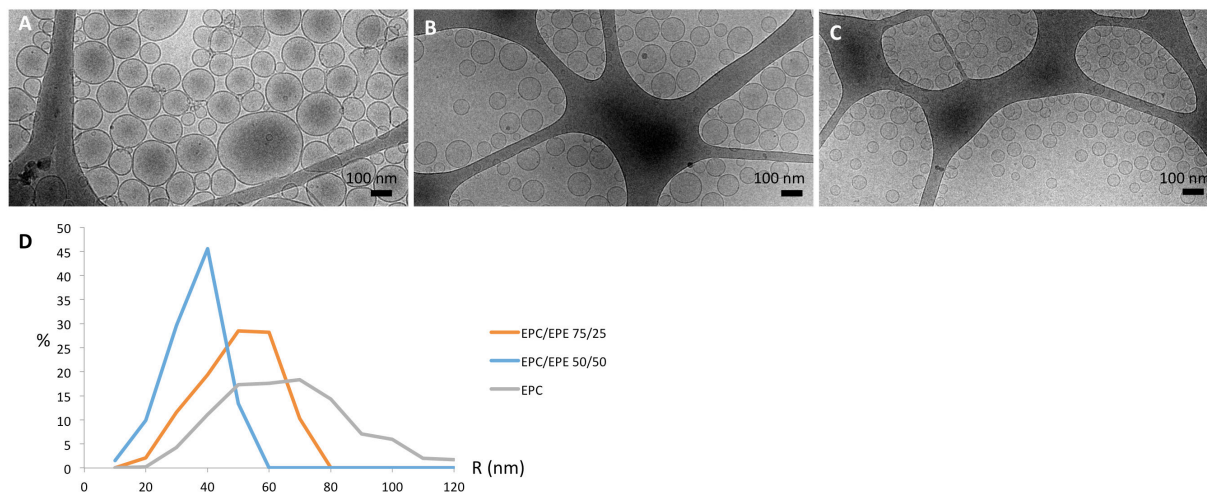


Figure 76 Decrease of sizes of liposomes with increasing amount of EPE in EPC vesicles.

(A) EPC, (B) EPC/EPE 75/25 w/w (C) EPC/EPE 50/50 w/w. (D) Approximately 1400, 900 and 1500 liposomes were analyzed.

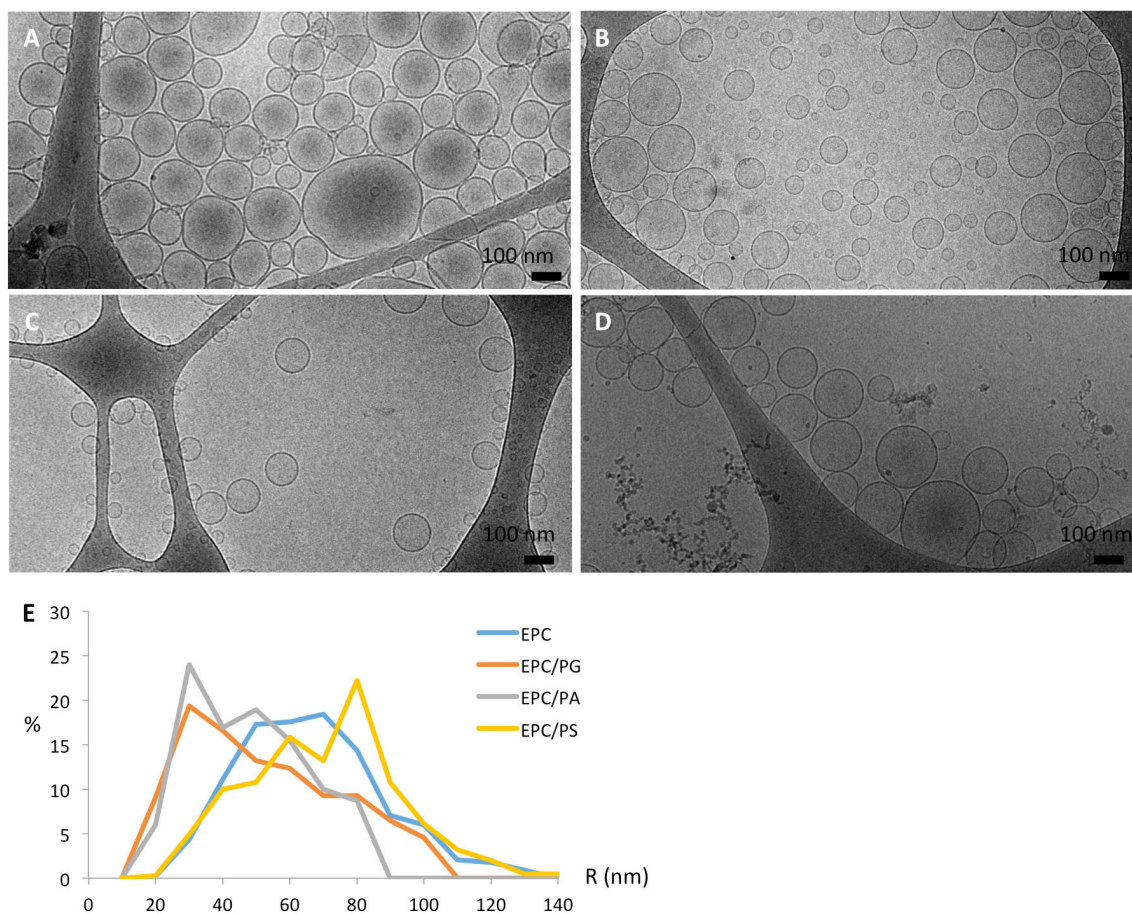


Figure 77 PG or PA but not PS in PC membranes led to the formation of heterogeneous populations of liposomes.

(A), EPC/PG 9/1 w/w (B), EPC/PA 9/1 w/w (C) and EPC/PS 9/1 w/w. Approximately 1400, 1300, 1700 and 400 liposomes were analyzed in (A), (B), (C) and (D) respectively. Small liposomes < 20 nm radius in (B) and (C) are slightly underestimated.

As EPC is a mixture of aliphatic chain lipids of variable lengths from C14 to C22 with 0, 1 to 2 unsaturations, we reconstituted liposomes with DOPC, mono-unsaturated C18 chains, mixed with DOPE or DOPG (Figure 78). Similar results as for EPC vesicles were found with DOPC; the presence of DOPE homogeneously decreases the size of liposomes and the presence of DOPG led to vesicles with small diameters.

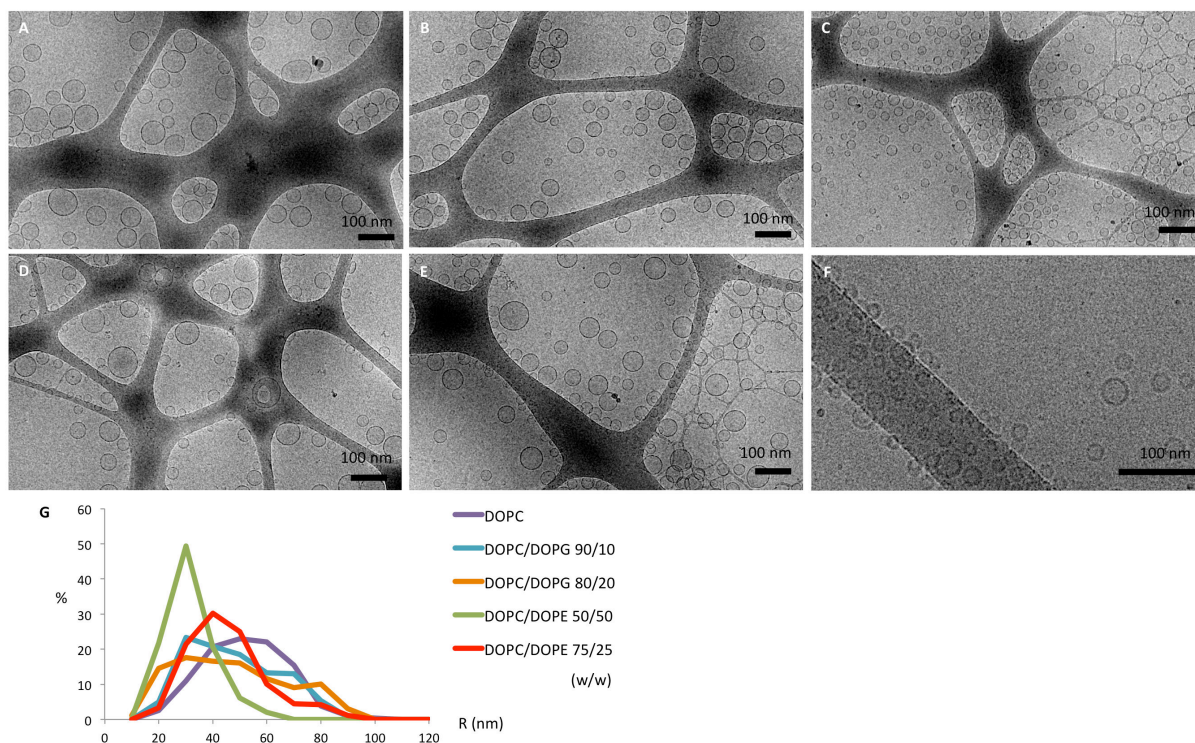


Figure 78 Liposome sizes of DOPC and DOPC mixtures.

DOPC (A), DOPC/DOPG 9/1 w/w (B), DOPC/DOPG 8/2 w/w (C), DOPC/DOPE 75/25 w/w (D), DOPC/DOPE 5/5 w/w (E) were reconstituted and their sizes were analyzed with approximately 800, 1600, 1200, 1100 and 1300 liposomes, respectively (G). (F) DOPC was reconstituted at 4 °C and small liposomes were observed. Images could not be analyzed because image contrast was not high enough to detect liposomes.

3. Liposome size modulation with same lipid composition

We varied reconstitution parameters such as ionic strength, temperature and rate of detergent removal that may interfere with the liposomes formation with EPC/PG 9/1, EPC/EPA 9/1, or E. coli lipid mixtures.

In the EPC/PG mixtures, increasing concentration of NaCl to 300 mM reduces the proportion of small vesicles (Figure 79). This confirmed that small liposomes observed in similar mixtures with negatively charged lipids are likely related to the presence of negatively charged lipids that are screened in the presence of high salts.

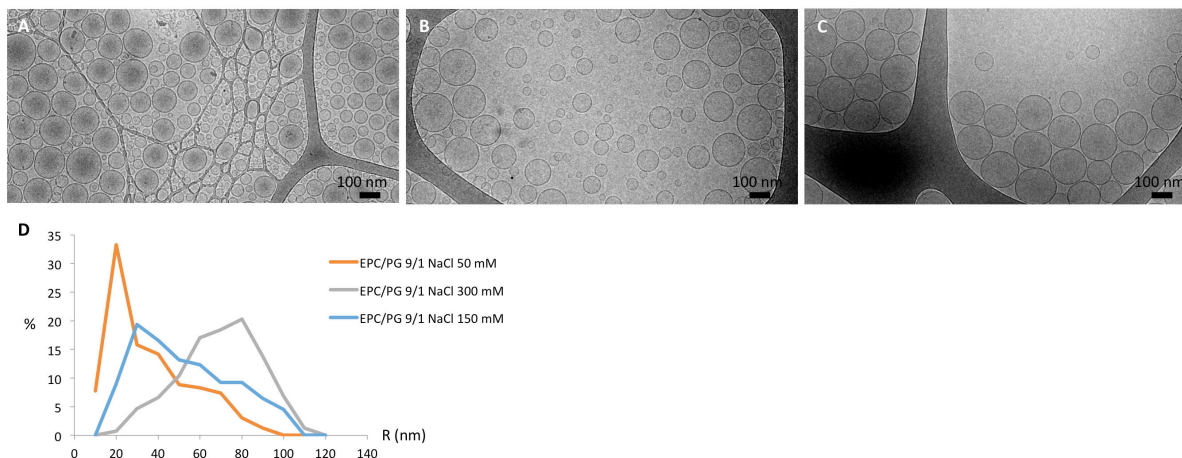


Figure 79 Effect of ionic strength on liposome size.

EPC/PG (9/1 w/w) was reconstituted at 50 mM (A), 150 mM (B) and 300 mM (C) of NaCl. (D) Size distributions were analyzed from cryo-EM images with approximately 2700, 1300 and 500 liposomes.

EPC/EPA liposomes reconstituted at 4 °C were small and homogeneous (\varnothing 20-40 nm) than those at 20 °C (Figure 80). This effect was also found with EPC vesicles alone and with PE, PA, PG, PS and CL and thus can be attributed to the presence of EPC lipids. It is worth noting that formation of DOPC vesicles at 4 °C also led to small liposomes (Figure 78F).

We also observed that liposome size decreased with increasing rates of detergent removal but decrease of sizes was not as drastic as the effect of temperature (data not shown).

We also tried to vary the size of *E. coli* liposomes by changing the reconstitution parameters such as temperature, detergent removal rate, and using other detergents but the size remained unchanged with always a homogeneous population of small vesicles.

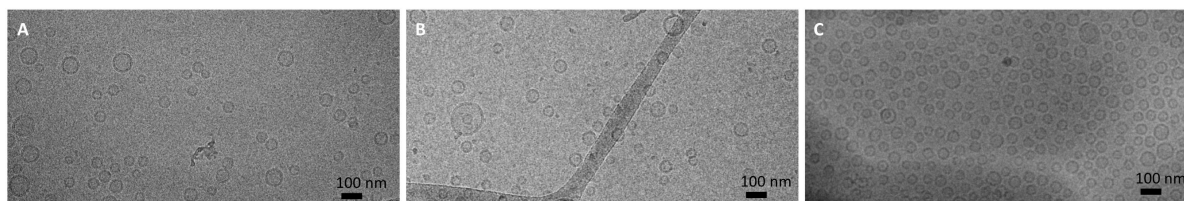


Figure 80 Reconstitution at 4 °C of EPC containing liposomes led to small liposomes.

Reconstitution at 4 °C led to formation of small liposomes of EPC (A), EPC/EPA 9/1 w/w (B) and EPC/PS 9/1 w/w (C). Images could not be analyzed because image contrast was not high enough to detect liposomes but the homogeneity and the averaged size can be estimated.

b. ATPase activity of BmrA is decreased in highly positively curved membrane

1. ATPase activity depending on membrane curvature

We compared ATPase activity of BmrA reconstituted with the same lipid mixture but forming two populations of very different sizes. For this, we reconstituted EPC/EPA and EPC/PS at 20 °C and 4 °C to obtain large and small liposomes, respectively and after reconstitution, ATPase activities were measured at 37 °C (Figure 81).

In all case, we observed a strong decrease of ATP hydrolysis by a factor of 2 when liposome size decreased by a factor of 2-3.

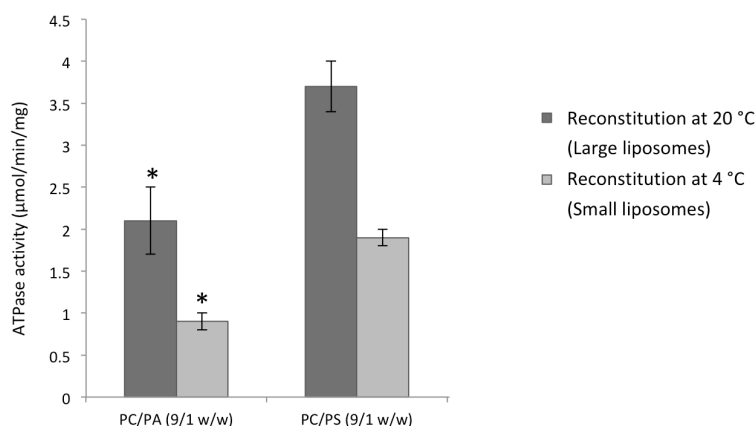


Figure 81 ATPase activity according to membrane curvature.

BmrA was reconstituted in EPC/EPA (9/1 w/w) or EPC/PS (9/1 w/w) either at 20 °C or at 4 °C. *ATPase activity of EPC/EPA proteoliposomes were measured at 25 °C instead of 37 °C.

2. Characterization of EPC/EPA proteoliposomes with two different sizes

To rule out the possibility that differences in activity in small and large proteoliposomes were related to proteoliposomes characteristics, we measured the orientation and incorporation efficiency of BmrA in both conditions.

The orientations of BmrA in EPC/EPA proteoliposomes reconstituted at RT and at 4 °C were 70% and 94% inside-out, respectively (Figure 82D). Proteins were fully incorporated into proteoliposomes of different sizes as shown by the colocalisation of lipid and protein fluorescence and the absence of protein aggregates at 30% sucrose (Figure 82C). The lipid-protein ratio in proteoliposomes is thus lower than in the initial solubilized mixture.

This experiment suggests that small proteoliposomes contained higher protein density and inside-out orientation than larger proteoliposomes although they hydrolyze ATP at significantly lower rate. This is first evidence that high membrane curvature may decrease the ATPase activity of BmrA, at least for vesicles smaller than 40 nm in diameter.

All together, we now can compare ATPase activity according to lipid composition and membrane curvature. As the highest activity was observed in small *E. coli* vesicles compared to larger EPC/PG or PC/PE vesicles, this suggests that the contribution of the lipid composition is predominant over membrane curvature to the ATPase activity.

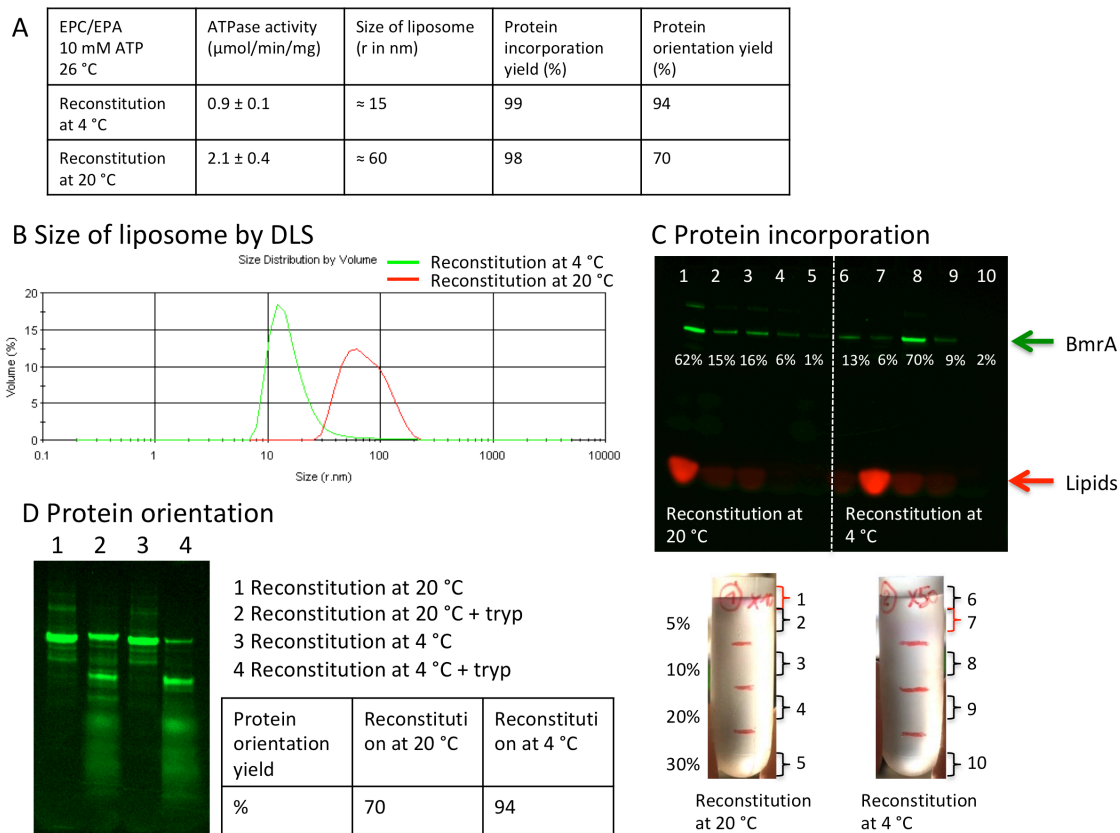


Figure 82 Characterization of EPC/EPA liposomes with different sizes.

However, the distribution of proteins in proteoliposomes was very different. In the large and small proteoliposomes formed at RT, proteins were overwhelmingly distributed throughout the vesicles and there were no protein-free vesicles (lane 1). The protein lipid ratio in proteoliposomes therefore corresponded to the initial solubilized mixture. In contrast, for reconstitutions in small liposomes, proteins were associated with few lipids (lane 8) and protein-free liposomes were formed (lane 6), similar to previously shown for *E. coli* proteoliposomes (see **Figure 68**).

III. Sorting and spatio-temporal distribution of BmrA in curved membrane according to its catalytic states

a. Experimental approaches

In order to understand the role of membrane curvature and tension on BmrA, we studied BmrA reconstituted in GUVs where these two parameters can be controlled (see Reconstitution into GUVs). **Nanotube-pulling experiments were performed by A. J. Kumar from the group of P. Bassereau (UMR 168, Institut Curie) with our continuous inputs on the formation of GUVs containing BmrA and on the design of functional experiments in GUVs.** A. K. Mahalka optimized the final steps of GUVs' growth by electroformation, performed tube pulling experiments and data analysis. **We discussed together the data that I present below.**

My main contributions in this work were:

- Optimization of the first steps of reconstitution of BmrA in GUVs
- Design of functional assays of BmrA in GUVs
- Design of experiments to measure the orientation of BmrA in GUVs
- Discussion and interpretation of the results

b. Reconstitution methods and challenges

1. Fusion of small proteoliposomes to GUVs

Preliminary experiments of reconstitution of BmrA in GUVs were performed by the methods of fusion of small proteoliposomes to GUVs in the presence of detergent or by direct incorporation into detergent destabilized GUVs, as successfully reported for different proteins (Dezi, PNAS 2013).

Fusion of small proteoliposomes containing Alexa488-BmrA to pure lipid GUVs was performed in the presence of sub-solubilizing concentrations of Triton X-100 (Figure 83A). Fluorescent lipids were only added in proteoliposomes as a fusion marker. Detergents were further removed by BioBeads.

Fluorescence of both lipids and proteins were observed in GUVs meaning that the proteoliposomes were fused to GUVs (Figure 83B-D, arrows). As the detergent concentration increased, there was more fusion with higher protein and lipid fluorescence intensities in GUVs. Successful reconstitutions were obtained but the reproducibility was low. Direct incorporation method was also performed, but no relevant results were observed. We thus turned to the method of the incorporation of BmrA starting from the swelling of a film of small proteoliposomes.

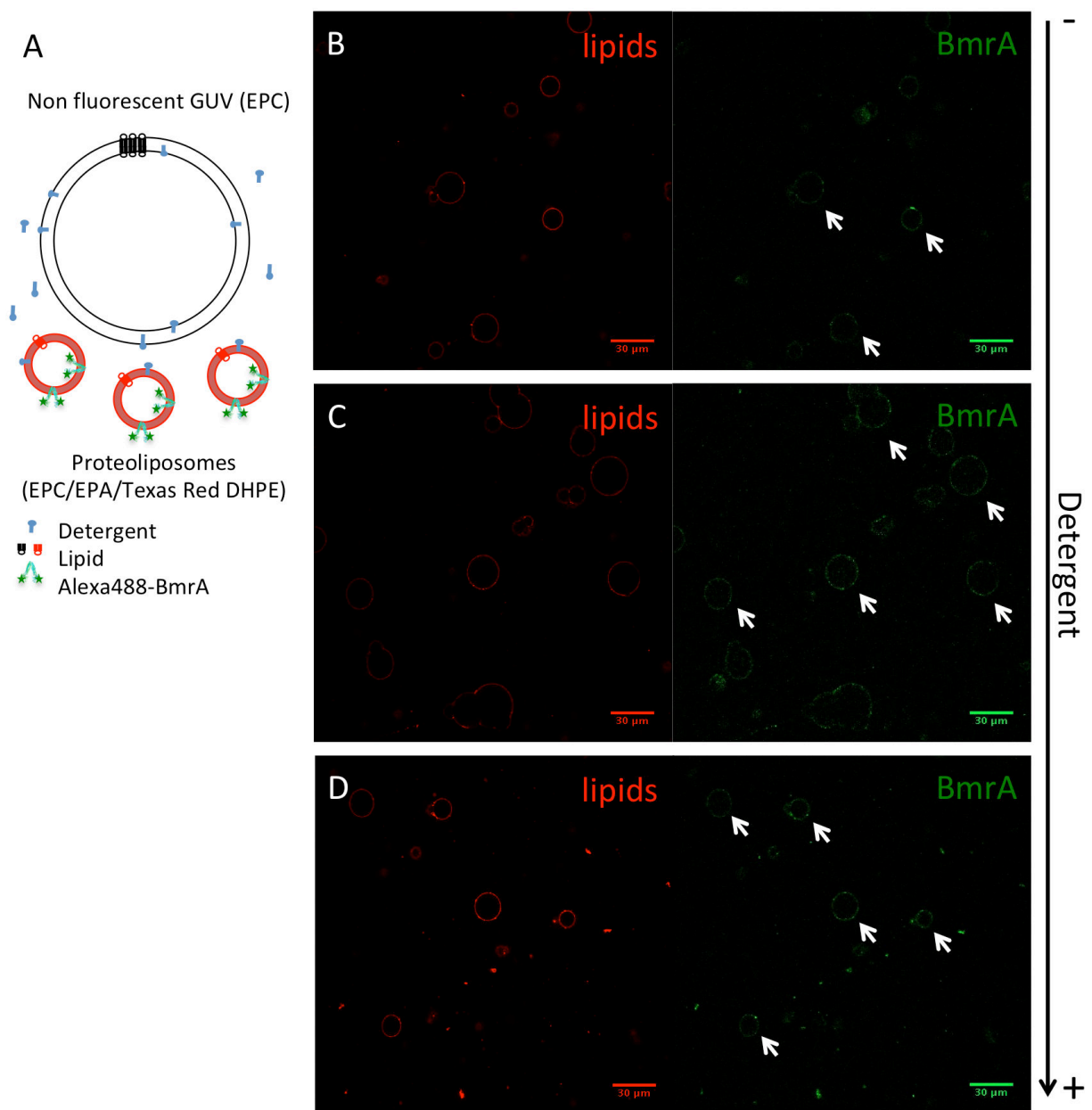


Figure 83 Fusion of proteoliposomes to GUVs.

(A) Scheme describes the principle of fusion of fluorescent proteoliposomes to non-fluorescent GUVs in the presence of detergent. Non-fluorescent GUVs (EPC) were incubated with proteoliposomes (EPC/EPA/Texas Red DHPE 9/1/0.5 w/w/w) in the presence of 75 μM DOTM (B), 0.3 (C) or 0.4 (D) Triton X-100/lipid mol/mol. Detergent was removed by BioBeads. Fluorescence signals of lipids (red) and BmrA (green) were observed by confocal microscopy. Arrows indicate protein signals in GUVs.

2. Electroformation method

In parallel, A. K. Mahalka optimized the growth of GUVs by electroformation method. This method has been used to reconstitution of KvAP, AQP0, which are robust protein channels. The principle consists of growing GUVs under electric field from proteoliposomes previously formed by detergent removal and partially dried on platinum wire (Figure 84). Moreover, growths of GUVs are performed at low salt conditions (< 50 mM salt).

However, when we applied to standard conditions for the growth of GUVs with BmrA, no GUVs were formed from the dried film. We found that most experimental conditions may lead to the denaturation or weakening of BmrA, e.g. a completely dried film or ionic strength above 50

mM prevented the formation of GUVs. The reconstitution steps had therefore been optimized for such fragile proteins. Reconstitution of BmrA in small proteoliposomes was readjusted back and forth along the optimization of the growth of GUVs. After a year of optimization, we found that the critical conditions were:

- Low salt buffer containing proteoliposome: the salt concentration was adjusted low enough to grow GUVs and high enough to preserve protein function: 5 mM MOPS pH 7.5, 20 mM NaCl.
- Drying time and temperature: the drying time should be long enough to form a protein/lipid film but not too long to aggregate the protein. Hence, drying at 4 °C rather than at 20°C prevented protein aggregation.

In these conditions, BmrA remained functional during the reconstitution in GUVs.

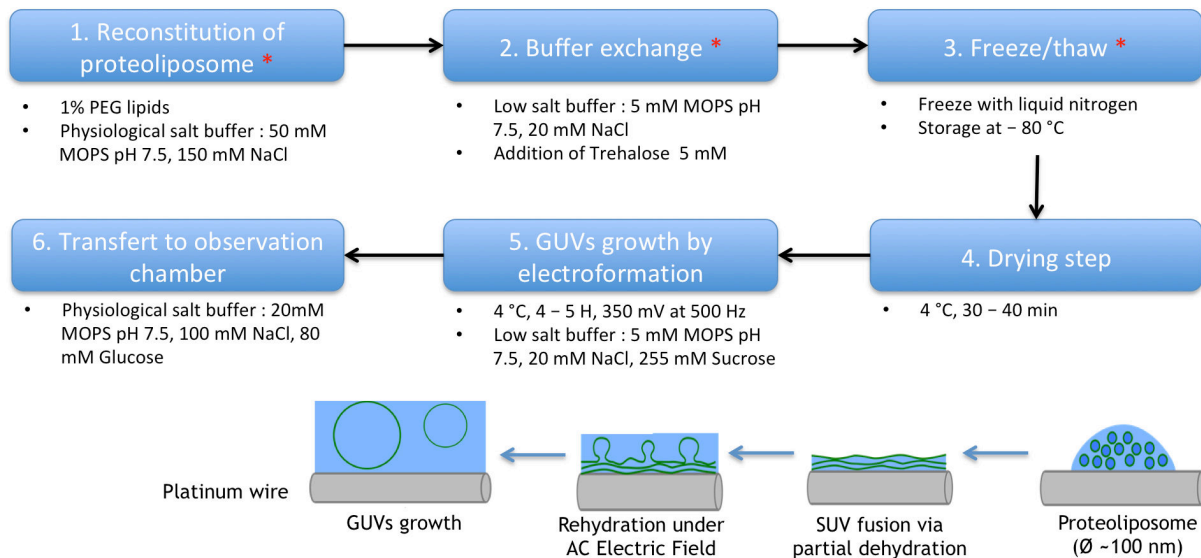


Figure 84 Reconstitution steps of BmrA into GUVs by electroformation method.

* indicates the steps I have been involved in for the reconstitution of BmrA in GUVs.

c. Characterization of reconstitution of BmrA in small liposomes for reconstitution in GUVs

We characterized the activity of BmrA along the different steps of the formation of GUVs:

- Formation of small proteoliposomes at high protein density (lipid/protein ratio 20 w/w)
- Aliquoting and freezing/thawing at -80 °C.
- Change of buffer to low salt
- Drying step in trehalose
- Growth at low salt
- Activity in physiological buffer and at 20 °C

1. Activity preservation after freezing in the presence of trehalose

Trehalose is a cryo-protectant and has been often used to protect transmembrane proteins upon drying and or freezing (Francia et al., 2008).

As depicted in Table 7, the activity of BmrA was conserved before and after freezing as after thawing steps in the range of 2 – 100 mM of trehalose. We found that GUVs better grew at 2 - 5 mM of trehalose.

EPC/EPA	ATPase activity ($\mu\text{mol}/\text{min}/\text{mg}$)	After inhibition with Vi 1 mM ($\mu\text{mol}/\text{min}/\text{mg}$)
2 mM trehalose	2.8	0.5
2 mM trehalose frozen/thawed	2.5	0.6
10 mM trehalose	2.3	0.6
10 mM trehalose frozen/thawed	2.1	0.6
100 mM trehalose	2.4	0.5
100 mM trehalose Freeze/thawed	2.1	0.5

Table 7 ATPase activity before and after freezing according to concentration of trehalose.

BmrA was reconstituted in EPC/EPA (9/1 w/w) and 2, 10, 100 mM of trehalose were added. Then, ATPase activities were compared before and after freezing with liquid nitrogen.

2. ATPase activity after buffer exchange to low salt

Proteoliposomes were reconstituted in 50 mM MOPS pH 7.5, 150 mM NaCl, then the buffer was exchanged to a lower salt buffer: 5 mM MOPS pH 7.5, 20 mM NaCl and 2 - 5 mM trehalose by SpinTrap.

ATPase activity measurement shows a 30 % decrease after buffer exchange (Figure 85 A). However, as calculated from fluorescence signals of protein and lipids before and after SpinTrap, $18 \pm 7\%$ of materials were lost during this step (Figure 85 B). Overall, this suggests that the proteins lose $22 \pm 6\%$ of activity after incubation at low salt buffer. Freezing and thawing steps in low salt buffer did not affect ATPase activity in the presence of trehalose.

It is worth noting that we could not measure ATP hydrolysis in low salt conditions that led to the precipitation of the cocktail of coupled enzymes.

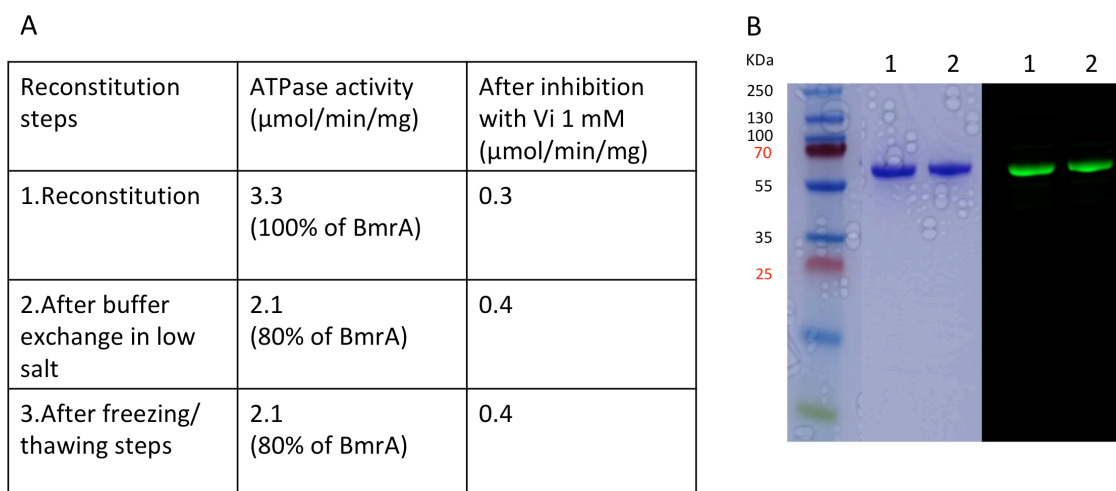


Figure 85 ATPase activity during reconstitution of proteoliposomes for GUVs.

BmrA was reconstituted to EPC/EPA/Texas Red DHPE (90/9.9/0.1 w/w) in MOPS buffer 50 mM pH 7.5, 150 mM NaCl (A 1). The buffer was exchanged by a pre-equilibrated SpinTrap column in MOPS 5 mM pH 7.5, trehalose 2 mM and NaCl 20 mM (A 2). Some fractions were then frozen with liquid nitrogen for 10 min and thawed (A 3). ATPase activity was measured at each step. The material lost during the SpinTrap was calculated by fluorescence on a 12% SDS-PAGE gel, comparing before (B 1) and after (B 2) buffer exchange.

3. ATPase activity in the presence of PEG lipids

Along the reconstitution assays, we figured out that the presence of 1-5 moles % DSPE-PEG2000 lipids helped growing GUVs and preventing GUVs from sticking each other. In addition, 0.01 moles % of biotinylated DSPE-PEG2000 lipids were added in order to pull nanotubes from GUVs with streptavidin functionalized beads by optical trap. Therefore, activity of BmrA in the presence of PEG lipid was investigated. BmrA was reconstituted in EPC/EPA/DSPE-PEG2000/DSPE-PEG2000-biotin/TexasRed-DHPE (89/8.9/1/0.01/0.1 mol%) at 60 w/w lipid to protein ratio in buffer 50 mM MOPS pH 7.5, 100 mM NaCl and 1 mM MgCl₂.

BmrA was highly active in the presence of DSPE-PEG2000, DSPE-PEG2000-biotin and Texas RED DHPE lipids (Table 8).

Lipid composition	ATPase activity (μmol/min/mg)
EPC/EPA (9/1 w/w)	3.9 ± 0.8
EPC/EPA/DSPE-PEG2000/DSPE-PEG2000biotin, TexasRed (89/8.9/1/0.01/0.1 mol)	4.9

Table 8 ATPase activity in the presence of PEG lipids.

BmrA was reconstituted in EPC/EPA/DSPE-PEG2000/DSPE-PEG2000biotin, TexasRed (3mg/ml) (89/8.9/1/0.01/0.1 mol) at 60 lipid/protein w/w in buffer MOPS 50 mM pH 7.5, 100 mM NaCl, 1 mM MgCl₂. ATPase activity was measured in buffer 50 mM MOPS pH 7.5, 150 mM NaCl, 10 mM MgCl₂ and 10 mM ATP for 4 min at 37 °C.

4. ATPase activity at 20 °C compared to 37 °C.

The experimental optical set-up did not allow to perform experiments at 37 °C. We measured the activity at 20 °C of BmrA reconstituted in small proteoliposomes in EPC/EPA, a

similar membrane environment of GUVs, and compared with reconstitutions with *E. coli* lipids, the standard conditions. ATP hydrolysis was 10 times slower at 20 °C compared to 37 °C for both lipid compositions (Figure 86). However, it is worth noting that although the activity was low at 20 °C, BmrA had a significant ATPase activity.

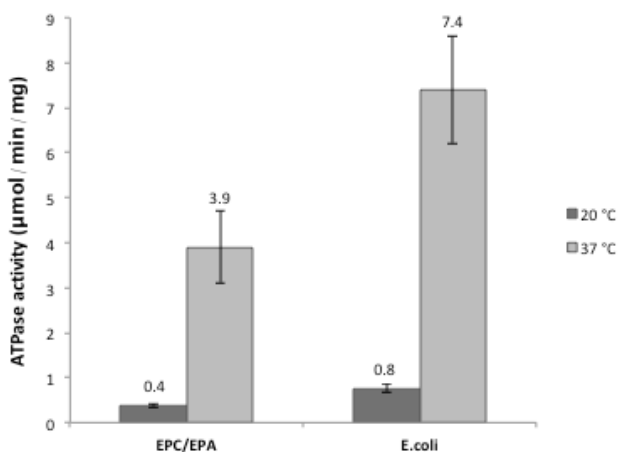


Figure 86 ATPase activity of EPC/EPA and *E. coli* proteoliposomes at 20 °C.

d. Reconstitution of BmrA into GUVs and tube pulling experiment

1. Reconstitution of BmrA in GUVs

BmrA was reconstituted into GUVs in both apo and orthovanadate-trapped states. GUVs grew faster and in larger amounts with orthovanadate trapped BmrA than with apo BmrA suggesting that apo-BmrA was more fragile according to this protocol of formation of proteoGUVs.

The density of proteins incorporated in the membranes of GUVs within the population of GUVs varied within a same experiments or when several experiments are compared, e.g. between 22 - 178 w/w lipid/protein (Figure 87). This is the case of apo and ATP-Vi BmrA. This was also observed for the reconstitution of KvAP and AQP0 in GUVs (Sophie Aimon et al., 2011). This is related to the process of formation of GUVs from the swelled proteoliposome films that may contain heterogeneous areas formed during the drying step. Some protein aggregates were observed by fluorescence on platinum wire during the GUVs growth.

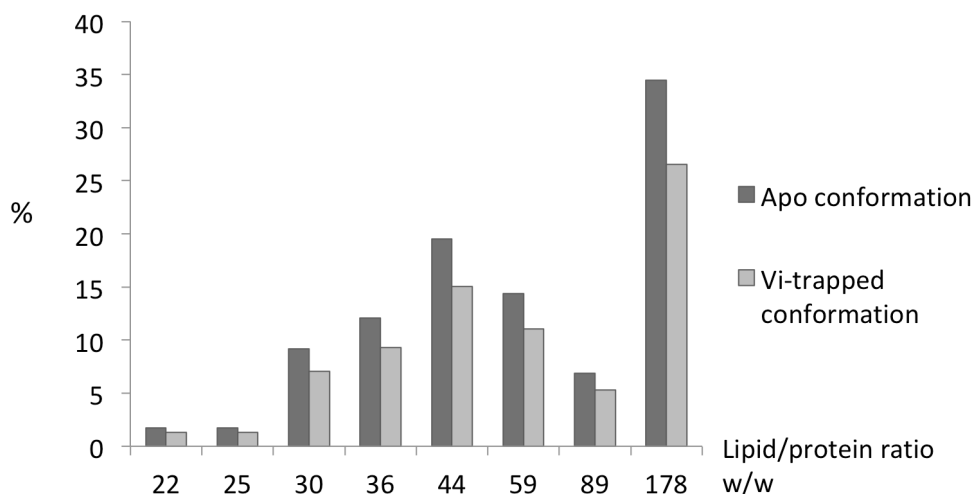


Figure 87 Lipid/protein ratio in GUVs according to conformational states.

Lipid/protein ratio in GUVs was calculated based on calibration with fluorescent lipids and molecular weight of lipids and BmrA. The frequency of lipid/protein ratio in GUVs was represented in apo (n=174 vesicles) and post-hydrolysis (n=130 vesicles) conformations.

However, it is worth noting that tube-pulling measurements are made with a single GUV that is characterized and repeated for correct statistics. In addition, experiments were only performed with GUVs at low protein density, less than 5% of membrane surface, as the curvature selectivity of BmrA was less pronounced above 5%. We have previously shown that between 20 and 320 lipid/protein w/w, no difference in ATPase activity was observed in small proteoliposomes (see ATPase activity does not depend on protein density).

2. Sorting of BmrA according to its catalytic state

The sorting of BmrA according to catalytic state was studied in tube pulling experiment. All experiments were carried out at 20 °C.

The distribution of apo-BmrA was sensitive to membrane curvature. Apo-BmrA sorted in large tubes of 80 nm in radius (green fluorescence, Figure 88 A, C) at low membrane tension ($\sigma < 0.01 \text{ mNm}^{-1}$). The sorting value increased with the increase of membrane curvature, reaching $S = 60$ for radius = 30 nm. This value is 15 times higher than the sorting values reported for KvAP, suggesting that the conicity of apo-BmrA is higher than KvAP (see conclusions: Membrane curvature and protein distribution).

Orthovanadate-trapped BmrA was only sorted in highly curved membrane (radius < 20 nm) when protein density was low, between 0.5 and 0.9% (Figure 88 B, D). The sorting value increased until 15 for radius = 30 nm that is 4 times higher than that of KvAP.

These experiments show that the apparent shape of BmrA in membrane is different in the apo and the post-hydrolysis conformations.

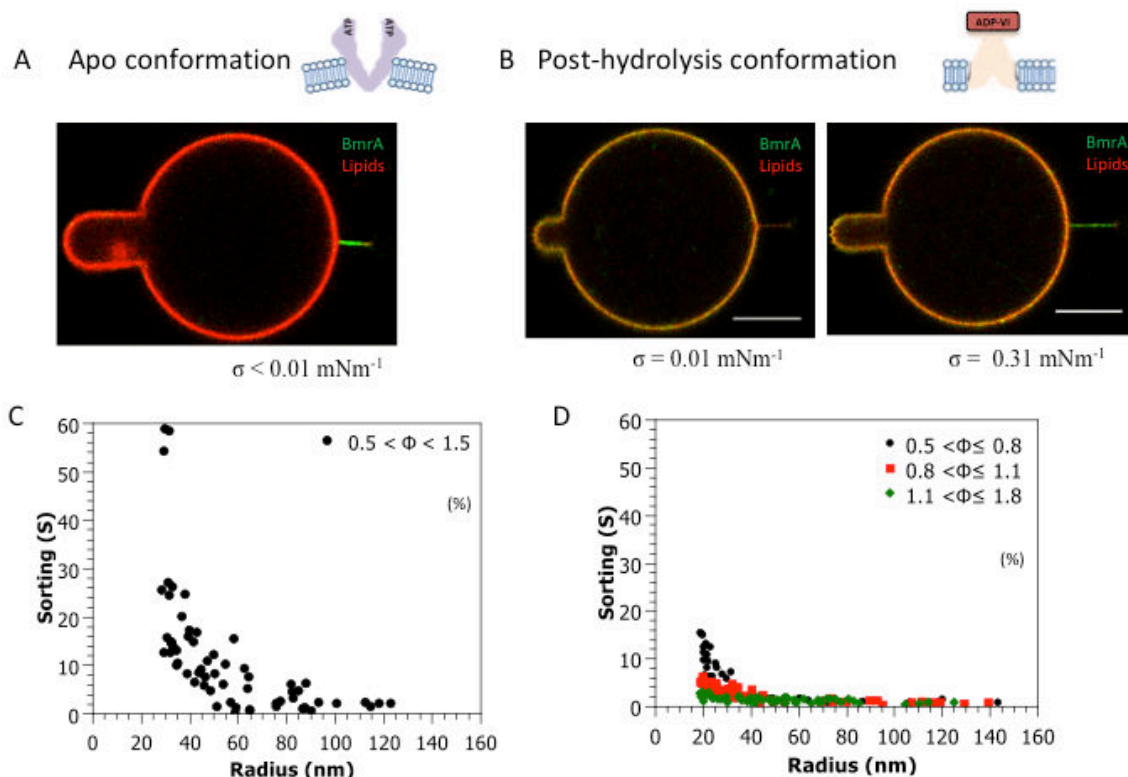


Figure 88 Sorting of BmrA according to catalytic states.

Alexa 488-BmrA was reconstituted in both apo- (A) and orthovanadate-trapped (B) states into lipid red labeled GUVs. Sorting was plotted as a function of radius of nanotube for apo- (C) and post-hydrolysis (D) conformations. (A, C) Apo-BmrA was highly sorted even in low curved membrane ($< 80 \text{ nm}$ radius of nanotube), suggesting that apo-BmrA is highly conical. Orthovanadate-trapped BmrA was only sorted in highly curved membrane (C, D) ($< 20 \text{ nm}$ radius of nanotube). Φ represents surface coverage of protein in %. The scale bar represents $5 \mu\text{m}$.

3. Clusters of apo-BmrA on the neck of nanotubes

During the sorting experiments, it was found that:

- The diffusion of apo BmrA in lipid nanotubes was extremely slow, compared to what we could expect from the diffusion rate of proteins in membranes (Figure 89 A, B). The time required for sorting apo-BmrA was approximately 10 to 12 min whatever the protein density. Even after 12 minutes, the system was not in equilibrium.
- BmrA clustered at the neck joining the GUVs and the tubes (Figure 89A arrows). Even after the protein was sorted in the tube, the proteins did not diffuse freely into the tube. This may be due to diffusion impairment of single proteins at the neck and/or slow diffusion of clusters.
- Apo-BmrA adjusted the size of nanotube itself to 30 nm of radius along the sorting (Figure 89B).

The enrichment of apo-BmrA seems to promote formation of clusters, which causes slow diffusion in nanotube and narrows the nanotube to 30 nm . The absolute value of lipid/protein ratio in nanotube cannot be calculated because it requires difficult calibrations of proteins fluorescence in nanotubes, but we can estimate it by following formula:

$$S = \Phi_{\text{tube}} / \Phi_{\text{GUVs}}$$

For $\Phi_{\text{GUVs}} = 1\%$, that corresponds to lipid/protein ratio 178 w/w, sorting values of 10 - 30 corresponding to lipid/protein ratio of 6 to 18 w/w.

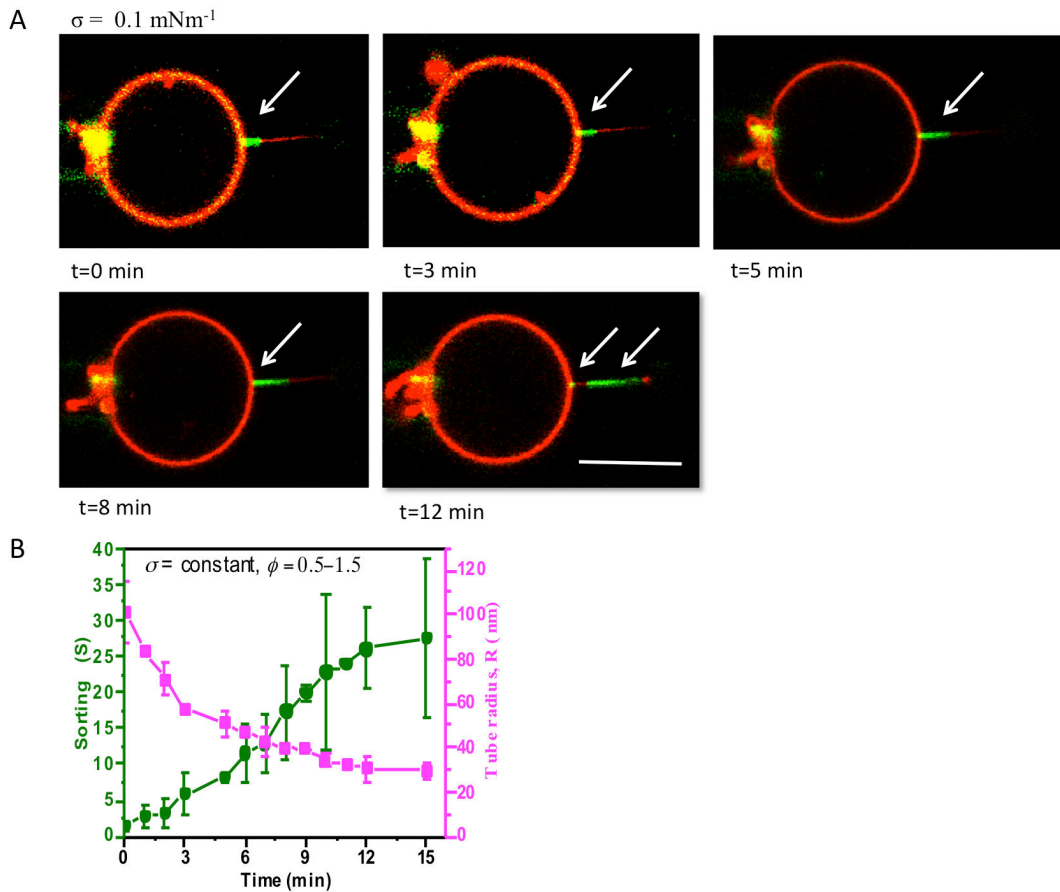


Figure 89 Sorting of apo-BmrA and clusters at the neck.

The sorting of apo-BmrA was studied over time (A) and analyzed (B). White arrows indicate the formation of clusters of BmrA. The scale bar represents 5 μm .

4. Orientation of apo-BmrA in GUVs and in nanotube

To determine the orientation of protein in GUVs and in nanotube, we used proteolysis by trypsin as used for proteoliposomes. Relative fluorescence of proteins and lipids was calculated over time.

In nanotube, apo-BmrA fluorescence decreased by 90% while lipid fluorescence remained constant, suggesting that 90% of BmrA are oriented with NBDs outside of GUVs (Figure 90). In GUVs and out of nanotubes, 50% of proteins were in inside-out orientation. This suggests that either only inside-out apo-BmrA is sorted in nanotubes or that during the sorting of both inside-in and inside-out apo BmrA in nanotubes, there is a backward diffusion of inside-in apo BmrA to GUVs.

We could not obtained reproducible results with orthovanadate-trapped BmrA maybe because proteolysis was less efficient than in apo-conformation as previously mentioned (see Different trypsin digestion in post-hydrolysis conformation).

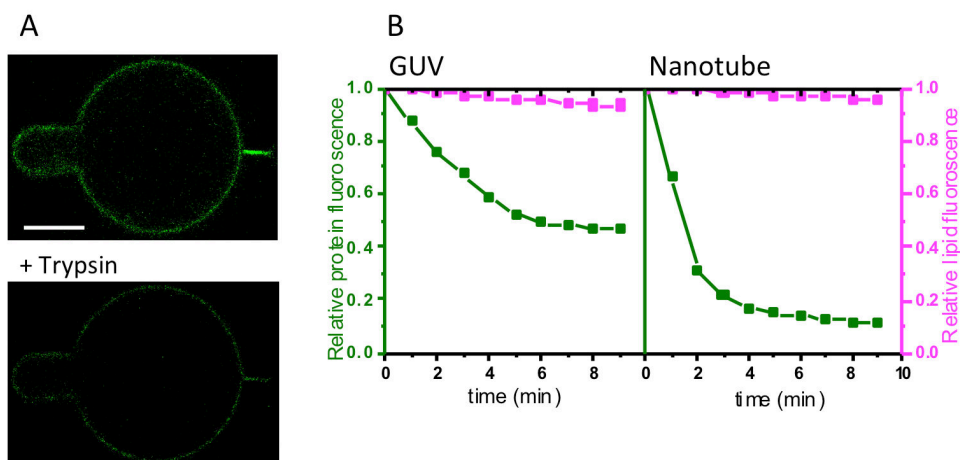


Figure 90 Orientation of apo-BmrA in GUVs and in nanotube by proteolysis.

(A, B) Trypsin was added to approximately 500 trypsin/BmrA w/w to sorted apo-BmrA in GUVs. Relative fluorescence of protein (green) and lipids (pink) were calculated over time. The scale bar represents 5 μm .

5. Addition of ATP- γ -S at sorted apo-BmrA

Since BmrA in two different conformational states was sorted at different sorting values, we next analyzed the changes of spatial distribution of BmrA when proteins change their conformation from apo to ATP-bound conformation. Apo-BmrA was first sorted in nanotubes and then ATP- γ -S was added. The sorting values decreased from 16 to 5 in a short time (Figure 91). This result unambiguously demonstrated that proteins were active. Sorting value of 5 as already found with ATP-Vi BmrA suggest a similar shape in pre- and post-hydrolytic conformations (Figure 90). The nanotube radius increased as the sorting decreased, which is the reverse of the decrease of nanotubes radius observed during the sorting of apo-BmrA. The decrease of sorting in a short time also suggests that ATP-bound BmrA diffuse more rapidly than in apo conformation and that proteins may less interacts between them.

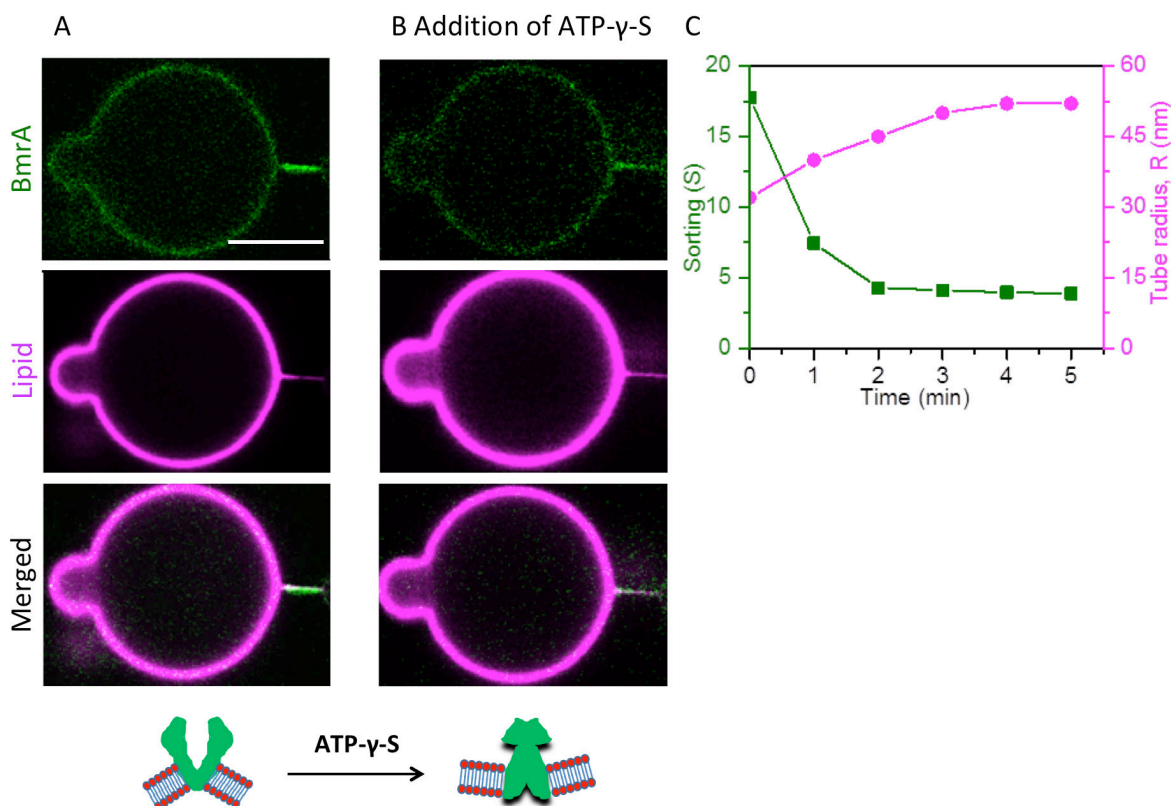


Figure 91 Redistribution of BmrA upon addition of ATP-γ-S.

At sorted apo-BmrA (A), 1-5 mM of ATP-γ-S was added (B) and sorting values were calculated over time (C). The scale bar represents 5 μm .

6. Redistribution of BmrA during catalytic cycle

We have previously determined snap-shots of the spatial distribution of BmrA locked in conformations. The spatial distribution of BmrA in curved membrane during catalytic cycle was then studied. After addition of ATP, sorting continuously decreased in nanotubes and stabilized at 5 min (Figure 92). Slow decrease could be related to long turnover of ATP hydrolysis due to low ATP concentration and low temperature, 20 °C rather than 37 °C. The ATP hydrolysis measured with small proteoliposomes show a 10 fold and a 20% decrease of ATP hydrolysis at 20 °C and 2 mM ATP compared to 37 °C and 10 mM ATP, respectively. Therefore in GUVs experimental condition, we can estimate the ATPase activity of 0.3 $\mu\text{mol}/\text{min}/\text{mg}$. If we assume that BmrA consumes 2 ATP per catalytic cycle, the turnover of a catalytic cycle is calculated at 2 s. Thus, although, apo-BmrA may diffuse differently from post-hydrolysis conformation due to neck crossing difficulties and clustering, the durations of the experiments were long enough for several turnovers and equilibrations. This suggests that BmrA prefers flat membrane to the curved membrane during the catalytic cycle.

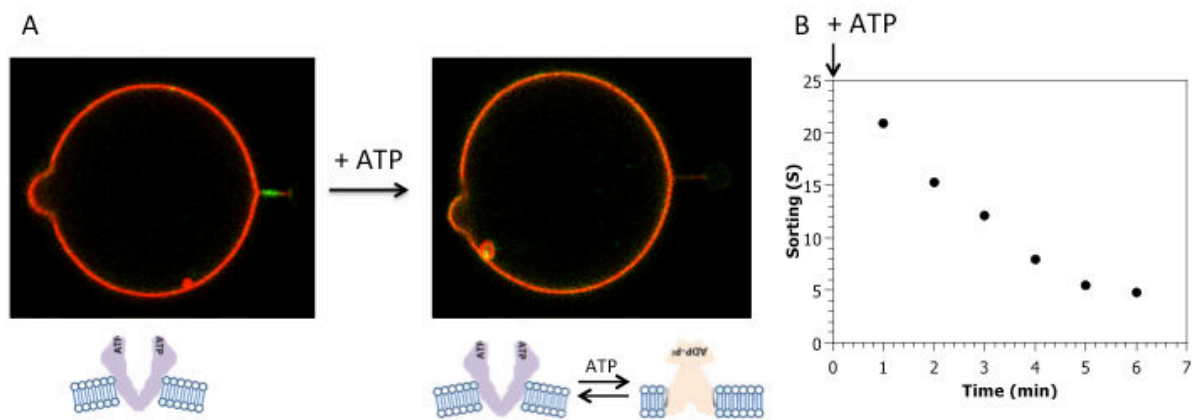


Figure 92 Redistribution of BmrA upon addition of ATP

ATP (1-2 mM) was added to apo-BmrA present in nanotubes (A) and (B) changes of sorting values were measured over the time.

IV. Fluorescent labeling for analysis of the dynamics of BmrA

Fluorescently labeled BmrA was used in tube pulling experiments and for FRET experiments. In both cases, we expected that the labeling does not modify the function and the structure of BmrA. In GUVs experiments, the fluorescent labeling was used to visualize and quantify the amount of incorporated proteins. In smFRET experiments, fluorescently labeled proteins were used for an accurate measurement of the dynamics and the distances between labeled amino acids. As described below, this has been a highly demanding task.

a. Labeling of BmrA at native single Cys residue

BmrA contains only a single cysteine residue located in NBDs that might be a good fluorescent labeling position and a good reporter of the NBDs dynamics. Since BmrA is a homodimer, two cysteine residues can be labeled and distances between these two could be measured. As stated in the introduction: BmrA, there is no structure of BmrA and the position of C436 is therefore putative. Different models were constructed based on bacterial homologues structures, i.e. MsbA for the apo-conformation and MsbA and SAV1886 for the post-hydrolysis conformation. C436 is located within or close to the helix 18 of the NBD. This helix participates in the conformational changes of NBDs during the catalytic cycle between the apo and the post-hydrolytic state. The amplitude of these changes is under debate and in the case of BmrA is not documented.

However, several data suggest that C436 is a good position for our studies: i) thiol-maleimide reaction on cysteine residue is highly specific; ii) a cysteine-less BmrA mutant, C436S, was reported to be highly active (Cao et al., 2009); iii) Cys436 is not a conserved residue among ABC transporters. C436 of BmrA corresponds to alanine (A438) for MsbA, leucine (L436) for SAV1866 and arginine (R485) or alanine (A1128) for mouse PgP; iv), equivalent residues are not positioned at the interface of functional NBD site in apo and post-hydrolysis conformations (Dawson & Locher, 2006; Esser et al., 2016; Mi et al., 2017; A. B. Ward et al., 2013). Residues are localized on the outer surface of NBDs, which suggests high accessibility to fluorescent dyes.

However, Cys436 is at the middle or at the end of the alpha helix depending on the calculated models of BmrA and thus we cannot rule out that this position is structurally important (Figure 93B, C).

Different strategies have been reported in the literature for the labeling of transmembrane proteins: (i) in native membranes before purification, (ii) labeling of purified proteins solubilized in detergent, (iii) in batch or bound to an affinity column, and after reconstitution in proteoliposomes. We tried all these strategies and finally used labeling of BmrA solubilized in DDM since results were more reproducible. The final protocol is depicted in Figure 46 in material and method.

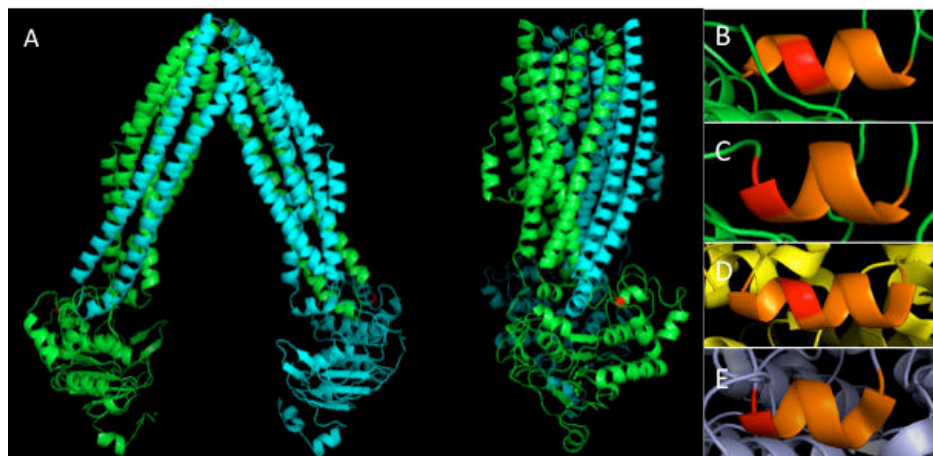


Figure 93 Front and side views of model of apo-BmrA.

(A) Calculated model of apo-BmrA based on *E. coli* apo MsbA structure (PDB : 3B5W). BmrA is a homodimer and each monomer is represented in green and blue colors. C436 residue is represented in red. C. Tavenau provided two others models of apo-BmrA computed with I-Tasser (B) or Raptor X (C). The position of cysteine in alpha helices (orange) slightly changes depending on the models. (D) Equivalent residues to C436 in ATP-Vi SAV1866 (D, PDB: 2HYD) and (E) ATP-Vi MsbA (PDB: 6BPP)

b. Labeling with a single fluorescent dye

1. Depending on time and temperature

BmrA in detergent was incubated with sulfo-Cy3 maleimide at different times, temperatures and concentrations of dyes.

BmrA labeling increased with increasing amount of dyes. Labeling was more efficient at 4 °C during over-night incubation than 1-2 hours at 20 °C (Figure 94). Therefore, labeling was performed at 4 °C overnight incubation for further experiments.

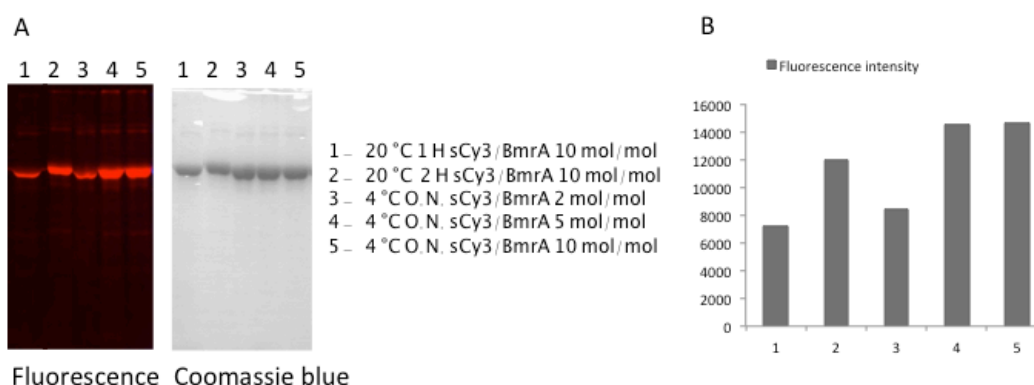


Figure 94 Labeling of BmrA in detergent according to time, temperature and concentration of dyes.

Sulfo-Cy3 dyes were incubated with BmrA in detergent at 4 or 20 °C, 1 h – overnight, with different dye/protein ratios 2-10 mol/mol. (A) 4 µg of BmrA was analyzed on 12% SDS-PAGE gel by fluorescence and stained with Coomassie blue. (B) The fluorescence on the gel was analyzed.

2. Concentration of dyes

BmrA in detergent was incubated with increasing amount of Alexa488 maleimide to dye/BmrA 1, 2, 5, 10, 20 and 50 mol/mol overnight at 4 °C. Sulfo-Cy3 and sulfo-Cy5 maleimide dyes were incubated at dye/protein 5, 10, 20, 50, 100 mol/mol, overnight at 4 °C. Labeled BmrA was analyzed on SDS-PAGE gel by fluorescence and stained with Coomassie blue.

BmrA labeling increased with increasing amount of Alexa488 and saturated at Alexa488/BmrA 20 mol/mol (Figure 95). For sulfo-Cy dyes, the labeling also increased with increasing concentration of dyes but was saturated at 40 mol/mol, suggesting that the labeling efficiency depends on fluorescent dyes.

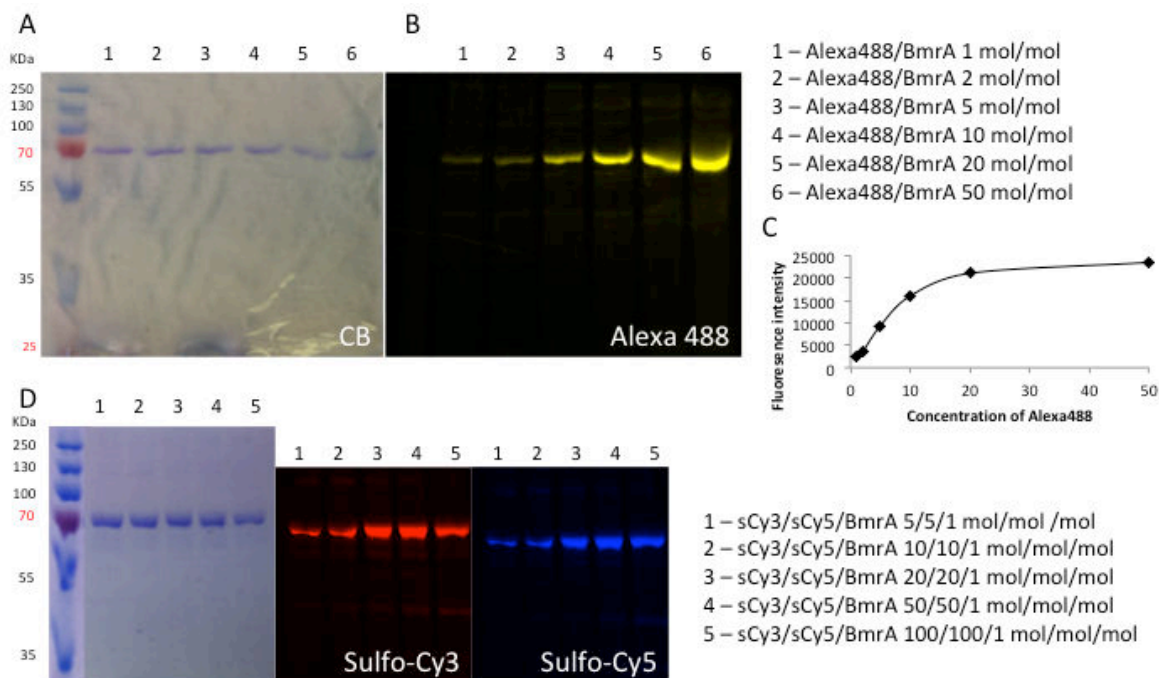


Figure 95 Labeling of BmrA with increasing concentration of fluorescent dyes.

BmrA was incubated with increasing amount of Alexa488 maleimide (A) or of sulfo-Cy3 and sulfo-Cy5 (D) in buffer 50 mM MOPS pH 7, 150 mM NaCl and 0.05% DDM, over-night at 4 °C. BmrA (1 µg for Alexa488 and 5 µg for sCy3/sCy5) was loaded on 12% SDS-PAGE gel, analyzed by fluorescence and stained by Coomassie blue. (C) The fluorescence intensity of Alexa488 on the gel was measured.

3. Specificity of labeling

BmrA WT and mutant Cys-less mutant solubilized in detergent were incubated with Alexa488 and the sulfo-Cy3 maleimide dyes and their fluorescence were analyzed on SDS-PAGE gel.

The signal of unspecific labeling corresponded to less than 4% compared to WT for both fluorescent dyes (Figure 96). This result demonstrates that the labeling is specific to C436 residue.

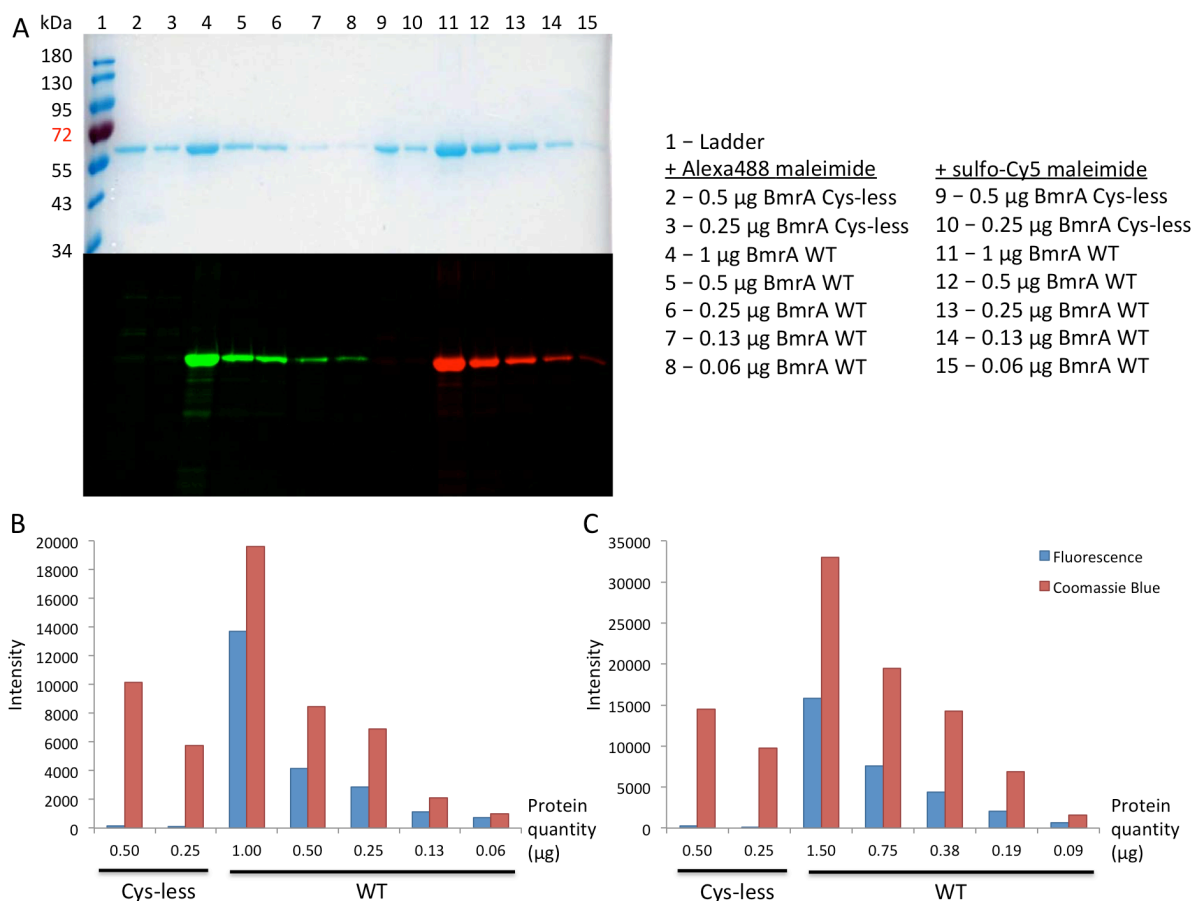


Figure 96 Absence of unspecific labeling of BmrA with maleimide-dyes.

(A) BmrA WT and BmrA Cys-less mutant (M1) were incubated at 10 dyes/protein mol/mol at 20 °C for 2 h with Alexa488 maleimide and sulfo-Cy3 maleimide in buffer 50 mM Tris pH 7, 100 mM NaCl, 0.05% DDM. Different amounts of protein were analyzed on 12% SDS-PAGE gel by fluorescence and stained with Coomassie blue. Fluorescence and Coomassie blue intensities on the gel were analyzed for Alexa488 (B) and sulfo-Cy5(C) labeled BmrA.

4. Rate of labeling and activities

We measured the ATPase activity of labeled BmrA (Table 9) and found that with all probes, BmrA was still highly active after labeling. For example, nearly 90% of BmrA can be labeled with Alexa488 and without loss of activity. This demonstrated that C436 residue is accessible and can be a good reporter of the function of BmrA. This is also consistent with our predictions based on the literature and computed models.

However, we also found that the rate of labeling as well as resulting ATPase activity strongly depends on the type of probes. In the cases of sulfo-Cy5 and Dy647P1, the activity decreased approximately 40%, suggesting that these dyes were toxic to proteins (see also Labeling with two fluorescent dyes for FRET).

Fluorescent dye	Dye/protein ratio (mol/mol)	Labeling rate for WT (%)	Activity conservation (%)	Population in homodimer
Alexa488 maleimide	10	87 ± 5.5	100	Dual-labeled: 76% 1-labeled: 22% Unlabeled: 2%
Atto610	10	94 ± 3.7	83	Dual-labeled: 88%

maleimide				1-labeled: 12% Unlabeled: 0%
Sulfo-Cy3 maleimide	20	58	nd	Dual-labeled: 34% 1-labeled: 48% Unlabeled: 18%
Sulfo-Cy5 maleimide	20	67	54	Dual-labeled: 45% 1-labeled: 44% Unlabeled: 11%
Cy3B maleimide	10	67± 5.6	79	Dual-labeled: 45% 1-labeled: 44% Unlabeled: 11%
Dy547P1 maleimide	10	50	88	Dual-labeled: 25% 1-labeled: 50% Unlabeled: 25%
Dy647P1 maleimide	10	62	66	Dual-labeled: 38% 1-labeled: 48% Unlabeled: 14%
Alexa647 maleimide	10	18	87	Dual-labeled: 3% 1-labeled: 30% Unlabeled: 67%

Table 9 Labeling yields and activity conservation of BmrA WT according to fluorescent dyes.

BmrA was labeled and purified with several fluorescent maleimide-dyes in DDM 0.05% (except for Dy547P1 and Dy647P1 in DDM 0.02%). Rate of labeling was calculated: concentration of fluorescent dyes measured by absorbance divided by concentration of protein measured by Bradford method. Activity conservation rate was established by comparing activity to unlabeled BmrA. Percentages of population were calculated by probability: dual labeled (=rate of labeling ^2), 1-labeled (=2*rate of labeling*(1- rate of labeling)), and unlabeled (=(1- rate of labeling)^2).

c. Labeling with two fluorescent dyes for FRET

In addition to BmrA WT, we designed two mutants of cys-less protein where cys residues were introduced at positions that may allow FRET measurements.

1. Different location of labeling by single mutagenesis

Labeling for FRET was performed as same method as labeling with one fluorescent dye. In parallel, two mutants were designed by site directed mutagenesis from cysteine-less C436S mutant M1 to select the best position, labeling yield, activity preservation for FRET experiments (Figure 97):

- M2: C436S, T444C;
- M3: C436S, T559C.

The choice of mutagenesis was based on reported studies on FRET and LRET experiments with homologues of BmrA (Cooper & Altenberg, 2013; Verhalen et al., 2012; Zoghbi et al., 2017) :

- T444 corresponds to T492 or S1137 of mouse PgP. FRET studies were carried out with T492C/S1137C PgP mutant with Alexa488/Atto610 dyes. PgP was as active as WT after mutation and labeling with fluorescent dyes.
- T559 corresponds to T561 of MsbA, and N607, T1252 of mouse PgP. LRET experiment were carried out with these mutants. For MsbA, the activity of mutant T561C was similar

to Cys-less. For mouse PgP, no significant difference of activity was observed after mutagenesis and labeling.

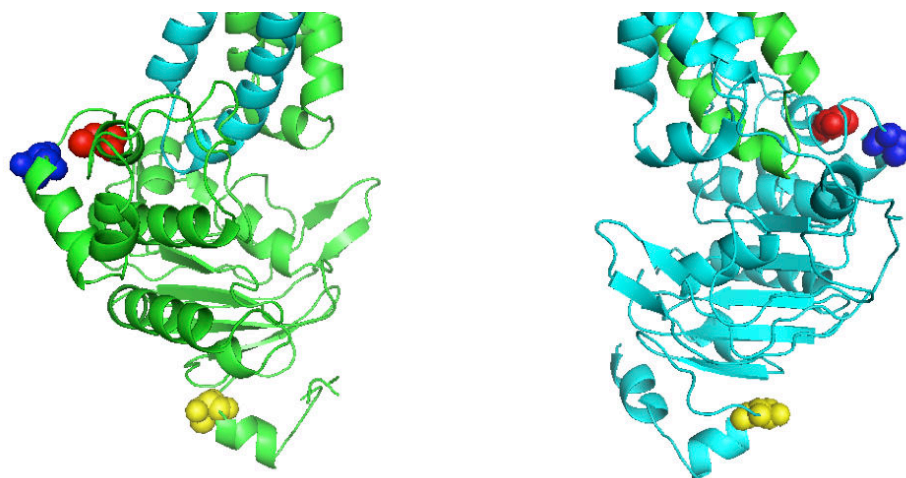


Figure 97 BmrA WT and mutants : introduction of Cys residue to other locations.

The figure above shows the NBD region in a putative model of BmrA, calculated based on *E. coli* apo MsbA structure (PDB: 3B5W). Native Cys436 (red) was mutated to serine residue C436S and 2 mutants were generated: T444C (blue) and T559C (yellow).

2. Optimization of ratio of two fluorescent dyes

Optimization of double labeling with dyes for FRET was performed to obtain 50% donors and 50% acceptors. FRET couples were selected based on spectrum overlap, dye photostability and published data: Alexa488/sulfo-Cy5, Alexa488/Atto610, sulfo-Cy3/sulfo-Cy5 and Cy3B/sulfo-Cy5. Two fluorescent dyes were incubated simultaneously with BmrA in DDM. As a result, several populations were present after labeling: BmrA without labeling, donor only, acceptor only, dual-labeled (donor-acceptor), donor/donor and acceptor/acceptor.

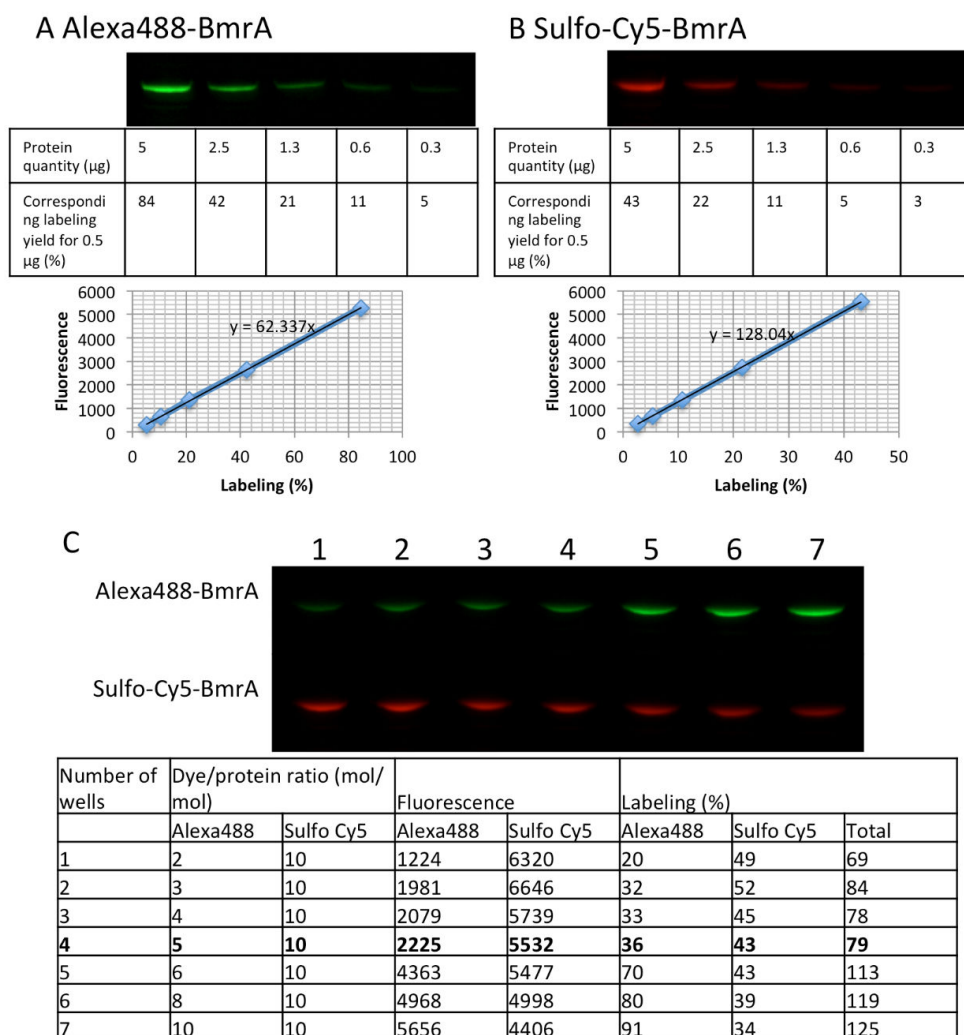


Figure 98 Example of optimization of ratio between two fluorescent dyes for dual-labeled BmrA.

(A, B) 0.5 µg of purified Alexa488-BmrA (84% labeling yield) and sulfo-Cy5-BmrA (43% labeling yield) were serially diluted and the fluorescence was calibrated from the 12% SDS-PAGE gel according to labeling rate. (C) A different ratio of two fluorescent dyes was incubated with purified BmrA in a detergent at 4 °C overnight under magnetic stirring. Fluorescence of 0.5 µg of protein was analyzed on 12% SDS-PAGE gel and labeling rates were determined from the calibration. The condition with a similar labeling rate for donor and acceptor was selected.

Based on this strategy described in Figure 98, ratio between 2 fluorescent dyes was determined for several FRET couples for WT BmrA and mutants (Table 10).

FRET couples	Dye/protein ratio (mol/mol)
Alexa488/Atto610	5/2
Alexa488/sulfo-Cy5	5/10
Sulfo-Cy3/sulfo-Cy5	10/10
Cy3B/sulfo-Cy5	5/10

Table 10 Ratio between two fluorescent dyes to obtain 50% of donor and 50% of acceptor labeled to BmrA WT

3. ATPase activity depending on labeling yield

WT

FRET couples	Labeling rate (%)	Activity conservation (%)	Population in homodimer
Alexa488/Atto 610	31 / 37	76	Alexa488/Atto610: 23% Alexa488/Alexa488: 10% Atto610/Atto610: 14% Alexa488: 20% Atto610: 24% Unlabeled: 10%
Alexa488/sulfo-Cy5	36/ 53	76	Alexa488/sulfo-Cy5: 38% Alexa488/Alexa488: 13% Sulfo-Cy5/sulfo-Cy5: 28% Alexa488: 8% Sulfo-Cy5: 12% Unlabeled: 1%
Sulfo-Cy3/sulfo-Cy5	32 / 39	80	Sulfo-Cy3/sulfo-Cy5: 25% Sulfo-Cy3/ sulfo-Cy3: 10% Sulfo-Cy5/sulfo-Cy5: 15% Sulfo-Cy3: 19% Sulfo-Cy5: 23% Unlabeled: 8%
Cy3B/sulfo-Cy5	50 / 36	73	Cy3B/sulfo-Cy5: 36% Cy3B/Cy3B: 25% Sulfo-Cy5/sulfo-Cy5: 13% Cy3B: 14% Sulfo-Cy5: 10% Unlabeled: 2%

Table 11 Rate of labeling and activity conservation for FRET couples of BmrA WT

As a first important result, all doubly labeled BmrA have a high ATPase activity (Table 11). However, ATP hydrolysis is never 100% and it is difficult to interpret the decrease of activity observed with doubly labeled proteins from what we observed with single labeling (Table 9). For instance, as depicted in Table 9, 100% single labeled Alexa 488 BmrA and 94% single Atto 610 BmrA conserved 100% and 83% ATPase activity. However, doubly labeled Alexa488/Atto610 BmrA is less active than expected with 76% activity. On the opposite, 67 % single labeled sulfo-Cy5 BmrA and 67% single labeled Cy3B BmrA conserved 54% and 79% activity respectively while doubly labeled BmrA has only a slightly decreased activity of 73%.

Moreover, the percentage of doubly labeled BmrA is often close to the percentage of decrease of ATPase activity and thus we cannot rule out that the doubly labeled BmrA are not active. Keeping this in mind we continued to characterize labeled BmrA.

Modification of membrane morphology with Alexa488- and Atto610-BmrA WT

To get more insights into the conformational changes of labeled BmrA, we reconstituted BmrA at high proteins density and analyzed the results by electron microscopy and negative staining. Previous experiments have shown that WT BmrA formed rings that dissociated after addition of ATP-Vi (Figure 99). Same experiments with Alexa488-, Atto610- and Alexa488/Atto610-BmrA led to the formation of fewer ring assemblies and more vesicles than

unlabeled BmrA. However, these rings and vesicles also changed their shapes after addition of ATP-vanadate. This suggests that fluorescent proteins are not identical than unlabeled BmrA but retained their ability of conformational changes in membrane.

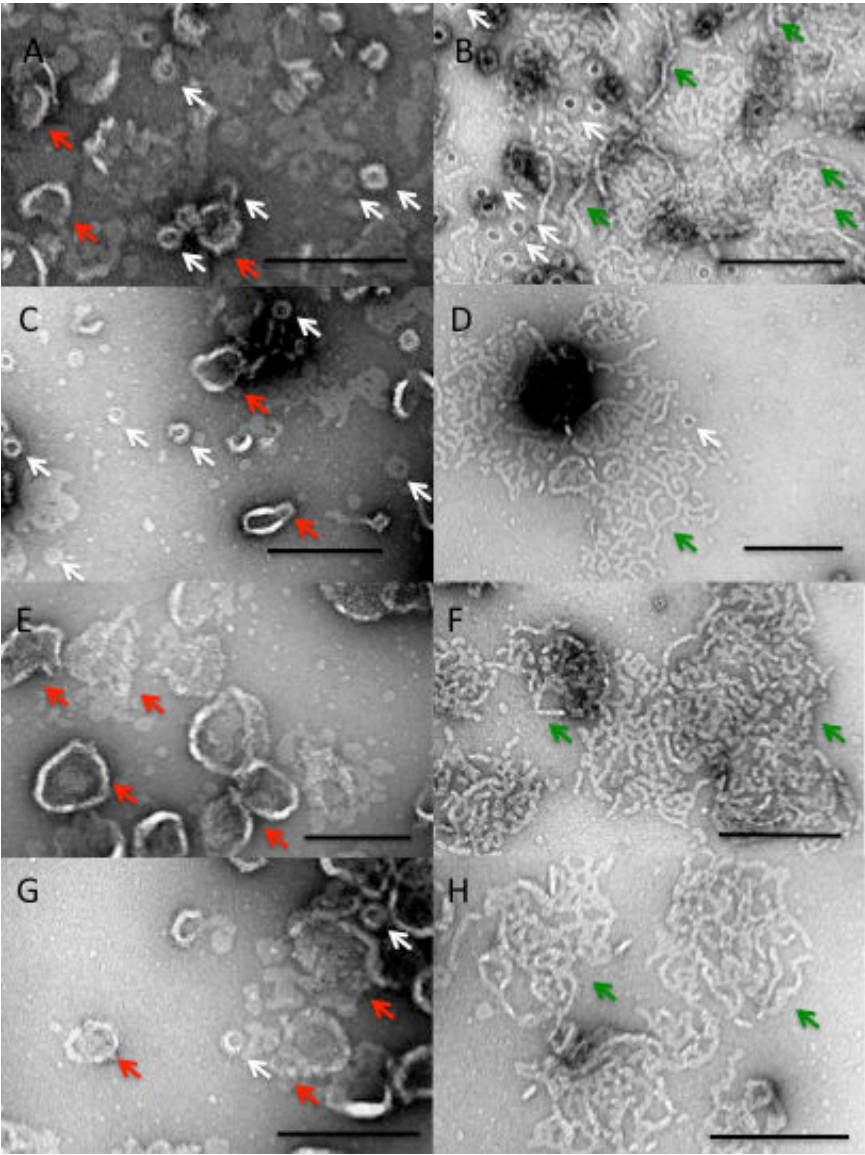


Figure 99 Membrane morphology changes according to catalytic states of labeled BmrA.

BmrA WT (A, B), WT Alexa488(C, D), WT Atto610 (E, F) and WT Alexa488/Atto610 (G, H) were reconstituted in apo conformation in DMPC at lipid/protein 2 w/w. In condition of formation of ring shape, the detergent removal was stopped and the images of reconstitution were taken by EM by negative staining (A, C, E, G). Then, 5 mM of ATP and 1 mM of orthovanadate was added and incubated 10 min at 20 °C under magnetic stirrer agitation (B, D, F, H). White, red and green arrows indicate ring, liposomes, flat membranes, respectively. The scale bar represents 200 nm.

M2

Fluorescent dyes	Labeling rate (%)	Activity conservation (%)	Population in homodimer
Unlabeled		95	
Alexa488	106	88	Alexa488/Alexa488: 100%

Cy3B	91	82	Cy3B/Cy3B: 83% Cy3B: 16% Unlabeled: 1%
Sulfo-Cy5	64	71	Sulfo-Cy5/sulfo-Cy5: 41% Sulfo-Cy5: 46% Unlabeled: 13%
Alexa488/sulfo-Cy5	36/ 47	71	Alexa488/sulfo-Cy5: 34% Alexa488/Alexa488: 13% Sulfo-Cy5/sulfo-Cy5: 22% Alexa488: 12% Sulfo-Cy5: 16% Unlabeled: 3%
Cy3B/sulfo-Cy5	39 / 47	60	Cy3B/sulfo-Cy5: 37% Cy3B/Cy3B: 15% Sulfo-Cy5/sulfo-Cy5: 22% Cy3B: 11% Sulfo-Cy5: 13% Unlabeled: 2%

Table 12 Rate of labeling and activity conservation for FRET couples of BmrA M2

M2 has same ATPase activity compared to WT (Table 12). The labeling yield and decrease of activity of doubly labeled M2 was also similar to WT. The rate of labeling of Alexa488 was slightly superior to 100%. This may be due to non-accurate measurement of BmrA concentration, unspecific labeling or the presence of a free probe.

M3

Fluorescent dyes	Labeling rate (%)	Activity conservation (%)	Population in homodimer
Unlabeled		51	
Alexa488	89	54	Alexa488/Alexa488: 79% Alexa488: 20% Unlabeled: 1%
Cy3B	106	35	Cy3B/Cy3B: 100%
Atto610	54	21	Atto610/Atto610: 29% Atto610: 50% Unlabeled: 21%
Sulfo-Cy5	72	41	Sulfo-Cy5/sulfo-Cy5: 50% Sulfo-Cy5: 40% Unlabeled: 8%
Alexa488/Atto 610	23/44	25	Alexa488/Atto610: 20% Alexa488/Alexa488: 5% Atto610/Atto610: 19% Alexa488: 15% Atto610: 29% Unlabeled: 11%

Alexa488/sulfo-Cy5	39/ 67	42	Alexa488/sulfo-Cy5: 52% Alexa488/Alexa488: 15% Sulfo-Cy5/sulfo-Cy5: 45%
Cy3B/sulfo-Cy5	39 / 47	35	Cy3B/sulfo-Cy5: 37% Cy3B/Cy3B: 15% Sulfo-Cy5/sulfo-Cy5: 22% Cy3B: 11% Sulfo-Cy5: 13% Unlabeled: 2%

Table 13 Rate of labeling and activity conservation for FRET couples of BmrA M3

Unlabeled M3 has a 50% decrease of activity compared to WT (Table 13). However, unlike to WT and M2, sulfo-Cy5 labeling did not affect M3-BmrA's activity. Therefore, Alexa488/sCy5 M3 was an interesting candidate with high labeling yield of dual-labeled protein and good preservation of activity compared to non-labeled protein.

Characterization of M3 and Alexa488/sulfo-Cy5 M3

We next investigated whether the effect on lipid composition on ATPase activity and inhibition rate were conserved in M3 and labeled M3 compared to WT.

As for WT, ATPase activities of M3 and Alexa488/sulfo-Cy5 M3 in EPC/EPA were two times lower than in *E. coli* liposomes (Figure 100). ATPase activity of Alexa488/sulfo-Cy5 M3 was inhibited approximately 80% and 85% by ATP- γ -S and AMP-PNP, respectively.

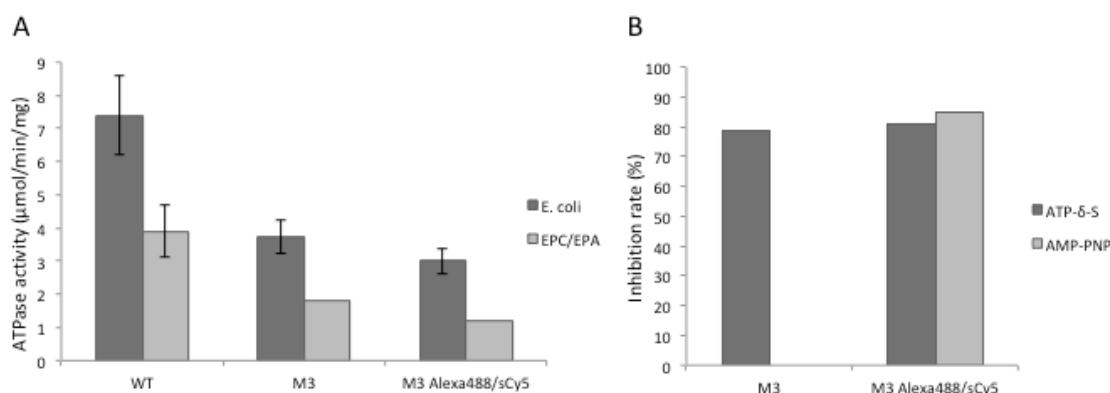


Figure 100 Characterizations of M3 and Alexa488/sulfo-Cy5 M3

(A) BmrA WT, M3 and Alexa488/sulfo-Cy5 M3 were reconstituted in *E. coli* or EPC/EPA (9/1 w/w) liposomes and their ATPase activity were measured. (B) Inhibition rate of M3 and Alexa488/sulfo-Cy5 M3 were investigated in *E. coli* liposomes in the presence of 10 mM ATP with 5 mM of ATP- γ -S or 10 mM of AMP-PNP.

d. Conclusion

We successfully labeled WT and mutants with several fluorescent probes at C436 residue. However, the labeling rate and toxicity appear to depend on the probe. Since the measured ATP activity results from a complex population of proteins (unlabeled/ donor-only labeled/ acceptor-only labeled / dual-labeled), we could not predict if the dual-labeled proteins were functional. In all cases, labeling with two dyes led to a decrease of ATPase activity even if protein remained very active.

We thus keep these results in mind when experiments with labeled BmrA were performed. Experiments with GUVs were performed with single labeled Alexa 488 BmrA and thus we were confident that all labeled proteins were active. In the case of FRET experiments, we decided to investigate it directly by observing the change in FRET related to its catalytic state. We selected some candidates for FRET studies with good activity and labeling rate: Alexa488/Atto610 WT, sulfo-Cy3/sulfo-Cy5 WT, Alexa488/sulfo-Cy5 WT, Alexa488/sulfo-Cy5 M3.

V. Dynamics of BmrA by smFRET

The objective was to study in more detail the effect on lipid composition and membrane curvature on the dynamics of BmrA at single molecule level.

We expect low FRET values in apo conformation if NBDs are separated and high FRET in post-hydrolysis where NBDs are closed (Figure 101). We have chosen two well characterized reconstituted systems: EPC/EPA (9/1) and *E. coli* proteoliposomes. FRET measurements were carried out by 3 different methods: fluorescence spectroscopy, measurements of the lifetime of donor by FCS (fluorescence correlation spectroscopy) of diffusing proteoliposomes in solution at single-molecule level by FCCS. In parallel, A. Damm, PhD student performed single molecule FRET of immobilized proteoliposomes on surface by TIRF microscopy.

Actually, we have optimized labeling of BmrA, single-molecule and ensemble FRET measurements in parallel. Since smFRET measurements on Pgp in liposomes have already been published (Verhalen et al., 2012), we started smFRET experiments with the same couples of probes Alexa488/Atto610 at similar position of cysteine residues, Cys436 of WT BmrA. Labeling and fluorescence spectroscopy measurements were done at Institut Curie (Paris, France) and measurement of donor lifetime and single-molecule FRET measurement by FCCS were performed at CBS (Montpellier, France) in collaboration with E. Margeat.

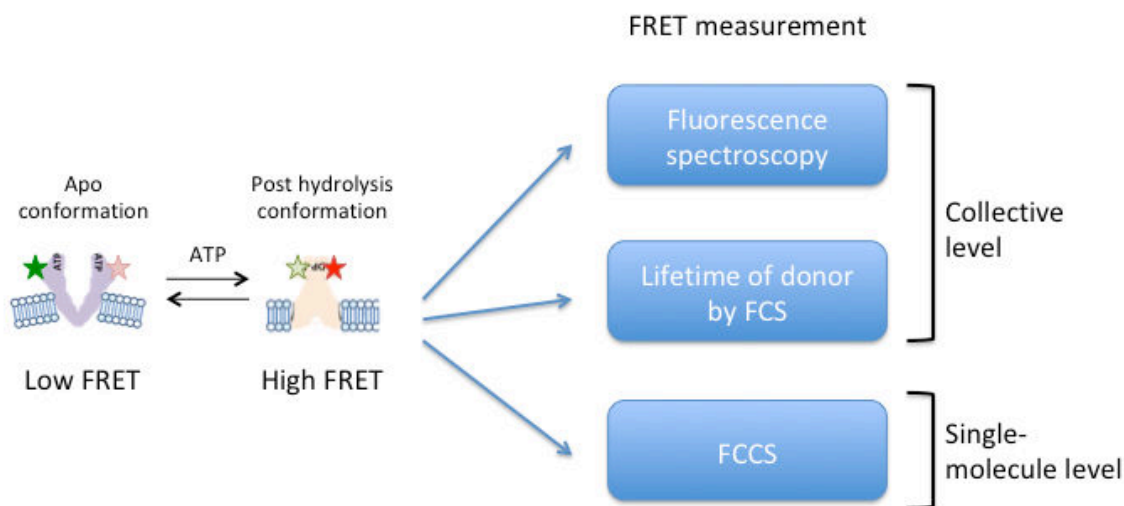


Figure 101 Different strategies to investigate dynamics of BmrA by FRET

We were not able to obtain a significant result in this part. We studied FRET changes between apo and post-hydrolysis conformations in detergent, detergent/lipids and membrane. We observed FRET signal in all conditions, but we did not observed FRET changes in post-hydrolysis conformation as shown in the Table 14. There were two conditions where possible FRET changes were observed in smFRET experiments: Alexa488/Atto610 WT and Alexa488/sulfo-Cy5 WT. But even then the results were not consistent with ensemble FRET measurement or the statistics in smFRET studies were low.

All the details on the experiments are available in Annexe I.

BmrA		Experimental approach		Condition	FRET changes after addition of inhibitor	Comment	
WT	Alexa488/Att o610	Ensemble FRET	FS	Liposome	No	See Table 15	
			Lifetime	Detergent	No	See Figure 118	
				Liposome	No	See Figure 118	
		smFRET		Detergent	No	See Figure 120	
				Liposome	Yes	See Figure 126 Low statistics	
		Alexa488/sulfo-Cy5	Ensemble FRET	FS	Liposome	No	See Table 15
	Lifetime			Detergent	No	See Figure 118	
				Liposome	No	See Figure 118	
	smFRET		Liposome	Yes	See Figure 126		
	Sulfo-Cy3/sulfo-Cy5		Ensemble FRET	FS	Liposomes	No	See Table 15
					smFRET		Detergent
		Liposome	No				See Figure 125
		Cy3B/sulfo-Cy5	smFRET		Liposome	No	See Figure 126
	Mutant 3	Alexa488/sulfo-Cy5	Ensemble FRET	FS	Detergent	No	See Table 15
					Lifetime	Detergent	No
Liposome				No		See Figure 118	
smFRET			Detergent/lipid	No	See Figure 121		

Table 14 Summary tables of FRET results. FS stands for Fluorescence Spectroscopy

Discussion

We studied the function and spatial distribution of BmrA, a bacterial ABC in different *in vitro* membrane models. We obtained significant results on the interaction between BmrA and membrane that could be extended to other homodimeric bacterial ABC transporters. We also discuss possible impact of these data on eukaryotic ABCs.

Mechanism of proteoliposomes formation

The formation of proteoliposomes with low protein density is believed to be similar to the formation of pure lipid vesicles by detergent removal. The simplest mechanism of liposome formation by detergent removal involves three steps (Figure 30): (I) detergent removal from mixed micelles increases the hydrophobicity of mixed micelles that coalesce to minimize their surface of interaction with water and form large lipid/detergent micelles; (II) further detergent removal leads to closure of vesicle to protect the edges of large micelles; (III) Once the vesicles are formed, the total elimination of detergent slightly changes the vesicle size.

The final size of the vesicles depends on intermediate states, especially the type of mixed lipid/detergent micelles. These intermediate states are poorly characterized because of their dynamics. However, micelles must coalesce to form vesicles and therefore parameters that influence the fusion between micelles determine final liposome size (Figure 102). The fusion of mixed micelles was temperature sensitive and the liposomes formed with PC by detergent removal at 4 °C are significantly smaller than those formed at 20 °C (Figure 80). Similarly, the rate of detergent removal modifies the final size of the liposomes (Lévy et al., 1990). Ionic strength also modulated the size of liposomes in the presence of anionic lipids with small and large vesicles formed at low, physiological and high salt, respectively (Figure 79). This suggests that high salt buffer reduces electrostatic repulsion allowing fusion between micelles.

However, at 20 °C and 150 mM of NaCl of reconstitution condition, PC vesicles decreased in size with anionic lipids except with PS lipid that led to large liposome (Figure 77). This suggests that the overall shape of lipids dominates the liposome size more than fusion of micelles (Figure 102B). PS, like PC, has cylindrical shape whereas other anionic lipids PA, PG, CL are conical shaped (Figure 103). Conical PE lipids also imposed the decrease of liposome size regardless the temperature, salt concentration or the rate of detergent removal.

According to literature, conical lipids are preferentially localized in inner leaflet and induce positive curvature (Callan-jones et al., 2011; Esteban-Martín, Jelger Risselada, Salgado, & Marrink, 2009; Kooijman, Chupin, de Kruijff, & Burger, 2003). Therefore, the asymmetry between two lipid leaflets may also contribute to the final size of liposomes. It is possible that the presence of detergent may facilitate lipid flip-flop concentrating conical lipids in inner leaflet. As a result, PC/PS liposomes should be symmetrically distributed between leaflets while in mixture of PC and conical lipids are asymmetrically distributed.

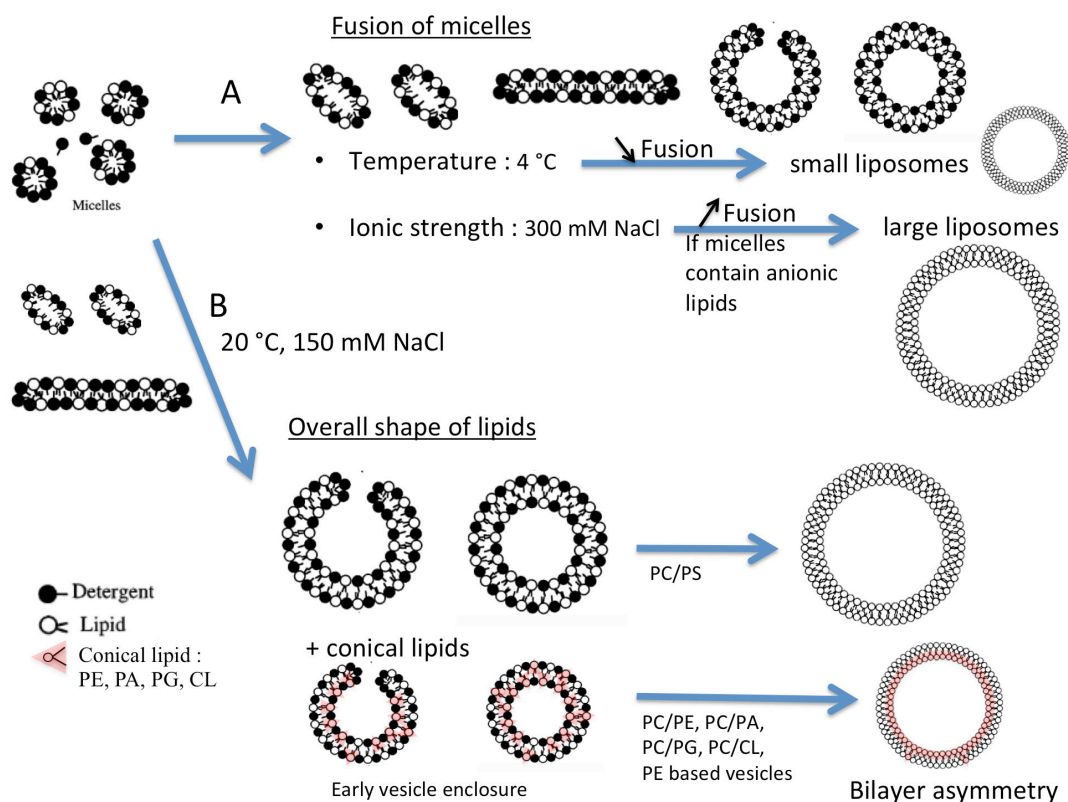


Figure 102 Mechanisms of liposome formation by detergent removal and factors that influence size of vesicles.

This figure is readapted from (J.-L. Rigaud et al., 1998) and completed with the current data.

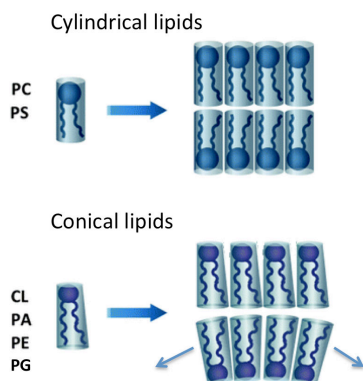


Figure 103 Overall shapes of lipids

Cylindrical lipids form flat lipid bilayer whereas conical lipids induce positive membrane curvature. The figure is readapted from (Marín-García, 2013).

These fusion properties of mixed micelles do not change with or without protein as shown by similar populations of reconstituted liposomes (Figure 73). However, we also showed that protein orientation in apo conformation in vesicles was not 50/50 inside-in/inside-out but rather 75% inside-out. Moreover, orientation depends on vesicle size with almost 100% inside-out in small vesicles. The fusion of the mixed micelles is accompanied by their curvature. It is possible that proteins are involved in membrane bending process (Figure 104). For example, proteins like BmrA, which have a non-zero intrinsic curvature (conicity), impose a spontaneous curvature to their close environment. Therefore, the protein conicity imposes the preferential orientation in the liposome. It can also be considered that protein orients itself during the protein diffusion within the micelles due to preference in positive curvature and/or to avoid steric hindrance of

large extramembrane domains of several proteins in inside-in orientation, especially for small liposomes.

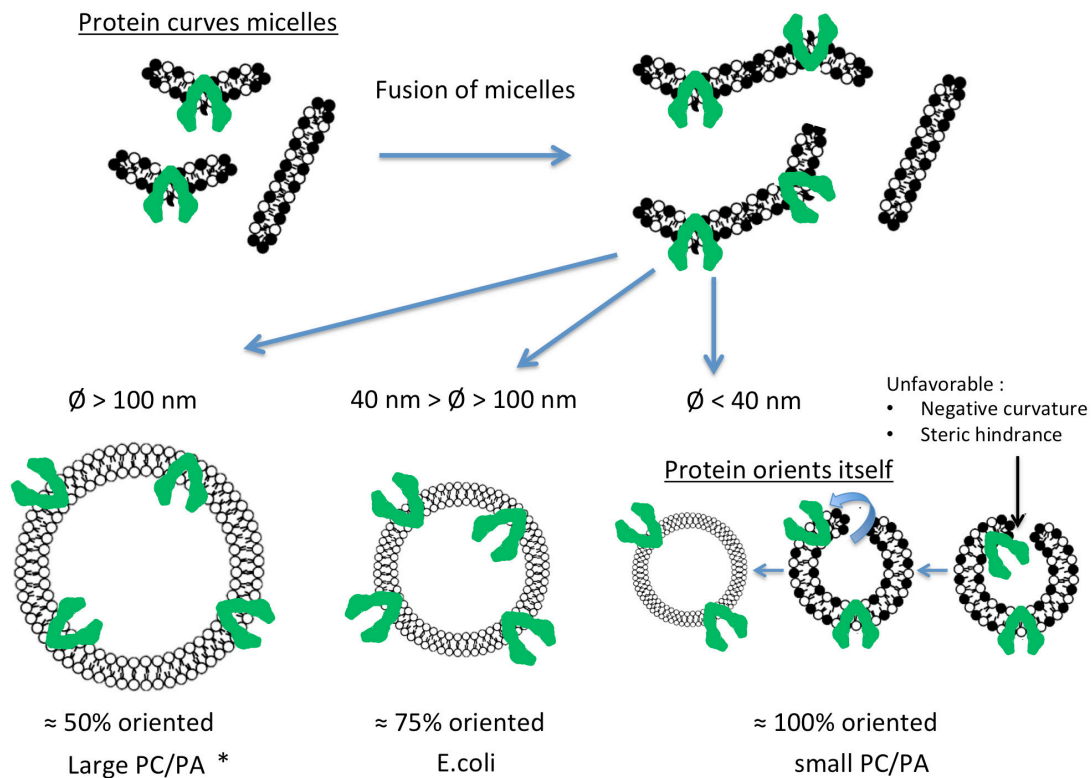
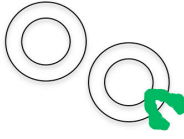
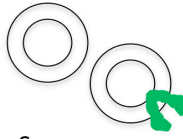
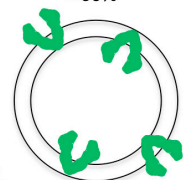


Figure 104 Protein orientation according to size of liposomes

* see Figure 105.

We have measured the orientation of protein reconstituted in EPC/EPA at 4 °C and at 20 °C, respectively, in small, 100 % inside-out, and in mixture of small and large liposomes, 75 % inside-out (Figure 82). We can calculate the protein orientation in large liposomes by comparing the two experiments. We have measured the percentage of liposomes vs. sizes, leading to 40% of small and 60% of large liposomes (Figure 71). We also know that there are 1 homodimer/2 liposomes of $\varnothing \approx 40 \text{ nm}$, and 4 homodimers in liposome of $\varnothing \approx 100 \text{ nm}$ (see Estimated number of BmrA according to diameter of liposome.). With the formula indicates in Figure 105, we calculated that proteins are oriented 50% inside-out in the large liposomes. This confirms that the protein orientation depends on the size of liposomes.

Similarly, we can infer the activity of BmrA in large PC/PA liposome in a mixture of small and large liposomes (Figure 105). We found that the activity in large liposomes was close to the average protein activity. Despite the high percentage of small liposomes of PC/PA and 100% inside-out orientation, protein activity in small liposomes weakly contributes to the average activity since few proteins with low activity are concerned. Therefore, protein activity might be two-fold underestimated in large liposomes due to 50% of protein orientation. This also suggests that the activity is actually 4 times greater in large liposomes than in small liposomes. Moreover, activities in PG, PA and PS were similar in PC based vesicles despite the differences in liposome distributions (Figure 63). Since only large liposomes contribute to the average activity, then the stimulation with negatively charged lipids are likely not specific to a particular headgroup.

EPC/EPA	Reconstitution at 4 °C	Reconstitution at 20 °C	
Liposome size	100%  ∅ < 40 nm	≈ 40%  S ∅ < 40 nm	≈ 60%  L ∅ > 40 nm
Protein distribution at 200 lipid/protein ratio w/w	0.5 homodimer/liposome	0.5 homodimer/liposome	4 homodimers/liposome
Protein orientation (%)	≈ 100	≈ 75	
		≈ 100	≈ 54 *
ATPase activity (μmol/min/mg)	0.9	2.1	
		0.9	2.3 **

$$* L_{\text{protein orientation}} = \frac{(\text{Total}_{\text{liposomes proportion}} \times T_{\text{protein distribution}} \times T_{\text{protein orientation}} - S_{\text{liposomes proportion}} \times S_{\text{protein distribution}} \times S_{\text{protein orientation}})}{(L_{\text{liposomes proportion}} \times L_{\text{protein distribution}})}$$

$$** L_{\text{protein activity}} = \frac{(T_{\text{liposomes proportion}} \times T_{\text{protein distribution}} \times T_{\text{protein orientation}} \times T_{\text{protein activity}} - S_{\text{liposomes proportion}} \times S_{\text{protein distribution}} \times S_{\text{protein orientation}} \times S_{\text{protein activity}})}{(L_{\text{liposomes proportion}} \times L_{\text{protein distribution}} \times L_{\text{protein orientation}})}$$

Figure 105 Calculation of protein orientations and activity in large PC/PA liposomes

The orientation and activity of BmrA (red) were calculated from the data of reconstitution characterization and activity measured at 26 degrees.

With regard to the reconstitution of BmrA in the GUVs, the experiments carried out in this thesis show that this remains very empirical. Among the eight methods of incorporation of protein in GUVs that have been published, I tried direct incorporation and fusion of proteoliposome and then abandoned for lack of time and A. Kumar did electroformation for BmrA reconstitution. These methods have been successfully used for numerous proteins, including a BmrCD, an ABC from *B. subtilis*, in our group and in the group of P. Bassereau. Although the protocols seemed already well established with other proteins, the reconstitution of BmrA was challenging. The electroformation method had to be readjusted to BmrA, probably because of the drying step, which destabilizes many membrane proteins. To overcome this problem, it was necessary to adjust the drying step by going through the step of pre-spreading the drop on the platinum wires. This optimization was performed by following the comparative evolution between the ATP hydrolysis activity measured in small proteoliposomes and GUVs growth. It is important to note that the optimization was rapid for Vi-trapped BmrA and much longer for apo-BmrA suggesting differences in stability between the two conformations. The protein orientation of BmrA is 50/50 in GUVs as shown in Figure 90 by proteolysis. BmrA was reconstituted in EPC/EPA GUVs, a lipid mixture for which we showed that proteins were active and where GUVs grow better than *E. coli* (P. Bassereau pers. com).

Once reconstituted, we showed unambiguously that apo-BmrA was active by response to ATP and also inhibited by ATP-γ-S during sorting experiments. This point is important to mention because it is difficult to prove that ABCs are functional in GUVs. Indeed, substrates are either too hydrophobic to accumulate in the internal volume or the internal volume is too big requiring long time of active transport that could compete with passive equilibration. Several studies report functional assays as an evidence of the incorporation of unlabeled protein. For example, the measurement of ATP hydrolysis in the medium, (Kim, Kim, & Lee, 2015) for PgP, may be due to proteins in small proteoliposomes or membrane fragments coexisting with GUVs. In our study,

we show direct evidences of functional BmrA reconstituted in GUVs with fluorescently labeled BmrA.

Protein density varies significantly compared to initial proteoliposomes but also between individual GUVs. The protein density varies between 200 to 1600 proteins/ μm^2 , which corresponds to lipid/protein ratio of 40 to 350 w/w whereas the lipid film is made from proteoliposomes of 20 w/w. This suggests that both drying and swelling steps of the lipid/protein film are heterogeneous processes. However, the size of GUVs allows a "unique" study of individual vesicles by fluorescence microscopy, and as in our experiments, allows a quantitative measurement of protein density for each GUV.

As shown in Figure 69, BmrA is active without any functional influence by protein density at these ranges of lipid/protein ratio in small proteoliposomes. Thus, results obtained between different GUVs are comparable whatever the proteins density.

Membrane states, lipids composition and ATPase activity of BmrA

The role of lipids and membrane on the activity of ABC transporters has been studied for several years and has been reported in several publications. We have fully characterized proteoliposomes in order to quantitatively compare ATPase activity. In some reports, protein orientation and liposome size are characterized, but the protein incorporation rate is rarely established and liposome lamellarity has never been shown. This can explain the important variability of activity reported for the same protein and between ABCs (e.g. MsbA (Kawai et al., 2011; Mi et al., 2017; Zoghbi et al., 2016).

As we have shown for BmrA, the activity depends on its environment in micelles of detergent and lipids or in membrane. We found qualitatively consistent results with other ABCs that ATPase activity of BmrA increases in the reconstituted system compare to in micelles of detergents, and that anionic lipids and PE stimulate activity.

BmrA was stable with high activity in different detergents. It has been reported that approximately 12 lipids are associated to purified BmrA homodimer in DDM (Chaptal et al., 2017; Ravaut et al., 2006). The addition of lipids led to increase of ATPase activity in micelles of detergent/lipids even though the quantity of detergent added was 2.5 – 4 times higher (mol) to lipids. This data suggests that lipids interact preferentially to BmrA more than detergent. This result is consistent with native mass spectroscopy studies of Pgp, TmrAB, McjD (Bechara et al., 2015; Marcoux et al., 2013; Mehmood et al., 2016) where lipids were tightly bound to the protein more than detergent. Moreover, lipids seem essential for optimal ATPase activity. Similar to our experiment, the addition of lipids to delipidated McjD led to increase of activity (Mehmood et al., 2016). The ATPase activity of BmrA was higher in micelles of Triton X-100 than DDM, suggesting that detergent modulates lipid-protein interaction. However, the interaction between lipids and proteins do not seem to be high in micelles since there was no lipid specificity.

The interaction between lipids and proteins increased in membrane. Anionic lipids stimulated the activity indifferently whatever the lipid-head group, PA, PG, PS and CL in PC vesicles, suggesting that the interaction is not highly specific. Moreover, the stimulation of activity by anionic lipids started from 10% (w). In a liposomes of 100 nm of diameter and lipid/protein ratio of 40 w/w, there are approximately 100 000 lipids and 15 homodimers/liposome. Therefore, 10% of anionic lipids represent approximately 700 lipids per homodimer. This suggests that an excessive amount of anionic lipids are required surrounding the protein to be able to stimulate the activity. Therefore, the interaction between anionic lipids and BmrA increases in membrane compared to micelles but remains weak. The interaction between BmrA and PE was weaker than anionic lipids, since the activity was stimulated starting from 40% for

PE in PC vesicles. This result is consistent with molecular dynamic simulations where negatively charged lipids were in closer proximity to ABCs than PE (Mehmood et al., 2016).

Compared to structurally important lipids that are tightly bound to proteins, here we discuss lipids that are continuously exchanging between annular belt and bulk lipid. Therefore, the residence time of these lipids surrounding the protein determines the lipid specificity. For example, molecular dynamic simulations on McjD showed a high number of contacts during a period of few μ sec between anionic lipids and positive residues (Mehmood et al., 2016). Since higher amount of positively charged amino acids were located at the cytoplasmic side anionic lipids were asymmetrically distributed between both leaflets.

According to a computed model of BmrA, there are 16 positively charged residues that can interact with anionic lipids per monomer (Figure 106). When compared to the amino acids involved in the interaction between MsbA and LPS (Mi et al., 2017), no equivalent residues were found in BmrA, suggesting that BmrA does not transport LPS (R78/R148/Q256/K299 in MsbA and A78/T148/S256/G299 in BmrA).

However, 14 positively charged residues are located on the cytoplasmic side, 2 others are located on extracellular side. Six other amino acids are located in TMDs and are conserved in MsbA. It is worth noting that the activity of MsbA is also sensitive to negatively charged lipids. Among them, three are in helix 4. Biochemical and NMR studies on MsbA suggested that helix 4 plays an important role in the transmission of conformational changes from TMDs to NBDs (Doshi et al., 2013; Spadaccini et al., 2018). This suggests a role of these conserved positive residues in the anionic lipid stimulation. BmrA has also 8 positive amino acids positioned in the elbow helix and located at the membrane-water interface. This is significantly higher than in MsbA or McjD with 3 and 2 positive amino acids, respectively. The role of these amino acids has never been documented. We can speculate that they contribute to the attraction of negatively charged lipids in the surrounding of BmrA.

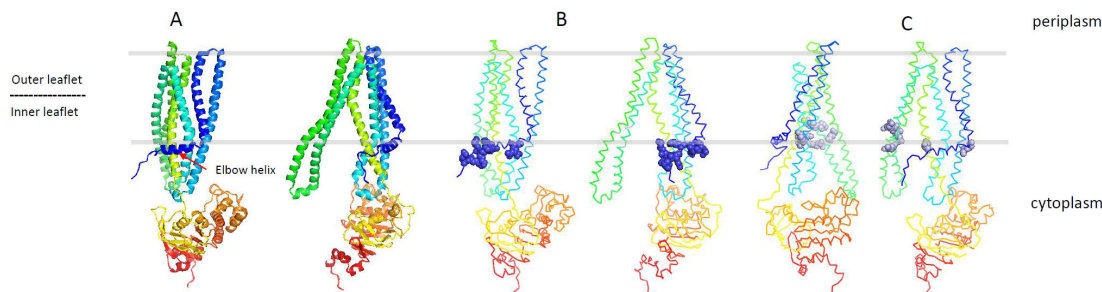


Figure 106 Distribution of positively charged amino acids of BmrA in the cytoplasmic side.

BmrA has been modeled with Raptor X. Only a monomer is depicted. The membrane region is depicted with gray lines according to the structure of MsbA in lipid nanodisc (Mi et al., 2017). Positive amino acids are present in the N-ter elbow helix (K4, K5, K7*, K9, K11, R20*, R21*), in helix 2 (K9), helix 4 (R186*, K187*, R194*) and helix 5 (K309*). Amino acids labeled with * are conserved in MsbA. K51 and K165 in the periplasmic side are not depicted.

However, it is not clear how membrane influences the hydrolysis of ATP at the NBDs that are far away from the membrane. It has been suggested that some lipids stabilize protein conformation at a close distance between NBDs, which promotes activity. (Gustot et al., 2010; Mehmood et al., 2016; Zoghbi et al., 2017). In our analysis, we do not have clear evidence of a direct modulation of conformation of BmrA by lipids. Our data from cryo-EM and EM experiment shows that ring shape assemblies are formed in PC, PC/PA and *E. coli* lipids suggesting that apo BmrA was in an identical conformation. This suggests that lipids might not be involved in the first step of ATP binding. Lipids can be involved in any following steps of the catalytic cycle, NBD dimerization, ATP hydrolysis and release of ADP (P. Tieleman, pers. com). This was the goal our studies by smFRET. We cannot interpret the data further.

Membrane curvature and ATPase activity

We have provided first evidence that membrane curvature can modulate the function of ABCs. We analyzed proteoliposomes (20 – 200 nm of diameter) with membrane curvature representative of intracellular vesicles, e.g. size of endosomes (60–500 nm), synaptic vesicles (20 – 80 nm) and lipid nanotubules (20 - 450 nm)(Zhang et al., 1998). We showed that the activity was decreased 4 times for liposomes size smaller than 40 nm of diameter than large liposomes in PC/PA and PC/PS.

Changing the size of the liposomes influences in bilayer asymmetry and physical modulations of membrane curvature and tension (Figure 107). In our reconstituted system, BmrA is oriented with NBDs outside of liposomes with positively charged residues at the outer leaflet of liposomes. We have previously suggested that inner leaflet contains more conical lipids, negatively charged lipids with a small head group and PE lipids, than outer leaflet. Due to the difference in surface area, 40 – 45% of lipids are localized in inner leaflet than outer leaflet in liposomes of 20 - 40 nm diameter (Marquardt, Geier, & Pabst, 2015). It is thus possible that the decrease of activity is related to the lower concentration of anionic lipids in the outer leaflet of liposomes.

The decrease of ATPase activity could also be influenced by membrane curvature and tension. Although only very few studies have been reported, Tonnesen and co-workers have shown that the pore size of α -hemolysin were modified in small vesicles, consequently decreasing pore permeability (Tonnesen, Christensen, Tkach, & Stamou, 2014). In the case of ABCs, like MsbA and other exporters, several apo conformation have been reported with variable separation of NBDs. Whatever their physiological reality, they demonstrate a great plasticity of ABCs. It is likely that apo BmrA also has the ability to adapt to high curvature in small liposomes. The hydrolysis of ATP must then overcome the membrane-bending barrier.

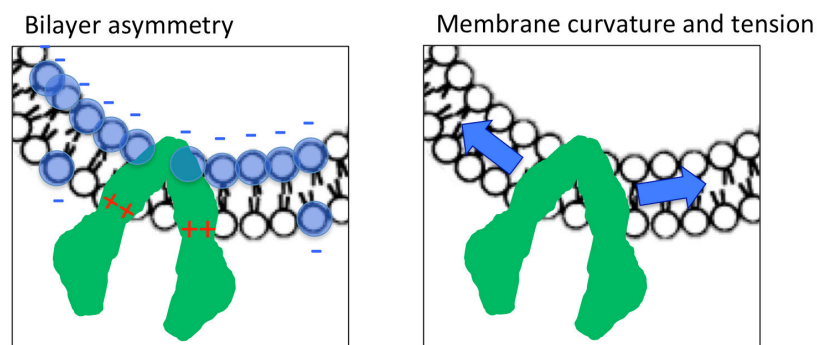


Figure 107 How geometrical membrane curvature influence protein activity.

Bilayer asymmetry: as conical anionic lipids are concentrated in the inner leaflet of small liposomes, anionic lipids do not interact to positively charged residues of BmrA, resulting an functional inhibition. Membrane curvature and tension physically prevent protein function.

Membrane curvature and protein distribution

We have investigated protein distribution in curved membranes of micron-sized reconstitution system. There was a significant difference in BmrA sorting between apo and post-hydrolysis conformation in curved membrane. In order to interpret the data, we need to understand if BmrA is sorted in positive or negative curvature. This can be deduced from the

knowledge of the orientation of BmrA in the nanotubes. We have experimentally demonstrated that apo BmrA is orientated 50/50 inside-in/inside-out in GUVs. We have also shown by trypsin digestion that when apo-BmrA is sorted in lipid nanotubes, proteins were in an inside-out conformation. This revealed that during the tube pulling, only inside-out proteins are sorted while inside-in BmrA are returned in the flat regions of GUVs. Thus, apo BmrA is sensitive to positive membrane curvature (Figure 110A).

In the case of post-hydrolytic conformation, ATP-Vi trapped, we did not succeed to performed trypsin digestion. However, one can deduce the orientation from the experiment where ATP- γ -S has been added to apo BmrA in inside-out orientation and already sorted in lipid nanotubes.

Then, upon the addition of the inhibitor, all proteins returned into flat GUVs (Figure 108C), suggesting that post-hydrolysis conformation of BmrA is not stabilized in positive curvature. Therefore, it is likely that in experiment where Vi-trapped BmrA were sorted, proteins were enriched in negative membrane curvature with the NBDs oriented inside of the nanotubes (Figure 108A). This result is consistent with theoretical models where inverted conical shaped proteins are sorted in negatively curved membrane (Figure 108D)(Sophie Aimon et al., 2014; McMahon & Boucrot, 2015).

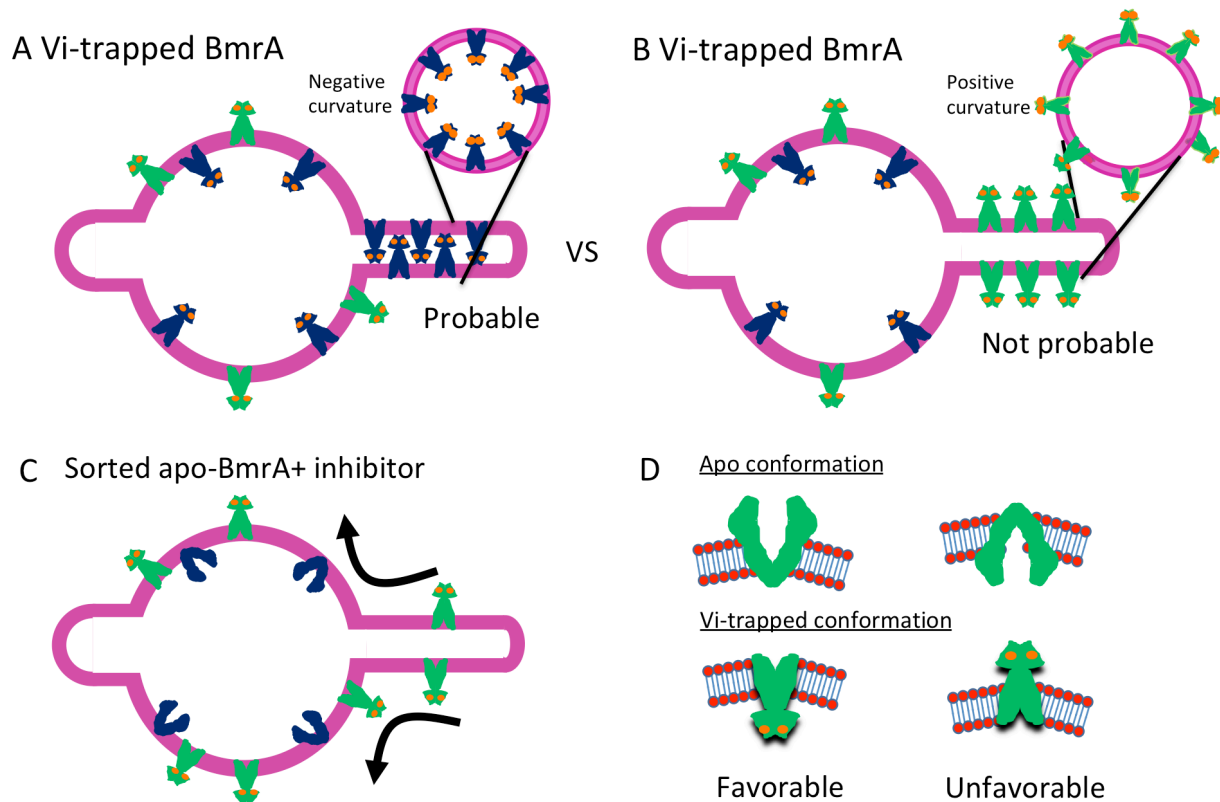


Figure 108 Schematic presentation of sorting of post-hydrolysis conformation.

(A, B) Two possible orientations of BmrA sorted in post-hydrolysis conformation. (C) Addition of inhibitor to apo-BmrA sorted in positive membrane curvature leads to complete decrease of sorting suggesting that BmrA in post-hydrolytic conformation prefers negative membrane curvature. (D) It is likely that inverted-conical shaped protein is inserted in positive membrane curvature.

In the case of KvAP and AQP0, two tetrameric proteins, sorting value revealed protein non-zero spontaneous curvature, which reflects to conicity of the protein in membrane. Experiments with BmrA are more complicated to interpret because the overall shape BmrA is not a square but has two different dimensions in the plane of the membrane (Figure 109 A, C). This means that the protein does not undergo the same membrane bending effect depending on the

side of BmrA. Moreover, the theoretical models established with KvAP and AQP0 considered a fixed conformation. In the case of BmrA, the protein undergoes several conformations. Therefore, a new theoretical model is required for calculation of BmrA's conicity.

The relative conicity can still be compared between apo- and post-hydrolysis conformations, which are 4 times more conical in apo than post-hydrolysis conformations in transmembrane domain.

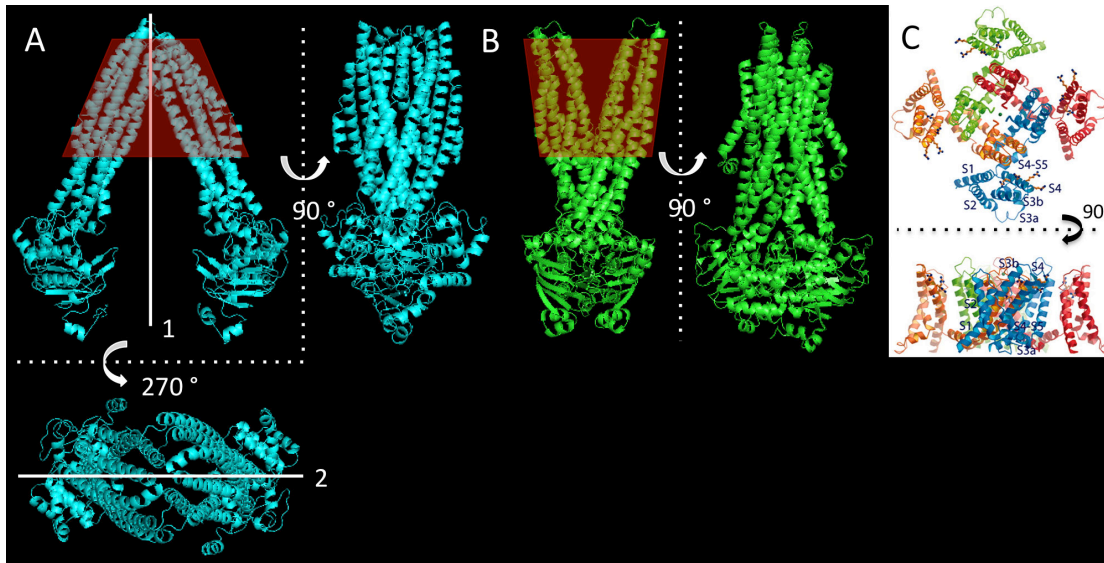


Figure 109 Models of BmrA and KvAP

(A) The models of apo-BmrA show two axes of symmetries. (B) The structure of SAV1866 (PDB: 2HYD) shows an opposite conical shape (red) to apo-conformation at the transmembrane part. (C) The model of KvAP shows a conical shape of the protein (S.-Y. Lee, Lee, Chen, & MacKinnon, 2005).

Furthermore, experiments with fixed conformations in apo and post-hydrolysis suggest that large conformational changes occur during the catalytic cycle in our experimental conditions, i.e. in curved membranes and at room temperature. This is also confirmed by the experiment where we studied protein distribution during the catalytic cycle (Figure 110). The addition of ATP to apo-BmrA sorted into positive membrane curvature results in the return of BmrA in a flat membrane, suggesting a conformational change during catalytic cycle.

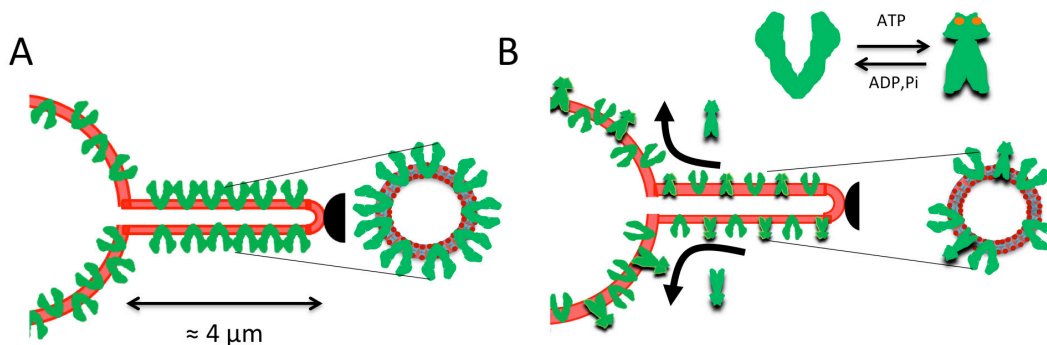


Figure 110 Schema illustrating sorting according to catalytic states

(A) Positive membrane curvature is unfavorable in post-hydrolysis conformation BmrA oriented with NBDs outside of membrane and in apo-conformation with NBDs inside. Sorting in post-hydrolysis (B), apo- (C) conformations and during catalytic cycle (D) in nanotube are illustrated.

Clustering of BmrA

Clustering of apo-BmrA was observed during tube-pulling experiments suggesting protein/protein interaction. The clustering of apo-BmrA was observed at the neck of GUVs (500 – 1500 lipids per BmrA) and not in GUVs flat regions (3800 – 30 000 lipids per BmrA). Protein/protein interaction was also shown in EM experiments, which BmrA form define highly curved assemblies at high protein density (lipid/protein ratio 0.5 – 2 w/w) in apo conformation (see Interplay between BmrA and membrane at high protein density). In this case, 45 – 170 lipids were present per BmrA. These assemblies of apo conformation were observed in various lipid compositions. However, FRET studies shows no evidence of protein interaction by interFRET experiments in liposomes at medium protein density (3400 – 17 000 lipids per BmrA) (Figure 119). All these data suggest that protein/protein interaction is sensitive to protein density and membrane curvature (Figure 111).

Besides, no evidence of clustering of post-hydrolysis BmrA was observed during the tube pulling experiment. Contrary to apo conformation, post-hydrolytic conformation appears to diffuse freely between nanotube and GUVs. This result suggests a weaker interaction between proteins in post-hydrolysis conformation than in apo-conformation.

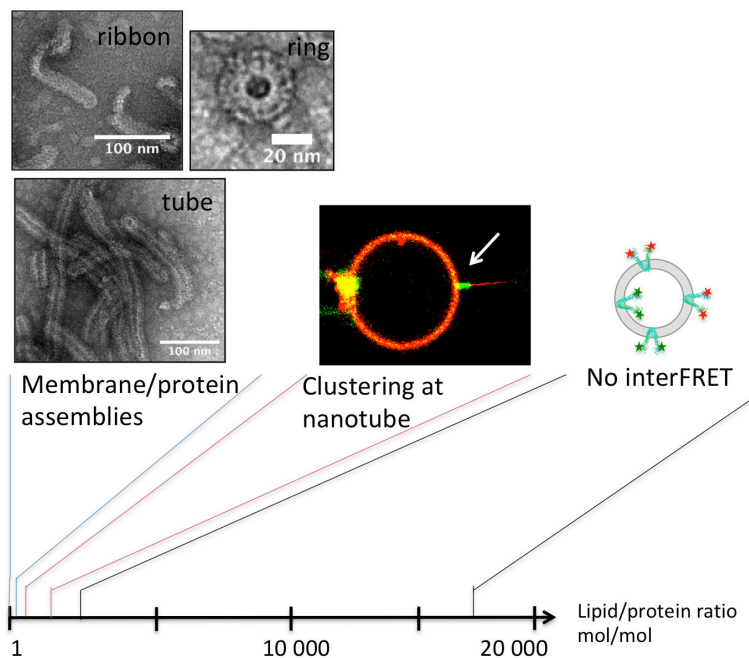


Figure 111 Clustering of apo-BmrA according to protein density

Spatial distribution of ABCs in cell membranes

BmrA can cluster if the protein density is high enough. Consequently, membrane conditions that may favor local protein density of BmrA will induce clustering of apo-BmrA, e.g. membrane raft or membrane curvature.

In a bacterial membranes, the curvature is nearly zero. There may be different curvatures during cell division or spore formation, but not as strong to promote clustering or sorting of BmrA. Therefore, there will be no consequences of membrane curvature in function or distribution of ABCs.

However, there are some lipid domains in bacteria (Lopez, 2015). The membrane of *B. subtilis* is mainly composed of PE, PG and CL (Muchová, Wilkinson, & Barák, 2011). It has been reported that lipid rafts have been discovered in *B. subtilis* associated to polyisoprenoids (Figure 112)(Barák & Muchová, 2013). Also lipid microdomains are present with preferential localizations (Figure 112): septal regions were enriched by PE-rich domains; CL are preferentially localized at in septal regions and at the cell poles; and PG are enriched in helix-like lipid structure extending along the long axis of the cell. Moreover, it has been reported that antibiotics preferentially interacts with lipid domains enriched in PG and forming macroscopic “helices” in the membrane of bacteria. The localization of BmrA is unknown but one can speculate that the function of BmrA is modulated according to its localization.

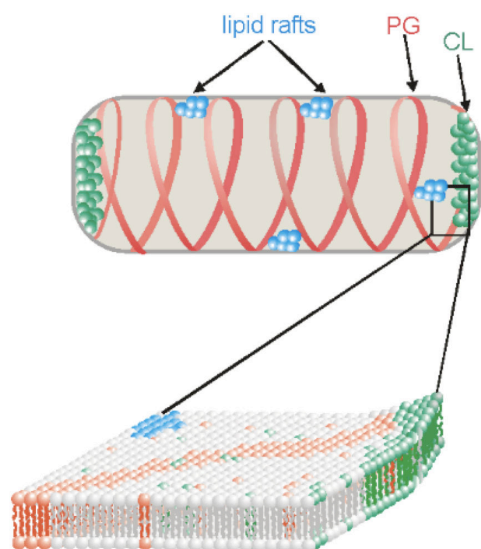


Figure 112 Lipid domains in *B. subtilis* (Barák & Muchová, 2013)

Besides, in eukaryotic cells, several membrane-remodeling processes occur with significantly different curvatures (Figure 113). In addition, lipid composition varies according to organelles, lipids form domains and are asymmetrically distributed. We can speculate that function and distribution varies according to the membrane curvature and local lipid composition. For example, several studies reported possible localization/enrichment of ABCs in caveolin or lipids raft enriched in cholesterol and sphingolipids (Klappe et al., 2009). In this case, function of ABC may be modulated according to its localization.

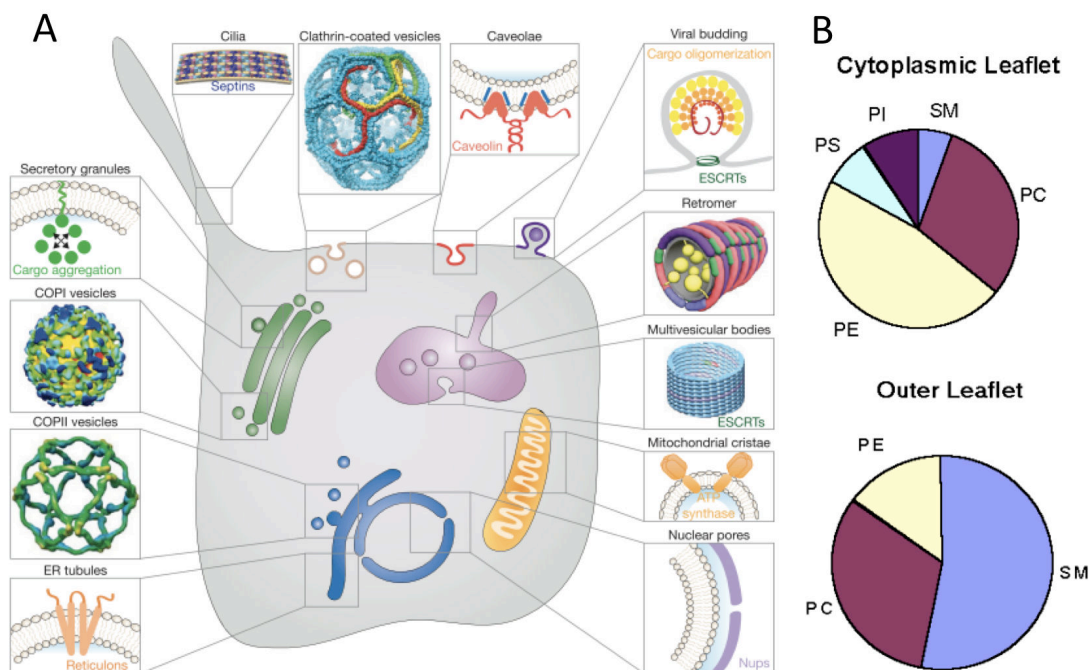


Figure 113 Membrane curvature and bilayer asymmetry in eukaryotic cell

(A) Membrane remodeling occurs with different range of membrane curvature. (B) Percent distribution of phospholipids between the outer and cytoplasmic leaflets of the human erythrocyte membrane. SM, sphingomyelin; PI, phosphatidylethanolamine. (Quinn, 2004; Stachowiak, Brodsky, & Miller, 2013)

The global cytoplasmic leaflet contains majority of PE lipids and 10% of PS lipids (Figure 113B). These lipids should interact with ABCs by their positively charged residues in the cytoplasmic side, suggesting a high protein activity.

The distribution of ABCs can be estimated according to membrane curvature (Figure 114). During any kind of invagination of vesicles with positive curvature, such as endocytosis, pinocytosis etc., ABCs would preferentially be localized in flat membrane without functional impairment as shown in tube pulling experiment. In the case of membrane protrusion such as membrane budding, filopodia or dendritic spines, the location of ABC will depend on the membrane curvature. For vesicle higher than 40 nm of diameter, ABCs would be excluded, such as in filopodia. For vesicles smaller than 40 nm of diameter, it is possible that ABCs in post-hydrolysis conformation are enriched in negatively curved membrane. How negative curvature affects function of ABCs is unknown.

However, this location may also depend on catalytic cycle. If ABC remains longer in apo conformation than in post-hydrolysis conformation, ABCs would be located preferentially in flat membrane in all cases without functional impairment. Therefore, the distribution of ABCs would not change during membrane remodeling.

In order to elucidate spatio-temporal distribution of eukaryotic ABC in curved membrane, we initiated collaboration with S. Wilkens (SUNY, New York), who has been studying and performing experiments on biochemical and molecular biological technique with eukaryotic PgP. We plan to incorporate PgP and perform tube pulling experiment with protocol established with BmrA.

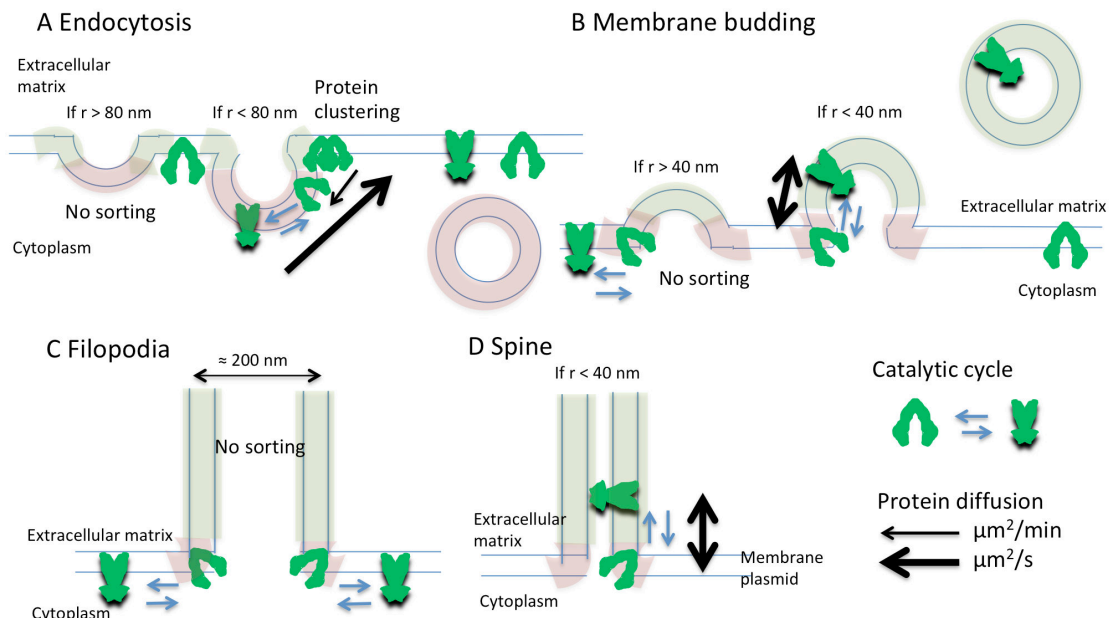


Figure 114 schematic representation of possible localization of ABCs in curved membranes

Positive and negative membrane curvatures are indicated in red and green colors.

Overall, we showed the contribution of lipid composition and membrane curvature on the membrane function, spatial distribution and domains clustering of BmrA (Figure 115). We also showed that BmrA in different conformations modulate membrane curvature. This revealed a functional interplay between the transmembrane proteins and its surrounding membrane environment.

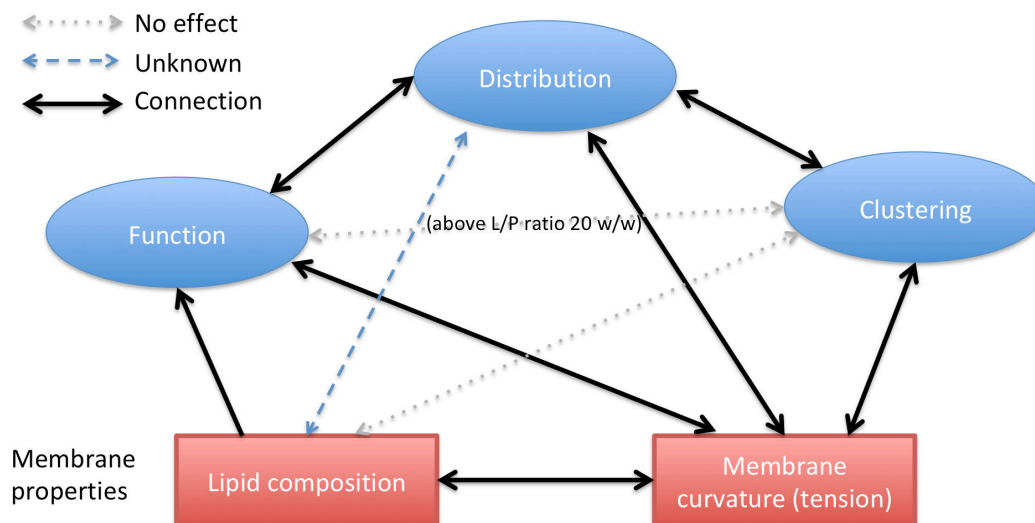


Figure 115 Interplay between BmrA and membrane

Annexe I : Dynamics of BmrA by smFRET

a. Optimization of experimental conditions for FRET measurements of reconstituted BmrA

Reconstituted BmrA in EPC/EPA or *E. coli* lipids were incubated at 20 or 37 °C, and ATPase activity was measured at different times to determine how long FRET experiments could be performed.

At 37 °C, the ATP hydrolysis of BmrA reconstituted in *E. coli* lipids was linearly decreased until the protein was completely inactivated after 1 h of incubation (Figure 116 A). Indeed, aggregation of *E. coli* proteoliposomes could be observed by eyes. In EPC/EPA lipids, activity was stable 1 h at 37 °C, then completely inactivated up to 2 h incubation. At 20 °C, activities were stable in both *E. coli* and EPC/EPA after incubation for 1 day at 20 °C and 3 days at 4 °C. But when we observed by cryo-EM images of *E. coli* proteoliposomes, we found that *E. coli* liposomes were fused, showing variable sizes and multilayered vesicles after 3 days of incubations at 4 °C. This likely explained the decrease of ATPase activity in *E. coli* liposomes. EPC/EPA proteoliposomes as seen by cryo-EM were stable at least for 3 days at 4 °C.

Therefore, further experiments were carried out at 20 °C where both proteoliposomes were stable. For experiments carried out at Montpellier, BmrA in EPC/EPA liposomes were reconstituted in Paris the day before the experiment and kept on ice, or freshly prepared while *E. coli* proteoliposomes were always freshly prepared just before FRET experiments to avoid any fusion of liposomes. Even though the activity was decreased 10 folds at 20 °C compared to 37 °C (Figure 86). BmrA was active and can be inhibited.

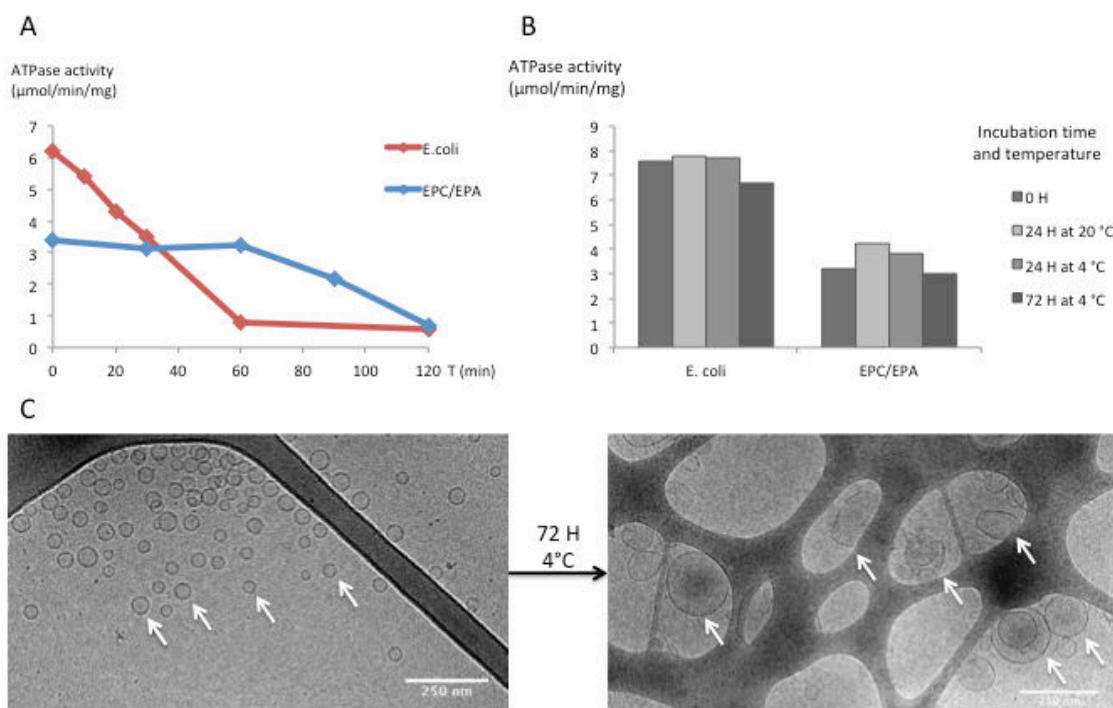


Figure 116 Stability of reconstituted system of *E. coli* and EPC/EPA liposomes according to temperature and time.

ATPase hydrolysis of BmrA was studied according to temperature and time. (A) ATPase activity of BmrA was investigated along the incubation at 37 °C in EPC/EPA (9/1 w/w) or *E. coli* liposomes with 10 mM of ATP. (B) Proteoliposomes were incubated at 4 or 20 °C during 3 days and their ATPase activity were studied with 10 mM of ATP. (C) Images of cryo-EM of *E. coli* proteoliposomes before and after incubation at 4 °C for 3 days shows mixture of fused, multilamellar vesicles and small vesicles (r ≈ 30 nm).

b. Ensemble FRET measurement

1. Fluorescence spectroscopy

BmrA WT were reconstituted in *E. coli* or EPC/EPA (9/1 w/w) liposomes at lipid/protein ratio 100 w/w. FRET efficiency (E_{FRET}) of BmrA in apo- and post-hydrolysis conformation were studied in cuvette with a fluorimeter. E_{FRET} was calculated from fluorescence spectra using the protocol described in material and methods (Figure 55). Then, E_{FRET} was compared before and after addition of ATP and orthovanadate. If there is a higher FRET in the post-hydrolysis conformation than in apo conformation, a decrease in the donor signal with an increase in the FRET signal in the fluorescence spectrum is expected (Figure 117, red arrows).

For the three FRET couples, FRET signal of WT BmrA could be observed in both EPC/EPA and *E. coli* proteoliposomes. E_{FRET} was higher in EPC/EPA than in *E. coli* proteoliposomes in all conditions. Addition of ATP-Vi did not change FRET values in all conditions except for Alexa488/Atto610 BmrA in *E. coli* liposome (see also FCS experiments below). In control experiment with mixtures of single labeled Alexa488-BmrA and single labeled Atto610-BmrA in proteoliposomes, E_{FRET} was 0 as expected.

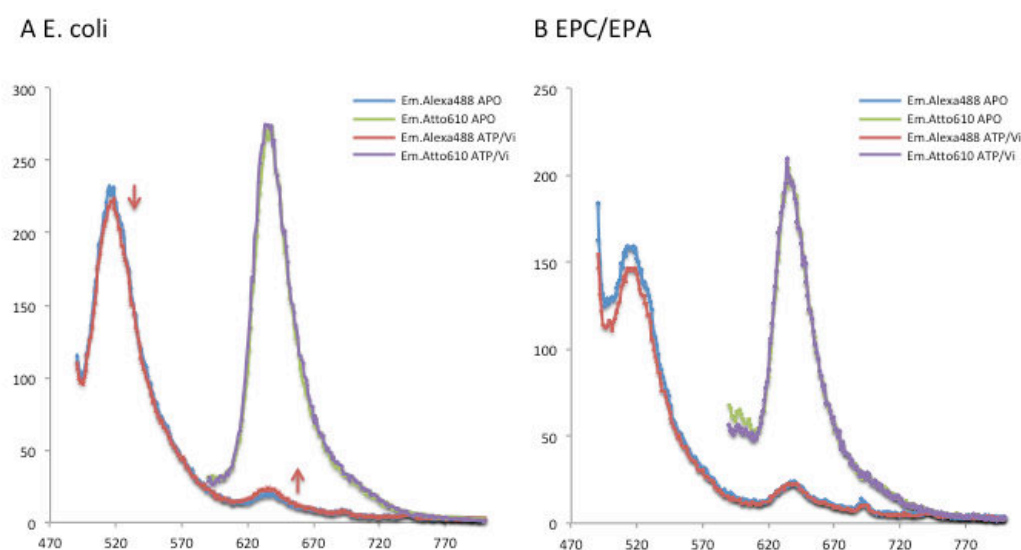


Figure 117 Example of ensemble FRET measurement by fluorescence spectroscopy.

Alexa488/Atto610 BmrA WT were reconstituted in *E. coli* (A) and EPC/EPA (B) proteoliposomes at 100 lipid/protein w/w. Emission spectra were registered before and after addition of 1.5 mM ATP for *E. coli* and 10 mM for EPC/EPA proteoliposomes and 1 mM of orthovanadate.

WT	Lipid composition	Apo E_{fret}	ATP/Vi E_{fret}
sCy3/sCy5	<i>E. coli</i>	0.17	0.17
	EPC/EPA	0.33	0.31
Alexa488/Atto610	<i>E. coli</i>	$0.16 \pm 0 *$	$0.21 \pm 0.01 *$
	EPC/EPA	0.39 ± 0.05	0.38 ± 0.06
Alexa488/sulfo-Cy5	EPC/EPA	0.15	0.12
Alexa488-BmrA + Atto610-BmrA	<i>E. coli</i>	0	0

Table 15 E_{FRET} of reconstituted BmrA WT.

BmrA was reconstituted at 100 lipid/protein w/w. 10 mM of ATP and 1 mM of orthovanadate were added. E_{FRET} were calculated by ratio of areas of donor, FRET and acceptor as described in material and methods. For *, see also **Figure 118**.

E_{FRET} of Alexa488/sulfo-Cy5 of mutant 3 of BmrA was measured in DDM 0.05% in apo conformation, in the presence of ATP and different inhibitors. No significant difference was observed between all the conditions.

M3	Apo Efret	ATP Efret	ATP/Vi Efret	AMP-PNP	ATP- γ -S
Alexa488/sulfo-Cy5	0.11 ± 0.01	0.14 ± 0.01	0.14 ± 0.02	0.12	0.11
Alexa488-BmrA + sulfo-Cy5-BmrA	0	0	0		

Table 16 E_{FRET} of Alexa488/sulfo-Cy5 M3 in detergent

These first experiments suggest a weak donor-acceptors transfer of fluorescence in apo conformation of BmrA but not significant changes of FRET after addition of ATP/vanadate both in membrane and in detergent for WT and M3.

2. Fluorescence lifetime measurement by FCS

We used another method to observe ensemble FRET changes by measuring donor lifetime. Fluorescence lifetime corresponds to an average time for a fluorophore that spent in excited state before returning to ground state. Fluorescence lifetime depends on the photochemistry of fluorophores and ranges from pico- to nanoseconds. When FRET occurs between donor and acceptor, donor fluorescence lifetime is decreased and allows determining E_{FRET} : $E = 1 - \tau_{\text{DA}}/\tau_{\text{D}}$, where τ_{DA} and τ_{D} are the quenched and free donor fluorescence lifetimes, respectively. Measuring donor lifetime therefore allows calculating the spatial proximity between donors and acceptors. The shorter the donor lifetime, the more FRET there is.

Here, we used Alexa488-labeled BmrA as donor because of its relatively long lifetime (≈ 4 ns).

No significant difference between apo and post-hydrolysis conformations

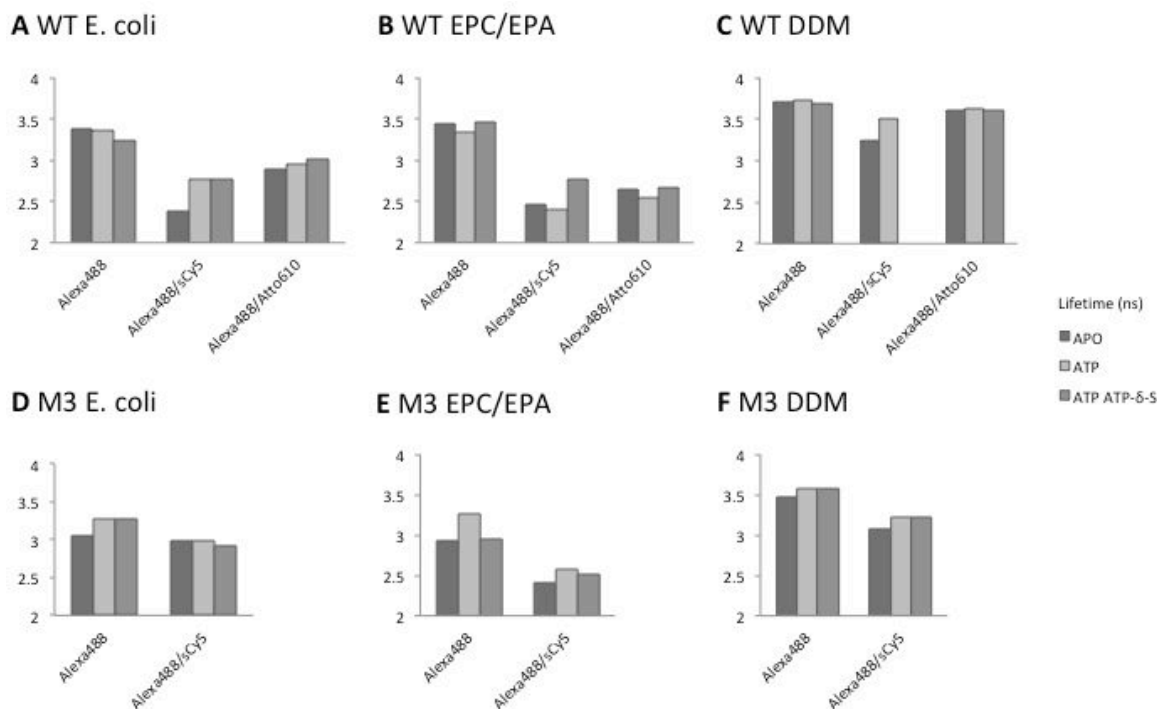


Figure 118 Alexa488 lifetime comparison between apo- and post-hydrolysis conformations.

10 mM of ATP and 10 mM of ATP-γ-S were added in detergent and in EPC/EPA. 1.5 mM of ATP and 1.5 mM of ATP-γ-S were added in *E. coli* to avoid aggregation of liposome.

Conformational changes of BmrA were investigated through changes in donor lifetime by adding ATP and inhibitor ATP-γ-S in detergent and in reconstituted systems.

In all conditions, addition of nucleotide or inhibitor did not change donor lifetime compared to apo conformation. This result is consistent with E_{FRET} measured by fluorescence spectroscopy. This suggesting that E_{FRET} changes observed for Alexa488/Atto610 in *E. coli* liposomes was not significant (Table 15 E_{FRET} of reconstituted BmrA WT., *).

The overall results suggest that either dual-labeled proteins are not active, or there is little or no conformational change between NBDs.

3. InterFRET

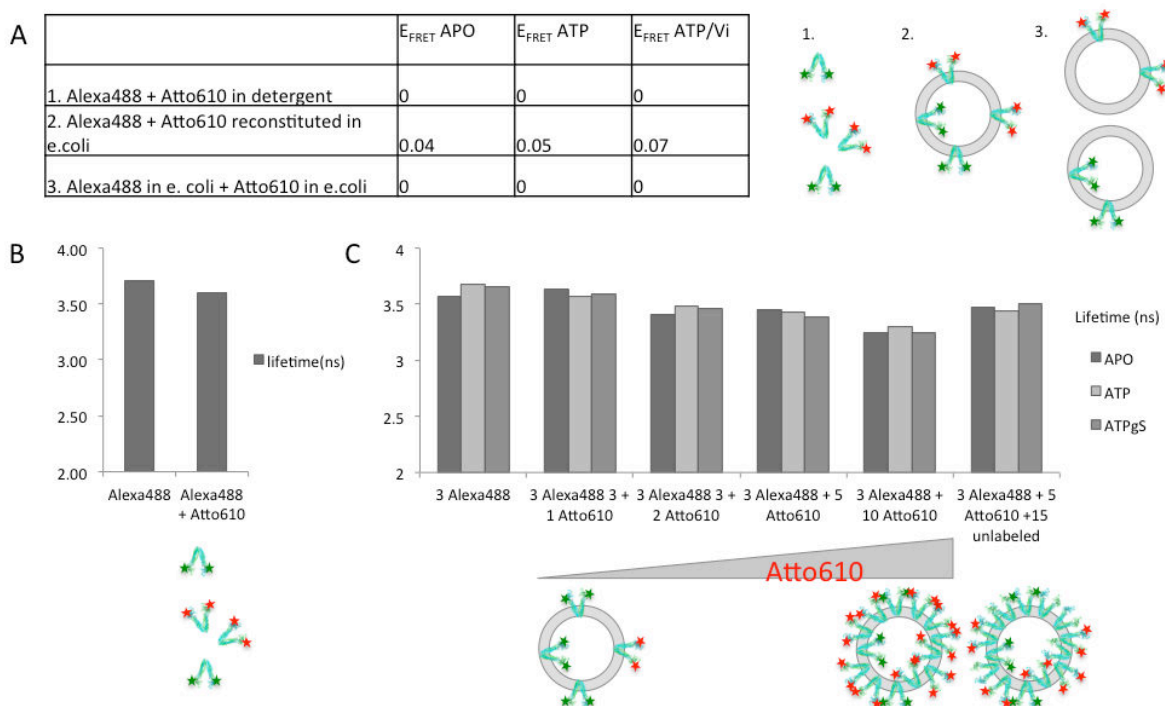


Figure 119 InterFRET measurement fluorescence spectroscopy and donor lifetime measurement.

E_{FRET} (A) and Alexa488 lifetime (B, C) were studied with single labeled Alexa488- and Atto610-BmrA in 0.05% DDM to 200 nM of fluorescent dyes (A1, B) or reconstituted in liposomes. coli (A2-3, C) in apo conformation, in the presence of 1.5 mM ATP, 1 mM orthovanadate and 1.5 mM ATP- δ -S. (A1, 3) BmrA was reconstituted at 100 w/w lipid/protein ratio. (C) Alexa488-BmrA was reconstituted at 120 w/w lipid/protein ratio in the condition of 3 homodimers/liposome. In the same condition, increasing amounts of Atto-BmrA were reconstituted at lipid/protein ratio of 40 - 400 w/w in the condition of 1, 2, 5, 10 homodimers/liposomes. Control experiment was performed with unlabeled protein at 20 w/w lipid/ protein ratio.

We performed an additional experiment to make sure that intermolecular FRET does not interfere with intramolecular FRET measurement. Alexa488 BmrA was reconstituted at 100 lipid/protein w/w ratio, which corresponds to 5 homodimers/proteoliposome and we performed E_{FRET} measurements. When Alexa488 and Atto610 were present in the same proteoliposome, a weak interFRET signal ($E_{\text{FRET}} = 0.04$) was observed in apo conformation, which increases 1.8 times in the ATP-Vi conformation ($E_{\text{FRET}} = 0.07$) (Figure 119 A2). E_{FRET} was 0 in detergent or in the mixture of proteoliposomes with Alexa488-BmrA only and proteoliposomes with Atto610-BmrA only (Figure 119 A1, A3). In Alexa488 lifetime measurement, no significant difference was observed in detergent and in the reconstituted system when Atto 610 BmrA was present (Figure 119). No difference was also observed by adding ATP or inhibitors to the apo conformation. In control experiment, addition of unlabeled BmrA resulted in a small decrease in lifetime.

All these data suggest that either BmrA proteins do not interact or weakly interact with each other when reconstituted in liposomes. Therefore, the intermolecular FRET would not interfere with on previous results in intramolecular FRET experiment based on the values measured in both cases.

c. smFRET by FCCS

1. Experimental approaches

We studied BmrA by single molecule FRET via FCCS in detergent, detergent/lipid and proteoliposomes. The fluorescence intensity was recorded while fluorescent proteins passed through the focal volume in the beam of two different wavelength lasers. We work in diluted protein concentration in pM so that one protein passes during the acquisition time. Each fluorescent signal was averaged to obtain relative raw FRET efficiency, EPR (relative proximity ratio). The intensity of the individual peaks shows that proteins were not aggregated.

We used ALEX (Alternating Laser excitation) system to select dual-labeled protein within the population of homodimers with single and with two identical or different probes. ALEX allows alternating between donor and acceptor excitation lasers for sample illumination. This way, stoichiometry could be calculated and only dual-labeled proteins were selected for EPR distribution (Figure 120 B3, C3).

2. smFRET of BmrA solubilized in micelles of detergent

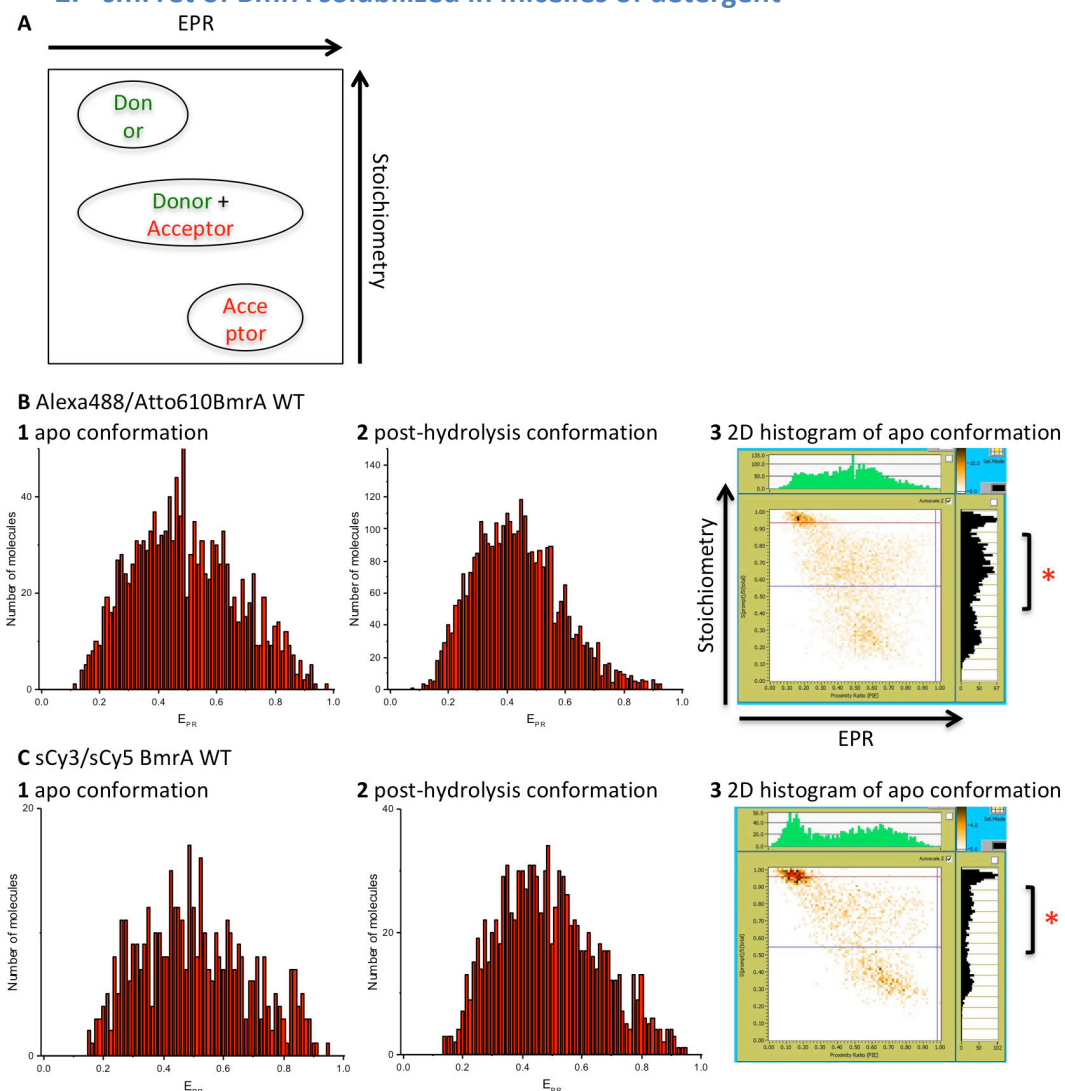


Figure 120 No difference of EPR between apo and post-hydrolysis conformations for BmrA WT Alexa488/Atto610 and sulfo-Cy3/sulfo-Cy5 in detergent.

(A) 2D histogram presents stoichiometry as function of EPR. Alexa488/Atto610 (B) and sulfo-Cy3/sulfo-Cy5 (C) BmrA WT were diluted to 50 pM in 0.05% of DDM. EPR histograms of dual-labeled protein were studied by FCCS between apo conformations (1)

and after addition of 5 mM of ATP and 1 mM of orthovanadate (2). 2D histograms of FRET couples showed 30% of dual-labeled BmrA, which corresponds to results obtained in biochemistry (3) * indicates dual-labeled BmrA.

Alexa488/Atto610 and sulfo-Cy3/sulfo-Cy5 of BmrA WT were studied in 0.05% DDM. The histograms of EPR were compared between apo- and post-hydrolysis conformations. The percentage of dual-labeled protein was calculated to approximately 30% for both FRET couples, which corresponded to results obtained by biochemistry (Figure 120 *B3, C3).

In apo conformation, a broad spectrum of EPR was observed from 0.15 to 0.95, with a main peak centered at 0.5 for both couple of FRET dyes (Figure 120 B1, C1). In post-hydrolysis conformation, no difference of EPR was observed in both cases (Figure 120 B2, C2).

3. smFRET of BmrA solubilized in micelles of lipid/detergent

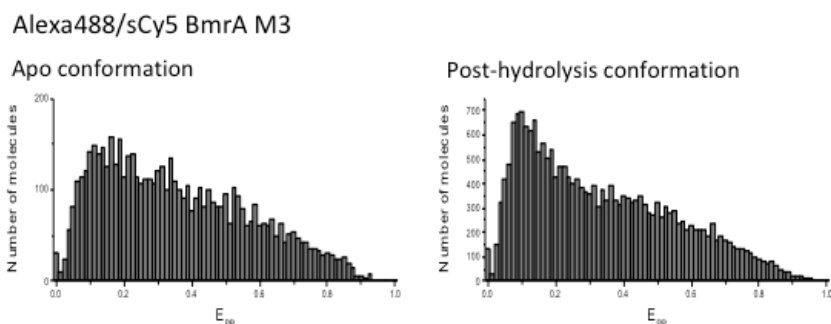


Figure 121 No changes in EPR between apo- and post-hydrolysis conformations of Alexa488/sCy5 BmrA M3 in micelles of lipid/detergent.

Alexa488/sulfo-Cy5 BmrA M3 were diluted to 50 pM in buffer containing 50 μM EPC/EPA (9/1 w/w), 0.01 % Triton X-100. Histogram of smFRET was compared between apo conformation and in the presence of 10 mM ATP and 10 mM AMP-PNP.

Alexa488/sulfo-Cy5 BmrA M3 was diluted in lipid/detergent micelles, and dual-labeled proteins' EPRs were studied between apo- and post-hydrolysis conformations.

In apo conformation, a broad spectrum was observed as in DDM from 0 to 0.95, centered at 0.15 (Figure 121). Addition of inhibitor did not affect the histogram.

4. smFRET of BmrA solubilized in proteoliposome

Estimation of lipid/protein ratio of reconstitution for single molecule studies

We calculated the lipid/protein ratio as a function of liposome diameter to obtain one homodimer/liposome. Estimated area of lipid head is around 65 Å² (Kučerka, Nieh, & Katsaras, 2011), the approximate number of lipids per liposome can be calculated, taking account that the membrane is a bilayer:

$$\text{Surface area of liposomes} = 4\pi R^2 * 2$$

$$\text{Number of lipids} = \text{Surface area of liposomes} / \text{Area of lipid} = 8\pi R^2 / 65$$

From the number of lipids, the ratio of molecular weight between lipids (MW 800) and a monomer of BmrA (MW 65 000) leads to the estimated number of BmrA per liposome per diameter of liposomes:

$$\text{Ratio Lipid/Protein} = \text{Number of lipids} * (\text{MW of lipids} / \text{MW of BmrA}) = \frac{8\pi R^2}{65} \times \frac{800}{65000} \quad (\text{Figure 122})$$

Lipid/protein ratio was calculated based on experimental average size of liposomes, which depends on the lipid composition (see Liposome size).

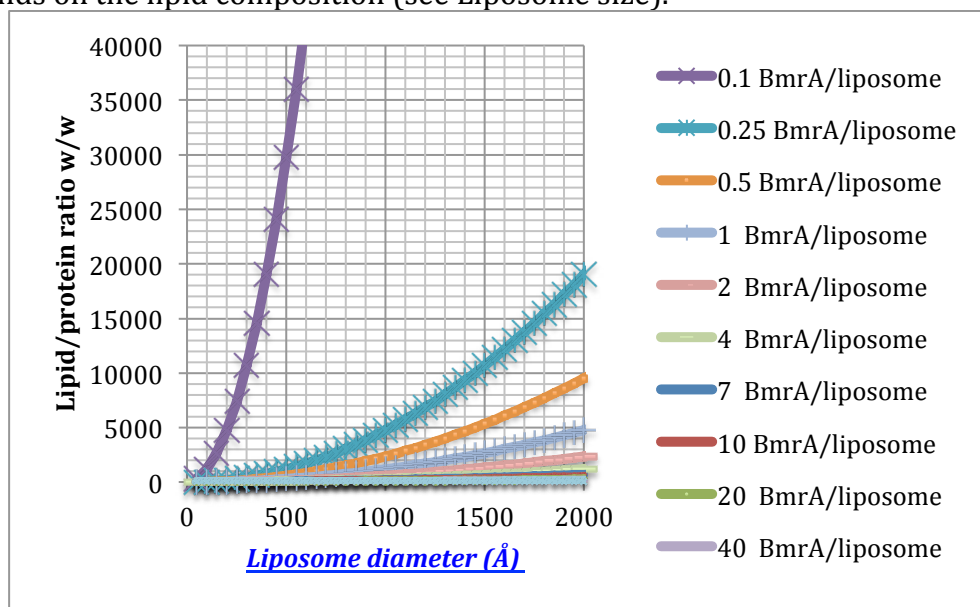


Figure 122 Estimated number of BmrA according to diameter of liposome.

Lipid/protein ratio according to diameter of liposomes is estimated based on lipid area (65 \AA^2), molecular weight of BmrA ($\approx 65 \text{ kDa}$) and lipids ($\approx 800 \text{ Da}$).

Analyze of one homodimer per liposome via FCS

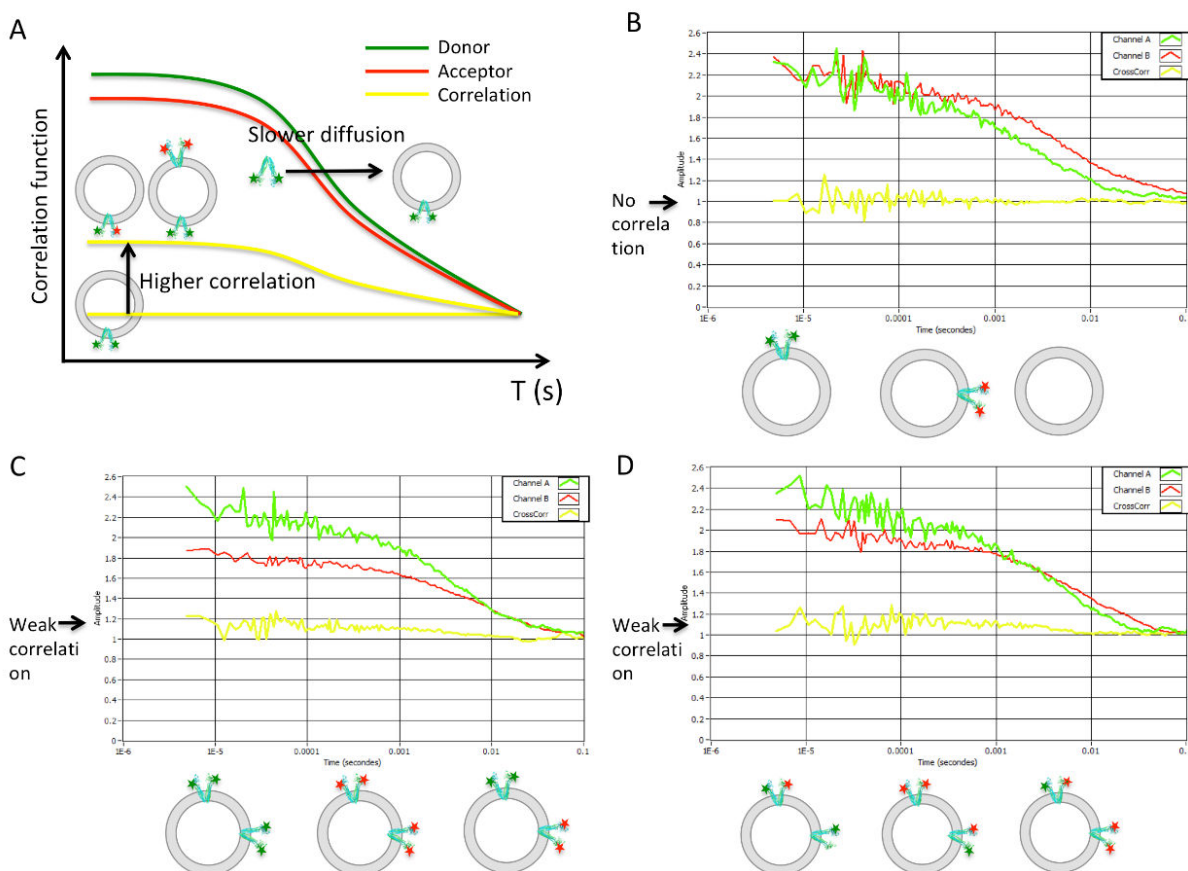


Figure 123 Correlation function according to protein density .

(A) Illustrative schema for FCS results. (B) Alexa488-BmrA and Atto610-BmrA were mixed and reconstituted in EPC/EPA liposomes at 8500 lipid/protein w/w. FCS was carried out showing no correlation between them. (C) In a same condition, protein were reconstituted at 430 lipid/protein w/w where a weak correlation was observed. (D) Dual-labeled Alexa488/Atto610 BmrA were reconstituted at 430 lipid/protein w/w as positive control where a weak correlation was observed.

We investigated by FCS whether calculated lipid/protein ratio actually led to one homodimer/proteoliposome. We mixed single labeled Alexa488-BmrA and Atto610-BmrA, and reconstituted in EPC/EPA in different lipid/protein ratios: at 8500 w/w at 430 w/w that would corresponded to 0.1 and 2 homodimer/liposome, respectively for liposome size < 90 nm. Then, we used fluorescence correlation spectroscopy (FCS) technique that allows measuring diffusion coefficient and also spatial-temporal correlation between two fluorophores. If there is only one homodimer/liposome, we expect no correlation. In the case of one or more Alexa488 and Atto610 within the same proteoliposomes, we expect correlation between two dyes. Dual-labeled Alexa488/Atto610 was also studied as a positive control.

Fluorescent signal of BmrA was diffusing during 10-30 ms in focal volume confirming that BmrA was reconstituted in liposomes and not aggregated (Figure 123). No correlation between Alexa488-BmrA and Atto610-BmrA was observed at 8500 w/w lipid/protein ratio demonstrating that BmrA can be reconstituted 1 homodimer/proteoliposomes. A lipid/protein ratio to 430 w/w, i.e. increasing protein density, leads to weak correlation. In control experiment, doubly labeled BmrA showed weak correlation as expected.

For further single molecules studies, we reconstituted in even more diluted protein condition, 40 000 ratio w/w to be sure that only 1 homodimer was present per liposome. It is

expected that for 60 nm *E. coli* liposome diameter (see Figure 75), 40 000 lipid/protein ratio corresponds to 0.01 homodimer/liposome.

Presence of unknown fluorescent contaminants in lipids

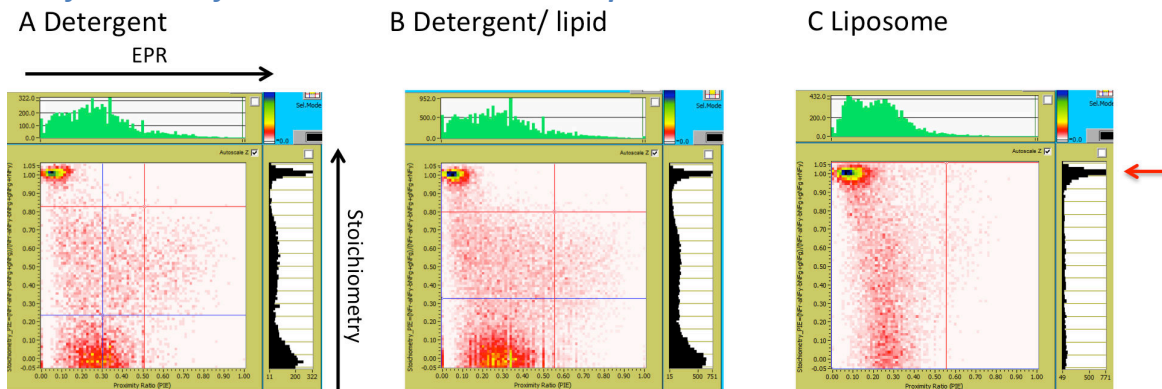


Figure 124 Presence of contaminants in lipids

Alexa488/sCy5 BmrA M3 was studied in single molecule level in 0.05% DDM (A), in micelles of EPC/EPA/Triton X-100 (B) and EPC/EPA liposomes (C). Red arrow indicates presence of contamination.

A fluorescent contaminant was detected by laser excitation between 488 nm and 532 nm in EPC/EPA and *E. coli* lipids. As shown in Figure 124, the presence of contamination (red arrow) was higher in liposomes compared to detergent and in micelles of detergent/lipid. This contamination was a major problem during the smFRET measurement in reconstituted system:

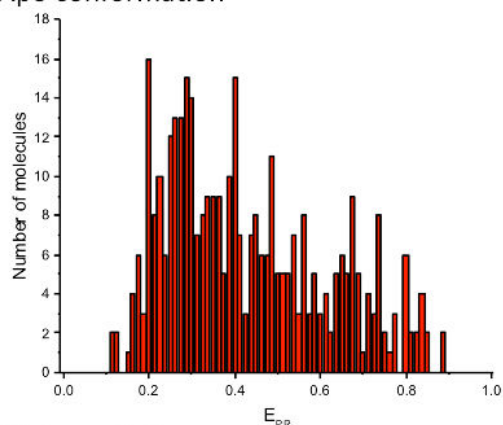
- The presence of contaminants prevents a good separation between donor, acceptor and dual-labeled proteins. As shown in Figure 56C, the dual-labeled and acceptor signals were masked by the contaminant signal.
- We could not obtain high statistics because we had to work in an even more diluted condition. For example, 3 hours was sufficient to collect data with good statistics in detergent, whereas in reconstituted conditions, even 12 hours of data collection was not sufficient to get good statistics.
- This contaminant had 4 ns fluorescent lifetime, therefore difficult to distinguish from Alexa488.
- Contaminants diffused with liposomes.
- The contaminants were more present in *E. coli* than EPC/EPA lipids and the intensity of this contamination was higher at the excitation wavelength of Cy3 (532nm) than at the one of Alexa488 (488nm).
- As contaminants were detected directly from pure lipids liposomes resuspended in water from lipid film, this suggests that contaminants were already present from the purchased lipids.

Fortunately, no FRET signal was detected among these contaminants (data not shown). Contaminants were not detected in buffer, detergent or BioBeads.

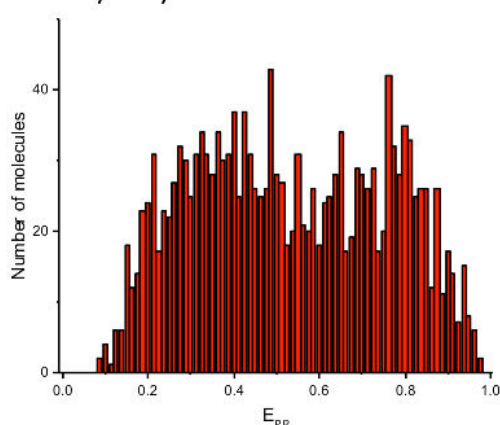
Importance of number of data points

A low statistics

Apo conformation

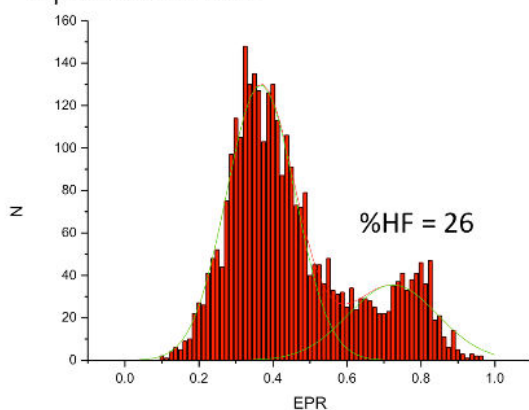


Post-hydrolysis conformation



B high statistics

Apo conformation



Post-hydrolysis conformation

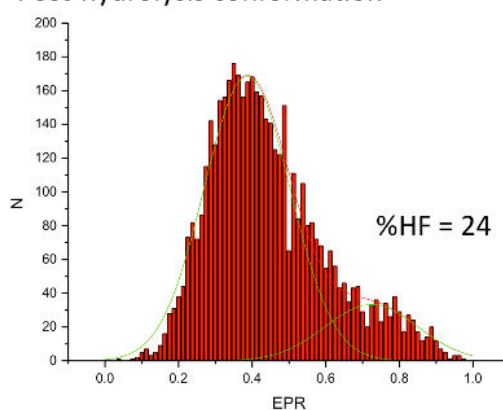


Figure 125 Comparison of EPR histograms between low and high statistics.

Sulfo-Cy3/sulfo-Cy5 BmrA WT were reconstituted in EPC/EPA and EPR distributions were compared between 2 hours (A) and 12 hours (B) of data collection. EPR distributions were studied in apo conformation and in post-hydrolysis conformations in the presence of 10 mM of ATP and 1 mM of orthovanadate. %HF stands for percentage of high FRET.

We compared the data collected in 2 hours and 12 hours with sulfo-Cy3/sulfo-Cy5 BmrA WT, reconstituted in EPC/EPA. Experiments were performed independently but with the same protein. EPR distributions were compared between apo- and post-hydrolysis conformations.

With low statistics, EPR distribution switches to high FRET in the presence of inhibitor (Figure 125A). Besides, with high statistics, no difference of distributions was observed (Figure 125B), which is consistent with results of ensemble FRET. This result would suggest that sulfo-Cy3/sulfo-Cy5 BmrA WT was not active. It is therefore essential to acquire data with good statistics, which would correspond to at least 10 000 particles.

EPR distribution according to conformational changes with different FRET couples

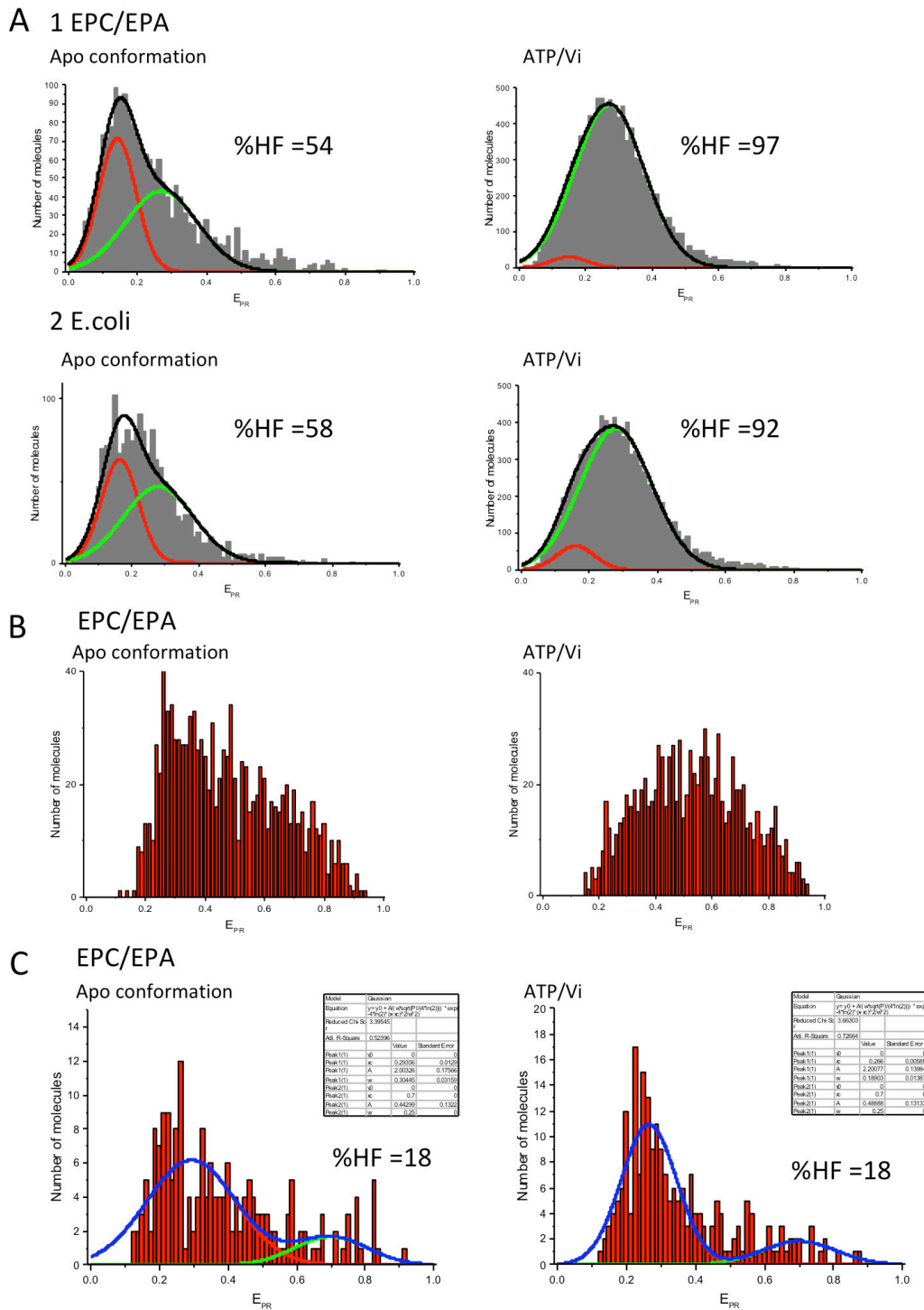


Figure 126 Comparison of EPR distribution between apo and post-hydrolysis conformation with different FRET couples.

BmrA WT Alexa488/sulfo-Cy5 (A), WT Alexa488/Atto610 (B), WT Cy3B/sulfo-Cy5 were reconstituted in EPC/EPA (9/1 w/w) (A1, B, C) or *E. coli* (A2) liposomes. EPR distributions between apo- and post-hydrolysis conformations were studied in the presence of 10 mM of ATP and 1 mM of orthovanadate for EPC/EPA or 1.5 mM of ATP and 1 mM of orthovanadate for *E. coli* proteoliposomes.

Alexa488/sulfo-Cy5, Alexa488/Atto610, Cy3B/sulfo-Cy5 BmrA WT were reconstituted in membrane and their EPR distributions were studied in apo- and post-hydrolytic conformations.

We only managed to get a good statistics with Alexa488/sulfo-Cy5 BmrA WT (Figure 126A). The shift to high FRET in post-hydrolysis conformation was observed in EPC/EPA and *E.*

coli liposomes. However, the width of the spectrum did not allow a clear separation between low and high FRET. Part of the population remained in low FRET after addition of inhibitor. This may be due to 25% protein oriented with NBDs inside the liposomes (See Protein orientation). No difference of distribution was observed between two lipid compositions.

In the case of Alexa488/Atto610, the shift to high FRET was observed in post-hydrolysis conformation with low statistics (Figure 126B).

For Cy3B/sulfo-Cy5, no significant change was observed as the sulfo-Cy3/sulfo-Cy5 couple (Figure 126C).

d. Conclusion

Unfortunately, we cannot conclude in this chapter because results in FRET measurement were not fully consistent with biochemical studies.

The main difficulty is that we ignore whether the dual-labeled protein is active and we could not confirm it biochemically. In ensemble FRET measurement, where all functional studies were performed in similar condition (protein density, reconstitution), we did observe FRET signal but we did not observe any change in FRET in micelles and membrane. In addition, when we studied the dual-labeled protein in single molecule level in detergent and lipid/detergent micelles, no difference of FRET distribution was observed before and after addition of inhibitor. We also encountered a difficulty related to the presence of contamination in lipids in single molecule measurement. This affected the data collection and analysis in reconstituted system with relevant statistics that is crucial for smFRET measurement.

But we do have some biochemical evidences suggesting that BmrA can be fully inhibited in both detergent and in membrane and dual-labeled proteins should be active in some condition. For example, Alexa488/sulfo-Cy5 mutant 3 has 50% of dual-labeled protein, with preserved activity as unlabeled mutant 3. Typically, in this condition, one can expect that dual-labeled Alexa488/sulfo-Cy5 BmrA were active.

This leads to the question whether the dual-labeled proteins are not active or whether there is no significant conformational change between NBDs during the catalytic cycle.

This study was taken over to A. Damm because of lack of time. A. Damm is currently performing smFRET studies with immobilized proteoliposomes on the surface and measuring FRET in ms time scale.

Résumé

a. Introduction

Les transporteurs ABC (ATP-binding cassette) sont l'une des plus grandes familles de protéines transmembranaires que l'on trouve dans tous les organismes vivants. Les ABC hydrolysent l'ATP pour importer ou exporter des substrats de différents types et tailles à travers la membrane : lipides, sels biliaires, hormones, micronutriments, nucléotides, sucres, vitamines, métaux, peptides, etc. (Beek et al., 2014; P. M. Jones & George, 2004). Certains ABC exporteurs confèrent un phénotype cellulaire de multirésistance (MDR : Multi Drug Resistance) par un efflux massif de molécules toxiques vers l'extérieur de la cellule (Figure 3)(Gottesman et al., 2002; Robey et al., 2018). Ce phénotype MDR est présent dans de nombreux organismes : bactéries, levures, plantes chez l'homme et confère une résistance aux antibiotiques, aux antifongiques, aux herbicides et aux médicaments anticancéreux, respectivement (Baral, 2017; Dawson & Locher, 2006; Kang et al., 2011; Thomas & Tampé, 2018). Les ABCs participant au MDR ont également été identifiés comme transporteurs de lipides et la relation entre l'ABC et la membrane a été mise en évidence (Higgins & Gottesman, 1992).

Les transporteurs ABC sont constitués d'un domaine transmembranaire (TMD) formant une cavité pour le substrat, et d'un domaine de fixation de nucléotides (NBD) qui contient un $\frac{1}{2}$ site catalytique (Figure 1). Tous les transporteurs ABC partagent une organisation fonctionnelle commune d'au moins deux NBDs et deux TMDs. Les ABC bactériens sont des demi-transporteurs et fonctionnent en homo- ou hétérodimères. Les homodimères contiennent deux sites catalytiques tandis que les hétérodimères contiennent un site catalytique et un site dégénératif, incapables d'hydrolyser l'ATP. Les NBDs sont conservés parmi les ABCs tandis que les TMDs sont variables (Robey et al., 2018; Wilkens, 2015).

Plusieurs structures de ABCs ont été résolues en cristallographie aux rayons X et en microscopie électronique (EM) (Locher, 2016; Moeller et al., 2015). Il existe trois conformations majeures (Figure 9): (i) les conformations apo- pré-hydrolytiques présentent des ouvertures variables entre les NBDs avec la cavité du substrat ouverte vers le cytoplasme; (ii) les conformations occlusives ont des NBDs dimérisés sans que la cavité soit accessible au cytoplasme ou à l'extérieur de la cellule ; (iii) les conformations post-hydrolytiques ont des NBDs dimérisés avec une cavité ouverte vers l'extérieur de la cellule. Cependant, l'amplitude de la séparation des NBDs dans la conformation apo est en discussion parce que : (i) des études fonctionnelles sur les ABCs humains PgP montrent que la protéine était active et capable de transporter des substrats après cross-linking des cys sur les NBDs (Loo & Clarke, 2014); (ii) la cristallisation des ABCs en détergent est souvent accompagnée d'une interaction protéine-protéine; (iii) des études dynamiques sur les PgPs montrent que les NBDs restent proches pendant le transport des substrats (Verhalen et al., 2012; Zoghbi et al., 2017).

Il existe plusieurs modèles de transport qui sont divisés en deux principes. D'une part, les modèles d'« accès alternatif » ou « switch » sont basés sur la séparation des deux NBDs (P. M. Jones & George, 2004). Les substrats amphiphiles se fixent sur la cavité par le cytoplasme ou par la membrane, puis la dimérisation et l'hydrolyse d'ATP conduisent à un changement important de conformation avec l'ouverture de la cavité et le relargage du substrat vers le milieu extracellulaire. D'autre part, les modèles « contact permanent » ou « outward-only » suggèrent que les NBDs restent en contact pendant le cycle (Hohl et al., 2014). Le modèle du contact permanent suggère que les ATP se lient et s'hydrolysent alternativement d'un site à l'autre, de sorte que les NBDs sont toujours en contact. Le modèle « outward-only » consiste en un changement conformationnel entre occlusif et post-hydrolytique. Ce modèle a été proposé pour le transport d'oligosaccharides lipidiques (LLO) pour PglK, un ABC bactérien (Perez et al., 2015).

Le rôle des lipides sur l'ABC est examiné par des études fonctionnelles, structurales et dynamiques. La clarification du rôle des lipides par des études fonctionnelles est compliquée

parce que: (i) les lipides peuvent être des substrats des ABCs ; (ii) les substrats amphiphiles se répartissent en bicouche lipidique et la distribution dépend de la composition lipidique ; (iii) certains détergents sont des substrats putatifs ; (iv) leurs substrats physiologiques sont souvent inconnus ; (v) les ABCs ont des fortes activités basales. Mais qualitativement, les ABCs ont une activité plus élevée dans la membrane que dans le détergent, de plus certains lipides spécifiques stimulent l'activité. Des études dynamiques montrent également que la conformation des protéines dépend de son environnement : détergent, composition de la membrane (Gustot et al., 2010; Zoghbi et al., 2016). Mais les résultats ne sont pas toujours en accord, ce qui peut être lié à différents systèmes de membranes, transporteurs et autres conditions comme des substrats variables. Dans l'ensemble, il existe clairement une relation complexe entre la fonction des protéines, les propriétés des membranes, les conformations et la dynamique. En outre, il n'y a pas d'informations sur l'ABC en ce qui concerne les effets physiques de la membrane i.e. la tension et la courbure de la membrane.

Nous avons constaté par EM qu'il existe des preuves de couplage entre la membrane (composition lipidique et courbure) et un ABC bactérien BmrA lorsqu'elle est reconstituée en haute densité protéique (Figure 38, 39, 40)(Fribourg et al., 2014). Nous avons ensuite exploré plus en détail ce couplage en condition diluée pour éviter l'interaction protéine-protéine.

Dans cette thèse, nous voulions nous concentrer sur l'importance de la membrane dans la fonction et l'organisation spatiale de BmrA. Nous avons purifié BmrA, puis étudié dans les liposomes de tailles différentes totalement caractérisés dont nous avons modulé et contrôlé les propriétés physico-chimiques. Nous avons combiné plusieurs stratégies complémentaires telles que la biochimie membranaire et la biophysique en collaboration avec des groupes de physiciens (Figure 43).

b. Résultats

1. Hydrolyse d'ATP de BmrA dans les micelles et reconstitué dans les membranes.

Nous avons caractérisé l'hydrolyse d'ATP en fonction de l'état de l'environnement : solubilisé en micelle de détergent, en micelles mixtes de détergent/lipide et membranaire.

En micelles de détergent et détergent/lipide

Nous avons tout d'abord étudié l'activité de BmrA dans différents détergents, DDM, Triton X-100 et LMNG au dessus de la concentration micellaire critique (Figure 59). BmrA était très actif dans les 3 détergents et complètement inhibée par l'ATP- γ -S. Les activités ATPasiques étaient similaires dans Triton X-100 ou LMNG et 3 fois plus lentes dans DDM.

Ensuite, les mélanges de lipides phosphatidylcholine (PC)/ phosphatidylglycérol (PG) ou de l'extrait d'*E. coli* sont ajoutés dans des micelles de DDM ou Triton X-100 (Figure 60, Table 5). La présence des lipides a augmenté d'environ 35% l'activité de BmrA solubilisé en DDM ou en Triton X-100 avec une activité toujours 3 fois inférieure en DDM qu'en Triton X-100. Aucune différence d'activité n'a été observée entre les deux compositions lipidiques.

En membrane

L'activité de BmrA a augmenté d'environ 10 fois lorsqu'il est reconstitué dans les liposomes par rapport au détergent (Figure 61). De plus, l'activité ATPasique dépend de la composition lipidique (Figure 62, 63). Premièrement, l'activité était deux fois plus importante

dans les liposomes PE que dans les PC. Deuxièmement, l'activité a été stimulée à partir de 10% (poids) de lipides chargés négativement (acide phosphatidique (PA), phosphatidylsérine (PS), PG et cardiolipides (CL)). Troisièmement, les lipides chargés négativement stimulent 2 fois et 3 fois dans les liposomes à base de PC et phosphatidyléthanolamine (PE), respectivement. Enfin, un mélange d'PE et de 10 % de PG était suffisant pour atteindre 89 % de l'activité en liposomes d'*E. coli* là où l'activité était la plus élevée.

Caractérisation complète du protéoliposome

Nous avons caractérisé des facteurs qui peuvent influencer la mesure de l'activité ATPasique dans les protéoliposomes:

- Orientation protéique : les liposomes étant imperméables à l'ATP, seules les protéines dont les NBDs sont orientés en dehors des protéoliposomes sont accessibles à l'ATP ;
- Incorporation de protéines : seules les protéines incorporées dans les liposomes sont pleinement actives ;
- Unilamellarité des liposomes : si les liposomes sont multilamellaires, seules les protéines des liposomes externes sont accessibles à l'ATP.

Nous avons sélectionné deux compositions lipidiques PC/PA et *E. coli* sachant que l'activité était deux fois plus importante en *E. coli* qu'en PC/PA. Nous avons caractérisé ces facteurs, comme indiqué dans la partie *matériel et méthodes*. Toutes les caractéristiques étaient similaires (Table 6). Cependant, les protéoliposomes d'*E. coli* étaient significativement plus petits que les liposomes EPC/EPA, ce qui soulève la question de savoir si la courbure membranaire peut influencer l'hydrolyse de l'ATP.

2. Analyse fonctionnelle en fonction de la courbure membranaire

Tailles des liposomes

Nous avons étudié la lamellarité et la taille des liposomes dans différentes compositions lipidiques par cryo-EM. Les liposomes étaient tous unilamellaires dans les liposomes à base de PC (Figure 77). Cependant la présence de lipides chargés négativement PA et PG a induit une apparition de petits liposomes ($40 \text{ nm} < \varnothing < 200 \text{ nm}$) avec une distribution de taille hétérogène à l'exception de PS. En ce qui concerne les liposomes à base de PE, les liposomes étaient de petite taille ($\varnothing \approx 40\text{-}70 \text{ nm}$) (Figure 75).

Nous avons varié les paramètres de reconstitution tels que la force ionique et la température pour obtenir des tailles variables avec la même composition lipidique. L'augmentation de la force ionique a induit une augmentation de la taille des liposomes PC/PG (Figure 79). La reconstitution à 4°C a permis d'obtenir de petits liposomes avec une population homogène pour des compositions lipidiques PC, PC/PA et PC/PS (Figure 80).

L'activité ATPasique en fonction de la taille des liposomes

Nous avons comparé l'activité ATPasique de BmrA reconstitué dans un même mélange lipidique mais formant deux populations de tailles très différentes. BmrA est reconstitué dans PC/PA et PC/PS à 20 °C et 4 °C pour obtenir des liposomes grands et petits, respectivement. Dans les deux cas, nous avons observé une forte diminution de l'activité d'un facteur 2 lorsque la taille des liposomes diminue d'un facteur 2 à 3 (Figure 81).

Nous avons ensuite caractérisé les protéoliposomes EPC/EPA de grandes et petites tailles (Figure 82). Les orientations BmrA étaient de 70 % et 94 % dans les liposomes grands et petits, respectivement. Les protéines ont été entièrement incorporées dans les deux cas.

Finalement, l'activité ATPasique en fonction de la composition lipidique et de la courbure membranaire peut être comparée. Puisque l'activité la plus élevée a été observée dans les petites vésicules d'*E. coli* par rapport aux grandes vésicules PC/PG ou PC/PE, cela suggère que la contribution de la composition lipidique est prédominante sur la courbure membranaire.

3. Tri et distribution spatio-temporelle de BmrA dans la membrane courbée en fonction de ses états catalytiques

Nous avons étudié le tri et la distribution de BmrA dans une membrane courbée. P. Bassereau (UMR 168, Institut Curie) et ses collaborateurs ont conçu un dispositif pour étudier la distribution spatio-temporelle des protéines transmembranaires dans une membrane courbée (Figure 35)(S Aimon, 2011). Le principe de l'expérience consiste à former un nanotube lipidique à partir d'une vésicule géante (GUV) dans laquelle la tension membranaire peut être contrôlée. Ainsi, la courbure de la membrane dans les nanotubes peut être modifiée et contrôlée avec différents diamètres correspondants à différentes tensions de la membrane. L'enrichissement protéique dans des nanotubes (S) a été quantifié en mesurant la fluorescence des protéines dans le nanotube par rapport aux GUVs, normalisé par la même fluorescence lipidique.

BmrA est reconstitué dans des GUVs. Les expériences de tirage de nanotubes ont été réalisées par A. K. Mahalka du groupe de P. Bassereau avec notre contribution sur la formation de GUV contenant de BmrA et sur la conception d'expériences fonctionnelles dans les GUV. A. K. Mahalka a optimisé les étapes finales de la croissance de GUVs par électroformation, réalisé des expériences de tirage de tubes et l'analyse des données.

Reconstitution de protéoGUVs

Pour la reconstitution BmrA dans GUVs, j'ai essayé l'incorporation directe et la fusion de protéoliposome (Figure 83) et ensuite abandonné par manque de temps et A. K. Mahalka a fait l'électroformation (Figure 84). Cette méthode d'électroformation a dû être réajustée à BmrA par l'étape de séchage. Cette optimisation a été réalisée en suivant l'évolution comparative entre l'activité d'hydrolyse de l'ATP mesurée dans les petits protéoliposomes et la croissance des GUVs (Figure 85,86, Table 8).

Tri et distribution de BmrA

Le tri de BmrA en fonction de l'état catalytique a été étudié dans le cadre d'une expérience de tirage de tubes (Figure 88). Toutes les expériences ont été effectuées à 20 °C. La distribution de l'apo-BmrA était sensible à la courbure de la membrane même dans de grands tubes de 80 nm de rayon à faible tension membranaire ($\sigma < 0,01 \text{ mNm}^{-1}$). La valeur de tri a atteint $S = 60$ pour un rayon = 30 nm. La protéine inhibée dans l'orthovanadate n'a été triée que dans la membrane fortement courbée (rayon < 20 nm) avec $S = 15$ pour un rayon = 30 nm. Ces expériences montrent que la forme apparente de BmrA dans la membrane est différente dans les conformations apo- et post-hydrolytiques.

Il a été constaté que la diffusion de l'apo-BmrA dans les nanotubes lipidiques était extrêmement lente avec formation de cluster de BmrA au niveau du cou (Figure 89). 50% et 90%

des apo-BmrA sont orientés avec des NBDs à l'extérieur de la vésicule dans le GUV et dans le nanotube, respectivement comme montré par l'attaque protéolytique (Figure 90).

L'ajout de l'ATP- γ -S à apo-BmrA triés en nanotubes a entraîné une diminution des valeurs de tri de 16 à 5 en peu de temps (Figure 91). Ce résultat a clairement montré que les protéines étaient actives et que apo-BmrA sont orientés avec des NBDs en dehors des GUVs.

De plus, l'ajout d'ATP à apo-BmrA triés en nanotubes a entraîné une diminution complète de tri dans les nanotubes (Figure 92). Ceci suggère que BmrA préfère la membrane plate à la membrane courbée pendant le cycle catalytique.

c. Discussion

Nous avons étudié la fonction et la distribution spatiale de BmrA, une ABC bactérienne dans différents modèles de membranes *in vitro*. Nous avons obtenu des résultats significatifs sur l'interaction entre BmrA et la membrane qui pourraient être étendus à d'autres transporteurs ABC bactériens homodimériques. Nous discutons également de l'impact possible de ces données sur les ABC eucaryotes.

Mécanisme de formation des proteoliposomes

La taille finale des vésicules dépend des états intermédiaires au cours desquels les micelles doivent fusionner pour former des vésicules (Figure 30). Les paramètres qui influencent la fusion entre les micelles déterminent donc la taille finale des liposomes comme la température, la force ionique et le taux d'élimination des détergents (Figure 102). Cependant, à 20 °C et 150 mM de NaCl, la forme globale des lipides domine la taille des liposomes plus que la fusion des micelles ; la présence de lipides coniques (PE, PA, PG) entraînent une diminution de taille des liposomes (Figure 103). De plus, selon la littérature, les lipides coniques sont localisés de préférence dans la feuille interne et induisent une courbure positive (Callan-jones et al., 2011 ; Esteban-Martín, Jelger Risselada, Salgado, & Marrink, 2009 ; Kooijman, Chupin, de Kruijff, & Burger, 2003). Par conséquent, il est possible que l'asymétrie entre deux feuillets lipidiques puisse contribuer à la taille finale des liposomes.

Nous avons également montré que l'orientation des protéines dans la conformation apo était de 75% et 100% dans un mélange de grandes/petites vésicules et les petites vésicules homogènes, respectivement. Il est possible que les protéines comme BmrA, qui ont une courbure intrinsèque non nulle (conicité), imposent une courbure spontanée à leur environnement proche (Figure 104). Par conséquent, la conicité protéique impose l'orientation préférentielle dans le liposome. On peut également considérer que la protéine s'oriente elle-même lors de la diffusion des protéines dans les micelles en raison d'une préférence pour une courbure positive et/ou pour éviter l'encombrement stérique des grands domaines extramembranaires, particulièrement pour les petits liposomes.

Nous avons calculé l'orientation des protéines dans les grands liposomes en comparant des caractérisations entre un mélange de grandes/petites vésicules et les petites vésicules homogènes (Figure 105). Avec la formule indiquée à la figure 105, nous avons calculé que les protéines sont orientées à 50 % avec les NBDs vers l'extérieur dans les grands liposomes. Ceci confirme que l'orientation des protéines dépend de la taille des liposomes.

De même, nous pouvons déduire l'activité de BmrA dans les grands liposomes PC/PA dans un mélange de petits et de grands liposomes. Nous avons constaté que l'activité des grands liposomes était proche de l'activité protéique moyenne. Par conséquent, l'activité des protéines pourrait être sous-estimée deux fois dans les grands liposomes en raison de 50% de l'orientation des protéines. Cela suggère également que l'activité est en réalité 4 fois plus élevée dans les

grands liposomes que dans les petits liposomes. De plus, puisque seuls les liposomes de grande taille contribuent à l'activité moyenne, les activités en PG, PA et PS sont comparables et identiques. La stimulation avec des lipides chargés négativement n'est donc pas spécifique à un groupe de tête lipidique particulier.

États membranaires, composition lipidique et activité ATPasique de BmrA

Nous avons étudié le rôle des lipides et de la membrane sur l'activité des ABC dans les vésicules entièrement caractérisées afin de comparer quantitativement l'activité. Nous avons trouvé des résultats qualitativement cohérents avec d'autres ABCs ; comme le fait que l'activité ATPase de BmrA augmente dans le système reconstitué par rapport à celle des micelles de détergents, et que les lipides anioniques et le PE stimulent l'activité.

L'interaction entre les lipides et les protéines ne semble pas être élevée car : (i) il n'y a pas de spécificité lipidique en micelles ; (ii) la stimulation de l'activité par les lipides anioniques commence à partir de 10% (w) suggérant qu'une quantité excessive de lipides anioniques est nécessaire autour de la protéine pour pouvoir stimuler l'activité.

Selon un modèle calculé de BmrA, il y a 16 résidus chargés positivement qui peuvent interagir avec les lipides anioniques par monomère (Figure 106). Cependant, 14 résidus chargés positivement sont situés du côté cytoplasmique, 2 autres sont situés du côté extracellulaire. Six autres acides aminés se trouvent dans les TMD et sont conservés dans le MsbA, suggérant un rôle de ces résidus positifs conservés dans la stimulation lipidique anionique. Le rôle de ces acides aminés n'a jamais été documenté mais nous pouvons spéculer qu'ils contribuent à l'attraction des lipides chargés négativement dans l'environnement de BmrA.

Courbure membranaire et activité ATPasique

Nous avons montré pour la première fois que la courbure de la membrane intervient dans la fonction de l'ABC et que l'activité était 4 fois plus faible pour les liposomes de taille inférieure à 40 nm de diamètre que pour les grands liposomes en PC/PA et PC/PS.

La modification de la taille des liposomes influence l'asymétrie de la bicouche et les paramètres physiques, tels que la courbure et la tension de la membrane (Figure 107). Dans notre système reconstitué, BmrA est orienté avec des NBDs à l'extérieur des liposomes avec des résidus chargés positivement au niveau du feuillet externe des liposomes. Nous avons déjà suggéré que le feuillet interne contient plus de lipides coniques, des lipides chargés négativement avec un petit groupe de tête et des lipides PE, que le feuillet externe. Il est donc possible que la diminution de l'activité soit liée à la plus faible concentration de lipides anioniques dans la feuille externe des liposomes.

La diminution de l'activité ATPasique pourrait également être influencée par la courbure et la tension de la membrane. Bien que très peu d'études aient été rapportées, Tonnesen et ses collaborateurs ont montré que la taille des pores de α -hemolysin a été modifiée dans de petites vésicules, diminuant ainsi la perméabilité des pores (Tonnesen, Christensen, Tkach, & Stamou, 2014). Il est probable que l'apo-BmrA ayant une forte flexibilité est capable de s'adapter à une forte courbure dans les petits liposomes. L'hydrolyse de l'ATP doit ensuite franchir la barrière de déformation de la membrane.

Courbure membranaire et distribution des protéines

Nous avons observé une différence significative dans le tri de BmrA entre les conformations apo et post-hydrolytique dans une membrane courbée.

Nous avons démontré expérimentalement que l'apo-BmrA est orienté 50% avec les NBDs extérieures de la vésicule dans une membrane plate dans le GUVs. Dans les nanotube, l'apo-BmrA était enrichi dans la courbure positive avec les NBDs orientés vers l'extérieurs des de vésicules.

Dans le cas de la conformation post-hydrolytique, nous n'avons pas réussi à réaliser la digestion à la trypsine. Cependant, on peut déduire l'orientation de l'expérience où de l'ATP- γ -S a été ajouté à l'apo-BmrA déjà triés en nanotubes (Figure 108). Une fois l'inhibiteur ajouté, toutes les protéines sont retournées dans la membrane de courbure nulle, ce qui suggère que la conformation post-hydrolytique de BmrA n'est pas stabilisée dans la courbure positive. Par conséquent, il est probable que BmrA en post-hydrolytique ont été enrichies en courbure négative de membrane avec les NBDs orientés à l'intérieur des nanotubes.

Il a été démontré que la conicité de la protéine détermine le tri dans une membrane courbée. La protéine conique a été triée dans une zone courbée alors que la protéine cylindrique ne l'était pas. La conicité relative peut être comparée entre les conformations apo et post-hydrolytique, qui sont 4 fois plus coniques en apo que les conformations post-hydrolyse dans le domaine transmembranaire (Figure 109).

De plus, des expériences avec des conformations fixes en apo et post-hydrolyse suggèrent que des changements conformationnels importants se produisent pendant le cycle catalytique dans nos conditions expérimentales, c'est-à-dire dans des membranes courbes et à température ambiante. Ceci est également confirmé par l'expérience où nous avons étudié la distribution des protéines au cours du cycle catalytique. L'ajout d'ATP à l'apo-BmrA trié en courbure de membrane positive entraîne le retour de BmrA dans une membrane plate, ce qui suggère un changement de conformation au cours du cycle catalytique (Figure 110).

Formation de cluster

La formation de cluster d'apo-BmrA a été observée au cours d'expériences d'extraction de nanotubes, ce qui suggère une interaction protéine/protéine. Le regroupement de l'apo-BmrA a été observé au niveau du cou des GUVs (500 à 1500 lipides par BmrA) et non dans les régions plates des GUVs (3800 à 30 000 lipides par BmrA). L'interaction protéine/protéine a également été montrée dans des expériences de microscopie électronique, dont la forme BmrA définit des assemblages très courbes à haute densité protéique (rapport lipide/protéine 0,5 - 2 poids/poids) dans la conformation apo. Dans ce cas, 45 à 170 lipides étaient présents par BmrA. Cependant, les études FRET ne montrent aucune preuve d'interaction protéique par des expériences interFRET dans les liposomes à densité protéique moyenne (3400 - 17 000 lipides par BmrA). Toutes ces données suggèrent que l'interaction protéine/protéine est sensible à la densité protéinique et à la courbure de la membrane (Figure 111).

Répartition spatiale de l'ABC dans les membranes cellulaires

BmrA peut se regrouper si la densité protéique est suffisamment élevée. Par conséquent, les conditions membranaires qui peuvent favoriser la densité protéique locale de BmrA induisent le regroupement d'apo-BmrA, par exemple le radeau membranaire ou la courbure de la membrane.

Dans une membrane bactérienne, la courbure est presque nulle. Par conséquent, il n'y aura aucune conséquence de la courbure de la membrane dans la fonction ou la distribution des ABCs. Cependant, il y a des domaines lipidiques dans les bactéries (Figure 112). Les microdomaines lipidiques sont présentes avec des localisations préférentielles: les régions septales ont été enrichies par des domaines riches en PE ; les CL sont localisées de préférence dans les régions septales et aux pôles cellulaires ; et les PG sont enrichies en structure lipidique

hélicoïdale s'étendant le long du grand axe de la cellule. La localisation de BmrA est inconnue mais on peut spéculer que la fonction de BmrA est modulée en fonction de sa localisation.

Dans les cellules eucaryotes, plusieurs processus de remodelage membranaire se produisent avec des courbures significativement différentes (Figure 113). De plus, la composition lipidique varie selon les organites, les lipides forment des domaines et sont distribués asymétriquement. On peut spéculer que la fonction et la distribution varient en fonction de la courbure de la membrane et de la composition lipidique locale. Dans ce cas, la fonction de l'ABC peut être modulée en fonction de sa localisation.

Le feuillet cytoplasmique global contient la majorité des lipides PE et 10% des lipides PS. Ces lipides devraient interagir avec les ABCs par leurs résidus positivement chargés dans le côté cytoplasmique, suggérant une activité protéique élevée.

La distribution des ABC peut être estimée en fonction de la courbure de la membrane (Figure 114). Au cours de tout type d'invagination des vésicules à courbure positive, comme l'endocytose, la pinocytose, etc., les ABCs seraient localisés de préférence dans une membrane plate sans altération fonctionnelle, comme le montre l'expérience de traction de tube. Dans le cas de protrusion membranaire comme le bourgeonnement membranaire, la filopodie ou les épines dendritiques, l'emplacement de l'ABC dépendra de la courbure membranaire. Pour les vésicules d'un diamètre supérieur à 40 nm, les ABCs seraient exclus, comme dans les filopodes. Pour des vésicules plus petites que 40 nm de diamètre, il est possible que les ABCs en conformations post-hydrolytiques soient enrichies en membrane négativement courbée. On ne connaît pas comment la courbure négative affecte la fonction de l'ABC.

Toutefois, cet emplacement peut également dépendre du cycle catalytique. Si l'ABC reste plus longtemps dans la conformation apo que dans la conformation post-hydrolyse, les ABCs seraient localisés de préférence dans une membrane plate dans tous les cas sans altération fonctionnelle. Par conséquent, la distribution des ABC ne changerait pas pendant le remodelage de la membrane.

Nous sommes en collaboration avec S. Wilkens (SUNY, New York), qui a étudié et réalisé des expériences sur les techniques de biochimie et de biologie moléculaire avec PgP. Nous prévoyons d'élucider la distribution de PgP eucaryote dans les GUVS avec le protocole établi avec BmrA.

Dans l'ensemble, nous avons montré la contribution de la composition lipidique et de la courbure membranaire sur la fonction, la distribution spatiale et la formation des domaines de BmrA (Figure 115). Nous avons également montré que BmrA dans différentes conformations modulent la courbure membranaire. Ceci a révélé une interaction fonctionnelle entre les protéines transmembranaires et l'environnement membranaire.

Figures and tables

Figure 1 Domains of ABC transporters	6
Figure 2 Seven superfamilies of ABC transporters.....	7
Figure 3 schematic representations of main functions leading to multidrug resistance in human cell.....	7
Figure 4 Schematic representations of MDR transporters in prokaryote	8
Figure 5 Topology, substrates and subcellular localization of human ABC	9
Figure 6 Structures of nucleotide-bound NBDs.....	10
Figure 7 Cryo-EM structure of MsbA.....	11
Figure 8 Two types of structures of ABC exporters.....	13
Figure 9 Several conformations of type I, B-family ABC-exporters.....	13
Figure 10 Large spectrums of conformations of MsbA and PgP in membrane mimicking system studied by negatively staining-EM	13
Figure 11 Two models of substrates transport.....	14
Figure 12 Rotation and translation movement for NBDs dimerization.....	15
Figure 13 Lipid translocation models by alternating access models	16
Figure 14 Schematic representations of NBDs for constant-contact model.....	17
Figure 15 Overall shapes of lipids and their assembling.....	18
Figure 16 Overall shapes of different lipids	18
Figure 17 Lipid distributions in eukaryotic cells.....	19
Figure 18 Cell components responsible for membrane remodeling in eukaryotic cell.....	19
Figure 19 Model of coupling between protein distribution and membrane curvature.....	20
Figure 20 Protein lateral mobility in fluctuating membranes	21
Figure 21 Hydrophobic mismatch.....	22
Figure 22 ATPase activity of MsbA according to ATP concentration and temperature.	23
Figure 23 Lipid densities surrounding McjD and PgP by MD.....	26
Figure 24 Membrane curvature and thickness surrounding PgP by MD	27
Figure 25 Oligomerization mechanism proposed for ABCA1	28
Figure 26 LRET results on MsbA and PgP.....	29
Figure 27 smFRET results of PgP	29
Figure 28 DEER experiment on PgP	30
Figure 29 Membrane models.....	31
Figure 30 Schematic representation of detergent mediated proteoliposome formation.....	33
Figure 31 Detergent elimination methods	34
Figure 32 Adsorption characteristics of BioBeads.....	35
Figure 33 Schematic representation of direct incorporation method.....	37
Figure 34 Reconstitution methods of integral membrane protein in GUVs.....	38
Figure 35 Sorting in curved membrane according to shape of protein	38
Figure 36 Common drug substrates between PgP, BmrA and MsbA	40
Figure 37 Model of BmrA	40
Figure 38 Structural studies of apo-BmrA by cryo-EM	41
Figure 39 Principal BmrA/membrane assemblies.....	42
Figure 40 Membrane morphology modification.....	43
Figure 41 Protein domain formation in post-hydrolysis conformation.	43
Figure 42 The presence of substrates induces membrane twisting.....	43
Figure 43 Strategies to study interplay between BmrA and its surrounding environment.	44
Figure 44 Overexpression of BmrA in membrane.....	47
Figure 45 Example of purification of BmrA.	48
Figure 46 Schema of purification of BmrA and labeled BmrA.....	49
Figure 47 Example of purification of labeled BmrA.	51

Figure 48 Schema of different strategies of reconstitution.....	51
Figure 49 Characterization of protein orientation in liposomes by proteolysis.....	55
Figure 50 Incorporation rate measured by flotation	56
Figure 51 Principle of fusion of proteoliposomes to GUVs.....	57
Figure 52 Principle of reconstitution of transmembrane proteins into GUVs	58
Figure 53 Principle of ATPase activity measurement coupled with oxidation of NADH.	59
Figure 54 Example of ATPase activity measurement	60
Figure 55 Analysis of E_{FRET} by fluorimeter.....	62
Figure 56 Functional analysis of BmrA according to its surrounding environment.....	66
Figure 57 Inhibition rate of different inhibitors.	67
Figure 58 Substrate effects on ATPase activity.	68
Figure 59 ATPase activity of BmrA solubilized in different detergents.	69
Figure 60 ATPase activity in lipid/detergent micelles.....	69
Figure 61 Lipid specificity on ATPase hydrolysis in reconstituted system.....	71
Figure 62 Increase of ATPase activity with increasing amount of negatively charged lipids in PE vesicles.	72
Figure 63 ATPase activity in PC vesicles with increasing amount of negatively charged lipids.....	73
Figure 64 Characterization of reconstituted system.....	73
Figure 65 Optimization of trypsin concentration for BmrA digestion in reconstituted system.	74
Figure 66 Orientation of BmrA according to lipids composition and reconstitution methods.....	75
Figure 67 Different accessibilities of trypsin to C436 in apo and ATP-Vi states.....	76
Figure 68 Protein incorporation rate in <i>E. coli</i> and EPC/EPA liposomes.....	77
Figure 69 ATPase activity according to lipid/protein ratio.....	77
Figure 70 Unilamellarity and size of liposomes studied by cryo-EM.....	78
Figure 71 Comparison of size distribution between DLS and cryo-EM images.	80
Figure 72 Detection of liposomes on cryo-EM images for homogeneous and heterogeneous sizes.	81
Figure 73 Same population of liposomes and proteoliposomes at low lipid/protein ratio.....	81
Figure 74 Different populations of liposomes reconstituted by detergent removal.....	82
Figure 75 Homogenous small liposomes made of <i>E. coli</i> lipid extract or EPE/PG 8/2 w/w lipid mixture.	82
Figure 76 Decrease of sizes of liposomes with increasing amount of EPE in EPC vesicles.....	83
Figure 77 PG or PA but not PS in PC membranes led to the formation of heterogeneous populations of liposomes.....	83
Figure 78 Liposome sizes of DOPC and DOPC mixtures.	84
Figure 79 Effect of ionic strength on liposome size.....	85
Figure 80 Reconstitution at 4 °C of EPC containing liposomes led to small liposomes.....	85
Figure 81 ATPase activity according to membrane curvature.	86
Figure 82 Characterization of EPC/EPA liposomes with different sizes.....	87
Figure 83 Fusion of proteoliposomes to GUVs.	89
Figure 84 Reconstitution steps of BmrA into GUVs by electroformation method.	90
Figure 85 ATPase activity during reconstitution of proteoliposomes for GUVs.....	92
Figure 86 ATPase activity of EPC/EPA and <i>E. coli</i> proteoliposomes at 20 °C.	93
Figure 87 Lipid/protein ratio in GUVs according to conformational states.	94
Figure 88 Sorting of BmrA according to catalytic states.	95
Figure 89 Sorting of apo-BmrA and clusters at the neck.....	96
Figure 90 Orientation of apo-BmrA in GUVs and in nanotube by proteolysis.....	97
Figure 91 Redistribution of BmrA upon addition of ATP- γ -S.....	98
Figure 92 Redistribution of BmrA upon addition of ATP.....	99

Figure 93 Front and side views of model of apo-BmrA.	101
Figure 94 Labeling of BmrA in detergent according to time, temperature and concentration of dyes.	101
Figure 95 Labeling of BmrA with increasing concentration of fluorescent dyes.....	102
Figure 96 Absence of unspecific labeling of BmrA with maleimide-dyes.	103
Figure 97 BmrA WT and mutants : introduction of Cys residue to other locations.	105
Figure 98 Example of optimization of ratio between two fluorescent dyes for dual-labeled BmrA.	106
Figure 99 Membrane morphology changes according to catalytic states of labeled BmrA.	108
Figure 100 Characterizations of M3 and Alexa488/sulfo-Cy5 M3.....	110
Figure 101 Different strategies to investigate dynamics of BmrA by FRET	112
Figure 102 Mechanisms of liposome formation by detergent removal and factors that influence size of vesicles.	116
Figure 103 Overall shapes of lipids.....	116
Figure 104 Protein orientation according to size of liposomes	117
Figure 105 Calculation of protein orientations and activity in large PC/PA liposomes	118
Figure 106 Distribution of positively charged amino acids of BmrA in the cytoplasmic side.	120
Figure 107 How geometrical membrane curvature influence protein activity.....	121
Figure 108 Schematic presentation of sorting of post-hydrolysis conformation.....	122
Figure 109 Models of BmrA and KvAP	123
Figure 110 Schema illustrating sorting according to catalytic states.....	123
Figure 111 Clustering of apo-BmrA according to protein density	124
Figure 112 Lipid domains in <i>B. subtilis</i> (Barák & Muchová, 2013)	125
Figure 113 Membrane curvature and bilayer asymmetry in eukaryotic cell.....	126
Figure 114 schematic representation of possible localization of ABCs in curved membranes....	127
Figure 115 Interplay between BmrA and membrane.....	127
Figure 116 Stability of reconstituted system of <i>E. coli</i> and EPC/EPA liposomes according to temperature and time.	129
Figure 117 Example of ensemble FRET measurement by fluorescence spectroscopy.....	130
Figure 118 Alexa488 lifetime comparison between apo- and post-hydrolysis conformations.	132
Figure 119 InterFRET measurement fluorescence spectroscopy and donor lifetime measurement.	133
Figure 120 No difference of EPR between apo and post-hydrolysis conformations for BmrA WT Alexa488/Atto610 and sulfo-Cy3/sulfo-Cy5 in detergent.	134
Figure 121 No changes in EPR between apo- and post-hydrolysis conformations of Alexa488/sCy5 BmrA M3 in micelles of lipid/detergent.	135
Figure 122 Estimated number of BmrA according to diameter of liposome.....	136
Figure 123 Correlation function according to protein density	137
Figure 124 Presence of contaminants in lipids	138
Figure 125 Comparison of EPR histograms between low and high statistics.....	139
Figure 126 Comparison of EPR distribution between apo and post-hydrolysis conformation with different FRET couples.	140
Table 1 List of fluorescent dyes.....	50
Table 2 List of lipids.....	53
Table 3 List of detergents.....	53
Table 4 List of laser and filter according to fluorescent dyes.....	62
Table 5 ATPase activity according to lipid composition in micelles of lipid/detergent	70
Table 6 ATPase activity measurement between EPC/EPA and <i>E. coli</i> proteoliposomes	78

Table 7 ATPase activity before and after freezing according to concentration of trehalose.....	91
Table 8 ATPase activity in the presence of PEG lipids.....	92
Table 9 Labeling yields and activity conservation of BmrA WT according to fluorescent dyes. ..	104
Table 10 Ratio between two fluorescent dyes to obtain 50% of donor and 50% of acceptor labeled to BmrA WT.....	106
Table 11 Rate of labeling and activity conservation for FRET couples of BmrA WT	107
Table 12 Rate of labeling and activity conservation for FRET couples of BmrA M2	109
Table 13 Rate of labeling and activity conservation for FRET couples of BmrA M3	110
Table 14 Summary tables of FRET results. FS stands for Fluorescence Spectroscopy	113
Table 15 E_{FRET} of reconstituted BmrA WT.	131
Table 16 E_{FRET} of Alexa488/sulfo-Cy5 M3 in detergent.....	131

Bibliography

- Aimon, S. (2011). Membrane shape modulates transmembrane protein distribution. *Dev Cell*, 30(2), 58–64. <https://doi.org/10.1016/j.immuni.2010.12.017>. Two-stage
- Aimon, S., Callan-Jones, A., Berthaud, A., Pinot, M., Toombes, G. E. S., & Bassereau, P. (2014). Membrane shape modulates transmembrane protein distribution. *Developmental Cell*, 28(2), 212–218. <https://doi.org/10.1016/j.devcel.2013.12.012>
- Aimon, S., Manzi, J., Schmidt, D., Larrosa, J. A. P., Bassereau, P., & Toombes, G. E. S. (2011). Functional reconstitution of a voltage-gated potassium channel in giant unilamellar vesicles. *PLoS ONE*, 6(10). <https://doi.org/10.1371/journal.pone.0025529>
- Aittoniemi, J., Fotinou, C., Craig, T. J., De Wet, H., Proks, P., & Ashcroft, F. M. (2009). SUR1: A unique ATP-binding cassette protein that functions as an ion channel regulator. *Philosophical Transactions of the Royal Society B: Biological Sciences*, 364(1514), 257–267. <https://doi.org/10.1098/rstb.2008.0142>
- Aller, S. G., Yu, J., Ward, A., Weng, Y., Chittaboina, S., Harrell, P. M., ... Chang, G. (2009). Structures of P-glycoproteins reveals a molecular basis for poly-specific drug binding. *Science*, 323(5922), 1718–1722. <https://doi.org/10.1126/science.1168750>. Structure
- Ambudkar, S. V. (1995). Purification and reconstitution of functional human P-glycoprotein. *Journal of Bioenergetics and Biomembranes*, 27(1), 23–29. <https://doi.org/10.1007/BF02110327>
- Andersen, O. S., & Koeppe, R. E. (2007). Bilayer Thickness and Membrane Protein Function: An Energetic Perspective. *Annual Review of Biophysics and Biomolecular Structure*, 36(1), 107–130. <https://doi.org/10.1146/annurev.biophys.36.040306.132643>
- Barák, I., & Muchová, K. (2013). The role of lipid domains in bacterial cell processes. *International Journal of Molecular Sciences*, 14(2), 4050–4065. <https://doi.org/10.3390/ijms14024050>
- Baral, B. (2017). Evolutionary Trajectories of Entomopathogenic Fungi ABC Transporters. *Advances in Genetics*, 98, 117–154. <https://doi.org/10.1016/bs.adgen.2017.07.002>
- Barreto-ojeda, E., Corradi, V., Gu, R., & Tieleman, D. P. (2018). Coarse-grained molecular dynamics simulations reveal lipid access pathways in P-glycoprotein, 1–13.
- Barthelme, D., Dinkelaker, S., Albers, S.-V., Londei, P., Ermler, U., & Tampé, R. (2011). Ribosome recycling depends on a mechanistic link between the FeS cluster domain and a conformational switch of the twin-ATPase ABCE1. *Proceedings of the National Academy of Sciences of the United States of America*, 108(8), 3228–33. <https://doi.org/10.1073/pnas.1015953108>
- Baumgart, T., Hammond, A. T., Sengupta, P., Hess, S. T., Holowka, D. A., Baird, B. A., & Webb, W. W. (2007). Large-scale fluid/fluid phase separation of proteins and lipids in giant plasma membrane vesicles. *Proceedings of the National Academy of Sciences*, 104(9), 3165–3170. <https://doi.org/10.1073/pnas.0611357104>
- Bechara, C., Nöll, A., Morgner, N., Degiacomi, M. T., Tampé, R., & Robinson, C. V. (2015). A subset of annular lipids is linked to the flippase activity of an ABC transporter. *Nature Chemistry*, 7(3), 255–262. <https://doi.org/10.1038/nchem.2172>
- Beck, A., Äänismaa, P., Li-Blatter, X., Dawson, R., Locher, K., & Seelig, A. (2013). Sav1866 from staphylococcus aureus and P-glycoprotein: Similarities and differences in ATPase activity assessed with detergents as allocrites. *Biochemistry*, 52(19), 3297–3309. <https://doi.org/10.1021/bi400203d>
- Beek, J., Guskov, A., & Slotboom, D. J. (2014). Structural diversity of ABC transporters, 419–435. <https://doi.org/10.1085/jgp.201411164>
- Belin, B. J., Busset, N., Giraud, E., Molinaro, A., Silipo, A., & Newman, D. K. (2018). Hopanoid lipids: From membranes to plant-bacteria interactions. *Nature Reviews Microbiology*, 16(5), 304–315. <https://doi.org/10.1038/nrmicro.2017.173>
- Bhatia, T., Husen, P., Brewer, J., Bagatolli, L. A., Hansen, P. L., Ipsen, J. H., & Mouritsen, O. G. (2015).

- Preparing giant unilamellar vesicles (GUVs) of complex lipid mixtures on demand: Mixing small unilamellar vesicles of compositionally heterogeneous mixtures. *Biochimica et Biophysica Acta - Biomembranes*, 1848(12), 3175–3180. <https://doi.org/10.1016/j.bbamem.2015.09.020>
- Biemans-Oldehinkel, E., Doeven, M. K., & Poolman, B. (2006). ABC transporter architecture and regulatory roles of accessory domains. *FEBS Letters*, 580(4), 1023–1035. <https://doi.org/10.1016/j.febslet.2005.11.079>
- Boël, G., Smith, P. C., Ning, W., Englander, M. T., Chen, B., Hashem, Y., ... Hunt, J. F. (2014). The ABC-F protein EttA gates ribosome entry into the translation elongation cycle. *Nature Structural and Molecular Biology*, 21(2), 143–151. <https://doi.org/10.1038/nsmb.2740>
- Borbat, P. P., Surendhran, K., Bortolus, M., Zou, P., Freed, J. H., & Mchaourab, H. S. (2007). Conformational motion of the ABC transporter MsbA induced by ATP hydrolysis. *PLoS Biology*, 5(10), 2211–2219. <https://doi.org/10.1371/journal.pbio.0050271>
- Brown, M. F. (2012). Curvature Forces in Membrane Lipid – Protein Interactions. *Biochemistry*, 51, 9782–9795. <https://doi.org/dx.doi.org/10.1021/bi301332v>
- Bryan, J., Muñoz, A., Zhang, X., Düfer, M., Drews, G., Krippeit-Drews, P., & Aguilar-Bryan, L. (2007). ABCC8 and ABCC9: ABC transporters that regulate K⁺ channels. *Pflügers Archiv European Journal of Physiology*, 453(5), 703–718. <https://doi.org/10.1007/s00424-006-0116-z>
- Callan-jones, A., Sorre, B., & Bassereau, P. (2011). Curvature-Driven Lipid Sorting in Biomembranes, 1–14.
- Cao, M. A. Do, Crouzy, S., Kim, M., Becchi, M., Cafiso, D. S., Di Pietro, A., & Jault, J. M. (2009). Probing the conformation of the resting state of a bacterial multidrug ABC transporter, BmrA, by a site-directed spin labeling approach. *Protein Science*, 18(7), 1507–1520. <https://doi.org/10.1002/pro.141>
- Chami, M., Steinfels, E., Orelle, C., Jault, J. M., Di Pietro, A., Rigaud, J. L., & Marco, S. (2002). Three-dimensional structure by cryo-electron microscopy of YvcC, an homodimeric ATP-binding cassette transporter from *Bacillus subtilis*. *Journal of Molecular Biology*, 315(5), 1075–1085. <https://doi.org/10.1006/jmbi.2001.5309>
- Chang, G., & Roth, C. B. (2001). Structure of MsbA from *E. coli*: a homolog of the multidrug resistance ATP binding cassette (ABC) transporters. *Science (New York, N.Y.)*, 293(5536), 1793–1800. <https://doi.org/10.1126/science.293.5536.1793>
- Chaptal, V., Delolme, F., Kilburg, A., Magnard, S., Montigny, C., Picard, M., ... Falson, P. (2017). Quantification of Detergents Complexed with Membrane Proteins. *Scientific Reports*, 7, 1–12. <https://doi.org/10.1038/srep41751>
- Chen, Z., Shi, T., Zhang, L., Zhu, P., Deng, M., Huang, C., ... Li, J. (2016). Mammalian drug efflux transporters of the ATP binding cassette (ABC) family in multidrug resistance: A review of the past decade. *Cancer Letters*, 370(1), 153–164. <https://doi.org/10.1016/j.canlet.2015.10.010>
- Cheniour, M., Brewer, J., Bagatolli, L., Marcillat, O., & Granjon, T. (2017). Evidence of proteolipid domain formation in an inner mitochondrial membrane mimicking model. *Biochimica et Biophysica Acta - General Subjects*, 1861(5), 969–976. <https://doi.org/10.1016/j.bbagen.2017.02.001>
- Clay, A. T., & Sharom, F. J. (2013). Lipid bilayer properties control membrane partitioning, binding, and transport of P-glycoprotein substrates. *Biochemistry*, 52(2), 343–354. <https://doi.org/10.1021/bi301532c>
- Clegg, R. M. (1992). Fluorescence resonance energy transfer and nucleic acids. *Methods in Enzymology*, 211, 353–388.
- Cooper, R. S., & Altenberg, G. A. (2013). Association/dissociation of the nucleotide-binding domains of the atp-binding cassette protein MSBA measured during continuous hydrolysis.

- Journal of Biological Chemistry*, 288(29), 20785–20796.
<https://doi.org/10.1074/jbc.M113.477976>
- Corradi, V., Mendez-Villuendas, E., Ingólfsson, H. I., Gu, R., Siuda, I., Melo, M. N., ... Tieleman, D. P. (2018). Lipid-Protein Interactions Are Unique Fingerprints for Membrane Proteins. *ACS Central Science*, acscentsci.8b00143. <https://doi.org/10.1021/acscentsci.8b00143>
- Dalmas, O., Do Cao, M. A., Lugo, M. R., Sharom, F. J., Di Pietro, A., & Jault, J. M. (2005). Time-resolved fluorescence resonance energy transfer shows that the bacterial multidrug ABC half-transporter BmrA functions as a homodimer. *Biochemistry*, 44(11), 4312–4321. <https://doi.org/10.1021/bi0482809>
- Davidson, A. L., Dassa, E., Orelle, C., & Chen, J. (2008). Structure, Function, and Evolution of Bacterial ATP-Binding Cassette Systems. *Microbiology and Molecular Biology Reviews*, 72(2), 317–364. <https://doi.org/10.1128/MMBR.00031-07>
- Dawson, R. J. P., & Locher, K. P. (2006). Structure of a bacterial multidrug ABC transporter. *Nature*, 443(7108), 180–185. <https://doi.org/10.1038/nature05155>
- De La Cruz, E. M., & Ostap, E. M. (2009). Kinetic and equilibrium analysis of the myosin ATPase. *Methods in Enzymology*, 455(08), 157–92. [https://doi.org/10.1016/S0076-6879\(08\)04206-7](https://doi.org/10.1016/S0076-6879(08)04206-7)
- Deleu, M., Brasseur, R., & Dufre, Y. F. (2008). Atomic force microscopy of supported lipid bilayers. *Nature Protocols*, 3(10), 1654–1659. <https://doi.org/10.1038/nprot.2008.149>
- Dezi, M., Fribourg, P. F., Cicco, A. Di, Jault, J. M., Chami, M., & Lévy, D. (2011). Binding, reconstitution and 2D crystallization of membrane or soluble proteins onto functionalised lipid layer observed in situ by reflected light microscopy. *Journal of Structural Biology*, 174(2), 307–314. <https://doi.org/10.1016/j.jsb.2010.12.001>
- Dietrich, C., Bagatolli, L. A., Volovyk, Z. N., Thompson, N. L., Levi, M., Jacobson, K., & Gratton, E. (2001). Lipid rafts reconstituted in model membranes. *Biophysical Journal*, 80(3), 1417–1428. [https://doi.org/10.1016/S0006-3495\(01\)76114-0](https://doi.org/10.1016/S0006-3495(01)76114-0)
- Doeven, M. K., Folgering, J. H. A., Krasnikov, V., Geertsma, E. R., Van Den Bogaart, G., & Poolman, B. (2005). Distribution, lateral mobility and function of membrane proteins incorporated into giant unilamellar vesicles. *Biophysical Journal*, 88(2), 1134–1142. <https://doi.org/10.1529/biophysj.104.053413>
- Doige, C. A., Yu, X., & Sharom, F. J. (1993). The effects of lipids and detergents on ATPase-active P-glycoprotein. *BBA - Biomembranes*, 1146(1), 65–72. [https://doi.org/10.1016/0005-2736\(93\)90339-2](https://doi.org/10.1016/0005-2736(93)90339-2)
- Dörr, J. M., Koorengevel, M. C., Schäfer, M., Prokofyev, A. V., Scheidelaar, S., van der Cruisen, E. A. W., ... Killian, J. A. (2014). Detergent-free isolation, characterization, and functional reconstitution of a tetrameric K⁺ channel: the power of native nanodiscs. *Proceedings of the National Academy of Sciences of the United States of America*, 111(52), 18607–12. <https://doi.org/10.1073/pnas.1416205112>
- Doshi, R., Ali, A., Shi, W., Freeman, E. V., Fagg, L. A., & Van Veen, H. W. (2013). Molecular disruption of the power stroke in the ATP-binding cassette transport protein MsbA. *Journal of Biological Chemistry*, 288(10), 6801–6813. <https://doi.org/10.1074/jbc.M112.430074>
- Eckford, P. D. W., & Sharom, F. J. (2008). Functional characterization of Escherichia coli MsbA: Interaction with nucleotides and substrates. *Journal of Biological Chemistry*, 283(19), 12840–12850. <https://doi.org/10.1074/jbc.M708274200>
- Eckford, P. D. W., & Sharom, F. J. (2010). The reconstituted Escherichia coli MsbA protein displays lipid flippase activity. *Biochemical Journal*, 429(1), 195–203. <https://doi.org/10.1042/BJ20100144>
- Eggensperger, S., Fisette, O., Parcej, D., Schäfer, L. V., & Tampé, R. (2014). An annular lipid belt is essential for allosteric coupling and viral inhibition of the antigen translocation complex TAP

- (Transporter Associated with Antigen Processing). *Journal of Biological Chemistry*, 289(48), 33098–33108. <https://doi.org/10.1074/jbc.M114.592832>
- El-Awady, R., Saleh, E., Hashim, A., Soliman, N., Dallah, A., Elrasheed, A., & Elakraa, G. (2017). The role of eukaryotic and prokaryotic ABC transporter family in failure of chemotherapy. *Frontiers in Pharmacology*, 7(JAN), 1–15. <https://doi.org/10.3389/fphar.2016.00535>
- Ernest, S., & Bello-reuss, E. (1999). Secretion of Platelet-Activating Factor Is Mediated by MDR1 P-Glycoprotein in Cultured Human Mesangial Cells, (15), 2306–2313.
- Esser, L., Zhou, F., Pluchino, K. M., Shiloach, J., Ma, J., Tang, W.-K., ... Xia, D. (2016). Structures of the Multidrug Transporter P-glycoprotein Reveal Asymmetric ATP Binding and the Mechanism of Polyspecificity. *J Biol Chem*, (1), jbc.M116.755884. <https://doi.org/10.1074/jbc.M116.755884>
- Esteban-Martín, S., Jelger Risselada, H., Salgado, J., & Marrink, S. J. (2009). Stability of asymmetric lipid bilayers assessed by molecular dynamics simulations. *Journal of the American Chemical Society*, 131(42), 15194–15202. <https://doi.org/10.1021/ja904450t>
- Francia, F., Dezi, M., Mallardi, A., Palazzo, G., Cordone, L., & Venturoli, G. (2008). Protein–Matrix Coupling/Uncoupling in “Dry” Systems of Photosynthetic Reaction Center Embedded in Trehalose/Sucrose: The Origin of Trehalose Peculiarity. *Journal of the American Chemical Society*, 130(31), 10240–10246. <https://doi.org/10.1021/ja801801p>
- Fribourg, P. F., Chami, M., Sorzano, C. O. S., Gubellini, F., Marabini, R., Marco, S., ... Lévy, D. (2014). 3D cryo-electron reconstruction of BmrA, a bacterial multidrug ABC transporter in an inward-facing conformation and in a lipidic environment. *Journal of Molecular Biology*, 426(10), 2059–2069. <https://doi.org/10.1016/j.jmb.2014.03.002>
- Galián, C., Manon, F., Dezi, M., Torres, C., Ebel, C., Lévy, D., & Jault, J. M. (2011). Optimized purification of a heterodimeric ABC transporter in a highly stable form amenable to 2-D crystallization. *PLoS ONE*, 6(5). <https://doi.org/10.1371/journal.pone.0019677>
- Garten, M., Aimon, S., Bassereau, P., & Toombes, G. E. (2015). Reconstitution of a transmembrane protein, the voltage-gated ion channel, KvAP, into giant unilamellar vesicles for microscopy and patch clamp studies. *J Vis Exp*, (95), 52281. <https://doi.org/10.3791/52281>
- Geertsma, E. R., Nik Mahmood, N. A. B., Schuurman-Wolters, G. K., & Poolman, B. (2008). Membrane reconstitution of ABC transporters and assays of translocator function. *Nature Protocols*, 3(2), 256–266. <https://doi.org/10.1038/nprot.2007.519>
- Geillon, F., Gondcaille, C., Raas, Q., Dias, A. M. M., Pecqueur, D., Truntzer, C., ... Trompier, D. (2017). Peroxisomal ATP-binding cassette transporters form mainly tetramers. *Journal of Biological Chemistry*, 292(17), 6965–6977. <https://doi.org/10.1074/jbc.M116.772806>
- Girard, P., Pécréaux, J., Lenoir, G., Falson, P., Rigaud, J. L., & Bassereau, P. (2004). A new method for the reconstitution of membrane proteins into giant unilamellar vesicles. *Biophysical Journal*, 87(1), 419–429. <https://doi.org/10.1529/biophysj.104.040360>
- Gottesman, M. M., Fojo, T., & Bates, S. E. (2002). Multidrug Resistance in Cancer: Role of Atp-Dependent Transporters. *Nature Reviews Cancer*, 2(1), 48–58. <https://doi.org/10.1038/nrc706>
- Greene, N. P., Kaplan, E., Crow, A., & Koronakis, V. (2018). Antibiotic Resistance Mediated by the MacB ABC Transporter Family: A Structural and Functional Perspective, 9(May). <https://doi.org/10.3389/fmicb.2018.00950>
- Gulati, S., Jamshad, M., Knowles, T. J., Morrison, K. A., Downing, R., Cant, N., ... Rothnie, A. J. (2014). Detergent-free purification of ABC (ATP-binding-cassette) transporters. *Biochemical Journal*, 461(2), 269–278. <https://doi.org/10.1042/BJ20131477>
- Gustot, A., Smriti, Ruysschaert, J. M., Mchaourab, H., & Govaerts, C. (2010). Lipid composition regulates the orientation of transmembrane helices in HorA, an ABC multidrug transporter. *Journal of Biological Chemistry*, 285(19), 14144–14151.

<https://doi.org/10.1074/jbc.M109.079673>

- Gutmann, D. A. P., Ward, A., Urbatsch, I. L., Chang, G., & van Veen, H. W. (2010). Understanding polyspecificity of multidrug ABC transporters: closing in on the gaps in ABCB1. *Trends in Biochemical Sciences*, 35(1), 36–42. <https://doi.org/10.1016/j.tibs.2009.07.009>
- Hassan, K. A., Fagerlund, A., Elbourne, L. D. H., Vörös, A., Kroeger, J. K., Simm, R., ... Kolstø, A. B. (2017). The putative drug efflux systems of the *Bacillus cereus* group. *PLoS ONE*, 12(5), 1–25. <https://doi.org/10.1371/journal.pone.0176188>
- Herget, M., Kreißig, N., Kolbe, C., Schölz, C., Tampe, R., & Abele, R. (2009). Purification and reconstitution of the antigen transport complex TAP. A prerequisite determination of peptide stoichiometry and ATP hydrolysis. *Journal of Biological Chemistry*, 284(49), 33740–33749. <https://doi.org/10.1074/jbc.M109.047779>
- Higgins, C. F. (2007). Multiple molecular mechanisms for multidrug resistance transporters. *Nature*, 446(7137), 749–757. <https://doi.org/10.1038/nature05630>
- Higgins, C. F., & Gottesman, M. M. (1992). Is the multidrug transporter a flippase? *Trends in Biochemical Sciences*, 17(1), 18–21. [https://doi.org/10.1016/0968-0004\(92\)90419-A](https://doi.org/10.1016/0968-0004(92)90419-A)
- Hirayama, H., Kimura, Y., Kioka, N., Matsuo, M., & Ueda, K. (2013). ATPase activity of human ABCG1 is stimulated by cholesterol and sphingomyelin. *Journal of Lipid Research*, 54(2), 496–502. <https://doi.org/10.1194/jlr.M033209>
- Ho, H., Miu, A., Alexander, M. K., Garcia, N. K., Oh, A., Zilberleyb, I., ... Koth, C. M. (2018). Structural basis for dual-mode inhibition of the ABC transporter MsbA. *Nature*, 557(7704), 196–201. <https://doi.org/10.1038/s41586-018-0083-5>
- Hohl, M., Hürlimann, L. M., Böhm, S., Schöppe, J., Grütter, M. G., Bordignon, E., & Seeger, M. A. (2014). Structural basis for allosteric cross-talk between the asymmetric nucleotide binding sites of a heterodimeric ABC exporter. *Proceedings of the National Academy of Sciences of the United States of America*, 111(30), 11025–11030. <https://doi.org/10.1073/pnas.1400485111>
- Infed, N., Hanekop, N., Driessen, A. J. M., Smits, S. H. J., & Schmitt, L. (2011). Influence of detergents on the activity of the ABC transporter LmrA. *Biochimica et Biophysica Acta - Biomembranes*, 1808(9), 2313–2321. <https://doi.org/10.1016/j.bbamem.2011.05.016>
- Jackson, S. M., Manolaridis, I., Kowal, J., Zechner, M., Taylor, N. M. I., Bause, M., ... Locher, K. P. (2018). Structural basis of small-molecule inhibition of human multidrug transporter ABCG2. *Nature Structural & Molecular Biology*, 25(4), 333–340. <https://doi.org/10.1038/s41594-018-0049-1>
- Jamshad, M., Lin, Y.-P., Knowles, T. J., Parslow, R. A., Harris, C., Wheatley, M., ... Dafforn, T. R. (2011). Surfactant-free purification of membrane proteins with intact native membrane environment. *Biochemical Society Transactions*, 39(3), 813–818. <https://doi.org/10.1042/BST0390813>
- Jin, M. S., Oldham, M. L., Zhang, Q., & Chen, J. (2012). Crystal structure of the multidrug transporter P-glycoprotein from *Caenorhabditis elegans*. *Nature*, 490(7421), 566–569. <https://doi.org/10.1038/nature11448>
- Johnson, Z. L., & Chen, J. (2017). Structural Basis of Substrate Recognition by the Multidrug Resistance Protein MRP1. *Cell*, 168(6), 1075–1085.e9. <https://doi.org/10.1016/j.cell.2017.01.041>
- Jones, P. M., & George, A. M. (2004). The ABC transporter structure and mechanism: Perspectives on recent research. *Cellular and Molecular Life Sciences*, 61(6), 682–699. <https://doi.org/10.1007/s00018-003-3336-9>
- Jones, P. M., & George, A. M. (2013). Mechanism of the ABC transporter ATPase domains: Catalytic models and the biochemical and biophysical record. *Critical Reviews in Biochemistry and Molecular Biology*, 48(1), 39–50. <https://doi.org/10.3109/10409238.2012.735644>

- Jørgensen, I. L., Kemmer, G. C., & Pomorski, T. G. (2017). Membrane protein reconstitution into giant unilamellar vesicles: a review on current techniques. *European Biophysics Journal*, 46(2), 103–119. <https://doi.org/10.1007/s00249-016-1155-9>
- Jungas, C., Ranck, J.-L., Rigaud, J.-L., Joliot, P., & Verméglio, A. (1999). Supramolecular organization of the photosynthetic apparatus of *Rhodobacter sphaeroides*. *The EMBO Journal*, 18(3), 534–542. <https://doi.org/10.1093/emboj/18.3.534>
- Jungwirth, H., & Kuchler, K. (2006). Yeast ABC transporters - A tale of sex, stress, drugs and aging. *FEBS Letters*, 580(4), 1131–1138. <https://doi.org/10.1016/j.febslet.2005.12.050>
- Kahya, N., Scherfeld, D., Bacia, K., Poolman, B., & Schwille, P. (2003). Probing lipid mobility of raft-exhibiting model membranes by fluorescence correlation spectroscopy. *Journal of Biological Chemistry*, 278(30), 28109–28115. <https://doi.org/10.1074/jbc.M302969200>
- Kang, J., Park, J., Choi, H., Burla, B., Kretschmar, T., Lee, Y., & Martinoia, E. (2011). Plant ABC Transporters. *The Arabidopsis Book*, 9, e0153. <https://doi.org/10.1199/tab.0153>
- Kaur, H., Andrea, L., Roberta, S., Ramona, V., Christian, H., Johanna, B.-B., ... Clemens, G. (2015). The ABC exporter MsbA probed by solid state NMR – challenges and opportunities. *Biological Chemistry*. <https://doi.org/10.1515/hsz-2015-0119>
- Kaur, H., Lakatos-Karoly, A., Vogel, R., Nöll, A., Tampé, R., & Glaubitz, C. (2016). Coupled ATPase-adenylate kinase activity in ABC transporters. *Nature Communications*, 7(May), 13864. <https://doi.org/10.1038/ncomms13864>
- Kawai, T., Caaveiro, J. M. M., Abe, R., Katagiri, T., & Tsumoto, K. (2011). Catalytic activity of MsbA reconstituted in nanodisc particles is modulated by remote interactions with the bilayer. *FEBS Letters*, 585(22), 3533–3537. <https://doi.org/10.1016/j.febslet.2011.10.015>
- Kispal, G., Csere, P., Guiard, B., & Lill, R. (1997). The ABC transport Atm1p is required for mitochondrial iron homeostasis. *FEBS Letters*, 418(3), 346–350. [https://doi.org/10.1016/S0014-5793\(97\)01414-2](https://doi.org/10.1016/S0014-5793(97)01414-2)
- Klappe, K., Hummel, I., Hoekstra, D., & Kok, J. W. (2009). Lipid dependence of ABC transporter localization and function. *Chemistry and Physics of Lipids*, 161(2), 57–64. <https://doi.org/10.1016/j.chemphyslip.2009.07.004>
- Kooijman, E. E., Chupin, V., de Kruijff, B., & Burger, K. N. J. (2003). Modulation of membrane curvature by phosphatidic acid and lysophosphatidic acid. *Traffic*, 4(3), 162–174. <https://doi.org/10.1034/j.1600-0854.2003.00086.x>
- Krügel, H., Licht, A., Biedermann, G., Petzold, A., Lassak, J., Hupfer, Y., ... Saluz, H. P. (2010). Cervimycin C resistance in *Bacillus subtilis* is due to a promoter up-mutation and increased mRNA stability of the constitutive ABC-transporter gene *bmrA*. *FEMS Microbiology Letters*, 313(2), 155–163. <https://doi.org/10.1111/j.1574-6968.2010.02143.x>
- Kučerka, N., Nieh, M. P., & Katsaras, J. (2011). Fluid phase lipid areas and bilayer thicknesses of commonly used phosphatidylcholines as a function of temperature. *Biochimica et Biophysica Acta - Biomembranes*, 1808(11), 2761–2771. <https://doi.org/10.1016/j.bbamem.2011.07.022>
- Lambert, O., Lévy, D., Ranck, J.-L., Leblanc, G., & Rigaud, J.-L. (1998). A new “gel-like” phase in dodecyl maltoside-lipid mixtures: implications in solubilization and reconstitution studies. *Biophysical Journal*, 74(2 Pt 1), 918–930. [https://doi.org/10.1016/S0006-3495\(98\)74015-9](https://doi.org/10.1016/S0006-3495(98)74015-9)
- Landau, E. M., & Rosenbusch, J. P. (1996). Lipidic cubic phases: A novel concept for the crystallization of membrane proteins. *Proceedings of the National Academy of Sciences*, 93(25), 14532–14535. <https://doi.org/10.1073/pnas.93.25.14532>
- Landry, Y. D., Denis, M., Nandi, S., Bell, S., Vaughan, A. M., & Zha, X. (2006). ATP-binding Cassette Transporter A1 Expression Disrupts Raft Membrane Microdomains through Its, 281(47), 36091–36101. <https://doi.org/10.1074/jbc.M602247200>
- Laub, K. R., Marek, M., Stanchev, L. D., Herrera, A., Kanashova, T., Dittmar, G., & Gu, T. (2017).

- Purification and characterisation of the yeast plasma membrane ATP binding cassette transporter Pdr11p. *Plos One*, 12(9), 1–18. <https://doi.org/10.6084/m9.figshare.5259457>
- Lee, A. G. (2003). *Lipid-protein interactions in biological membranes: A structural perspective. Biochimica et Biophysica Acta - Biomembranes* (Vol. 1612). [https://doi.org/10.1016/S0005-2736\(03\)00056-7](https://doi.org/10.1016/S0005-2736(03)00056-7)
- Lee, J. Y., Kinch, L. N., Borek, D. M., Wang, J., Wang, J., Urbatsch, I. L., ... Rosenbaum, D. M. (2016). Crystal structure of the human sterol transporter ABCG5/ABCG8. *Nature*, 533(7604), 561–564. <https://doi.org/10.1038/nature17666>
- Lee, S.-Y., Lee, A., Chen, J., & MacKinnon, R. (2005). Structure of the KvAP voltage-dependent K⁺ channel and its dependence on the lipid membrane. *Proceedings of the National Academy of Sciences*, 102(43), 15441–15446. <https://doi.org/10.1073/pnas.0507651102>
- Levental, K. R., & Levental, I. (2015). *Giant Plasma Membrane Vesicles: Models for Understanding Membrane Organization. Current Topics in Membranes* (Vol. 75). Elsevier Ltd. <https://doi.org/10.1016/bs.ctm.2015.03.009>
- Lévy, D., Bluzat, A., Seigneuret, M., & Rigaud, J. L. (1990). A systematic study of liposome and proteoliposome reconstitution involving Bio-Bead-mediated Triton X-100 removal. *BBA - Biomembranes*, 1025(2), 179–190. [https://doi.org/10.1016/0005-2736\(90\)90096-7](https://doi.org/10.1016/0005-2736(90)90096-7)
- Lévy, D., Gulik, A., Bluzat, A., & Rigaud, J. L. (1992). Reconstitution of the sarcoplasmic reticulum Ca²⁺-ATPase: mechanisms of membrane protein insertion into liposomes during reconstitution procedures involving the use of detergents. *BBA - Biomembranes*, 1107(2), 283–298. [https://doi.org/10.1016/0005-2736\(92\)90415-I](https://doi.org/10.1016/0005-2736(92)90415-I)
- Li-Blatter, X., Nervi, P., & Seelig, A. (2009). Detergents as intrinsic P-glycoprotein substrates and inhibitors. *Biochimica et Biophysica Acta - Biomembranes*, 1788(10), 2335–2344. <https://doi.org/10.1016/j.bbamem.2009.07.010>
- Locher, K. P. (2016). Mechanistic diversity in ATP-binding cassette (ABC) transporters. *Nature Structural & Molecular Biology*, 23(6), 487–93. <https://doi.org/10.1038/nsmb.3216>
- Loo, T. W., & Clarke, D. M. (2002). Vanadate trapping of nucleotide at the ATP-binding sites of human multidrug resistance P-glycoprotein exposes different residues to the drug-binding site. *Proceedings of the National Academy of Sciences*, 99(6), 3511–3516. <https://doi.org/10.1073/pnas.022049799>
- Loo, T. W., & Clarke, D. M. (2014). Cysteines introduced into extracellular loops 1 and 4 of human P-glycoprotein that are close only in the open conformation spontaneously form a disulfide bond that inhibits drug efflux and ATPase activity. *Journal of Biological Chemistry*, 289(36), 24749–24758. <https://doi.org/10.1074/jbc.M114.583021>
- Loo, T. W., & Clarke, D. M. (2017). Thiol-reactive drug substrates of human P-glycoprotein label the same sites to activate ATPase activity in membranes or dodecyl maltoside detergent micelles. *Biochemical and Biophysical Research Communications*, 488(4), 573–577. <https://doi.org/10.1016/j.bbrc.2017.05.106>
- Lopez, D. (2015). Molecular composition of functional microdomains in bacterial membranes. *Chemistry and Physics of Lipids*, 192, 3–11. <https://doi.org/10.1016/j.chemphyslip.2015.08.015>
- Lubelski, J., Konings, W. N., & Driessen, A. J. M. (2007). Distribution and Physiology of ABC-Type Transporters Contributing to Multidrug Resistance in Bacteria. *Microbiology and Molecular Biology Reviews*, 71(3), 463–476. <https://doi.org/10.1128/MMBR.00001-07>
- Marcoux, J., Wang, S. C., Politis, A., Reading, E., Ma, J., Biggin, P. C., ... Robinson, C. V. (2013). Mass spectrometry reveals synergistic effects of nucleotides, lipids, and drugs binding to a multidrug resistance efflux pump. *Proceedings of the National Academy of Sciences*, 110(24), 9704–9709. <https://doi.org/10.1073/pnas.1303888110>
- Marín-García, J. (2013). Mitochondrial Biogenesis BT - Mitochondria and Their Role in

- Cardiovascular Disease. In J. Marín-García (Ed.) (pp. 59–97). Boston, MA: Springer US. https://doi.org/10.1007/978-1-4614-4599-9_4
- Marquardt, D., Geier, B., & Pabst, G. (2015). Asymmetric lipid membranes: Towards more realistic model systems. *Membranes*, 5(2), 180–196. <https://doi.org/10.3390/membranes5020180>
- McMahon, H. T., & Boucrot, E. (2015). Membrane curvature at a glance. *Journal of Cell Science*, 128(6), 1065–1070. <https://doi.org/10.1242/jcs.114454>
- McMahon, H. T., & Gallop, J. L. (2005). Membrane curvature and mechanisms of dynamic cell membrane remodelling. *Nature*, 438(7068), 590–596. <https://doi.org/10.1038/nature04396>
- Mehmood, S., Corradi, V., Choudhury, H. G., Hussain, R., Becker, P., Axford, D., ... Beis, K. (2016). Structural and functional basis for lipid synergy on the activity of the antibacterial peptide ABC transporter McjD. *Journal of Biological Chemistry*, 291(41), 21656–21668. <https://doi.org/10.1074/jbc.M116.732107>
- Mehmood, S., Domene, C., Forest, E., & Jault, J.-M. (2012). Dynamics of a bacterial multidrug ABC transporter in the inward- and outward-facing conformations. *Proceedings of the National Academy of Sciences of the United States of America*, 109(27), 10832–6. <https://doi.org/10.1073/pnas.1204067109>
- Mi, W., Li, Y., Yoon, S. H., Ernst, R. K., Walz, T., & Liao, M. (2017). Structural basis of MsbA-mediated lipopolysaccharide transport. *Nature*, 549(7671), 233–237. <https://doi.org/10.1038/nature23649>
- Mishra, S., Verhalen, B., Stein, R. A., Wen, P. C., Tajkhorshid, E., & Mchaourab, H. S. (2014). Conformational dynamics of the nucleotide binding domains and the power stroke of a heterodimeric ABC transporter. *ELife*, 3, e02740. <https://doi.org/10.7554/eLife.02740>
- Moeller, A., Lee, S. C., Tao, H., Speir, J. A., Chang, G., Urbatsch, I. L., ... Zhang, Q. (2015). Distinct Conformational Spectrum of Homologous Multidrug ABC Transporters. *Structure*, 23(3), 450–460. <https://doi.org/10.1016/j.str.2014.12.013>
- Morrison, K. A., Akram, A., Mathews, A., Khan, Z. A., Patel, J. H., Zhou, C., ... Rothnie, A. J. (2016). Membrane protein extraction and purification using styrene-maleic acid (SMA) co-polymer: Effect of variations in polymer structure. *Biochemical Journal*, 473(23), 4349–4360. <https://doi.org/10.1042/BCJ20160723>
- Muchová, K., Wilkinson, A. J., & Barák, I. (2011). Changes of lipid domains in *Bacillus subtilis* cells with disrupted cell wall peptidoglycan. *FEMS Microbiology Letters*, 325(1), 92–98. <https://doi.org/10.1111/j.1574-6968.2011.02417.x>
- Mühleip, A. W., Joos, F., Wigge, C., Frangakis, A. S., Kühlbrandt, W., & Davies, K. M. (2016). Helical arrays of U-shaped ATP synthase dimers form tubular cristae in ciliate mitochondria. *Proceedings of the National Academy of Sciences*, 113(30), 8442–8447. <https://doi.org/10.1073/pnas.1525430113>
- Nagata, K. O., Nakada, C., Kasai, R. S., Kusumi, A., & Ueda, K. (2013). ABCA1 dimer-monomer interconversion during HDL generation revealed by single-molecule imaging. *Proceedings of the National Academy of Sciences*, 110(13), 5034–5039. <https://doi.org/10.1073/pnas.1220703110>
- Neumann, J., Rose-Sperling, D., & Hellmich, U. A. (2016). Diverse relations between ABC transporters and lipids: An overview. *BBA-Biomembranes*. <https://doi.org/10.1016/j.bbamem.2016.09.023>
- Neyfakh, A. A. (1997). Natural functions of bacterial multidrug transporters. *Trends in Microbiology*, 5(8), 309–313. [https://doi.org/10.1016/S0966-842X\(97\)01064-0](https://doi.org/10.1016/S0966-842X(97)01064-0)
- Olofsson, L., & Margeat, E. (2013). Pulsed interleaved excitation fluorescence spectroscopy with a supercontinuum source. *Optics Express*, 21(3), 3370–8. <https://doi.org/10.1364/OE.21.003370>

- Orelle, C., Dalmas, O., Gros, P., Di Pietro, A., & Jault, J. M. (2003). The Conserved Glutamate Residue Adjacent to the Walker-B Motif is the Catalytic Base for ATP Hydrolysis in the ATP-binding Cassette Transporter BmrA. *Journal of Biological Chemistry*, 278(47), 47002–47008. <https://doi.org/10.1074/jbc.M308268200>
- Orelle, C., Gubellini, F., Durand, a, Marco, S., Levy, D., Gros, P., ... Jault, J. M. (2008). Conformational change induced by ATP binding in the multidrug ATP-binding cassette transporter BmrA. *Biochemistry*, 47(8), 2404–2412. <https://doi.org/10.1021/bi702303s>
- Palsdottir, H., & Hunte, C. (2004). Lipids in membrane protein structures. *Biochimica et Biophysica Acta - Biomembranes*, 1666(1–2), 2–18. <https://doi.org/10.1016/j.bbamem.2004.06.012>
- Parmar, M. J., Lousa, C. D. M., Muench, S. P., Goldman, A., & Postis, V. L. G. (2016). Artificial membranes for membrane protein purification, functionality and structure studies. *Biochemical Society Transactions*, 44(3), 877–882. <https://doi.org/10.1042/BST20160054>
- Perez, C., Gerber, S., Boilevin, J., Bucher, M., Darbre, T., Aebi, M., ... Locher, K. P. (2015). Structure and mechanism of an active lipid-linked oligosaccharide flippase. *Nature*, 524(7566), 433–438. <https://doi.org/10.1038/nature14953>
- Phillips, R., Ursell, T., Wiggins, P., & Sens, P. (2009). Emerging roles for lipids in shaping membrane-protein function. *Nature*, 459(7245), 379–85. <https://doi.org/10.1038/nature08147>
- Pierman, B., Toussaint, F., Bertin, A., Lévy, D., Smargiasso, N., De Pauw, E., & Boutry, M. (2017). Activity of the purified plant ABC transporter NtPDR1 is stimulated by diterpenes and sesquiterpenes involved in constitutive and induced defenses. *Journal of Biological Chemistry*, 292(47), 19491–19502. <https://doi.org/10.1074/jbc.M117.811935>
- Pignataro, M. F., Dodes-Traian, M. M., González-Flecha, F. L., Sica, M., Mangialavori, I. C., & Rossi, J. P. F. C. (2015). Modulation of plasma membrane Ca²⁺-ATPase by neutral phospholipids: Effect of the micelle-vesicle transition and the bilayer thickness. *Journal of Biological Chemistry*, 290(10), 6179–6190. <https://doi.org/10.1074/jbc.M114.585828>
- Popot, J.-L. (2010). Amphipols, Nanodiscs, and Fluorinated Surfactants: Three Nonconventional Approaches to Studying Membrane Proteins in Aqueous Solutions. *Annual Review of Biochemistry*, 79(1), 737–775. <https://doi.org/10.1146/annurev.biochem.052208.114057>
- Prasad, R., Khandelwal, N. K., & Banerjee, A. (2016). Yeast ABC transporters in lipid trafficking. *Fungal Genetics and Biology*, 93, 25–34. <https://doi.org/10.1016/j.fgb.2016.05.008>
- Procko, E., Ferrin-O'Connell, I., Ng, S. L., & Gaudet, R. (2006). Distinct Structural and Functional Properties of the ATPase Sites in an Asymmetric ABC Transporter. *Molecular Cell*, 24(1), 51–62. <https://doi.org/10.1016/j.molcel.2006.07.034>
- Pyle, E., Kalli, A. C., Amillis, S., Hall, Z., Lau, A. M., Hanyaloglu, A. C., ... Politis, A. (2018). Structural Lipids Enable the Formation of Functional Oligomers of the Eukaryotic Purine Symporter UapA. *Cell Chemical Biology*, 25(7), 840–848.e4. <https://doi.org/10.1016/j.chembiol.2018.03.011>
- Quemeneur, F., Sigurdsson, J. K., Renner, M., Atzberger, P. J., Bassereau, P., & Lacoste, D. (2014). Shape matters in protein mobility within membranes. *Proceedings of the National Academy of Sciences*, 111(14), 5083–5087. <https://doi.org/10.1073/pnas.1321054111>
- Quinn, P. J. (2004). Plasma membrane phospholipid asymmetry. *Phospholipid Metabolism in Apoptosis*, 36, 39–60. https://doi.org/10.1007/0-306-47931-1_3
- Ramachandra, M., Ambudkar, S. V., Chen, D., Hrycyna, C. A., Dey, S., Gottesman, M. M., & Pastan, I. (1998). Human P-glycoprotein exhibits reduced affinity for substrates during a catalytic transition state. *Biochemistry*, 37(14), 5010–5019. <https://doi.org/10.1021/bi973045u>
- Ravaud, S., Do Cao, M.-A., Jidenko, M., Ebel, C., Le Maire, M., Jault, J.-M., ... Aghajari, N. (2006). The ABC transporter BmrA from *Bacillus subtilis* is a functional dimer when in a detergent-

- solubilized state. *The Biochemical Journal*, 395(2), 345–353. <https://doi.org/10.1042/BJ20051719>
- Rees, D. C., Johnson, E., & Lewinson, O. (2009). ABC transporters: the power to change. *Nature Reviews Molecular Cell Biology*, 10(3), 218–227. <https://doi.org/10.1038/nrm2646>
- Reuter, G., Janvilisri, T., Venter, H., Shahi, S., Balakrishnan, L., & Van Veen, H. W. (2003). The ATP binding cassette multidrug transporter LmrA and lipid transporter MsbA have overlapping substrate specificities. *Journal of Biological Chemistry*, 278(37), 35193–35198. <https://doi.org/10.1074/jbc.M306226200>
- Reyes, C. L., Ward, A., Yu, J., & Chang, G. (2006). The structures of MsbA: Insight into ABC transporter-mediated multidrug efflux. *FEBS Letters*, 580(4), 1042–1048. <https://doi.org/10.1016/j.febslet.2005.11.033>
- Rigaud, J.-L., & Levy, D. (2003). Reconstitution of membrane proteins into liposomes. *Methods in Enzymology*, 372(2000), 65–86. [https://doi.org/10.1016/S0076-6879\(03\)72004-7](https://doi.org/10.1016/S0076-6879(03)72004-7)
- Rigaud, J.-L., Lévy, D., G, M., & Lambert, O. (1998). Detergent removal by Bio-Beads. Application to membrane protein reconstitution and two-dimensional crystallisation. *Eur J. of Biophysics. (Review)*, 27, 305–319.
- Rigaud, J. L., Pitard, B., & Levy, D. (1995). Reconstitution of membrane proteins into liposomes: application to energy-transducing membrane proteins. *BBA - Bioenergetics*, 1231(3), 223–246. [https://doi.org/10.1016/0005-2728\(95\)00091-V](https://doi.org/10.1016/0005-2728(95)00091-V)
- Riordan, J. R. (2008). CFTR Function and Prospects for Therapy. *Annual Review of Biochemistry*, 77(1), 701–726. <https://doi.org/10.1146/annurev.biochem.75.103004.142532>
- Ritchie, T. K., Kwon, H., & Atkins, W. M. (2011). Conformational analysis of human ATP-binding cassette transporter ABCB1 in lipid nanodiscs and inhibition by the antibodies MRK16 and UIC2. *Journal of Biological Chemistry*, 286(45), 39489–39496. <https://doi.org/10.1074/jbc.M111.284554>
- Robey, R. W., Pluchino, K. M., Hall, M. D., Fojo, A. T., Bates, S. E., & Gottesman, M. M. (2018). Revisiting the role of ABC transporters in multidrug-resistant cancer. *Nature Reviews Cancer*, 18(July), 1–13. <https://doi.org/10.1038/s41568-018-0005-8>
- Römer, W., Pontani, L. L., Sorre, B., Rentero, C., Berland, L., Chambon, V., ... Johannes, L. (2010). Actin Dynamics Drive Membrane Reorganization and Scission in Clathrin-Independent Endocytosis. *Cell*, 140(4), 540–553. <https://doi.org/10.1016/j.cell.2010.01.010>
- Romsicki, Y., & Sharom, F. J. (1999). The membrane lipid environment modulates drug interactions with the P-glycoprotein multidrug transporter. *Biochemistry*, 38(21), 6887–6896. <https://doi.org/10.1021/bi990064q>
- Rosetti, C. M., Mangiarotti, A., & Wilke, N. (2017). Sizes of lipid domains: what do we know from artificial lipid membranes? What are the possible shared features with membrane rafts in cells? *Biochimica et Biophysica Acta (BBA) - Biomembranes*. <https://doi.org/10.1016/j.bbamem.2017.01.030>
- Sayaka Inagakia, Rodolfo Ghirlandob, and R. G. (2014). Biophysical Characterization of Membrane Proteins in Nanodiscs, 59(3), 287–300. <https://doi.org/10.1016/j.ymeth.2012.11.006>
- Schmidt, U., & Weiss, M. (2010). Hydrophobic mismatch-induced clustering as a primer for protein sorting in the secretory pathway. *Biophysical Chemistry*, 151(1–2), 34–38. <https://doi.org/10.1016/j.bpc.2010.04.009>
- Schölz, C., Parcej, D., Ejsing, C. S., Robenek, H., Urbatsch, I. L., & Tampe, R. (2011). Specific lipids modulate the transporter associated with antigen processing (TAP). *Journal of Biological Chemistry*, 286(15), 13346–13356. <https://doi.org/10.1074/jbc.M110.216416>
- Sharom, F. J. (2014). Complex Interplay between the P-Glycoprotein Multidrug Efflux Pump and the Membrane: Its Role in Modulating Protein Function. *Front Oncol*, 4(March), 41.

<https://doi.org/10.3389/fonc.2014.00041>

- Shen, H. H., Lithgow, T., & Martin, L. L. (2013). Reconstitution of membrane proteins into model membranes: Seeking better ways to retain protein activities. *International Journal of Molecular Sciences*, 14(1), 1589–1607. <https://doi.org/10.3390/ijms14011589>
- Shintre, C. A., Pike, A. C. W., Li, Q., Kim, J.-I., Barr, A. J., Goubin, S., ... Carpenter, E. P. (2013). Structures of ABCB10, a human ATP-binding cassette transporter in apo- and nucleotide-bound states. *Proceedings of the National Academy of Sciences*, 110(24), 9710–9715. <https://doi.org/10.1073/pnas.1217042110>
- Siarheyeva, A., & Sharom, F. J. (2009). The ABC transporter MsbA interacts with lipid A and amphipathic drugs at different sites. *The Biochemical Journal*, 419(2), 317–28. <https://doi.org/10.1042/BJ20081364>
- Simons, K., & Sampaio, J. L. (2011). Membrane organization and lipid rafts. *Perspect Biol*, 3(10), a004697. <https://doi.org/10.1101/cshperspect.a004697>
- Skrzypek, R., Iqbal, S., & Callaghan, R. (2018). Methods of reconstitution to investigate membrane protein function. *Methods*. <https://doi.org/10.1016/j.ymeth.2018.02.012>
- Spadaccini, R., Kaur, H., Becker-Baldus, J., & Glaubitz, C. (2018). The effect of drug binding on specific sites in transmembrane helices 4 and 6 of the ABC exporter MsbA studied by DNP-enhanced solid-state NMR. *Biochimica et Biophysica Acta - Biomembranes*, 1860(4), 833–840. <https://doi.org/10.1016/j.bbamem.2017.10.017>
- Stachowiak, J. C., Brodsky, F. M., & Miller, E. A. (2013). A cost-benefit analysis of the physical mechanisms of membrane curvature. *Nature Cell Biology*, 15(9), 1019–1027. <https://doi.org/10.1038/ncb2832>
- Starling, A. P., East, J. M., & Lee, A. G. (1993). Effects of phosphatidylcholine fatty acyl chain length on calcium binding and other functions of the (Ca(2+)-Mg2+)-ATPase. *Biochemistry*, 32(6), 1593–1600.
- Steinfels, E., Orelle, C., Dalmas, O., Penin, F., Miroux, B., Di Pietro, A., & Jault, J. M. (2002). Highly efficient over-production in *E. coli* of YvcC, a multidrug-like ATP-binding cassette transporter from *Bacillus subtilis*. *Biochimica et Biophysica Acta - Biomembranes*, 1565(1), 1–5. [https://doi.org/10.1016/S0005-2736\(02\)00515-1](https://doi.org/10.1016/S0005-2736(02)00515-1)
- Steinfels, E., Orelle, C., Fantino, J. R., Dalmas, O., Rigaud, J. L., Denizot, F., ... Jault, J. M. (2004). Characterization of YvcC (BmrA), a multidrug ABC transporter constitutively expressed in *Bacillus subtilis*. *Biochemistry*, 43(23), 7491–7502. <https://doi.org/10.1021/bi0362018>
- Stolarczyk, E. I., Reiling, C. J., & Paumi, C. M. (2011). Regulation of ABC transporter function via phosphorylation by protein kinases. *Current Pharmaceutical Biotechnology*, 12(4), 621–35. <https://doi.org/10.2174/138920111795164075>
- Szöllösi, D., Rose-Sperling, D., Hellmich, U. A., & Stockner, T. (2018). Comparison of mechanistic transport cycle models of ABC exporters. *Biochimica et Biophysica Acta - Biomembranes*, 1860(4), 818–832. <https://doi.org/10.1016/j.bbamem.2017.10.028>
- Taylor, N. M. I., Manolaridis, I., Jackson, S. M., Kowal, J., Stahlberg, H., & Locher, K. P. (2017). Structure of the human multidrug transporter ABCG2. *Nature*, 546(7659), 504–509. <https://doi.org/10.1038/nature22345>
- Terasawa, H., Nishimura, K., Suzuki, H., Matsuura, T., & Yomo, T. (2012). Coupling of the fusion and budding of giant phospholipid vesicles containing macromolecules. *Proceedings of the National Academy of Sciences*, 109(16), 5942–5947. <https://doi.org/10.1073/pnas.1120327109>
- Thomas, C., & Tampé, R. (2018). Multifaceted structures and mechanisms of ABC transport systems in health and disease. *Current Opinion in Structural Biology*, 51, 116–128. <https://doi.org/10.1016/j.sbi.2018.03.016>
- Tonnesen, A., Christensen, S. M., Tkach, V., & Stamou, D. (2014). Geometrical membrane curvature

- as an allosteric regulator of membrane protein structure and function. *Biophysical Journal*, 106(1), 201–209. <https://doi.org/10.1016/j.bpj.2013.11.023>
- Toussaint, F., Pierman, B., Bertin, A., Lévy, D., & Boutry, M. (2017). Purification and biochemical characterization of NpABCG5/NpPDR5, a plant pleiotropic drug resistance transporter expressed in *Nicotiana tabacum* BY-2 suspension cells. *Biochemical Journal*, 474(10), 1689–1703. <https://doi.org/10.1042/BCJ20170108>
- Toyoshima, C., Sasabe, H., & Stokes, D. L. (1993). Three-dimensional cryo-electron microscopy of the calcium ion pump in the sarcoplasmic reticulum membrane. *Nature*, 362(6419), 467–471.
- Ujwal, R., & Bowie, J. U. (2011). Crystallizing membrane proteins using lipidic bicelles. *Methods (San Diego, Calif.)*, 55(4), 337–341. <https://doi.org/10.1111/j.1743-6109.2008.01122.x> Endothelial
- Van Den Brink-Van Der Laan, E., Antoinette Killian, J., & De Kruijff, B. (2004). Nonbilayer lipids affect peripheral and integral membrane proteins via changes in the lateral pressure profile. *Biochimica et Biophysica Acta - Biomembranes*, 1666(1–2), 275–288. <https://doi.org/10.1016/j.bbamem.2004.06.010>
- van Meer, G., & de Kroon, A. I. P. M. (2011). Lipid map of the mammalian cell. *Journal of Cell Science*, 124(Pt 1), 5–8. <https://doi.org/10.1242/jcs.071233>
- van Veen, H. W., Margolles, A., Müller, M., Higgins, C. F., & Konings, W. N. (2000). The homodimeric ATP-binding cassette transporter LmrA mediates multidrug transport by an alternating two-site (two-cylinder engine) mechanism. *The EMBO Journal*, 19(11), 2503–2514. <https://doi.org/10.1093/emboj/19.11.2503>
- Vanni, S., Hirose, H., Barelli, H., Antonny, B., & Gautier, R. (2014). A sub-nanometre view of how membrane curvature and composition modulate lipid packing and protein recruitment. *Nature Communications*, 5. <https://doi.org/10.1038/ncomms5916>
- Verhalen, B., Dastvan, R., Thangapandian, S., Peskova, Y., Koteiche, H. A., Nakamoto, R. K., ... Mchaourab, H. S. (2017). Energy transduction and alternating access of the mammalian ABC transporter P-glycoprotein. *Nature*, 543(7647), 738–741. <https://doi.org/10.1038/nature21414>
- Verhalen, B., Ernst, S., Börsch, M., & Wilkens, S. (2012). Dynamic ligand-induced conformational rearrangements in P-glycoprotein as probed by fluorescence resonance energy transfer spectroscopy. *Journal of Biological Chemistry*, 287(2), 1112–1127. <https://doi.org/10.1074/jbc.M111.301192>
- Verhalen, B., & Wilkens, S. (2011). P-glycoprotein retains drug-stimulated ATPase activity upon covalent linkage of the two nucleotide binding domains at their C-terminal ends. *Journal of Biological Chemistry*, 286(12), 10476–10482. <https://doi.org/10.1074/jbc.M110.193151>
- Wang, Y., Botelho, A. V., Martinez, G. V., & Brown, M. F. (2002). Electrostatic properties of membrane lipids coupled to metarhodopsin II formation in visual transduction. *Journal of the American Chemical Society*, 124(26), 7690–7701. <https://doi.org/10.1021/ja0200488>
- Wang, Y. H., Li, Y., Yang, S. L., & Yang, L. (2005). Classification of substrates and inhibitors of P-glycoprotein using unsupervised machine learning approach. *Journal of Chemical Information and Modeling*, 45(3), 750–757. <https://doi.org/10.1021/ci050041k>
- Ward, A. B., Szewczyk, P., Grimard, V., Lee, C., Martinez, L., Doshi, R., ... Chang, G. (2013). Structures of P-glycoprotein reveal its conformational flexibility and an epitope on the nucleotide-binding domain. *Proceedings of the National Academy of Sciences*, 110(33), 13386–91. <https://doi.org/10.1073/pnas.1309275110>
- Ward, A., Reyes, C. L., Yu, J., Roth, C. B., & Chang, G. (2007). Flexibility in the ABC transporter MsbA: Alternating access with a twist. *Proceedings of the National Academy of Sciences of the United States of America*, 104(48), 19005–10. <https://doi.org/10.1073/pnas.0709388104>
- Wen, P. C., Verhalen, B., Wilkens, S., Mchaourab, H. S., & Tajkhorshid, E. (2013). On the origin of

- large flexibility of P-glycoprotein in the inward-facing state. *Journal of Biological Chemistry*, 288(26), 19211–19220. <https://doi.org/10.1074/jbc.M113.450114>
- Wilkens, S. (2015). Structure and mechanism of ABC transporters. *F1000Prime Reports*, 7(February), 1–9. <https://doi.org/10.12703/P7-14>
- Wiseman, B., Kilburg, A., Chaptal, V., Reyes-Mejia, G. C., Sarwan, J., Falson, P., & Jault, J. M. (2014). Stubborn contaminants: Influence of detergents on the purity of the multidrug ABC transporter BmrA. *PLoS ONE*, 9(12), 1–25. <https://doi.org/10.1371/journal.pone.0114864>
- Xie, Y., Xu, K., Linn, D. E., Yang, X., Guo, Z., Shimelis, H., ... Qiu, Y. (2008). The 44-kDa Pim-1 kinase phosphorylates BCRP/ABCG2 and thereby promotes its multimerization and drug-resistant activity in human prostate cancer cells. *Journal of Biological Chemistry*, 283(6), 3349–3356. <https://doi.org/10.1074/jbc.M707773200>
- Xu, Y., Seelig, A., & Bernèche, S. (2017). Unidirectional Transport Mechanism in an ATP Dependent Exporter. *ACS Central Science*, 3(3), 250–258. <https://doi.org/10.1021/acscentsci.7b00068>
- Zarrabi, N., Ernst, S., Verhalen, B., Wilkens, S., & Borsch, M. (2014). Analyzing conformational dynamics of single P-glycoprotein transporters by Forster resonance energy transfer using hidden Markov models. *Methods (San Diego, Calif.)*, 66(2), 168–179. <https://doi.org/10.1016/j.ymeth.2013.07.026>
- Zhang, B., Koh, Y. H., Beckstead, R. B., Budnik, V., Ganetzky, B., & Bellen, H. J. (1998). Synaptic vesicle size and number are regulated by a clathrin adaptor protein required for endocytosis. *Neuron*, 21(6), 1465–1475. [https://doi.org/10.1016/S0896-6273\(00\)80664-9](https://doi.org/10.1016/S0896-6273(00)80664-9)
- Zoghbi, M. E., Cooper, R. S., & Altenberg, G. A. (2016). The lipid bilayer modulates the structure and function of an ATP-binding cassette exporter. *Journal of Biological Chemistry*, 291(9), 4453–4461. <https://doi.org/10.1074/jbc.M115.698498>
- Zoghbi, M. E., Mok, L., Swartz, D. J., Singh, A., Fendley, G. A., Urbatsch, I. L., & Altenberg, G. A. (2017). Substrate-induced conformational changes in the nucleotide-binding domains of lipid bilayer-associated P-glycoprotein during ATP hydrolysis. *Journal of Biological Chemistry*, 292(50), 20412–20424. <https://doi.org/10.1074/jbc.M117.814186>
- Zou, P., Bortolus, M., & Mchaourab, H. S. (2009). Conformational Cycle of the ABC Transporter MsbA in Liposomes: Detailed Analysis Using Double Electron-Electron Resonance Spectroscopy. *Journal of Molecular Biology*, 393(3), 586–597. <https://doi.org/10.1016/j.jmb.2009.08.050>
- Zou, P., & Mchaourab, H. S. (2009). Mapping Daunorubicin-binding Sites in the ATP-binding Cassette Transporter MsbA Using Site-specific Quenching by Spin Labels * □, 284(20), 13904–13913. <https://doi.org/10.1074/jbc.M900837200>
- Zutz, A., Hoffmann, J., Hellmich, U. A., Glaubitz, C., Ludwig, B., Brutschy, B., & Tampé, R. (2011). Asymmetric ATP hydrolysis cycle of the heterodimeric multidrug ABC transport complex TmrAB from *Thermus thermophilus*. *Journal of Biological Chemistry*, 286(9), 7104–7115. <https://doi.org/10.1074/jbc.M110.201178>

Résumé

Les ABC (ATP binding cassettes) transporteurs constituent une grande famille de protéine transmembranaire présentent dans tous les organismes. Les ABC hydrolysent l'ATP pour transporter une quantité immense de substrats amphiphiles, comme les lipides, stéroïdes, peptides... Certains ABCs confèrent un phénotype cellulaire de multiresistance aux drogues des bactéries contre les antibiotiques à l'homme contre les agents anticancéreux, antiviraux ...

Une question fondamentale pour comprendre le transport de drogues est comment les propriétés de membranes modulent la fonction et l'organisation spatio temporelle des ABCs transporteurs. Nous avons étudié en détails ces couplage avec BmrA, un ABC bactérien de *B. subtilis* en utilisant différents systèmes membranaires *in vitro* et différentes approches de biochimie et de biophysique membranaire. Dans un premier temps, après expression et purification des protéines en détergent, nous avons caractérisé l'hydrolyse d'ATP en fonction de l'état de l'environnement membranaire, solubilisé en micelle de détergent et en micelles mixtes. Les proteoliposomes ont été caractérisés en fonction de l'orientation des protéines, leur taux d'incorporation, leur taille et la lamellarité. Cela nous a permis de moduler de façon contrôlée la composition lipidique, la densité et la conformation des protéines et la courbure membranaire pour déterminer de façon quantitative les contributions respectives de ces paramètres de membranes. Ainsi, nous montrons que l'hydrolyse d'ATP est sensible à la spécificité lipidique quand la protéine est dans une bicouche et que les lipides négatifs et les lipides de type phosphatidylethanolamine stimulent de façon synergique l'activité hydrolytique. L'hydrolyse d'ATP diminue pour les fortes courbure positives. Dans un second temps, nous avons déterminé les conditions de reconstitution de BmrA dans des vésicules géantes qui ont ensuite permis d'étudier les rôles respectifs de la courbure et de la tensions membranaire dans l'organisation spatiale de BmrA par des approches de nanotube pulling. Les expériences en collaboration montrent que BmrA a une préférence marquée pour les régions membranaires à forte courbure conduisant à la formation de cluster de protéines et que cette préférence varie en fonction de l'état catalytique de la protéine. Finalement, nous avons mis au point une méthode pour étudier la dynamique des NBDs par transfert d'énergie de résonance de Förster au niveau de la molécule unique dans un système reconstitué par spectroscopie de fluorescence et de corrélation croisée.

L'ensemble des données suggère que organisations spatiales des ABC transporteurs dans les cellules bactériennes et eucaryotes sont différentes avec la possibilité de tris dans des zones de fortes courbures lors de remodelages membranaires mais sans modification importante de la fonction.

Mots Clés

Transporteur ABC, protéine transmembranaire, reconstitution, propriétés membranaires, GUV

Abstract

ABCs (ATP binding cassettes) transporters constitute a large family of transmembrane proteins present in all organisms. ABC transporters hydrolyze ATP to translocate an immense quantity of amphiphilic substrates, such as lipids, steroids, peptides... Some ABCs confer a multiresistance cellular phenotype to drugs from bacteria against antibiotics to humans against anticancer agents, antivirals...

A fundamental question for understanding drug transport at the molecular level is how the properties of membranes modulate the function and spatial temporal organization of ABCs. We studied in detail these coupling with BmrA, a bacterial ABC of *B. subtilis* using different *in vitro* membrane systems and different biochemical and membrane biophysical approaches. Firstly, after expression and purification of proteins in detergent, we characterized the hydrolysis of ATP of BmrA according to its membrane environment, solubilized in detergent micelles and in mixed lipid/detergent micelles. Proteoliposomes were characterized according to protein orientation, incorporation rate, size and lamellarity. This allowed us to modulate in a controlled manner lipid composition, protein density and conformation and membrane curvature to quantitatively determine the respective contributions of these membrane parameters. Thus, we show that ATP hydrolysis is sensitive to lipid specificity when the protein is embedded in a bilayer. This lipid specificity is provided by negative lipids and phosphatidylethanolamine type lipids that synergistically stimulate hydrolytic activity. However, ATP hydrolysis was decreased in high positive membrane curvature. Secondly, we determined the conditions of reconstitution of BmrA in Giant Unilamellar Vesicles, which then allowed our collaborator to study the respective roles of membrane curvature and tension in the spatial organization of BmrA. Nanotube pulling experiments performed in collaboration show that BmrA has a strong preference for highly curved membrane regions leading to protein cluster formation and that this preference varies according to the catalytic state of the protein. Finally, we developed a method to study the dynamics of NBDs by Förster resonance energy transfer at the single molecule level in reconstituted system via fluorescence cross-correlation spectroscopy.

The data set suggest that spatial organizations of ABC transporters in bacterial and eukaryotic cells are different with the possibility of sorting during membrane remodeling of eukaryotic membranes in areas of strong membrane curvatures but without significant change in function.

Keywords

ABC transporter, transmembrane protein, reconstitution, membrane properties, GUV